JHU/APL DST-12
FISCAL YEAR 1984

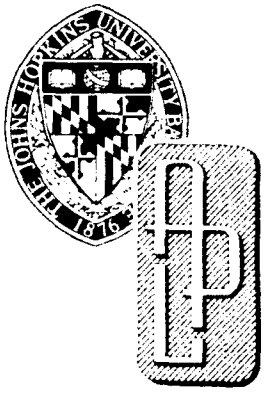

APPLIED PHYSICS LABORATORY

DEVELOPMENTS IN SCIENCE AND TECHNOLOGY

Approved for public release, distribution unlimited

THE JOHNS HOPKINS UNIVERSITY • APPLIED PHYSICS LABORATORY
Johns Hopkins Road, Laurel, Maryland 20707
Operating under Contract N00024-85-C-5301 with the Department of the Navy

JHU/APL DST-12
FISCAL YEAR 1984

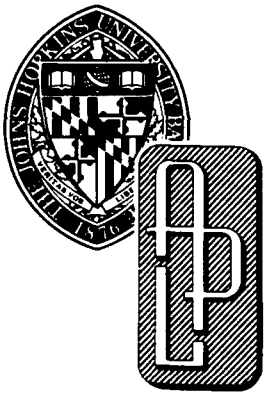

APPLIED PHYSICS LABORATORY

DEVELOPMENTS IN SCIENCE AND TECHNOLOGY

THE JOHNS HOPKINS UNIVERSITY • APPLIED PHYSICS LABORATORY
Johns Hopkins Road, Laurel, Maryland 20707
Operating under Contract N00024-85-C-5301 with the Department of the Navy

FOREWORD

The Applied Physics Laboratory (APL), a division of The Johns Hopkins University, is located in Howard County, Maryland, midway between Baltimore and Washington. Its work is carried out under contractual agreements between the University and the federal, state, and local governments by a staff of more than 2700, including 1500 professional scientists and engineers, of whom more than half have advanced degrees. Their ideas are implemented and extended through several field activities and a network of associate contractors and collaborators from coast to coast.

The primary mission of APL is to enhance national security by applying advanced science and technology to the solution of problems important to national objectives. The Laboratory conducts programs in fundamental and applied research, exploratory and advanced development, component engineering, system engineering and integration, and test and evaluation of operational systems. About 80% of the Laboratory's effort is for the Department of the Navy, and 10% is for other Defense agencies. About 10% is applied to nondefense areas, including space research.

APL, established in 1942 under the auspices of the Office of Scientific Research and Development, successfully developed a proximity (VT) fuze for antiaircraft defense that was highly effective during World War II. The University agreed to continue the Laboratory after the war as an important national resource. During the era of emerging guided-missile technology from about 1944 to 1956, APL concentrated on developing a family of shipborne surface-to-air missiles. The Navy-sponsored Bumblebee program pioneered many basic guided-missile technologies used later in other missile programs.

The era of weapons system engineering began in 1956 with the commissioning of the first guided-missile cruiser. The experience gained in integrating missiles with radars, computers, displays, and other elements of a complete weapon system has found application in many systems of interest to the Navy in various warfare areas and to other branches of the government. Significant activities are proceeding in areas of special APL competence, including advanced radar techniques, missile propulsion, missile guidance, countermeasures, data processing and display, and combat systems integration.

As Technical Advisor to the Navy in the design, development, and operation of the Aegis Weapon System, APL now has the broader challenge of integrating the operation of Aegis cruisers with other ships and aircraft of the battle group. Other areas of tactical systems support include aviation countermeasures and a major role as Technical Direction Agent of the Navy Tomahawk cruise missile program. APL also has a major role in the area of command, control, and communications (C^3) systems to facilitate the operation of Naval forces. Both strategic and tactical aspects of the C^3 process are being examined.

APL provides technical evaluation of the operational Fleet Ballistic Missile (FBM) System. Quantitative test and evaluation procedures are applied to every newly commissioned ballistic missile submarine. Similarly, APL currently provides precise evaluation of the Army's Pershing missile systems. Significant programs are also under way for Naval strategic communications and tactical targeting. Since 1970, APL has had the responsibility for planning and conducting a significant technical program to ensure the security of the FBM submarine fleet against possible technological or tactical countermeasures. The approach is to quantify all physical and tactical means that might be developed to detect, identify, and track our submarines and to propose and evaluate suitable countermeasures and tactics.

The APL space program started with the Navy Navigation Satellite System, originally known as Transit, an accomplishment comparable in importance to the wartime proximity fuze and the surface-to-air missile program. APL invented the concept, designed and built the initial satellite constellation, and set up and operated a worldwide satellite tracking network. The APL space program now also includes the design and construction of a broad range of scientific satellites and space-borne scientific experiments for NASA and DoD.

With the encouragement of DoD, APL is applying its talent and experience to civil programs in areas of national importance. Some areas to which attention has been devoted in recent years are biomedical research and engineering; power plant siting; urban transport; navigation aids; reduction of pollution of the biosphere; ocean thermal, geothermal, and flywheel energy systems; and advanced education.

To support its R&D activities through knowledge and experience in advanced research, the Laboratory performs fundamental research in biological, chemical, mathematical, and physical sciences related to its missions. Through unique applications of system engineering, science, and technology to the needs of society, APL has enhanced the University's tradition of excellence while gaining worldwide recognition of its own.

This report contains only selected samples of APL technical accomplishments that were completed during fiscal year 1984 and are suited to reporting in a concise format for unlimited distribution. Some major programs were omitted because their broad scope or long-term, continuing nature are not suited to this format or because of classification. While this publication does not sample all APL areas of effort and accomplishment, it does provide an indication of the scope and variety of the technical work carried out during the reporting period.

CONTENTS

SYSTEMS ENGINEERING

SURVEILLANCE AND TRACKING

COMMAND, CONTROL, AND COMMUNICATIONS

TEST AND EVALUATION

NAVAL WARFARE ANALYSIS

SPACE SCIENCE AND TECHNOLOGY

OCEAN SCIENCE AND TECHNOLOGY

BIOMEDICAL SCIENCE AND ENGINEERING

ENVIRONMENTAL SCIENCE AND TECHNOLOGY

FUNDAMENTAL RESEARCH

SYSTEMS ENGINEERING

INTRODUCTION

The history of the Laboratory is replete with accomplishments that span a wide range of technological activities. A systems approach has been characteristic of many of those activities. Over the years, the complexity of the systems involved has greatly increased. In its formative years, APL supervised the research, development, and production of proximity fuzes. That activity led to guided missile research and development and later to the development of ship combat systems. APL has applied the principles of systems engineering in its work on the development of the basic structure of shipboard combat systems such as the Aegis Combat System, Terrier and Tartar New Threat Upgrades, and the multimission DDG-51 Combat System. In recent years, the Laboratory has expanded its use of the systems engineering approach to formulate a concept wherein the resources of many ships and their aircraft are coordinated at the battle group level to achieve new levels of antiair-warfare effectiveness.

The development of long-range cruise missiles also has required the integration of ever-larger collections of systems that must work together coherently. The missiles must be related not only to ship combat systems but also to command, control, and communications (C^3) networks and to sensor systems. APL has taken a leading role in the needed integration effort since the inception of the Tomahawk program. The Laboraotry's experience in this program and in a NAVELEX program to engineer a tactical C^3 system for the Navy for the year 2000 has provided a synergistic basis to achieve desired goals.

Representative of numerous APL contributions in support of defense objectives is the system design, fabrication, and testing of a compact oceanographic data acquisition system for submarine use.

APL has applied systems engineering principles to a number of civilian programs. Noteworthy examples are found in the evaluation for the Department of Energy of alternative, long-range, nondepleting sources of energy. Solar and geothermal energy sources have been identified as being especially attractive to meet future national requirements. Tests exploiting one aspect of solar energy—the thermal gradient between the surface and the deep ocean—indicate that Ocean Thermal Energy Conversion (OTEC) may provide a practical and economical way to produce electricity, chemicals such as ammonia for fertilizers, and synthetic fuels such as methanol. Methanol has promise both for fuel-cell use to generate electricity and as an automotive vehicle fuel. One article evaluates the feasibility and cost of producing methanol by OTEC. Another compares the cost and efficiency of three kinds of geothermally enhanced OTEC plants.

A SMALL OCEANOGRAPHIC DATA ACQUISITION SYSTEM FOR SUBMARINE USE

R. E. Ball and V. Vigliotti

APL has completed the design, development, fabrication, and testing of a submarine-deployable Small Oceanographic Data Acquisition system. The system incorporates the data acquisition, processing, recording, and display functions of the previously deployed Minimal Installation Data Acquisition System II in one-fourth the space. In addition to significant hardware development, new software has been developed to use a touch-sensitive menu-driven display for system control.

BACKGROUND

The primary mission of the Ocean Data Acquisition Program (ODAP) from its inception in 1976 has been the collection and post-test analysis of oceanographic data. To fulfill this mission, ODAP has developed and deployed on board U.S. Navy submarines three generations of oceanographic data collection systems. In 1984, the development, fabrication, and testing of the submarine-deployable Small Oceanographic Data Acquisition (SODA) system was completed. This fourth-generation system expanded deployment opportunities through miniaturization while maintaining or improving established system capabilities.

DISCUSSION

System Requirements

Design guidelines governing the SODA system development minimized new design efforts where suitable existing components could be identified. Applied equally to hardware and software elements, this approach produced an architecture similar to the previously developed Minimal Installation Data Acquisition System (MIDAS) and MIDAS-II[1] suites, which encompass commercial microcomputer equipment and peripherals, a standard operating system, and special-purpose hardware and software when necessary. The design satisfies the following standing ODAP collection system requirements:

1. Acquire oceanographic sensor data in both analog and multiplexed digital formats,
2. Acquire ship position and motion data in either synchro and event or multiplexed digital formats,
3. Record data on digital and analog magnetic tape,
4. Display acquired data in real time on a cathode ray tube and a strip-chart recorder,
5. Permit the operator to interact with the data acquisition and display software.

Figure 1 shows the major data acquisition units and the equipment with which they interact.

The principal SODA design specifications were intended to reduce system size significantly, maintain compatibility with MIDAS-II high-level language software, and improve system performance through enhancement and simplification of the operator-to-system interaction.

System Design and Hardware Development

The feasibility of the design depended on finding a suitably small and powerful microcomputer and supporting peripherals having the required MIDAS-II compatibility. This need fostered the development of a benchmark test[2] of representative ODAP data collection processes as a tool for the quantitative evaluation of selected commercial units. The performance of the MIDAS-II minicomputer (DEC PDP 11/34A) was established as the ODAP system benchmark requirement.

Candidate microcomputers were selected for their degree of compatibility with the MIDAS-II high-level applications and operating system software. Two microcomputers satisfying the software compatibility requirement were identified: the DEC LSI 11/23, and an enchanced version of the LSI 11/23 offered by General Robotics Corp. The latter was chosen because it required a lower percentage of its processing power (69.4%) under the benchmark regime, allowing for greater future expansion.

Two special-purpose hardware units were also developed to reduce the size from MIDAS-II equivalents. The analog processing unit printed circuit board (PCB) and the synchronized time code generator were developed under the direction of the ODAP Office by Interstate Electronics Corp. and Datum Inc., respectively.

Processing of low-level analog sensor signals is performed on four-channel PCBs. Each channel of a PCB applies selectable gain, filtering, and root-mean-square averaging functions. Two output signals are available from each channel: a wideband signal for recording on the wideband analog recorder and a narrowband signal that is routed to the analog-to-digital (A/D) converter. As many as eight PCBs may be included in a SODA sys-

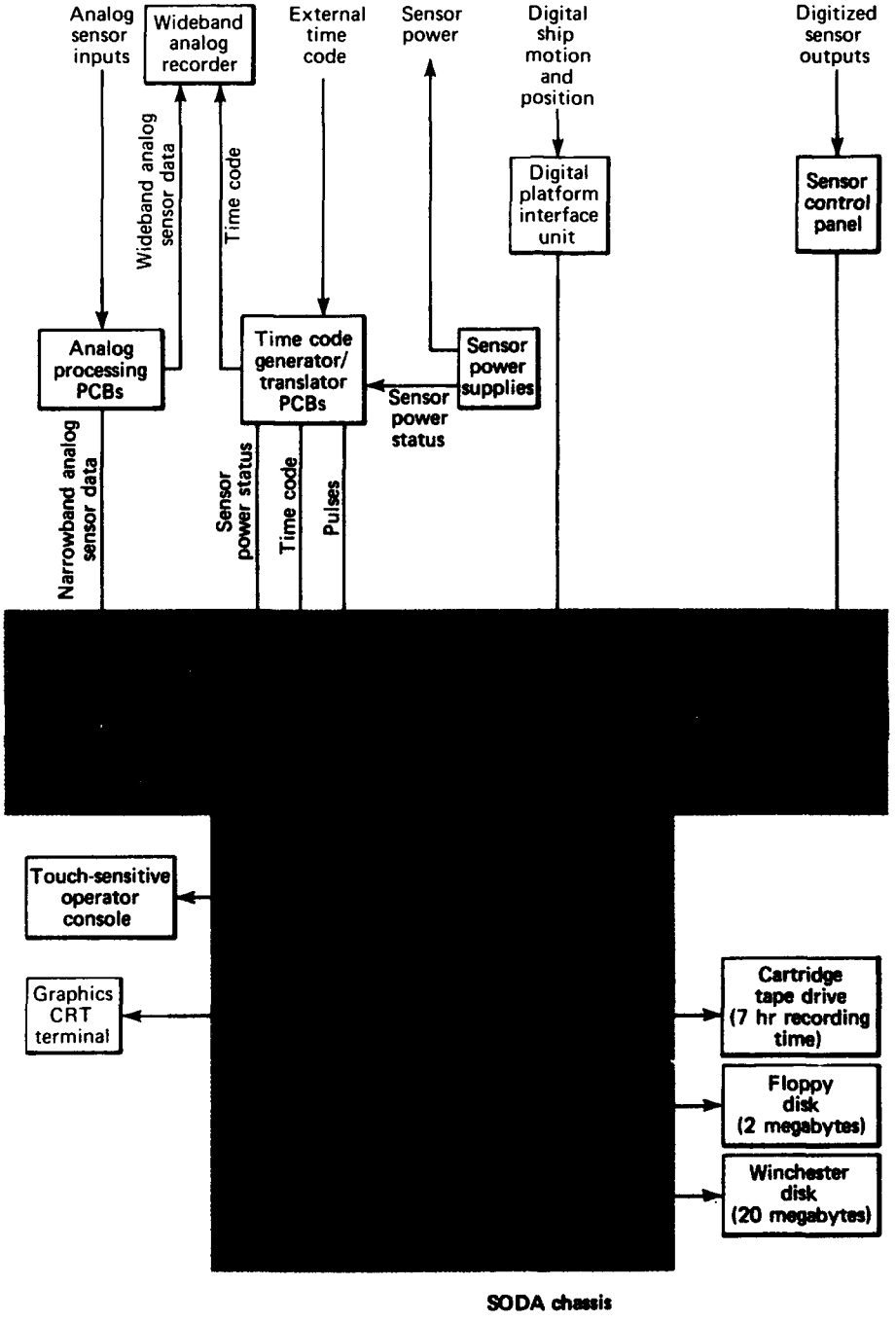

Figure 1—Functional diagram of the SODA system.

tem configuration. The new design reduces the size of each channel to 25% of the MIDAS-II equivalent.

The SODA system requires precision timing-rate and time-of-day inputs synchronized to an externally generated time code. The synchronized time code generator, implemented on three PCBs, performs this function. It generates the timing pulses used to synchronize the software-controlled A/D sampling and data display outputs and accumulates time-of-day information.

The operator console provides for interaction with the data acquisition and display software and is implemented on a commercial touch-sensitive gas plasma display manufactured by General Digital Corp. The unit contains 51 individually addressable pages, each capable of sensing touch inputs and displaying software-generated outputs. This hardware feature is coupled with the special-purpose operator interaction software to present the operator with a menu-driven set of displays to perform all required system operations.

The SODA system is packaged in rugged module shells for protection and for ease of stacking aboard ship. The sensor control panel, digital platform interface unit, and wideband analog recorder packages were designed previously; the SODA chassis package was developed by APL. The chassis (Fig. 2) is 12.5 by 20 by 32 in. and occupies only 25% of the space required by comparable units of previous ODAP systems.

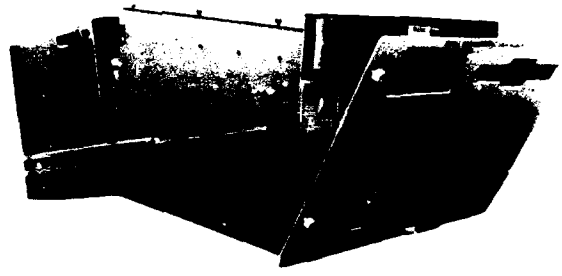

Figure 2—The SODA system chassis.

Software

The real-time software system consists of concurrently executing data acquisition, recording, processing, and display programs and an operator interaction program. Major data flow paths through program modules are shown in Fig. 3. Program interaction and synchroni-

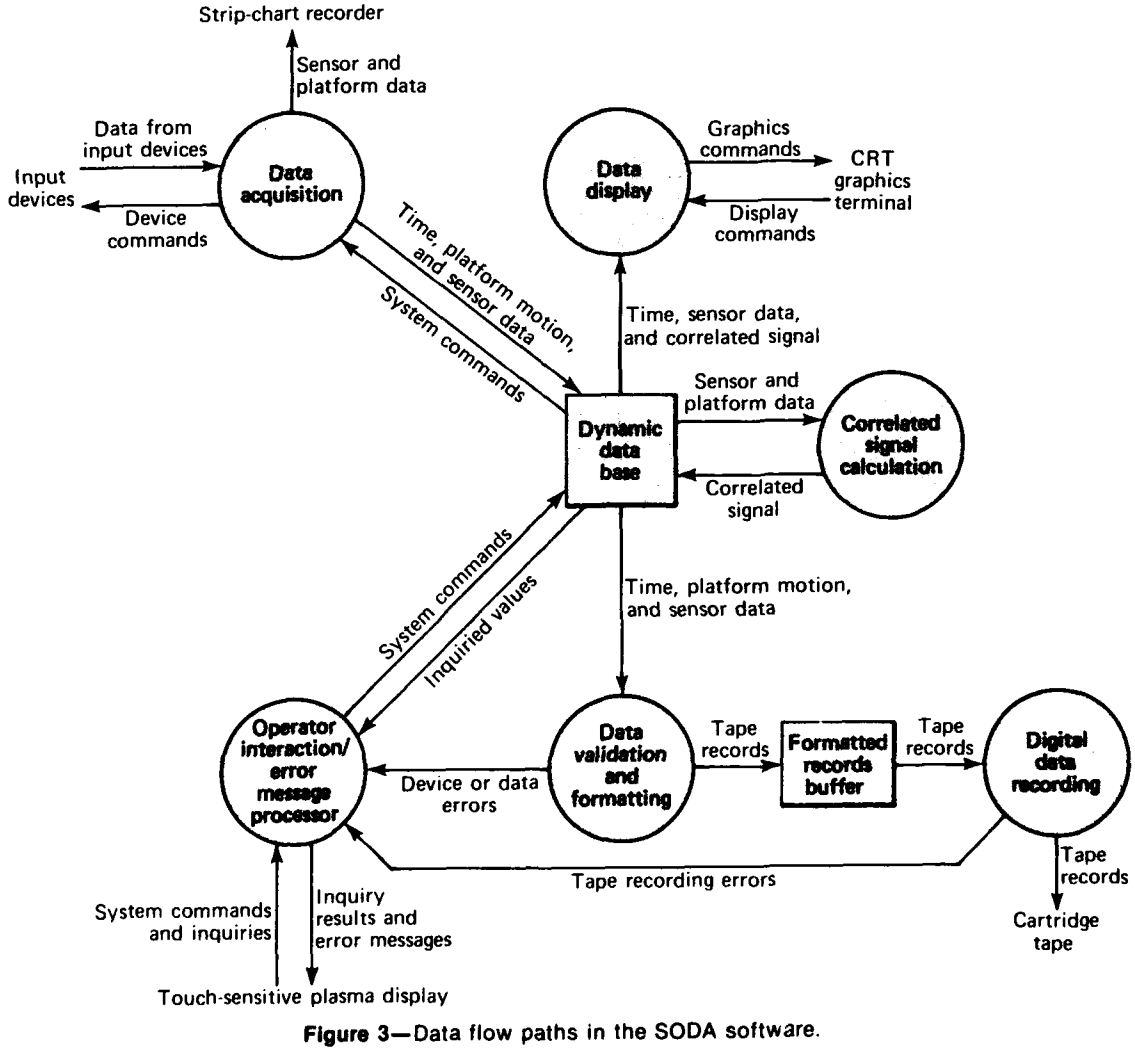

Figure 3—Data flow paths in the SODA software.

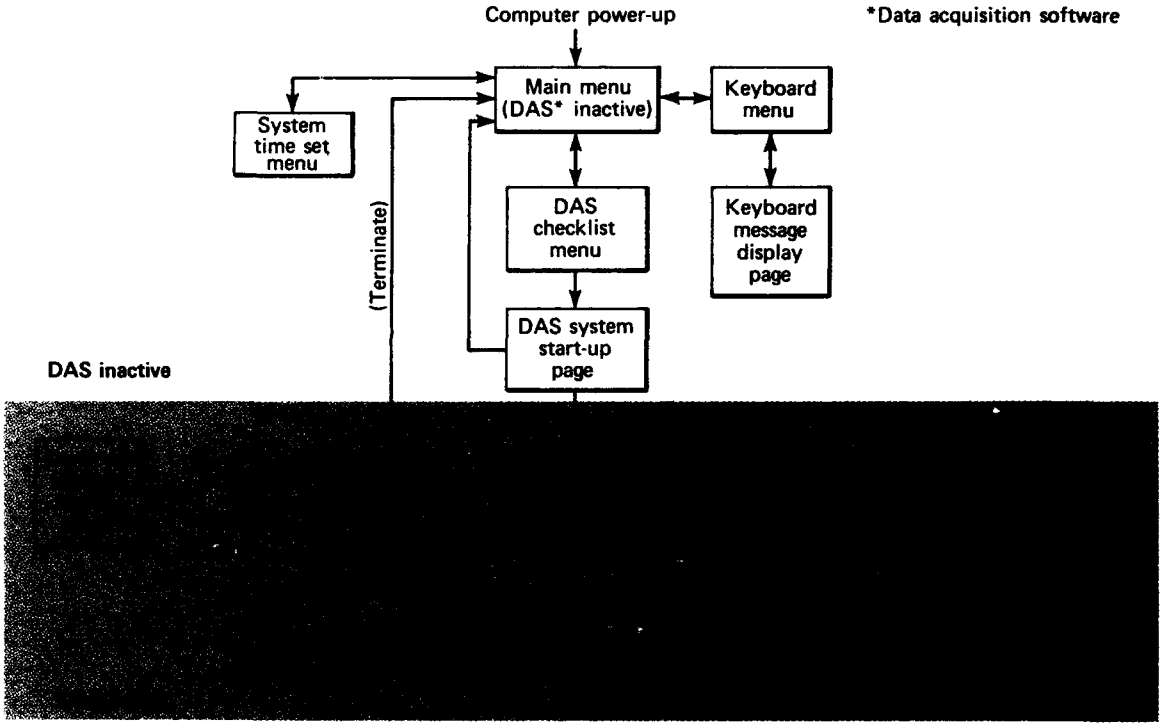

Figure 4—Structure of the menu architecture.

zation are handled through the standard DEC RSX-11M time-sharing operating system. The choice of the LSI 11/23 microcomputer, a member of the PDP 11 family, as the SODA processor allowed virtually all of the existing MIDAS-II software to be transferred directly to the SODA system. However, significant software development was needed to improve the operator-to-system interaction program.

Operator interaction with the data acquisition system is through the system's operator console, which is used to initiate or terminate data acquisition, command the system to perform required functions, ask for system status or data values, observe error messages generated during data acquisition, and interact (under abnormal conditions) with RSX-11M utility programs. The previous MIDAS-II console, a standard alphanumeric cathode ray tube, required the operator to memorize (or look up) and correctly type all required commands or responses. The touch-panel terminal with menu-driven displays in the SODA system removes this burden from the operator, simplifies the mode of interaction, and reduces possibilities of errors.

Figure 4 shows the structure of the menu display architecture. Each menu, which corresponds to a memory page of the terminal that can be individually updated and displayed, provides positive feedback to the operator, and the operator can always return to some previous menu state. Included in the menu is a keyboard emulation module that allows the operator to type specific commands in the unusual case when more than a standard touch response is required.

SYSTEM STATUS

Hardware and software testing completed during 1984 verified that the SODA system met all operational requirements. Its first operational deployment is scheduled for the spring of 1985. The smaller package size enhances submarine installation flexibility and should increase deployment opportunities, while the touch-sensitive console and improved software greatly simplify operation, thereby reducing training requirements and increasing system utility.

REFERENCES

[1] R. E. Ball, J. E. Coolahan, V. Vigliotti, and R. E. Cohn, "A Shipboard Real-Time Data Acquisition System for Oceanographic Measurements," in *Developments in Science and Technology, Fiscal Year 1982*, JHU/APL DST-10.

[2] V. Vigliotti and R. E. Ball, *LSI 11/23 Benchmark Test*, JHU/APL ODAP-M-268/83 (1983).

[3] R. E. Ball, *Small Oceanographic Data Acquisition System Design*, JHU/APL ODAP-M-359/83 (1983).

This work was supported by the Office of the Chief of Naval Operations, OP-009V.

EVALUATION OF PROCESS AND COST FOR METHANOL PRODUCTION BY OCEAN THERMAL ENERGY CONVERSION

W. H. Avery, D. Richards, E. J. Francis, and G. L. Dugger

Three industrial organizations experienced in offshore oil technology and synthetic fuel production have cooperated with APL in evaluating the feasibility and cost of producing methanol on Ocean Thermal Energy Conversion (OTEC) plantships sited in the tropical oceans. The concept involves using OTEC electric power for the on-board electrolysis of water to form hydrogen and oxygen, followed by combining those gases with coal (transported to the ship) to form methanol. The commercial availability of OTEC methanol would create an abundant source of high octane fuel that could significantly reduce future United States and world requirements for gasoline and other petroleum-based fuels.

BACKGROUND

The investigation by APL in 1974 of alternative energy sources that could reduce or replace United States imports of petroleum fuels showed that OTEC offered outstanding promise in two respects: (a) the estimated costs of energy and products were attractive, and (b) the technology is based on a resource that could provide nonpolluting renewable energy in quantities that are far larger than forseeable total United States demands.

With support from the U.S. Department of Energy, and in conjunction with industrial contractors, conceptual and preliminary design studies initiated in 1978 defined the configuration, marine engineering requirements, and costs of 40-MWe OTEC plantships using OTEC-produced electrolytic hydrogen in combination with nitrogen extracted from the air to produce ammonia.

The program showed the feasibility of producing an OTEC energy product on plantships designed to cruise slowly ("graze") throughout the year in the warmest areas of the tropical oceans. A baseline design and a cost estimate were documented for a 40-MWe OTEC demonstration plantship designed to produce 110 metric tons per day of liquid ammonia for shipment to United States ports on conventional ammonia tankers. The study also yielded a baseline design for a 35-MWe OTEC power plant to be moored two miles off shore at Punta Tuna, Puerto Rico, and to deliver power to the on-shore utility grid.[1]

Since 1982, the APL OTEC program has focused on the technological requirements for producing methanol, a liquid fuel with an octane number of 108. Methanol has been demonstrated as a direct, economical replacement for gasoline in present automobiles.

The concept proposed by APL for preparing methanol on OTEC plantships involves the reaction of oxygen and hydrogen (prepared by efficient on-board water electrolysis) with coal (transported to the plantship). Detailed analysis has shown the technical feasibility of the approach, and the commercial prospects look favorable compared with new plants designed for the production of methanol from natural gas or coal by less efficient conventional methods.

DISCUSSION

The feasibility and cost of producing methanol on OTEC plantships have been evaluated in two successive engineering studies conducted by industrial organizations with wide experience in synfuel development and marine engineering, under subcontract to APL. In the first study, an OTEC plantship was designed to generate 160-MWe net of electric power for use on board ship to produce 1000 metric tons per day of fuel-grade methanol. The plant was designed by Brown and Root Development, Inc. (BARDI) using state-of-the-art engineering and cost data derived from their designs for full-scale methanol and amonia plants.[2] Engineering design information for the OTEC power plant and plantship was based on scale-up of the dimensions and performance from the baseline 40-MWe ammonia plantship design.[1]

The BARDI study showed the technical feasibility of the OTEC methanol concept and indicated that the cost of producing methanol and delivering it to United States ports would be low enough to make the process interesting. An artist's concept of the plantship based on the BARDI layout is shown in Fig. 1. It became apparent that major improvements in cost would be possible if a more advanced coal gasification process such as that developed by Rockwell International, Inc., were substituted for the older Texaco gasification process selected for the BARDI design. Accordingly, Rockwell International and Ebasco Services, Inc., who supplied process and marine engineering support, contracted to revise the BARDI results and incorporate the design data for the advanced gasification process. That work showed that the methanol output could be raised to 1750 metric tons per day for the same basic OTEC power and plantship dimensions.[3]

The large increase in methanol output for the revised process relative to the BARDI design results primarily from the higher efficiency and smaller size of the

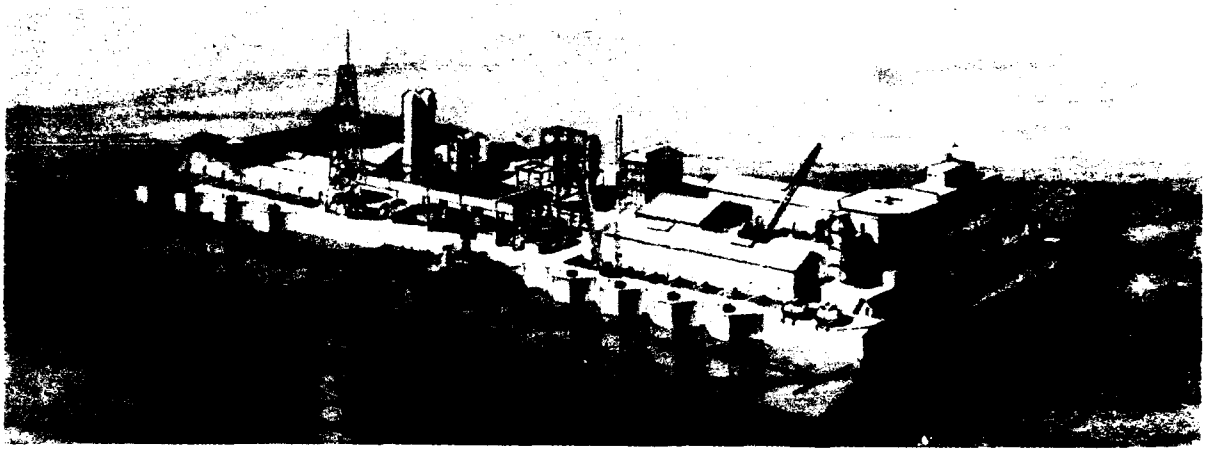

Figure 1—Artist's concept of the OTEC plantship.

Rockwell gasifier compared to the much older Texaco design. In the Texaco gasification process, a slurry of coal and water is introduced along with oxygen into a large vessel where the reaction proceeds in the gas phase at temperatures above 2200°F to form a gas mixture containing approximately equal molar amounts of carbon monoxide, carbon dioxide, and hydrogen. Sulfur in the coal reacts to form sulfur dioxide; the ash in the coal forms a liquid slag that is drained from the bottom of the vessel. The hot product gases are cooled and treated to remove the sulfur and carbon dioxide, the composition is adjusted to the correct ratio of carbon monoxide to hydrogen by reacting part of the carbon monoxide with water to form hydrogen and carbon dioxide ("shift conversion"), the excess carbon dioxide is removed, and the purified gas is finally passed through a catalytic converter to form methanol.

In the Rockwell process, dry pulverized coal is injected with steam and oxygen at the bottom of a reaction vessel, which is filled with molten sodium carbonate at a temperature of 1800°F. The molten bath produces a very high rate of heat transfer so that an equilibrium composition of the exhaust gases is attained in the compact reaction vessel. Thus, less than 10 mole percent of the gas is unwanted carbon dioxide. Furthermore, the sulfur and ash in the coal react with the melt and stay in the liquid phase. The result is high gasifier efficiency and a reduction in the size and complexity of the gasifier and the gas clean-up and process equipment. Additional gains in coal preparation and shipping result from the use of dry coal instead of a slurry. Finally, the total process has been optimized to operate at maximum power throughout the year by using process heat and standby power to compensate for lower output during times when the ocean's thermal gradient is lower. A schematic of the process is shown in Fig. 2.

The delivered cost of methanol to United States ports using this process is estimated to be 50 to 65 cents per gallon (1983 dollars), equivalent on a miles-per-gallon basis to a sales price of 88 cents to $1.14 per gallon for high octane gasoline. The price comparison is based on results of tests on methanol-powered cars in fleet operations in California by the Bank of America. Details of the cost evaluations are given in Table 1.

Final reports describing the engineering design studies, process details, and costs have been issued.[4-6] Those reports indicate that OTEC could become a major new energy source, potentially able to supply all United States fuel needs if fully developed.

CONCLUSION

In 1982, proved reserves of oil and equivalent natural gas liquids in the United States (including Alaska) were 33 billion barrels,[7] while the consumption of those fuels was 5.5 billion barrels.[8] Thus, if no new reserves were discovered and the nation were forced to depend entirely on its own resources, our proved oil supplies would be exhausted in six years (from 1982) at current rates of consumption. The situation would be alarming if imports and the ability to find new reserves had not sufficed to keep the reserves at an approximately constant level. Surprisingly, the record shows that the proved reserves have been maintained at approximately six times the annual fuel consumption since 1960, when disquieting questions about impending shortages of oil first began to be expressed. Thus, new oil sources have been discovered and proved as needed to sustain the ratio.

There is now a complacent public belief that oil consumption in the United States can be balanced indefinitely by new discoveries and modest oil imports.

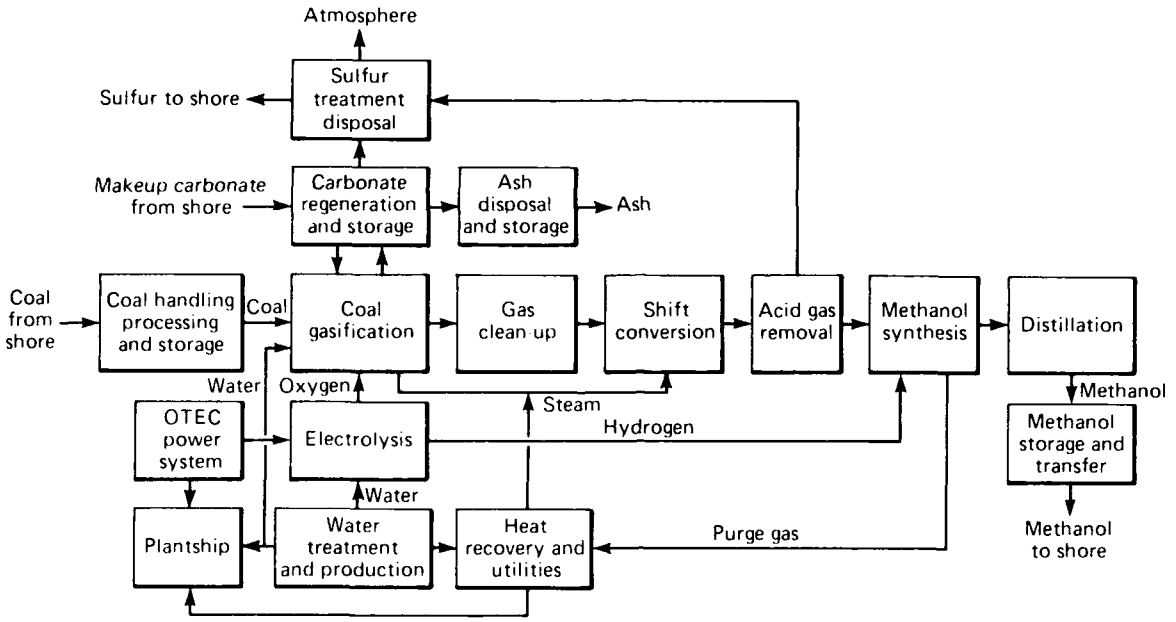

Figure 2—Schematic of the Rockwell gasification process.

Table 1—Estimated cost of OTEC methanol (1983 dollars).*

Plant investment (millions of dollars)		
Basic plantship	389	
Methanol plant	305	
Subtotal	694	
Interest during construction (14.8% of PI)	86	
Total 0% contingency	780	
Total 30% contingency	1014	
Annual cost (millions of dollars)	**0% contingency**	**30% contingency**
Real fixed cost	46.0	59.8
Operating cost		
Crew	8.8	11.4
Catalysts and materials	7.0	9.1
Coal, $50 per metric ton	23.3	30.3
Coal shipping, $11 per metric ton	5.2	6.8
Methanol shipping	6.6	8.6
General managers	0.3	0.4
Total annual cost	97.2	126.4
Annual production	2×10^8 gallons	
Methanol cost (dollars per gallon at U.S. port)	0.49	0.63
Methanol sales price (dollars per gallon at U.S. port)	0.66	0.86
Equivalent unleaded gasoline sales price (dollars per gallon)	0.88	1.14

*First commercial plantship, 160 MWe, 1750 metric tons per day.

However, the costs of finding and developing new domestic reserves have increased steadily and recently have begun to rise sharply. Between 1977 and 1982, the cost of adding a barrel of oil to the proved reserves rose from $5.86 to $12.95 (both in 1983 dollars), an increase of 120% in just five years. (The prices are derived from the data of Refs. 7 and 8 and are adjusted to 1983 dollars by means of the producer price index.) If this steep rise continues, the cost of discovering domestic oil will make further exploration uneconomic in the early 1990s, forcing increasing dependence on foreign sources unless alternative motor vehicle fuels can be developed. Since it takes a number of years to obtain substantial production, it is urgent that the development of the most attractive alternative fuel options, such as OTEC methanol, be given high priority now, in order that significant quantities of domestic fuel can be in production when they are needed.

REFERENCES

[1] J. F. George and D. Richards, *Baseline Designs of Moored and Grazing 40 MW OTEC Pilot Plants,* JHU/APL SR 80-1A (Jun 1980).

[2] W. H. Avery, D. Richards, W. G. Niemeyer, and J. D. Shoemaker, "OTEC Energy via Methanol Production," 18th Intersociety Energy Conversion Engineering Conf., Orlando, Fla. (Aug 21-26, 1983).

[3] D. Richards, W. H. Avery, and E. J. Francis, "OTEC Methanol-from-Coal Process Plantship Studies," 1984 ASME Winter Annual Meeting, New Orleans (Dec 9-14, 1984).

[4] *Coal to Methanol Study Using OTEC Technology,* Brown & Root Development, Inc., APL Contract 601700 (Jan 19, 1983).

[5] *Rockgas Facility for the Coal-to-Methanol OTEC Plantship,* Final Report, Rockwell International, APL Contract 601862-L (Aug 1983).

[6] *Coal-to-Methanol OTEC Plantship Study Using the Rockwell Molten Carbonate Coal Gasification System,* Final Report, Ebasco Services, Inc. (Mar 1984).

[7] Table 33 in *Annual Energy Review 1983,* Energy Information Administration, Washington, DOE/EIA-0384(83).

[8] Table 32 in *Annual Energy Review 1983,* Energy Information Administration, Washington, DOE/EIA-0384(83).

This work was supported by the U.S. Department of Energy.

COMPARISON OF HYBRID GEOTHERMAL-OTEC PLANT ALTERNATIVES

G. L. Dugger, L. L. Perini, and D. Richards

Estimated costs of three kinds of geothermally enhanced, ocean thermal energy conversion plants—binary, dual-binary, and flash-binary—have been compared for sites having moderate geothermal water temperatures. A binary plant using ammonia or isobutane as the working fluid yields the lowest estimated cost unless there is a strong need for fresh water (a by-product of a flash-binary plant), in which case a flash-binary plant may be best.

BACKGROUND

In 1981, the Department of Energy's Division of Ocean Energy Technology asked APL to investigate the extension of ocean thermal energy conversion (OTEC) technology to sites where modest geothermal resources are available. Hybrid geothermal-OTEC (GEOTEC) plants using seawater cooling at island or coastal sites could produce electricity from geothermal resources previously thought to be inadequate for power production. With assistance from the Naval Weapons Center (NWC), China Lake, Calif., and the Naval Civil Engineering Laboratory, Port Hueneme, Calif., we considered potential applications at Naval stations including Adak Island in the Aleutians chain and Lualualei on Oahu, Hawaii. A computer program for cycle analysis and cost estimation was developed.[1] Resource assessments by NWC indicated that Adak Island was, indeed, a promising site.[2] Our preliminary analysis indicated that a dual-binary plant was an attractive candidate for Adak.[3]

In August 1983, NWC let a subcontract to an industry team headed by TRW to do a conceptual design of a GEOTEC plant at Adak.[4] Meanwhile our attention was directed toward generic GEOTEC plants for sites with geofluid temperatures substantially lower than the 180°C estimated for Adak. An improvement was made in the computational procedure for binary plants, and binary plants now yield more attractive results than dual-binary plants. This article compares estimated costs for generic binary, dual-binary, and flash-binary plants.[5]

DISCUSSION

The GEOTEC Cycles

The binary cycle is analogous to the OTEC cycle, but with the warm seawater replaced by geofluid. A working fluid is evaporated by heat exchange with the geofluid; it drives a turbine-generator, is condensed by heat exchange with cold seawater, and then is pumped back into the evaporator to repeat the cycle. In the dual-binary cycle, two closed loops are interconnected by a heat exchanger that serves as the condenser for the higher temperature (isobutane) loop and handles the preheating and part of the vaporization load for the lower temperature (ammonia) loop (Fig. 1). In comparison to a binary cycle, this use of two working fluids, each chosen for its characteristics in a portion of the overall temperature difference between the geofluid and the seawater, leads to slightly greater efficiency with respect to the geofluid requirement for a given power output. However, the interloop heat exchanger adds substantially to the total heat exchanger surface area and cost.

In a flash-binary cycle (Fig. 2), part of the geofluid is flashed to drive a turbine-generator and then is condensed and used as potable water. The remainder of the geofluid is used in an amonia binary cycle and is then reinjected into the earth. If potable water has a high value at the site being considered, the higher the geofluid temperature, T_{GF}, the greater the percentage of the geofluid that should be flashed. However, as the geofluid temperature decreases, the total geofluid flow, $\dot{w}_{GF}$, needed to produce a given total net power output (10 MWe) increases. It turns out that the optimum performance and minimum cost correspond to potable water outputs near 600,000 gal/day, regardless of the T_{GF} in the 90° to 140°C range. Thus, the comparisons with the other cycles are made for the case of producing this water output level.

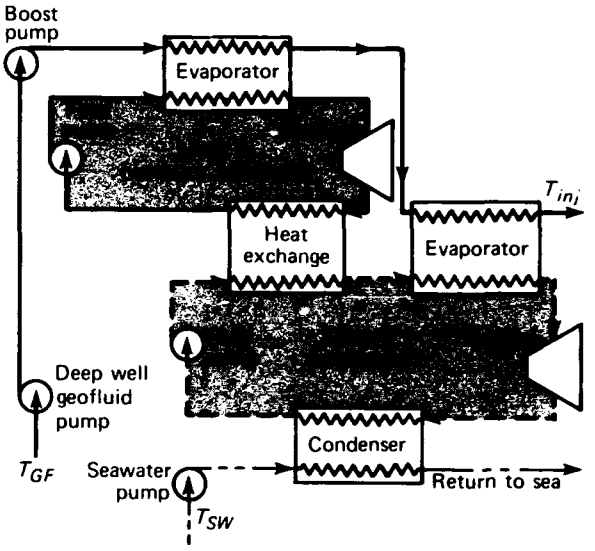

Figure 1—Simplified diagram of GEOTEC plant using a dual-binary cycle.

Major Inputs for the Analysis

The following assumptions were made for the geofluid and seawater systems. Each production well has a 100-m drawdown and a flow rate of 1000 gal/min. The

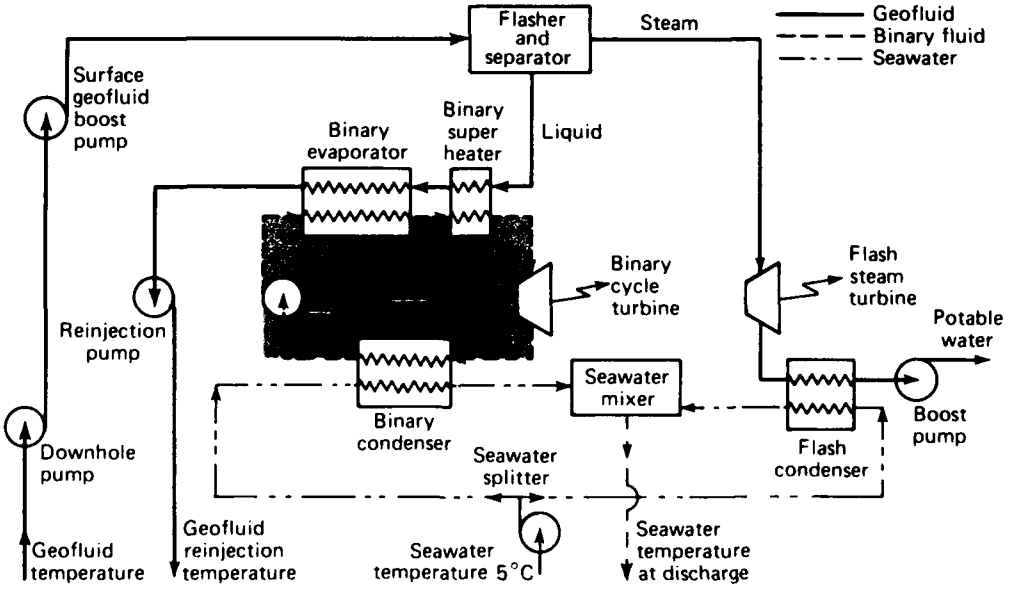

Figure 2—Simplified diagram of GEOTEC plant using a flash-binary cycle.

cost estimates are based on proportionate well costs; i.e., a 2400 gal/min flow requirement results in a cost for 2.4 wells. There is one reinjection well for every two production wells. The offshore bathymetry is assumed to be similar to that off Oahu (a potential GEOTEC site), where a depth of 820 m is required to obtain 5°C seawater at an offshore distance of 5620 m. The plant is located 1000 m inland from the shoreline, and the seawater is discharged 1000 m offshore. The diameter of the seawater pipe varies from 0.73 to 1.7 m as the T_{GF} varies from 180° to 90°C.

All heat exchangers are of the shell-and-tube type with the geofluid or the seawater inside the tubes. Pool-type evaporators are postulated. The evaporators include preheating sections; for a water or ammonia working fluid, a superheater is added between the evaporator and the turbine. The condensers use film-type condensation on horizontal tubes. In the interloop heat exchanger for the dual-binary cycle, the evaporation of the ammonia occurs inside the tubes and the condensation of the isobutane, outside. Details of assumptions on efficiencies and head losses are given elsewhere.[1,5]

Cost estimates are compared by first estimating the cost of the power cycle equipment, including the heat exchangers at $\$25/ft^2$, the turbine generator at \$300/kWe gross power, the geofluid pumps at \$0.15M per production well, and seawater and working-fluid pumps at $\$261X^{0.35}$ each, where X is the product of head (in pounds per square inch absolute) and flow rate (in gallons per minute). For the flash-binary system, a cost of $\$26{,}000\dot{w}_{GF}{}^{0.7}$ (where $\dot{w}_{GF}$ is the geofluid flow rate in pounds per second) is added for a noncondensables removal system. Related costs for piping, electrical subsystems and wiring, steel, instrumentation, insulation, and building are given by the sum of 24% of the equipment costs and $\$5/ft^2$ of heat exchanger surface area to bring in the size effect. A field installation cost equal to 35% of the equipment and related costs is added to give the total installed cost. We add 12% of the total installed cost for engineering and management fees and 18% of equipment and related costs for interest during construction.

We assume \$1M for each production and reinjection well. The well-field piping costs for the geofluid have been increased by 20% to provide for insulation. To the seawater piping costs we add \$200/ft of length for deployment of the offshore piping and \$6/ft for the onshore portion. These well and piping costs are added to the plant and equipment costs to arrive at the estimated total power plant cost.

Results of the Analysis

Figure 3 shows that the dual-binary isobutane/ammonia cycle requires slightly less geofluid flow than the binary cycle using ammonia, which in turn requires less than the flash-binary (ammonia) cycle to produce 10 MWe net. For the latter cycle, a flashed-steam-turbine exit pressure of 0.95 psia (T = 120°F) is assumed. A booster pump on the steam condenser outlet pressurizes the potable water.

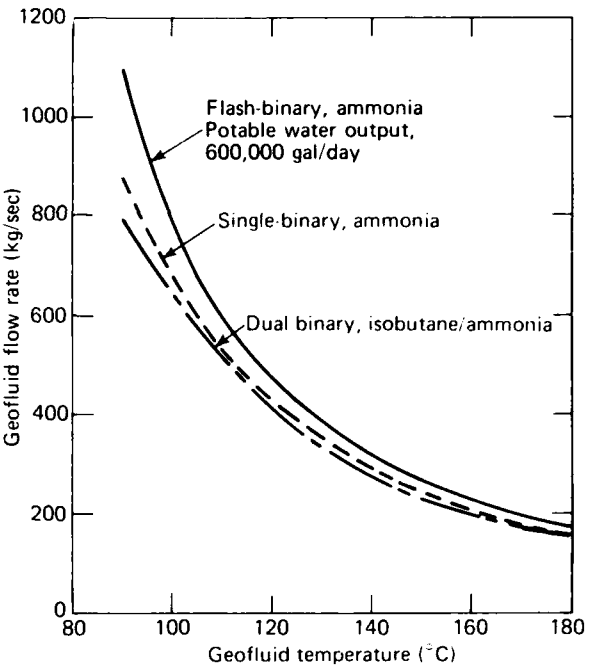

Figure 3—Comparison of geofluid flow rates for flash-binary, single-binary, and dual-binary cycles as a function of geofluid temperature, to produce 10 MWe (net).

Figure 4 shows that the estimated costs for the dual-binary plant are 8 to 20% higher than the best binary plant costs found for ammonia. (The results for isobutane, not shown, were almost as good as those for ammonia.) The estimated costs for the flash-binary plant range from 10 to 37% higher than those for the binary plant. However, for many islands or coastal sites the value of the 600,000 gal/day of potable water could make the flash-binary cycle the more attractive one.

To estimate the value of the fresh water needed in order to make the flash-binary plant break even with the binary plant, let us assume a 15% fixed charge plus an operation and maintenance cost based on a crew of 12 at \$0.05M/yr each and 2% of the capital cost for maintenance materials. For a geofluid temperature of 180°C, the ammonia binary plant would cost \$21M, yielding an annual cost of \$4.17M/yr and an electricity cost, with a 90% availability factor, of 53 mills/kWh. The flash-binary plant would cost \$24.5M, which converts to \$4.77M/yr or 60 mills/kWh. To make up the difference in annual costs, the 600,000 gal/day of water would have to be valued at \$2.70/1000 gal, a moderate price.

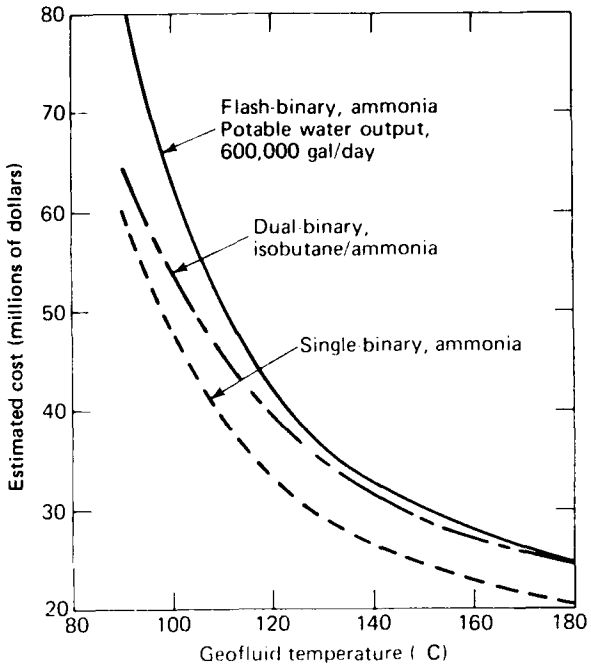

Figure 4—Comparison of estimated costs for flash-binary, single-binary, and dual-binary cycles as a function of geofluid temperature, to produce 10 MWe (net).

For a geofluid temperature of 90°C, however, the annual costs for the binary and flash-binary plants are $10.8M and $14.4M, respectively, and the water would have to be valued at $16/1000 gal to make up the difference, which would be too high because multistage flash desalination can be done for $10/1000 gal.[6] The electricity cost for the binary plant (excluding distribution cost and profit) would be 137 mills/kWh, which would be competitive at some islands.[6]

In conclusion, a GEOTEC performance/cost computer program developed at APL has been applied to estimate the costs of various cycles. An ammonia or isobutane binary plant will offer the lowest electricity cost, but flash-binary plants with fresh water production may be attractive where fresh water is needed and the geofluid temperature is above approximately 130°C. For remote sites such as Adak, costs may be nearly three times the estimated "generic" plant costs, which were based on equipment and drilling cost estimates for the lower 48 states.[3,4]

REFERENCES

[1] G. L. Dugger, L. L. Perini, and D. Richards, "Hybrid Geothermal-Ocean Thermal Energy Conversion (GEOTEC) Power Plant Analysis and Cost Estimates," 5th Miami Conf. on Alternative Energy Sources, Miami Beach (Dec 13-15, 1982).

[2] G. L. Dugger, L. L. Perini, and D. Richards (APL), J. A. Whelan (NWC), and P. J. Ritzcovan (DOE), "Geothermal-Enhanced OTEC (GEOTEC) Resources and Plant Performance Estimates," Oceans '82 MTS-IEEE Conf. and Exposition, Washington (Sep 20-22, 1982).

[3] G. L. Dugger, L. L. Perini, D. Richards, and F. C. Paddison, "The Potential for a Hybrid Geothermal-Ocean Thermal Energy Conversion (GEOTEC) Power Plant Installation at Adak Island, Alaska," in *18th Intersociety Energy Conversion Engineering Conference*, pp. 355-363 (Aug 16-21, 1983).

[4] *GEOTEC Engineering Concept Study*, TRW Energy Development Group, SN42646, Redondo Beach, Calif., prepared for Naval Facilities Engineering Command, Naval Weapons Center, China Lake, Calif. (Mar 1984).

[5] L. L. Perini, D. Richards, and G. L. Dugger, "Comparison of Hybrid Geothermal OTEC Plant Alternatives," ASME Winter Annual Meeting, New Orleans (Dec 9-14, 1984).

[6] M. H. Hall et al., "Thermo-Economic Analysis of Open Cycle OTEC Plants," ASME Winter Annual Meeting, New Orleans (Dec 9-14, 1984).

This work was supported by the Department of Energy, Division of Ocean Energy Technology.

SURVEILLANCE AND TRACKING

INTRODUCTION

APL's involvement in surveillance and tracking systems covers a wide spectrum of programs. The work is generally directed toward improving the present and future capabilities of Navy combatant radars used in antiair warfare. The radars maintain surveillance of the air space surrounding the ship and track engaged targets in support of the fire-control process. Functionally, surveillance includes detecting aircraft and missiles and tracking them to develop and display a complete and accurate picture of air activity. The fire-control tracking function differs from surveillance with respect to the requisite precision and accuracy of target position and rate measurements. Recently, expertise gained in developing combat system radars has been applied to infrared detection and track development and to upgrading Navy test range control radars.

In the mid 1960s, APL began the design of an advanced development radar to demonstrate principles of phased array radars, waveform design, signal processing, and microwave power generation. That radar, known as AMFAR, was demonstrated in 1968. The demonstrated principles formed the basis for the Aegis Weapon System, which is now at sea in an increasing number of Aegis-equipped fighting ships. The commissioning of USS *Ticonderoga* (CG-47) early in 1983 marked the beginning of a new era in Naval surface ship antiair warfare. As many as 24 CG-47 class cruisers and 50 DDG-51 class destroyers equipped with Aegis are planned for deployment in the Fleet by the end of this century.

Current efforts in surveillance and tracking include the operational evaluation of the Terrier New Threat Upgrade, which is aboard USS *Mahan*. Test and evaluation of the Phase II upgrade for the Mk 92 system is being conducted. Operational testing is in progress for the Aegis radar upgrade now entering production. An engineering basis for the next Aegis upgrade is being developed to ensure that a sound technical base will exist should technological factors and changes in the nature of the threat indicate the need for it.

This section reports on a portion of this work that is suitable for general distribution. The first article illustrates advanced work in an extremely important aspect of surveillance and tracking, the presentation of the data to the users. Color and other graphics capabilities are shown to aid materially the presentation of a substantial amount of information in a readily assimilable manner.

The next article shows that the beta distribution fits the statistics of radar cross section more accurately than do the Rayleigh and chi squared distributions in use since the classic work of Marcum and Swerling. In addition to improved accuracy, the amount of stored data required to characterize experimental radar cross section is greatly reduced.

The final article in this section describes a model for water vapor absorption over the 4 μm infrared window. A more accurate prediction of attenuation may now be made that, for the first time, includes the effects of temperature.

ADVANCED GRAPHICS FOR THE AEGIS DISPLAY SYSTEM

F. J. Willey and D. W. Nesbitt

A set of guidelines has been developed to provide a method and structure for designing displays that are presented to commanders in Combat Information Centers; command, control, communication, and information fusion centers; and other command and control theaters. The method, which develops displays from a primary system requirement, includes a computer program (a rule-based expert system) that assigns color (and other hardware attributes) to components of the picture (display elements). The resultant color display is very data intensive without being overwhelmingly complex.

BACKGROUND

The display system of current Aegis ships includes four large-screen, monochrome display sets that are used to present the tactical warfare picture to a commander and his staff. Future Aegis ships will have four large-screen color display sets, as well as color television monitors. Displays produced on that equipment are intended to aid a commander who may need to see large amounts of data so that he can determine the interrelationships among various elements of a tactical situation. The current monochrome system creates displays like the one shown in Fig. 1, which is cluttered and not easily usable but is representative of the type of tactical picture that may be needed by a commander.

The use of color and other graphics capabilities can provide an improvement in the ability to display larger amounts of data coherently.

DISCUSSION

Methodology

The developed method and system of applying color (and other display parameters) create a display as is illustrated in Fig. 2. The method used (Fig. 3) is one of soliciting system designers and human factors engineers to establish tables of values that reflect their design intentions and display needs. An embedded computer program called the Color Display Control System (CDCS) provides an automated way to assign color and other parameters to the display's graphic elements.

Systems engineers assign various display attributes or features to each display element or separate piece or kind of display data. Human factors engineers determine how to achieve the various display features by using color and other hardware capabilities. The assignment tables are used to drive the CDCS, which assigns basic colors to displayed elements, selects bit-plane addresses, and reassigns color to overlying or intersecting regions based on sets of rules (see Fig. 4) that depend on the ap-

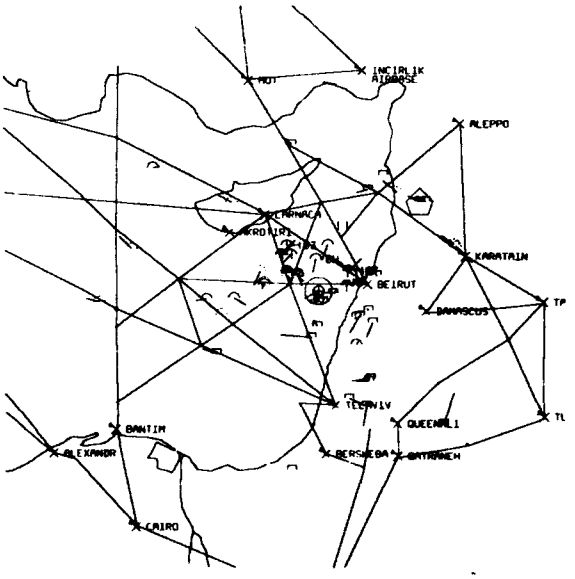

Figure 1—A monochrome tactical picture.

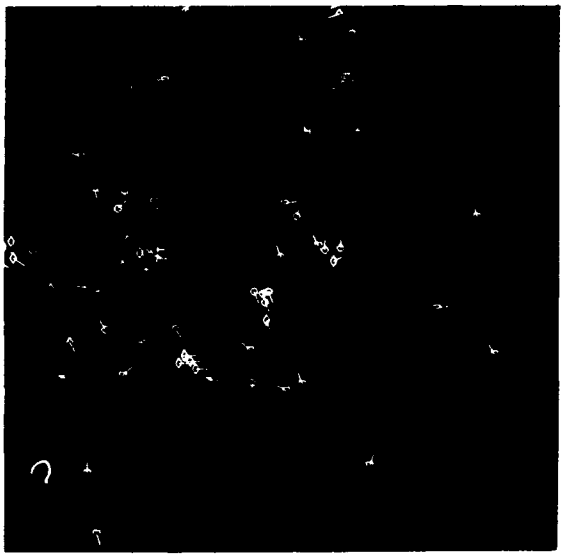

Figure 2—The same area with color applied, based upon the method.

plication. Different display applications require different sets of rules to produce the desired results. The CDCS is structured like a rule-based expert system, allowing the system to perform its task under many different sets of rules. Thus, it can accommodate a large variety of display applications simply by developing a new set of rules as specified by the method.

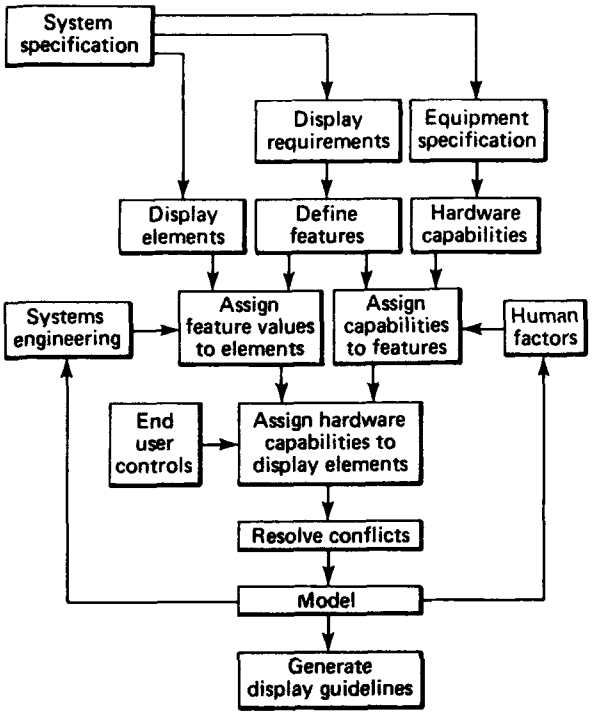

Figure 3—Display design method.

Each display element (the separate user-selectable pieces of data that make up a display such as land areas or commercial airways) has been assigned various levels of certain display features based on the system requirement. In the Aegis display system, the display features include area emphasis, recognizability, differentiability, and edge treatment. Other display applications may require display features from which a feature-element table could be derived and used as an input to the CDCS.

The other input to the CDCS—the assignment of hardware capabilities to display features—is based on the hardware's capability. This set of assignments is used by the CDCS to assign color (hue, brightness, and saturation) and other hardware capabilities to the various display elements based on the feature value assignments. The rules choose a color. Depending on the application, the color system will contain a number of brightness levels, saturation levels, and hue divisions. For example, the palette used in Fig. 2 consisted of white, three brightness levels, and two saturation levels (off-whites) for each of seven other hues. The two saturation levels provide "transparency" to overlying filled areas. If the saturation level of a colored area is shifted to another value, the area retains its sense of emphasis while allowing an-

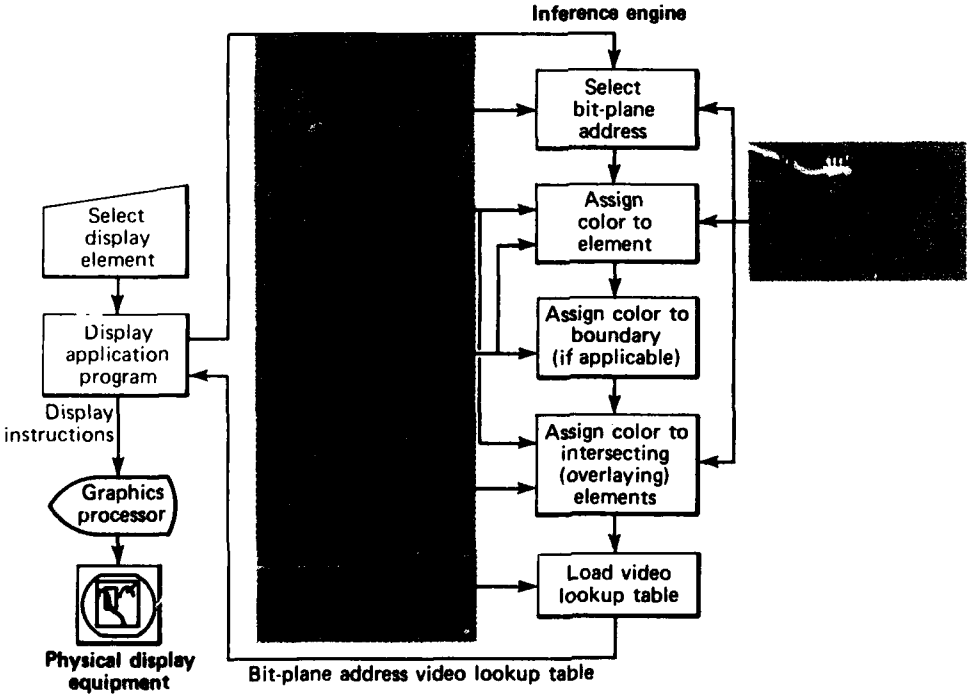

Figure 4—Functional diagram of the color display control system.

other area to appear within (or beneath) it. The system maintains minimum levels of color contrast between all colors.

RESULTS

The displays developed using this method and the CDCS have changed the way we view the use of color in tactical displays. They use color for clarity without being color coded, are fault tolerant because they are not color coded, and are more data intensive, with lower levels of display clutter.

The method and the CDCS that has been designed provide an effective way to combine the needs of users with the requirements of the system and the capabilities of the equipment. Because of its structure, the method, and the embedded computer program, the CDCS can be used to produce a variety of rule bases and to support a number of different display applications.

This method was first used to develop a series of color displays in the APL Combat Systems Evalution Laboratory. The displays were instrumental in leading the Navy to pursue the installation of advanced color graphics capability in Aegis ships. The guidelines have gained wide acceptance by the Naval Surface Weapons Center and other Navy laboratories and contractors participating in the Aegis Program.

This work was supported by NAVSEASYSCOM, PMS-400.

VERIFICATION OF A TECHNIQUE TO EXTEND THE STATISTICAL DESCRIPTION OF RCS SCINTILLATION

J. W. Follin, Jr., F. C. Paddison, and A. L. Maffett

A complex radar target at selected aspects will present enough scatterers that the radar cross section (RCS) scintillation will be Rayleigh distributed. However, a more flexible distribution is required for other aspects where the cross section is dominated by a very few scatterers. APL has developed a theoretical description of lobe widths and scintillations and has correlated them with measured RCS data. The results for the Boeing 727-100C and a drone aircraft show that for half of the target aspects, the RCS scintillations cannot be described by the "classical" Rayleigh and chi-square distributions; rather, the more flexible beta distribution is required. These results apply for bistatic as well as monostatic geometries.

BACKGROUND

Radar targets are usually large compared to the RF wavelength; as a result, the RCS shows a complex constructive and destructive interference pattern. The RCS typically can change by orders of magnitude for very small changes in radar frequency or aspect angle or for slight flexure of parts of the aircraft. Changes in the target's RCS are called scintillations. Early in the development of radar, Marcum and Swerling[1] proposed a methodology to quantify the detection probability of a radar for a given target cross section in the presence of receiver noise. Swerling postulated that the scintillation of a complex target composed of many scatterers could be represented by the Rayleigh or the chi-square distribution. The type of distribution is important because the performance of the radar or the survivability of the target often depends on the tails of the actual distribution. Surprisingly, there have been few attempts, until this effort, to verify how well the Rayleigh (chi-square) distribution fit real data. The problem is aggravated by the complexity of scintillation data (illustrated in Fig. 1) that usually results

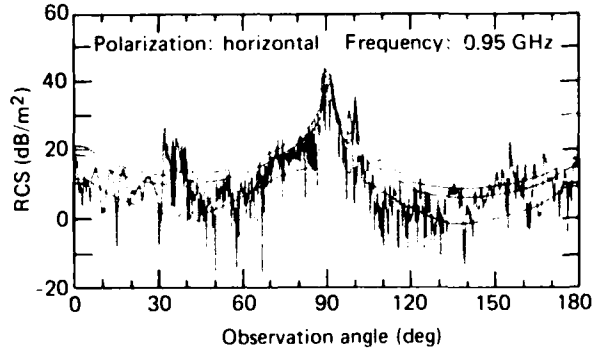

Figure 1—Measured RCS of the Boeing 727-100C with superposed theoretical curves.

in a smoothing of the cross-sectional data to eliminate the scintillation, rather than a processing of the data to determine the appropriate statistical description for future use by the system analyst.

The program discussed here started with measurements of the RCS of several classified targets, and an attempt was made to find the best statistical description of their scintillations. Although at some aspects one or another of the common probability distributions fits the scintillation data, at other aspects no fit was found.

Part of the task was to calculate the RCS to validate the measurements (and the theory) and to permit prediction of the RCS at all aspects in order to avoid expensive measurements. A computer program was developed to calculate the RCS and the scintillation statistics. We also have enlarged upon earlier work on lobe widths and glint and have added them to the computer program for bistatic and monostatic geometries.

DISCUSSION

For a finite target, there is a maximum RCS, and if one component dominates near some aspect, there is a minimum RCS near that aspect. We have shown that for a target of three spheres fixed on a nonreflecting frame, there are three RCS values for which there is a logarithmic singularity in the probability density function. However, the integrals under the singularities are small, and an adequate representation can be obtained by fitting the mean, variance, and third and fourth moments. To do this, we work with dimensionless statistical variables such as width (w = variance/mean^2) and modified skewness (g = third moment/(mean × variance)).

Figure 2 is a plot of the w, g plane showing the Rayleigh point ($w = 1$, $g = 2$) and the locus of the chi-square distribution ($g = 2w$). The locus of the log-normal distribution is the parabola, $g = w(w + 3)$. The beta distribution covers the shaded part of the physical region, while the plotted points show the statistical parameters for the RCS of long cylinders.

Our attempt to validate the beta distribution by means of unclassified data brought into sharp focus the problem of the RCS data archivist. Although RCS ranges have been in operation for at least 25 years, little classified and almost no unclassified data are retained to provide a measure of scintillation. The RATSCAT range, for example, makes analog plots of raw data; it retains magnetic tapes for three years and then erases the data.

Thomas Dalby of the Boeing Co. measured a 1:100 scale model of their 727-100C commercial aircraft, and Floyd D. Amburgey of RATSCAT supplied a magnetic tape of the drone. The Boeing 727 at 0.95 GHz can be

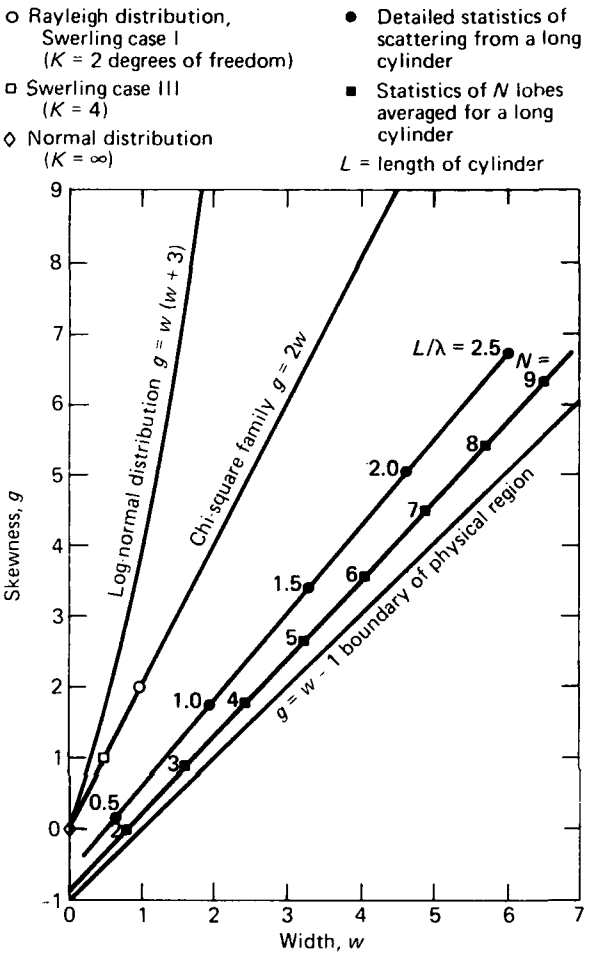

Figure 2—Selected statistical descriptions used to describe RCS scintillations on skewness width plane.

represented by 50 independent scatterers. Considering the restricted viewing aspect (a 10° aspect window is used in this discussion), only a few of the scatterers are in view at a time as the aspect angle changes from nose to tail. At aspects where a large number of scatterers of comparable size may be presented, the distribution is Rayleigh. As the number of scatterers in view is reduced, Rayleigh is no longer a good representation, particularly where a single scatterer tends to dominate the RCS.

The means and variances of the RCS have been calculated; the mean and the mean plus or minus the standard deviation are plotted in the overlay of Fig. 1 to illustrate the accuracy of the theoretical approach. That approach assumes random relative phases in a two-dimensional average about a given aspect, while the relative phases are somewhat restricted in a single traverse.

The data (measured for every 0.1°) were processed in 10° windows for the mean, variance, and third and fourth moments, and fits were made to the beta distri-

bution. The fit to the 727-100C at 90° aspect is shown in Fig. 3 with superposed Rayleigh, chi-square, and log-normal curves. The 90° point is at $w = 2.5$, $g = 2.0$ in Fig. 2. It clearly does not fit the Rayleigh or chi-square distribution because of the strong singularity at small RCS and the small skewness. About half of the aspects of the 727-100C and the drone require the greater flexibility of the beta distribution for an adequate fit.

SIGNIFICANCE

This work solves the problem of the data archivist for cases where storing scintillation data is important. With radar frequencies being extended higher and higher, it is an important parameter. The beta parameters represent a convenient and simple way to store accurate data on the calculated or measured scintillation in each data window—a compression of data by many orders of magnitude.

Calculations on the probability of detection using a calculated or experimentally determined beta fit should be more accurate when in the tails of the distribution, the location where detection is usually desired.[3]

The statistical moments can be calculated directly from an ensemble of scatterers. The ability to calculate a scintillation spectrum is significant because one does not have to build a physical model to measure the RCS and its fine structure. This development makes the calculation process much simpler. One previously had to calculate the constructive and destructive interference pattern, assuming relative phases, and then process the calculated data to develop statistics.

The theoretical calculations have also been shown to agree with lobe widths for a change of aspect or a change in bistatic angle.[4] Finally, theoretical results for glint (apparent target centroid motion) are available that agree with measured data.

The ability to develop an accurate statistical description of the calculated or measured static RCS should aid considerably in the comparison with dynamic data, where geometries cannot be established accurately and

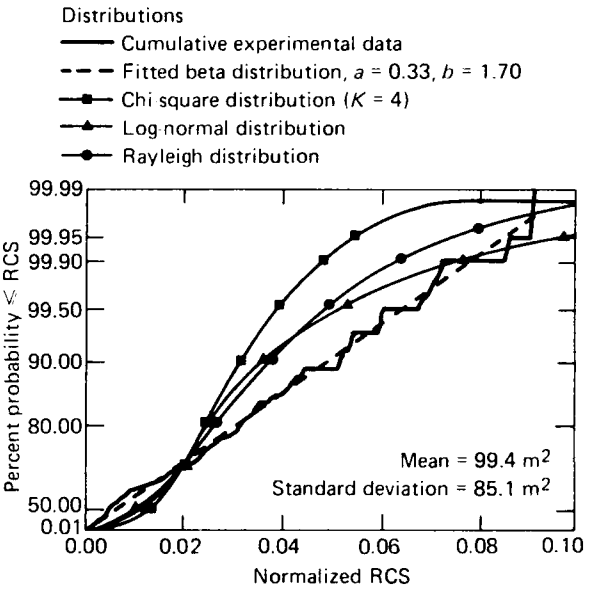

Figure 3—RCS of Boeing 727-100C in the wing plane; 0.95 GHz; horizontal polarization; data window 85° to 95°.

yet a statistical measure of RCS is possible. This has been a problem for many years but now can be solved easily. This work is reported more fully in Refs. 4 and 5.

REFERENCES

[1] J. I. Marcum and P. Swerling, "Studies of Detection by Pulse Radar," *IRE Trans. Inf. Theory* **IT-6**, 145-267 (1960).

[2] J. W. Follin, *Statistical Properties of RCS*, JHU/APL QM-81-115 (1981).

[3] R. L. Kulp, "Detection Probabilities for Beta Distributed Scatter Cross Sections," *Electromag. J.* (Dec 1984).

[4] J. W. Follin, Jr., F. C. Paddison, and A. L. Maffett, "Statistics of RCS Scintillations," *Electromag. J.* (Dec 1984).

[5] F. C. Paddison, A. L. Maffett, J. W. Follin, Jr., and N. W. Klimack, *The APL-RCS/Statistics Code Description, Illustrations of Output and Users Guide*, JHU/APL TG 1345 (1984).

This work was supported by the Rome Air Development Center and Independent R&D.

INFRARED ABSORPTION BY WATER VAPOR IN THE TROPOSPHERE

M. E. Thomas

A complete representation of infrared absorption by water vapor as a function of frequency, water vapor partial pressure, and temperature is accomplished by a total line shape model.

BACKGROUND

Infrared propagation in the atmosphere is influenced by scattering, turbulence, and absorption. The most important contributor to infrared absorption in the troposphere is water vapor. This is particularly true for the infrared window regions.

The propagation characteristics of infrared energy in the atmosphere are important criteria for the design of effective infrared seekers on missiles, forward looking infrared systems, laser radar, and other military instrumentation. In addition to military applications, such knowledge is important to infrared astronomy and remote sensing of the atmosphere.

A previously developed total line shape model for nitrogen broadened water vapor[1-3] has been improved. It now predicts the observed temperature dependence of the absorption coefficient, k, defined as

$$k = -\frac{1}{l} \ln T \quad , \tag{1}$$

where T is the transmission and l the path length. The model now agrees with the temperature, pressure, magnitude, and frequency dependence of experimental data. The model is based on the impact approximation or interruption broadening for near-line-center phenomena and the quasi-static or statistical broadening for the far wing. The formalism considers only binary collisions and satisfies detailed balance in the infrared region. The line shape is called "total" because the near-line-center profile is empirically connected to the far-wing profile, forming a complete line shape. The far-wing profile also contains empirical parameters chosen by near-band far-wing experimental data.[3] The result is a semiempirical line shape featuring the basic physics of the temperature, partial pressure, and frequency dependence over the entire profile.

DISCUSSION

The far wings of a line shape are influenced by the intermolecular potentials of strong collisions. Therefore, an accurate model of such potentials is critical for a meaningful model of far wings. The temperature dependence of strong water-vapor/water-vapor interactions is now specified by experimentally determined second virial coefficients of steam. This manifests itself in the line shape parameter[3]

$$\lambda_{a6} = \lambda\,(T = 296)\; 10^{2.1115[(296/T)-1]} \quad ,$$

where T is the temperature in Kelvin units. The factor λ_{a6} comes from the phase shift contributions of the statistical (quasi-static) line shape. It does not represent contributions from level shift effects. They have been accounted for approximately by a first-order perturbation theory solution of the statistical line shape by Fomin and Tvorogov.[4] However, the perturbation approach is not valid for the rotational band because the collisional perturbation energy is much greater than the internal molecular energy. Therefore, the temperature dependence of the Fomin-Tvorogov factor for the rotational band was changed to agree with experimental data.

RESULTS

The major results of the improved temperature modeling are:

1. Good agreement with experimentally observed temperature dependence at all infrared frequencies,
2. Improved prediction of the room temperature 4-μm continuum based on an extrapolation of the data of Burch et al.[5] and White et al.[6] for high temperature and high-water-vapor partial pressure.

Figure 1 (a compilation of data from Refs. 5 and 7 through 9) illustrates the ability of the total line shape model to predict the observed temperature dependence of k at 944.195 cm^{-1}. The total line shape model agrees with the dimer model approach at this frequency. Fur-

thermore, the model agrees with the near rotational band (300 to 600 cm^{-1}), where far wings are known to exist and dimer models are not considered important.

The 4-μm-window room-temperature continuum is difficult to characterize experimentally because the absorption is weak, contaminants are a problem, and mirror reflectivity can change as a function of the water-vapor partial pressure in White-type cells. For these reasons, the 4-μm-window data sets are not as credible as the 10-μm-window data sets. Figure 2 shows one of the high-temperature data sets of Burch et al.[5] These data were used to extrapolate to the k prediction at T = 296 K. Overall, the Burch extrapolation is considered the most believable in light of the previously mentioned problems. The total line shape model agrees with the high-temperature data but is lower than the room-temperature Burch extrapolation because Burch assumed that the self-broadening coefficient did not change from the observed high-temperature data to room temperature. The model has a temperature dependence in the self-broadening coefficient. This proved to be important in the 12- to 8-μm region and certainly belongs in the 4-μm region as well. Thus, the model predicts a new level of the 4-μm continuum absorption under that of Burch.

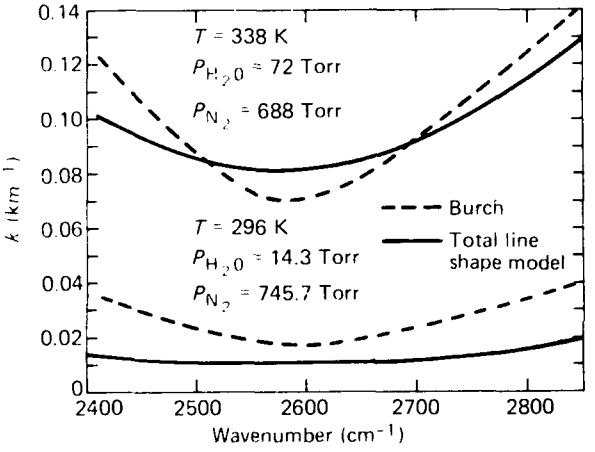

Figure 1—The absorption coefficient, k, versus temperature at 944.195 cm^{-1}.

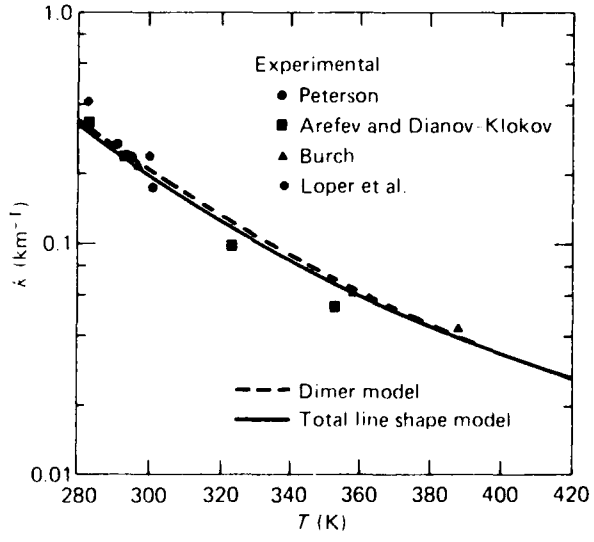

Figure 2—The absorption coefficient, k, versus wavenumber and temperature in the 4-μm window.

CONCLUSIONS

The total line shape model is a semiempirical approach toward representing the observed water-vapor absorption in the troposphere. The line shape formulas are theoretically founded, but the far-wing formulas contain parameters that must be chosen empirically. There are three parameters per gas type for the rotational band and two parameters per gas type per band otherwise.

The result is a reasonably accurate representation of experimental data at any frequency, pressure, and temperature in the infrared region. Because of its theoretical basis, the model can accurately interpolate and extrapolate between and beyond experimental data points, whereas a strictly empirical model cannot. These results make a case for the far-wing representation of the water vapor continuum, rather than the strictly empirical models used heretofore.

ACKNOWLEDGMENTS

The author gratefully acknowledges the support and guidance of W. J. Tropf and the assistance of J. P. Skura in preparing the code.

REFERENCES

[1] M. E. Thomas, *Tropospheric Water Vapor Absorption in the Infrared Window Regions*, Ph.D. Dissertation, The Ohio State University (Aug 1979).

[2] R. J. Nordstrom and M. E. Thomas, "The Water Vapor Continuum as Wings of Strong Absorption Lines," in *Atmospheric Water Vapor*, A. Deepak, T. D. Wilkerson, and L. H. Ruhnke, eds., Academic Press, New York (1980).

[3] M. E. Thomas and R. J. Nordstrom, "The N_2-Broadened Water Vapor Absorption Line Shape and Infrared Continuum Absorption—Part I, Theoretical Development, and Part II, Implementation of the Line Shape," *J. Quant. Spectrosc. Radiat. Transfer* **28**, 81-101 and 103-112 (1982).

[4] V. V. Fomin and S. D. Tvorogov, "Formation of the Far Wings Contour of Spectral Lines Broadened by a Foreign Gas; Analysis of Exponential Decrease of Continuous Absorption beyond the Band Head of the 4.3-μ Band of CO_2," *Appl. Opt.* **12**, 584-589 (1973).

[5] D. E. Burch, D. A. Gryvnak, and J. D. Pembrook, *Investigation of the Absorption of Infrared Radiation by Atmospheric Gases: Water, Nitrogen, Nitrous Oxide,* AFCRL-71-0124 (1971).

[6] K. O. White, W. R. Watkins, C. W. Bruce, R. E. Meredith, and F. G. Smith, "Water Vapor Continuum Absorption in the 3.5-4.0 μm Region," *Appl. Opt.* **17**, 2711-2720 (1978).

[7] J. C. Peterson, *A Study of Water Vapor Absorption at CO_2 Laser Frequencies Using a Differential Spectrophone and White Cell,* Ph.D Dissertation, The Ohio State University (Jun 1978).

[8] V. N. Aref'ev and V. I. Dianov-Klokov, "Attentuation of 10.6 μm Radiation by Water Vapor and the Role of $(H_2O)_2$ Dimers," *Opt. Spectrosc.* **42**, 488 (1977).

[9] G. L. Loper, M. A. O'Neill, and J. A. Gelbwachs, "Water-Vapor Continuum CO_2 Laser Absorption Spectra between 27° and -10°C," *Appl. Opt.* **23**, 3701 (1983).

This work was supported by NAVSEASYSCOM, SEA-62R1.

COMMAND, CONTROL, AND COMMUNICATIONS

INTRODUCTION

Command, Control, and Communications (C^3) are required to support the several military commanders in the integrated use of available service forces in deterring war or in prosecuting warfare to achieve national objectives. C^3 supports that mission by assembling and formatting the information needed to make and render decisions as required, to develop and promulgate orders to implement the decisions, and to monitor the course of events resulting from the promulgated orders.

APL became involved in the C^3 program in 1971 when the Chief of Naval Operations requested an evaluation of the performance of TACAMO, the airborne strategic communication link to Fleet Ballistic Missile submarines. That successful test program led to an ever-increasing participation in test and evaluation, methodology development, equipment design, and the development of computer software in strategic naval communication. In 1976, additional facets of C^3 were added to APL's task, including evaluation of Fleet Command Centers, study of requirements for Tactical Flag Command Centers afloat, and testing of C^3 support for the Army's Pershing missile system.

In 1977, the Naval Electronic Systems Command requested APL's assistance in the systems engineering of a tactical C^3 system for the U.S. Navy in the year 2000. The objective of the program is to provide NAVELEX with engineering design guidance and transition planning for the development of that future system. In 1978, another increase in effort occurred with the addition of tasks in the fields of electronic warfare, surveillance, and over-the-horizon detection, classification, and targeting. The latter are closely related to APL work in Tomahawk and Harpoon, the cruise missile programs. A year later, a strategic connectivity study defined the qualitative improvements that are required for the communications support of sea-based strategic forces of the future.

Additional areas of APL involvement have been to assist several agencies outside of the Navy in resolving C^3 problems. The following articles describe the Laboratory's support provided to the Naval Regional Medical Center in Portsmouth, Va., the United States Information Agency, and the Army.

One article describes the battlefield automated systems interfaces that APL identified for Army organizations at echelons above corps.

The second article describes the installation of a broadband coaxial-cable local area network at the Naval Regional Medical Center in Portsmouth for communication between clinical data processing systems and their associated remote terminals.

The third article addresses the development and installation of a communications-oriented computer at the United States Information Agency headquarters in Washington, D.C.

AUTOMATION OF COMMAND AND CONTROL IN THE THEATER ARMY

J. K. Beam and J. M. DuBrul

Battlefield automated system interfaces have been identified by APL for U.S. Army organizations at echelons above corps. The interfaces were based on an examination of five Army theaters and were categorized by functional areas of the command, control, and communications architecture for automated systems that was developed for corps level and below. The examination led to the identification of automated system interfaces for a generic Theater Army as defined in evolving Army doctrinal publications.

BACKGROUND

Within the past decade, advances in computer technology and the need to handle large quantities of data associated with battlefield operations in a timely manner have led the Army to develop automated systems to support battlefield operations. These systems have been fielded largely as an independent development to support the accomplishment of a particular function, with little consideration given to interoperability requirements among the battlefield systems. In 1978, recognizing the need for an automation architecture that would provide a synergistic effect for command and control, the Army commenced an effort that resulted in a Command, Control, and Subordinate Systems (CCS2) architecture for automated systems at corps level and below. The architecture, shown graphically in Fig. 1, envisioned the interconnection of battlefield automated systems in five functional areas directly related to battle management: fire support, maneuver control, air defense artillery, intelligence/electronic warfare, and combat service support.

The Combined Arms Combat Development Activity, Fort Leavenworth, Kans., requested that the Laboratory extend the CCS2 architecture to echelons above corps (EAC), the Army Theater Command level. Such an extension was considered necessary in view of the increasing reliance on automated systems to perform critical battlefield functions at EAC (particularly in the areas of intelligence/electronic warfare and combat service support) and the concommitant requirement for these systems at EAC to interface with battlefield systems at corps level and below. APL had previously examined command and control within the U.S. Navy. [1]

DISCUSSION

Technical Approach

Our approach to the application of the CCS2 architecture to EAC involved the identification of automated systems from source documents and surveys of selected Army theaters. This led to a set of system definitions of the automated interfaces in each theater. Using Army plans for each theater, we based the theater system configuration on planned wartime requirements and Army doctrinal statements. We selected the theaters by examining a full range of potential Army operations, from those heavily involved with allies (U.S. Army, Europe) to those that involved no allies (U.S. Third Army).* Such considerations were necessary because Army EAC organizations are tailored to the requirements of the theater they support.

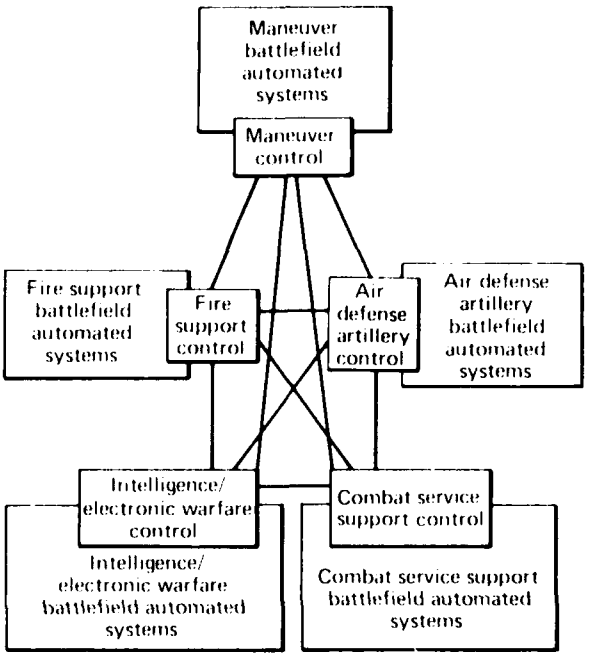

Figure 1—The CCS2 architecture.

Having identified the range of operations, we developed the automation interfaces for a generic mature theater organization. A generic theater army organization represents many major commands, each responsible for activities in its own functional area. Most of these commands (e.g., air defense artillery, personnel, and transportation) are supported by their own individual automated systems, and the commands themselves may be widely separated within a theater of operations (e.g., Eu-

*The U.S. Third Army supports the Commander-in-Chief Central Command; it has replaced the Rapid Deployment Joint Task Force.

rope or the Pacific), which places a demand on communications to establish the identified interfaces.

Automation Requirements Definition

We examined automated systems for each of the five functional areas of the CCS2 architecture. Because the combat service support functional area contained most of the automated systems, that area was divided into three categories—logistics, medical, and personnel—and logistics was subdivided into ammunition, maintenance, supply, and transportation. For example, automated ammunition systems are used to maintain centralized theater management of all conventional ammunition assets. The theater commander acts as theater coordinator for the wholesale suppliers of ammunition. The Standard Army Ammunition System (SAAS) is an automated system that deals with all tactical levels of ammunition management. It consists of both automated and manual subsystems, provides for the integrated supply and maintenance of conventional ammunition, and has the following components:

1. SAAS-1: Theater inventory control at the Theater Army Materiel Management Center;
2. SAAS-3: Stock control activity at the Theater Army Area Command and the Corps Support Command levels;
3. SAAS-4: Storage activity within the theater and corps, at the theater storage area, corps storage area, or ammunition supply points.

The interaction of the SAAS system within a theater is shown in Fig. 2. Since there may be several Theater Army Area Commands within a given theater, there are likely to be several SAAS-3 systems providing data to the SAAS-1 system at the Theater Army Materiel Management Center. Figure 2 shows that the SAAS system must also interface with an automated system in the Transportation Command in order to be able to control the movement of ammunition within the theater or to divert that movement should the tactical situation so dictate.

A diagram similar to Fig. 2, depicting automated system interfaces, was prepared for each functional category examined in each theater. About 50 existing or planned systems that had battlefield application under wartime conditions through the year 1990 were considered. Future systems and system replacements are indicated on those diagrams. For example, Fig. 2 shows that the SAAS-1 system is to be replaced by an improved SAAS-3 system in 1987 at the Theater Army Materiel Management Command and that the SAAS-4 system is to be installed in 1985. If planned systems were not fully supported in procurement plans, they were shown as dashed ovals to indicate that they are planned but not programmed. We expressed automation interface data

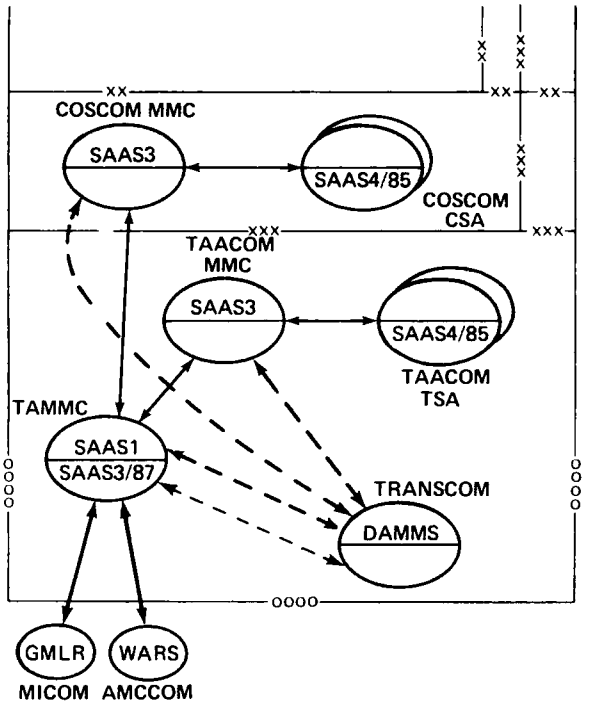

Legend

←——→	= Automated information flow
←– –→	= Required interface, not programmed
—x x—	Division boundary
—xxx—	Corps boundary
—oooo—	Echelons above corps boundary
AMCCOM	Armament, Munitions, and Chemical Command
COSCOM	Corps Support Command
CSA	Corps storage area
DAMMS	Department of the Army Movement Management System
GMLR	Guided missile large rocket
MICOM	Missile Command
MMC	Materiel Management Center
SAAS	Standard Army Ammunition System
TAACOM	Theater Army Area Command
TAMMC	Theater Army Materiel Management Center
TRANSCOM	Transportation Command
TSA	Theater storage area
WARS	Worldwide Ammunition Reports System

Figure 2—Interaction of the SAAS system within a theater.

transfer in terms of the JCS Publication 12 information categories,[2] the direction of information flow, and the content of the information to be exchanged. For each year between 1983 and 1990, we prepared an interface diagram showing the effect of introducing automated systems into each theater by functional area. This examination provided a basis for the Army to identify automation interfaces at EAC.

FINDINGS AND CONCLUSIONS

We reached the following findings:

1. No automated system interoperability requirements were applicable to the fire support functional area at EAC.
2. At the theater level, maneuver control is more appropriately designated "operations control." Although several theaters are developing automated operations control systems, there is no Army-wide automated system planned for application to EAC.
3. Air defense artillery was found to have no automation at EAC headquarters level but was automated at the brigade and battalion level.
4. There are automated systems to support the functions of the major subordinate commands at EAC; little automation was found to tie together the functions among the major subordinate commands.
5. Each EAC examined contained only a subset of the generic organization; the degree of similarity was associated with the size of the Army component.

In conclusion, we found the CCS2 architecture to be generally applicable to EAC; however, not all functions addressed by the CCS2 architecture are supported by automated systems at EAC.

The Army Battlefield Interface Concept-Echelons Above Corps study provides the first complete analysis of a totally integrated automation architecture for the Theater Army. Its findings will provide the basis for the Army's requirements documents to ensure total system interoperability.

ACKNOWLEDGMENT

The authors gratefully acknowledge the assistance of Dennis Mahoney and Jerry Moore of the U.S. Army Combined Arms Combat Development Activity in all phases of this study. The guidance and assistance by the U.S. Army Study Advisory Group also proved to be invaluable.

REFERENCES

[1] G. D. Halushynsky and J. K. Beam, "A Concept for Navy Command and Control in the Year 2000," *Johns Hopkins APL Tech. Dig.* **5**, 9-18 (1984).

[2] *Tactical Command and Control Planning Guidance and Procedures for Joint Operations*, JCS Publication 12 (Apr 1974).

This work was supported by the U.S. Army Combined Arms Combat Development Activity.

BROADBAND COAXIAL-CABLE TELECOMMUNICATION SYSTEM

G. H. Laird

The installation of a broadband coaxial-cable local area network for communication between clinical data processing systems and their associated remote terminals was completed at the Naval Regional Medical Center in Portsmouth, Va. The system, which has been operational for nearly a year, provides a communications capability that can be adapted to the diverse needs of a health care facility.

BACKGROUND

The Department of Defense is procuring automated data processing systems to support various hospital activities within the Naval Regional Medical Centers (NRMCs). Each automated data processing system must have a communications capability to support interactions between central processing units and their associated remote terminals.

In recent years, broadband technology has been developed and applied to the growing demands for high-capacity, multichannel communications networks. A state-of-the-art broadband telecommunication system has been installed at the Portsmouth NRMC. In addition to meeting the local needs, it permits the evaluation of broadband technology in an operational hospital enviro-

ment to determine if this type of technology should be adopted for all Navy health care facilities.

APL acted as the technical agent of the Naval Medical Data Services Center in all phases of system specification, installation, and testing of the initial system installed in a Navy health care facility. The task included preparing the telecommunication system performance and interface requirements and approving the technical specification based on those requirements, preparing a Request for Proposal, evaluating competitive bidding responses to it, and recommending award of the installation contract for the telecommunication system. APL also monitored the installation and testing of the components of the communication system to ensure that it was installed as designed, and specified and conducted the final tests to certify that the entire system met design specifications and was ready for use.

DISCUSSION

The Portsmouth NRMC system provides bidirectional communications capability to handle audio, data, and television services on a broadband coaxial-cable system. The system interconnects four buildings on the Portsmouth campus. Figure 1 shows the campus layout, the underground coaxial-cable routing, and the four buildings connected by the system. The system carries electronic signals between computers located in the building 250 computer room and associated devices located in the three health care facility buildings: 1, 123, and 215.

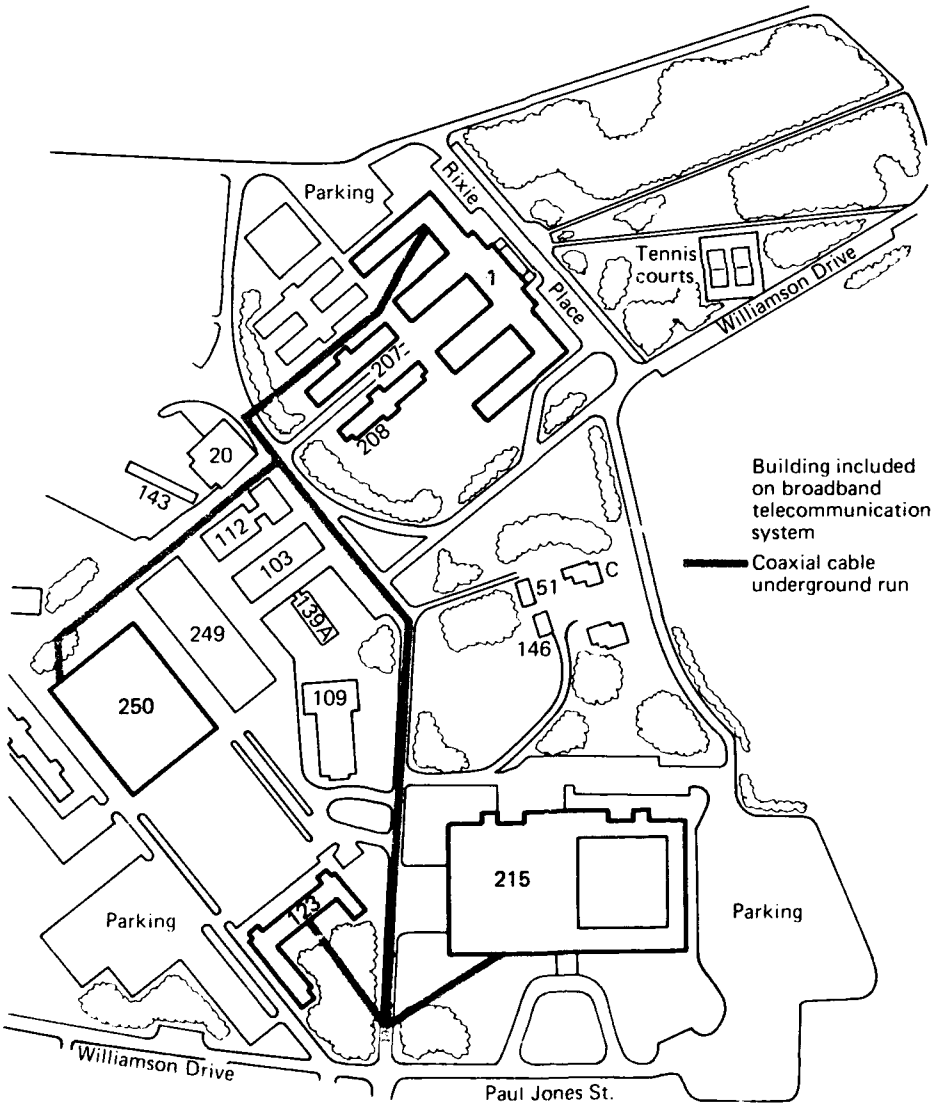

Figure 1—The main hospital layout of the Portsmouth NRMC.

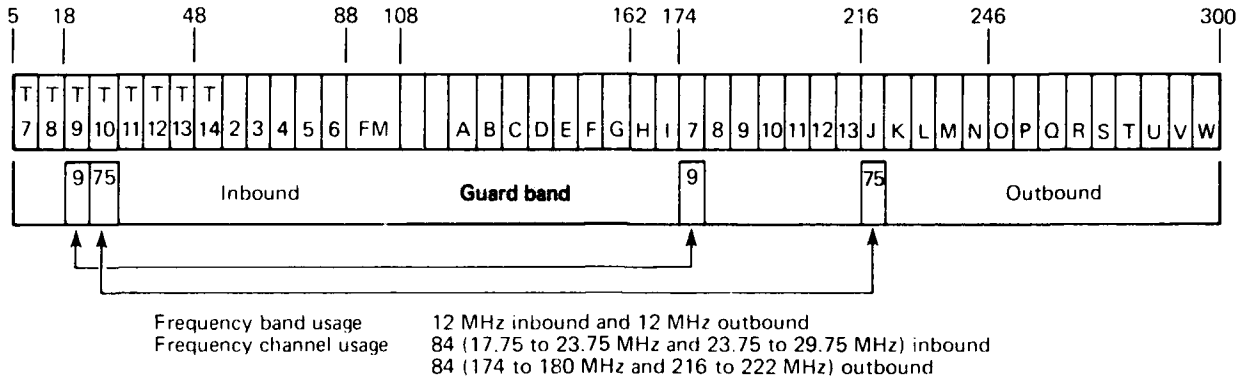

Frequency band usage — 12 MHz inbound and 12 MHz outbound
Frequency channel usage — 84 (17.75 to 23.75 MHz and 23.75 to 29.75 MHz) inbound
84 (174 to 180 MHz and 216 to 222 MHz) outbound

Figure 2—Channel allocation chart.

The system headend (the location in the system where signals can be checked, monitored, and inserted) is installed in the computer room. Signals from the headend to the data terminal equipment locations are designated outbound, and signals from the terminals to the headend are designated inbound. The outbound frequency band is from 162 to 300 MHz and the inbound from 5 to 112 MHz. The configuration with the single-cable mid-split (the separation of the outbound and inbound frequency bands) requires that a guard band be provided to ensure that the outbound and inbound signals do not mutually interfere. The guard band is from 112 to 162 MHz, and no channel assignments can be made there.

The 3M Interactive Systems Telecommunications Division model 925/926 modems provide a serial data link interface for terminals, printers, and computer ports to the broadband telecommunication system. The modems operate asynchronously in full duplex mode at data rates up to 9600 bits per second. They translate and transmit the modulated bit stream at assigned frequencies on the system.

A channel allocation chart (Fig. 2) shows the channel allocation and the modem frequency assignment for the Portsmouth NRMC and how the 300 MHz bandwidth of the coaxial cable is divided into the standard cable television channel assignments. Selected frequency assignments are noted along the top of the figure, starting at 5 MHz and ending at 300 MHz. The chart also shows that most standard television channels are able to share the system with the data equipment.

The 84 modem pairs initially installed at Portsmouth and assigned to the system are located on cable television channels J (75 channel assignments) and 7 (9 channel assignments) in the outbound frequency band and on companion channels T10 and T9, respectively, in the inbound frequency band.

The system was tested and aligned in accordance with procedures based on cable television system measurements. During the installation, seven major test phases were completed in the following sequence: preinstallation testing of the coaxial cable, amplifiers, and power supplies; cable system setup and amplifier alignment; cable system acceptance; carrier-to-noise ratio measurement; cable system radiation measurement; data communications equipment checkout; and telecommunication system testing.

CONCLUSIONS

The broadband telecommunication system has been operating continuously since certification in November 1983, supporting five clinical automated data processing systems with terminals located throughout three buildings interconnected on the system. The clinical systems that are supported are the laboratory, patient appointment and scheduling, pharmacy, radiology, and hypertension. A total of 343 four-port taps were installed in the local distribution cable to accomodate 1372 devices (video and data terminal devices) in the four buildings. The ability to interface with other local area networks has also been designed into the system.

The test procedures and test sequence followed at the NRMC were designed so that each phase of testing depended on the successful completion of the preceding phase. This approach to alignment and testing increased the probability that the system would meet the overall specifications for certification when installation had been completed. The system has been operating reliably for nearly a year. It provides a capability that can be adapted or expanded to the diverse communications needs of a health care facility.

This work was supported by the Naval Medical Data Services Center.

COMMUNICATIONS ENGINEERING IN SUPPORT OF THE UNITED STATES INFORMATION AGENCY

N. K. Brown and S. P. Yanek

A communications-oriented computer to upgrade the United States Information Agency's Wireless File electronic news system has been installed at the agency's Washington, D.C., headquarters. It is connected direct-'·· to circuitry that distributes news items to remote terminals worldwide. APL has provided the agency with an integrated system for communicating Arabic, English, French, and Spanish text via telegraph, radio telegraphy, telephone, and leased-line networks.

BACKGROUND

The United States Information Agency (USIA), an independent agency of the executive branch of the U.S. Government, provides diverse information services to a worldwide foreign constituency of cultural organizations, academicians, and students as well as political, business, and media representatives. Among its most timely information services is the daily Wireless File, a :ollection of news items and background articles prepared, edited, translated, and distributed electronically to approximately 300 locations overseas (e.g., embassies, consulates, information centers), whence it is distributed. There are six editions of the file. Five are daily editions prepared for the major geographic regions of the world (Africa, Europe, East Asia and the Pacific Islands, the Americas, and the Near East and South Asia). The sixth, an administrative file, is sent to all regions every second Sunday. Typical regional files consist of up to 20,000 words of English text; three of the five regional files are also translated into French, Spanish, and Arabic.

Each edition of the Wireless File undergoes text preparation, transmision, reception, and distribution. A mixture of electromechanical and electronic text generation and communications equipment has been used to perform these functions. Information flow in the Wireless File System before the upgrade is shown in Fig. 1.

The text entry of original material was performed by typists using keyboard video display terminals on a text editing system known as the ATEX. After being entered and edited, the articles were printed in optical character reader format, manually inserted into an optical scanner of the Scandisk system, and punched on paper tape. The articles stored on paper tape were then broadcast to teleprinters within the USIA to provide paper copies for proofreading. English and foreign language articles were separated into regional files within the ATEX, reprinted in optical character reader format, and rescanned into the Scandisk. Then, instead of being punched on paper tape, they were assembled into separate regional files on removable floppy disks of the Scandisk. At the scheduled times, the regional files were transmitted to the regional posts via a combination of leased circuits and high-frequency radio links. If part of the regional files was incorrectly received because of transmission errors, the affected articles were retransmitted

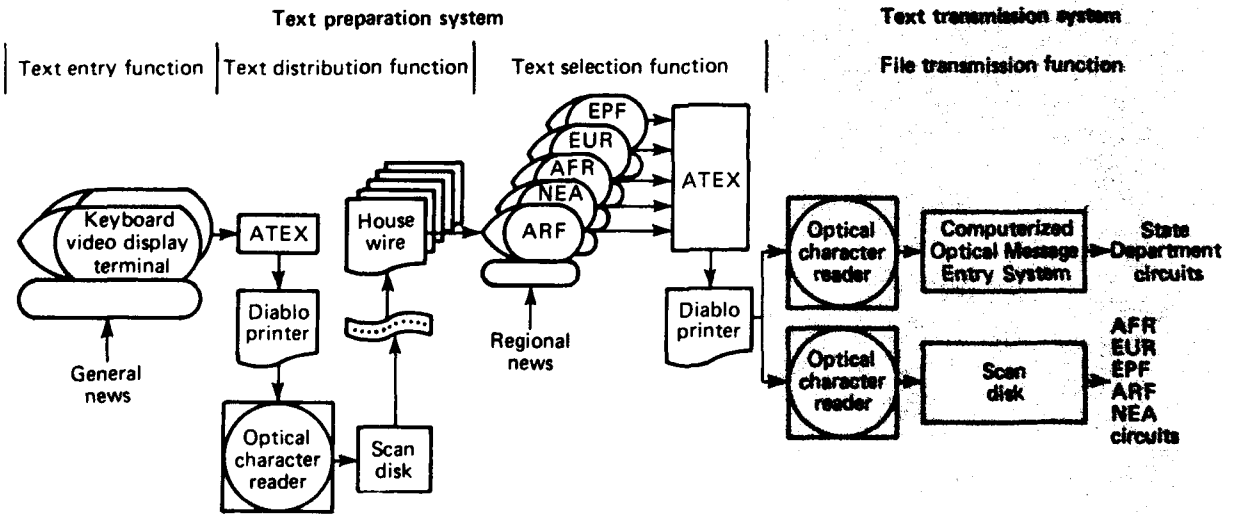

Figure 1—The previous Wireless File System.

via special State Department circuits in the form of "USINFO" messages.

DISCUSSION

APL was requested to identify areas for potential improvements and to recommend and implement a way to improve the efficiency of communications processing in the Wireless File System.[1] The USIA released an independent Request for Proposal for an enhanced News and Editorial Support System to supplant the ATEX. The existing assemblage of electronic and electromechanical communications equipment had evolved over many years; it lacked compatible technology and was characterized by labor-intensive information handling. A modern communications processing capability was needed as the first step in enhancing the Wireless File System. Commercial processors were identified that support computer-to-computer interfaces, transmit various data codes at different speeds, handle different types of circuits and protocols, and offer automated data handling procedures. An informal survey of the telecommunications industry produced a list of nearly 100 devices described as communications processors.

APL recommended and implemented the following methodology in selecting a Wireless File communications processor:

1. Description of requirements,
2. Description of proposed system operation,
3. Statement of the requirements and specifications in detail,
4. Development of a Request for Proposal package,
5. Evaluation of the proposals for communications processors,
6. Installation and integration of the communications processor into the Wireless File System,
7. Acceptance testing of the communications processor.

The requirements were stated from a functional perspective to allow the data communications industry a degree of flexibility in proposing a system concept and an equipment configuration.[2]

RESULTS

As a result of the responses from industry, a modern communications processing subsystem was selected, acquired, installed, and tested.[1] The integrated system includes the subsystem interacting with the USIA-furnished systems: the enhanced News and Editorial Support System and the existing Computerized Optical Message Entry System.

The communications processing subsystem is based on store-and-forward message processing technology with built-in archival capabilities. This type of processing permits users who possess keyboard-equipped terminals to compose and submit messages to the communications processor, which forwards the message to the proper destination at the appropriate time over the designated communications links. The communications processing subsystem has been connected to the News and Editorial Support System via a data communications circuit (Fig. 2) and software developed to encapsulate each article by a message-oriented header and trailer. In addition to that connection, the subsystem is interfaced to a remote teletypewriter with an Arabic keyboard. For the first time, USIA was able to achieve direct entry, storage, and transmission of Arabic Wireless File material to compatible terminals.

Until transmission is enabled, the communications processing subsystem accumulates Wireless File articles in five regional message queues that overflow to disk as needed. At a scheduled transmission time, the queues are released and the articles are code translated (except for Arabic) to accommodate the teletypewriter-like remote printers that are connected to the technical control unit. As articles exit from the message switch (X-32) to leased direct circuits, their message-oriented headers and trailers are removed by external microprocessors. To provide compatible signal levels to the technical control unit, each output circuit is also equipped with a signal converter.

To facilitate the retransmission of articles whose text becomes unreadable because of transmission errors, the subsystem archives every transmitted article for up to 14 days. Occasionally, articles are retransmitted to recipients by an alternative set of secure circuits provided by the State Department. To do this, the subsystem also contains a microprocessor-based format converter to route articles retrieved from archival storage through an approved interface directly to the Computerized Optical Message Entry System. That system retains the original optical scanner as a switchable, alternative means of text entry. A Diablo printer with an optical character reader printwheel may be attached to the communications processor for backup purposes. The subsystem includes uninterruptible power supplies to safeguard operational integrity.

CONCLUSIONS

The installation of a communications processor has increased the efficiency and accuracy of USIA's daily Wireless File operations. The handling of information in the form of paper, floppy disks, and paper tape has been greatly reduced. The need for manual intervention during transmission has been virtually eliminated. The mul-

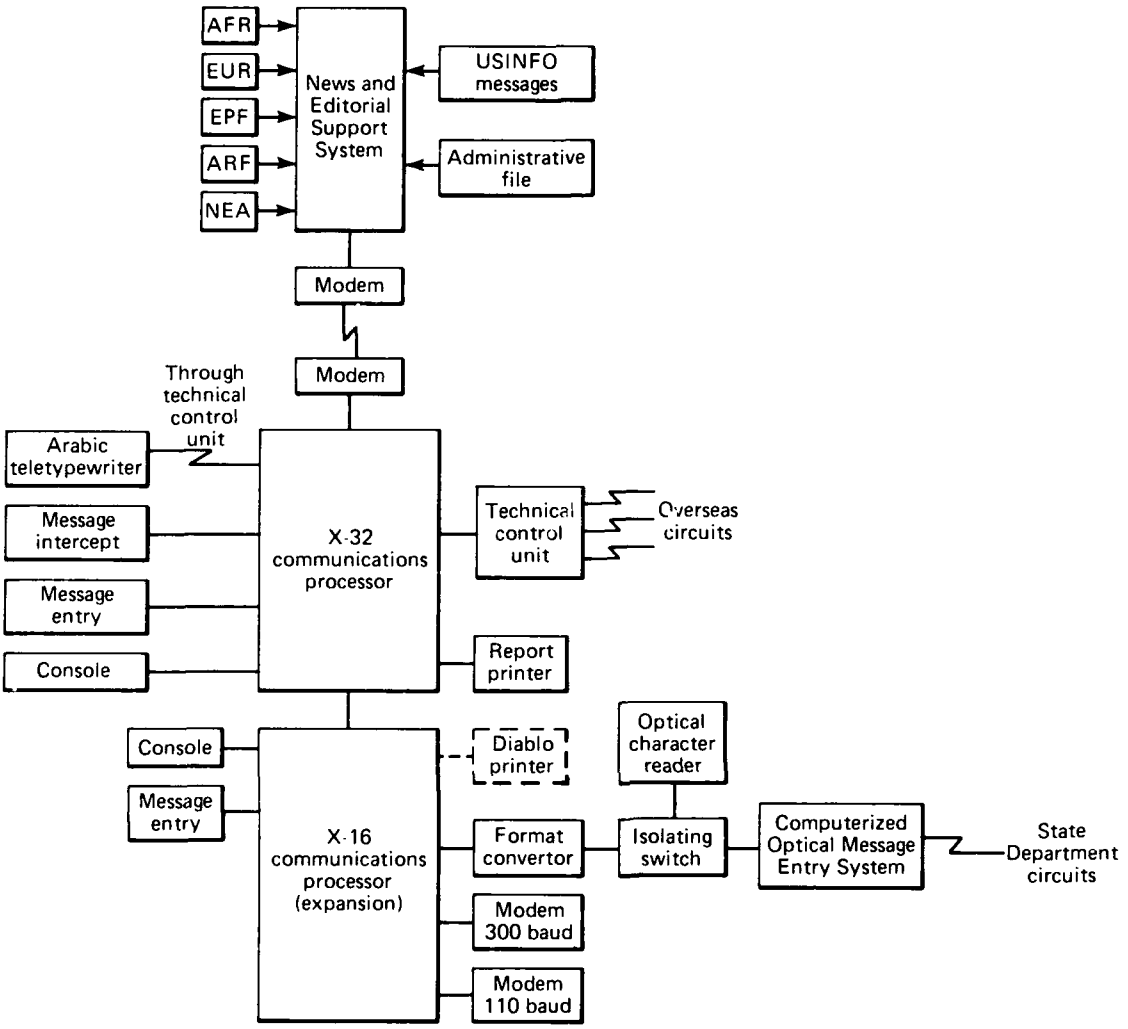

Figure 2—The upgraded Wireless File System.

tiplicity of obsolete, expensively maintained electromechanical equipment has been discontinued. New techniques for Wireless File distribution are feasible in the form of support for dial-up delivery and connection to common carriers. USIA now has an expandable device controlling telephone, telegraph, leased-line, and radio broadcast modes of communication for the dissemination of Arabic, English, French, and Spanish text.

ACKNOWLEDGMENTS

The authors would like to acknowledge the support provided by C. S. Perry and B. L. Kirchhofer of APL and by C. Cantrell, formerly with Hadron, Inc., and now with AT&T Information Systems.

REFERENCES

[1] Fleet Systems Department, *USICA Wireless File Conclusions and Recommendations*, JHU/APL FS-82-135 (Jun 1982).

[2] Fleet Systems Department, *United States Information Agency (USIA) Requirements and Specifications for Wireless File Communications Processing Subsystem*, JHU/APL FS-83-015 (Feb 1983).

[3] Fleet Systems Department, *United States Information Agency (USIA), Communications Processing Subsystem Test Analysis Report*, JHU/APL FS-84-004 (Jan 1984).

This work was supported by the United States Information Agency.

TEST AND EVALUATION

INTRODUCTION

Test and evaluation has long been an important part of APL's involvement in weapon systems technology. It is a significant factor in programs for the development of new weapons systems, combat systems, and their major components, and in improving or upgrading existing systems. In other programs, test and evaluation is the primary task, with the Laboratory acting as an independent evaluator of weapon system performance. Those programs have led to many others such as the development of data acquisition systems having unique requirements, the evaluation and improvement of instrumentation and facilities on test ranges, and the determination of test instrumentation requirements.

Programs for the development of surface ship combat systems, such as Aegis, or the upgrading of existing systems, such as the Terrier and Tartar New Threat Upgrade, require extensive test and evaluation effort, including at-sea testing to verify the combat system's performance. The Laboratory has now taken a further step, that of evaluating several ships and their aircraft integrated into the fighting unit of a naval battle group. Recent at-sea testing conducted by APL initiated that process; APL began a quantitative study of the interactions of the ships in a battle group and investigated innovative and cooperative surveillance and engagement methods.

The Laboratory's participation in cruise missile programs includes the performance evaluation of Harpoon and Tomahawk. APL's recently expanded role in the Tomahawk program calls for greater responsibility in the test and evaluation of that weapon system.

For many years, APL has served the Navy as an independent evaluator of the submarine launched ballistic missile (SLBM) weapon systems and has served the Army similarly on behalf of the Pershing weapon systems. APL has a key role in the development and conduct of test and evaluation programs for these operational systems that will continue throughout the time of their deployment. A major new effort is the Trident II Accuracy Evaluation Program, with the objectives of in-depth understanding of the accuracy of the weapon system and prediction of its performance. A principal design goal is a substantial increase in accuracy.

Closely related to the SLBM evaluation is the Communications Continuing Evaluation Program, which has the objective of assessing the efficacy and reliability of the command message communications to operational SSBNs. A major program to ensure the security of the SSBN forces has, for a number of years, conducted full-scale at-sea testing aimed at producing useful threat and countermeasure assessments; special exercises are conducted to evaluate SSBN security during certain evolutions. Yet another effort, important to security, is the evaluation of the SSBN sonar suite.

Various APL programs involve development, improvement, or evaluation of instrumentation systems for test and evaluation. Development tasks include

SATRACK II for the precise tracking of Trident II test flights using the Global Positioning System satellites; a small, high-capacity data acquisition system for use on E-2C aircraft to collect the large amount of data required to evaluate that aircraft's role in the outer air battle; and the System Data Recorder to acquire Pershing II test data. Developments for test range facilities include a multiradar surface tracking system that integrates data from noncolocated radars and generates an accurate, composite display of the range area, and also an Air Launched Deep Ocean Transponder to facilitate maintenance of the bottom-mounted transponder arrays used for launch and impact measurements during SLBM test firings. APL recently determined the quality of meteorological instrumentation required for the test flight impact area in order to fulfill specific accuracy evaluation objectives.

This introduction attempts to provide an overview of the rather extensive APL programs in this important area of defense technology. The articles that follow do not begin to provide a representative sample of the overall effort but do indicate the nature of certain selected accomplishments in test and evaluation.

CARTRIDGE MAGNETIC TAPE SYSTEMS FOR SHIPBOARD AND AIRCRAFT APPLICATIONS

D. M. Bullis, C. E. Dorsett, and J. F. Jaworski

New high-data-capacity cartridge drive systems for magnetic tape recording have been adapted for use in selected aircraft and shipboard data collection systems for the reconstruction of Fleet exercises. Known as streamer cartridge tapes, they have replaced previous systems using reel-to-reel recorders with their limited data-handling capacity and excessive bulk.

BACKGROUND

The Fleet Analysis Center, Corona, Calif., has indicated a need for an assessment of the role of the E-2C aircraft in the outer air battle during exercises where the ability to collect and store a large amount of pertinent data is of utmost importance in determining Fleet performance. In those operations, recording of the data output of the on-board Airborne Tactical Data System (ATDS) computer, particularly in E-2C radar surveillance aircraft, puts a premium on size, weight, and ease of operation of the recording system. The Hawkeye Airborne Recording Digital Instrumentation (HARDI), a data recording system for the E-2C, has been developed by APL in response to the requirement for a small recorder.

DISCUSSION

The current tactical data recording system in the E-2C, the Digital Data Recorder/Reproducer (DDRR), has a 9-track, 800-bits-per-inch tape containing 630 ft of magnetic tape. The DDRR has a tactical operational program that uses most of the space available on the tape, so that only about 15 minutes of data can be recorded. As on-station time during Fleet exercises approaches 4 hours, the DDRR would require the loading of a new blank tape approximately every 15 minutes to provide continuous data records. This is a reel-to-reel recorder, and not only is changing tapes in the aircraft difficult, but many tapes are required.

The advantage of the high-data-rate and capacity system for Fleet exercises is clearly indicated. A small, very portable, easily operated recording device built around the data cartridge drive system was found to meet those needs.

The HARDI System

During data extract in Fleet exercises, the L304 computer in the E-2C aircraft records data on the HARDI system instead of the DDRR. HARDI is lightweight and is easily and quickly installed in or removed from the E-2C aircraft. No modification to hardware or wiring is required. Data for an entire flight reside in a single, hand-carried cartridge, and the format is compatible with Fleet Analysis Center requirements. HARDI requires no operator intervention, an important asset in aircraft use. It operates without degradation to IFF, navigation, or ATDS performance. It consists of two units installed in the ATDS computer cabinet in place of blank drawer panels.

Data recorded during Fleet exercises are normally analyzed at the Fleet Analysis Center. The use of the HARDI data recording system together with a small portable computer, a plotter, and a printer makes possible on-site reconstruction of an exercise.

The major subsystem in HARDI is the 3M magnetic recorder, which is a high-capacity data cartridge drive system. The drive module is 4.56 in. high, 6.85 in. wide, and 8.625 in. deep; it weighs 6 lb. The controller board is 6.5 in. wide and 12 in. long. The HARDI unit is shown in Fig. 1.

The Scotch DC 615 HC formatted data cartridge uses high-capacity, high-performance bidirectional magnetic tape. With 150 ft of ¼-in.-wide tape, it provides up to 16.7 megabytes of user storage capacity in a package only 4 by 6 in. The spring-loaded dust door opens automatically and closes automatically when the cartridge is removed.

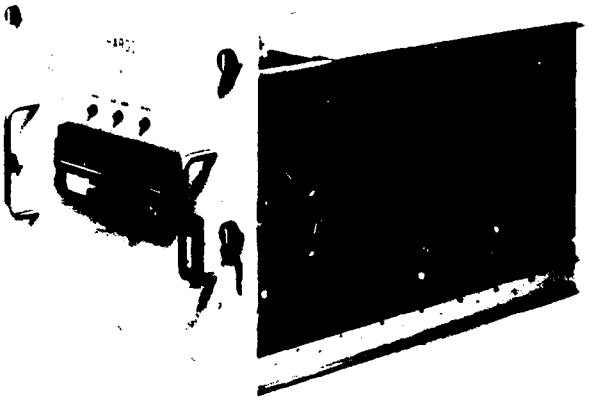

Figure 1—The Hawkeye Airborne Recording Digital Instrumentation.

3M Cartridge Magnetic Tape Unit

Following the successful demonstration of the advantages of using the high-capacity data cartridge in E-2C aircraft, the next step was to extend the concept to taking data aboard ship during Fleet exercises. Each ship has data recording facilities, but they are dedicated to ship's use rather than to exercise evaluation. A separate data recording system was needed.

The task of adapting the cartridge data system to shipboard use was complicated by the variety of host computer systems on the ships where the only common feature is that they all communicate with peripheral devices by MIL-STD 1397 parallel channels. The problem therefore was to provide a single unit that included all the electronics and intelligence needed to permit the use of the new data cartridge in any data system, without modifying the host computer.

A single unit to accomplish this has been built around the cartridge drive system. It is designated the 3M Cartridge Magnetic Tape Unit (3M/CMTU) to distinguish it from the shipboard AN/USH 26 data cartridge system, a limited capability system found on some ships. With the 3M/CMTU, the tape systems in the various ships are simulated by means of a simple front panel control change.

The 3M/CMTU consists of a chassis that can be mounted on a single rack (Fig. 2). Powered by 115 VAC, 60 to 400 Hz, it consumes 120 W of power. Internally, the unit features Eurocard industry standard construction and a VME data bus.

The unit contains a 3M HCD-75 cartridge tape system consisting of a formatter/controller and two transport units. It also contains a 68000-based microcomputer with operational firmware, host interface, and 3M interface cards. Its storage capacity is 67 million bytes per cartridge, and the maximum data throughput is 35 thousand bytes per second. Two transport units operating "ping-pong" fashion extend the recording period. A block diagram of 3M/CMTU is shown in Fig. 3.

Figure 2—The 3M Cartridge Magnetic Tape Unit.

All primary functions performed by the 3M/CMTU are under control of the internal microcomputer card program. Front panel switches select modes of operation. The microprocessor reads the desired mode. Commands received from the host computer are interpreted by the microprocessor and are translated into appropriate control signals.

Streaming devices such as the 3M data cartridge have "repositioning delays" at the end of data transfer bursts. If left uncorrected, that characteristic would seriously limit data throughput. The microprocessor provides a 32 thousand byte data buffer function to allow for such delays, thus maintaining maximum throughput.

An additional microprocessor function accommodates logical block length (logical block length is the number of bytes contained in a logic data group, referred to

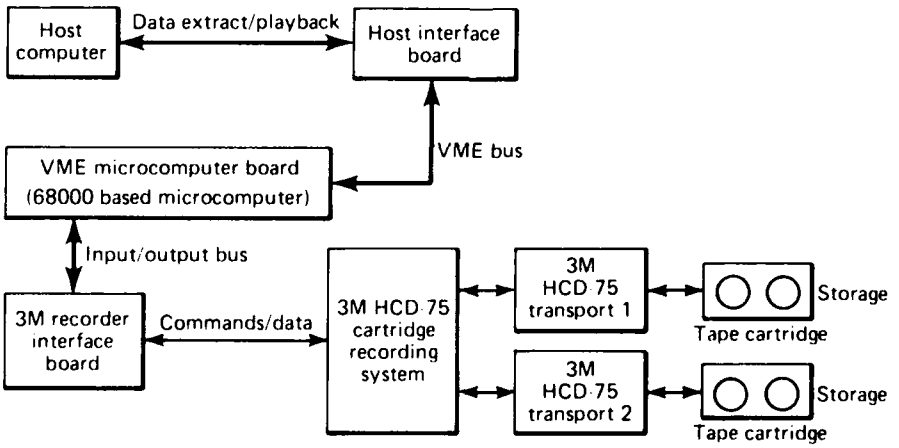

Figure 3—Block diagram of the 3M/CMTU.

as a block, and varies from one computer to another). The physical block length of the 3M tape subsystem is fixed at 1024 bytes. Ways have been provided to accommodate the block requirements of the various host computers. The microprocessor adds appropriate preambles to the normal data stream to allow faithful reproduction of the data from tape.

SUMMARY

To date, E-2C aircraft in 12 Fleet exercises have been instrumented with HARDI. Much of the ATDS database for various projects such as E-2C tracker studies has been obtained using the new system.

3M/CMTU units have been deployed in support of some ten Fleet exercises, including Gridlock and New Threat Update, during which no failures have occurred. These recording systems provide previously unobtainable reliability, flexibility, and performance in airborne, shipboard, and land-based test applications.

This work was supported by NAVSEASYSCOM, SEA-06 and PMS-400.

RESULTS OF THE PRECISE INTEGRATED NAVIGATION SYSTEM LONARS TEST

L. F. Fehlner and W. J. Peters III

In support of the development of the AN/SSN-2 Precise Integrated Navigation System, an assessment of the quality of loran service in the San Diego, Calif., area was undertaken. Data gathered using the Loran Navigation Receiving System (LONARS) and the Internav LC-404 Loran-C receiver were evaluated and compared.

BACKGROUND

The Precise Integrated Navigation System (PINS), being developed for installation in a new class of minesweepers, incorporates multiple radionavigation and acoustic navigation systems. The performance of the PINS Loran-C receiver (Internav LC-404) had been substandard in both the hyperbolic and the circular modes during development testing aboard USS *Pluck* (MSO-464) in the San Diego area. A test to quantify Loran-C performance using LONARS as the primary reference was requested by the Navy.

LONARS, the Loran-C radionavigation system developed by APL for use as the position reference system when evaluating the performance of the Strategic Submarine Weapons System, is essentially immune to atmospherics and cross-rate interference and has a measurement resolution of less than 1 nsec. Real-time geodetic performance has been on the order of 60 ft (root sum squared (rss) one standard deviation (one sigma), and post-mission performance has been less than 50 ft (rss one sigma).

DISCUSSION

One LONARS was installed ashore at the Naval Ocean Systems Center (NOSC), Point Loma, Calif., and a second was installed on *Pluck* to quantify the quality and characteristics of the loran signal in San Diego at a fixed site and on board the minesweeper.

Loran Interference

It was observed immediately that the loran signal at NOSC was contaminated by low-frequency interference, which was traced to the local Naval transmitting facilities. When all four of the manually operated notch filters of LONARS were properly tuned, the interference was reduced to an acceptable level and had negligible effect on the positional information. The filters of the PINS Loran-C receiver also required manual adjustment to operate normally in the presence of the interference.

A complicating characteristic of the interference was its temporal variability. To achieve satisfactory LONARS performance, it was necessary to monitor the receiver and retune the filters periodically to notch the interference.

Sky-Wave Contamination

LONARS could not maintain accurate phase tracking of the loran signal between local sunset and sunrise. The difficulty was traced to sky-wave interference that was evident in three modes: (1) very slow ground-wave speed of propagation, (2) long-delayed sky wave from stations being tracked, and (3) sky wave from stations not being tracked.

Mode 1, illustrated in Fig. 1a, involves a relationship between ground wave and sky wave whereby the first-hop sky wave contaminates the ground wave as far forward as the standard track point. All eight pulses are affected the same way. This causes the receiver to report times of arrival that no longer can be attributed to the ground wave and results in errors in computed position. If the contamination is severe, phase lock at the standard track point may be lost, leading to very large positional errors. Long-delayed sky wave (Mode 2) resulting from multiple hops contaminates the later pulses in each group of eight (Fig. 1b), causing the shape of the last seven pulses (of the eight) to be distorted. This leads to loss of phase lock at the standard track point. Phase tracking could be limited to the first pulse but that would compromise receiver performance in the absence of sky wave. Tracking only the first pulse would avoid the problems of Mode 2 but is subject to Mode 1 sky wave and to increased disturbances arising from a lower signal-to-noise ratio.

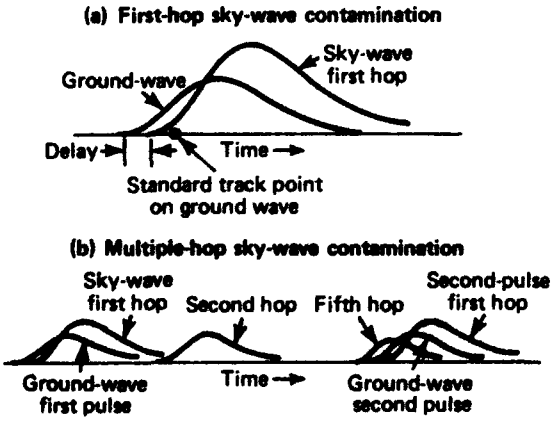

Figure 1—Schematic representation of the sky-wave problems.

Mode 3 is sky-wave contamination resulting from signals received from loran transmitters other than those being tracked. Under certain atmospheric conditions, sky waves can be received from distant transmitters at significant signal levels. Such contamination has an unpredictable effect and varies with time and receiver position, but it can be reduced and, under some circumstances, eliminated by appropriate real-time editing of the measurement data.

All three modes of sky-wave contamination were observed at night in San Diego, making the present loran service in that area virtually unusable for navigation from approximately local sunset to local sunrise.

Geometric Dilution of Precision

The San Diego area is located where the hyperbolic solution for geodetic position is poor. The geometric dilution of precision (GDOP) is worst in the north-south direction. Its value is about 7; i.e., a 10-nsec error in time difference produces a position error of 70 ft. The GDOP is about 1.2 in the east-west direction; i.e., a 10-nsec time error is about 12 ft of position error. Calculations show that the GDOP in the circular (rho-rho) mode is better (about 1.2 both north-south and east-west) than in the hyperbolic mode of coordinate conversion.

Receiver Performance

On November 30, 1983, data were recorded by LONARS at the NOSC facility, tracking Fallon, Nev., Middletown, Calif., and Searchlight, Nev., signals (GRI 9940), using Middletown as the reference for time differences (denoted by F-M and S-M). The mean and standard deviations were computed for contiguous 15-min intervals and were sampled every 1.0934 seconds. The recorded data are essentially uncorrelated at a lag of 6 sec, and every sixth data point was used in the 15-min intervals to produce statistics for independent samples. The data, plotted in Fig. 2, show the sequence of the mean deviations of time differences from their very-long-term average and of two sigma deviations from the means. The abscissa scale is seconds from midnight Universal Time Coordinated (UTC).

The wild excursions shown in Fig. 2 indicate loss of lock on the standard track point at the end of the third cycle. Figure 3 shows that LONARS maintained phase lock on the signal but could not satisfy its envelope shape criterion because of sky-wave contamination. In attempting to find the standard track point, the time differences did not deviate more than about 120 μsec, indicating that the phase tracking point did not move off the pulse. Had it moved off, the return to the standard track point would not have occurred.

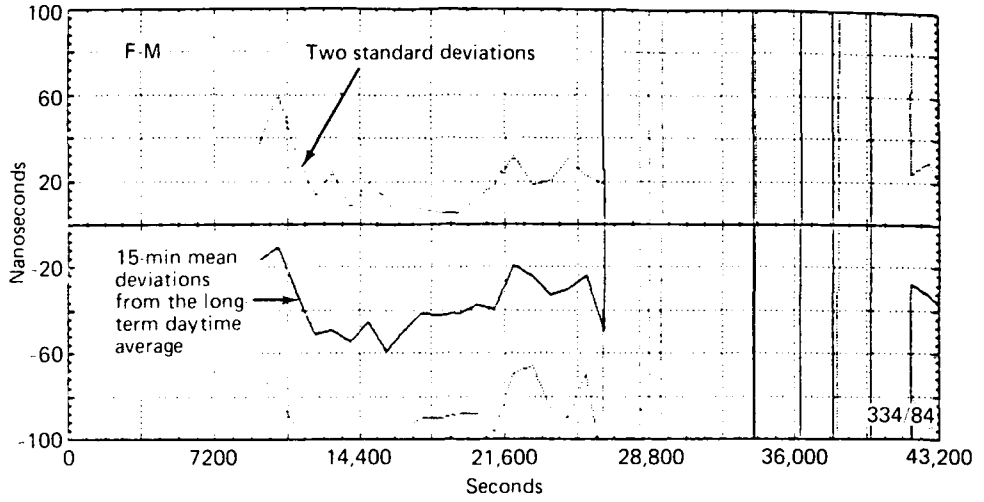

Figure 2—Loran performance recorded by LONARS at NOSC, Nov 30, 1983. The S-M time-difference data, not shown, are similar in nature to the F-M data.

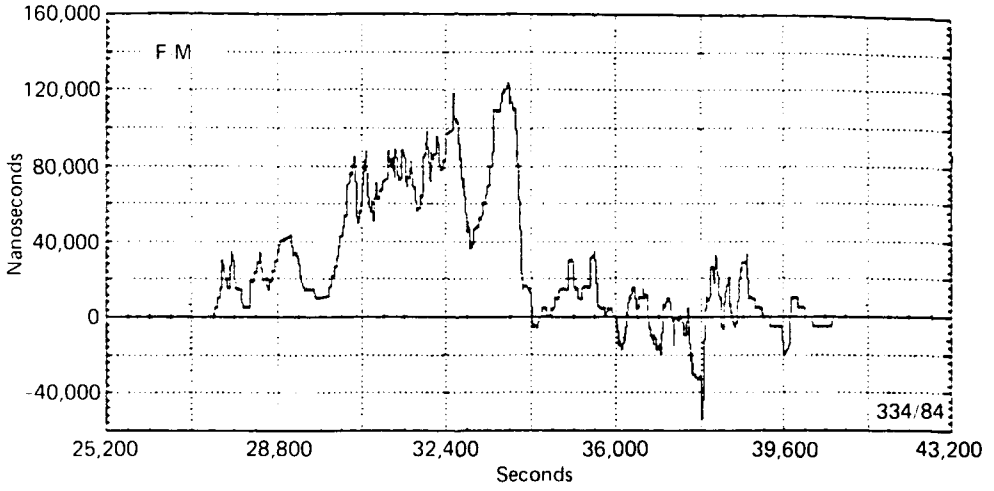

Figure 3—Nighttime time-difference deviations from the long-term daytime average recorded by LONARS at NOSC, Nov 30, 1983. The S-M time-difference data, not shown, are similar in magnitude and shape to the F-M data.

Loran reception in the San Diego area is unreliable for position fixing from sunset to sunrise. However, the daytime loran reception is well within U.S. Coast Guard stated emission tolerances[1] and exhibits the same characteristics as those in the southeast United States.[2] Estimates made from the LONARS data recorded at NOSC are that the daytime standard deviation of the F-M time difference is about 25 nsec and the S-M time difference is about 15 nsec at NOSC. By inference, the standard deviation of time of arrival is about 11 nsec for Searchlight and Middletown and about 22 nsec for Fallon.

Data recorded by LONARS on board *Pluck* while at the wharf indicated a daytime standard deviation of about 50 nsec for F-M and 20 nsec for S-M. The corresponding standard deivations of time of arrival is about 11 nsec for Searchlight, 17 nsec for Middletown, and 46 nsec for Fallon.

On December 8, 1983, the LONARS and the PINS Loran-C receiver were operated simultaneously at NOSC; data are shown in Figs. 4 and 5, respectively. The time differences are computed differently by the two receivers. The daytime standard deviations of the LONARS time differences are as stated previously. The daytime standard deviation of both of the time differences as measured by the PINS Loran-C receiver is about 60 nsec. Under the assumption that all three standard deviations of time of arrival are equal, their value is 42 nsec. The large excursions in Figs. 4 and 5 before sunrise are in-

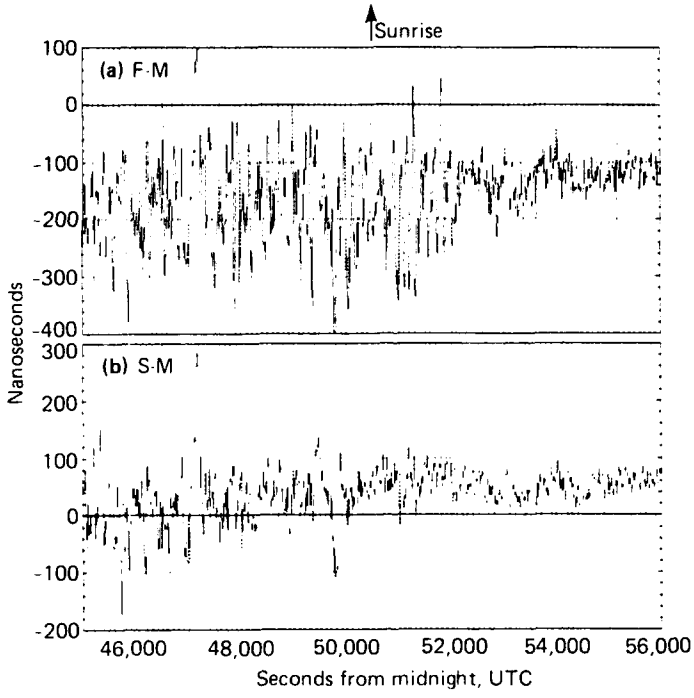

Figure 4—Time-difference deviations from the long-term daytime average recorded by LONARS at NOSC, Dec 8, 1983.

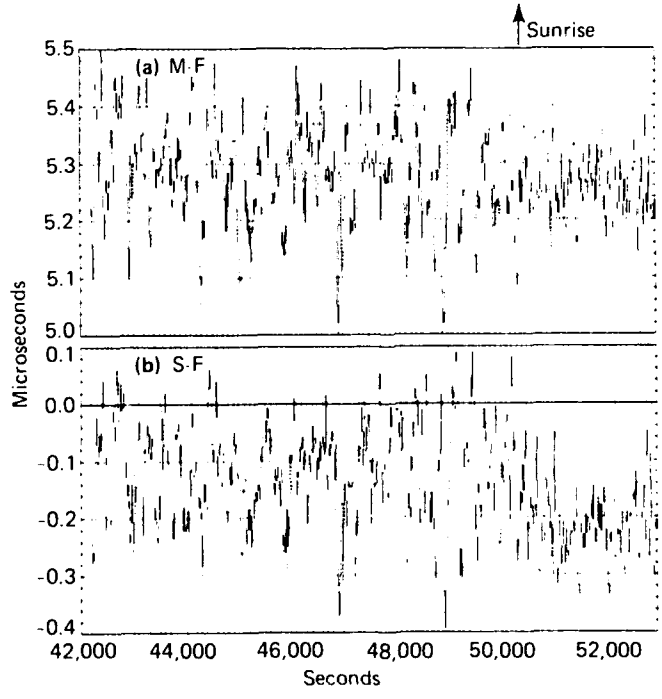

Figure 5—Time-difference deviations from the long-term daytime average recorded by the Loran-C receiver at NOSC, Dec 8, 1983.

dicative of the unreliable nightime reception of loran in San Diego.

CONCLUSIONS

The temporal stability of the loran signals of the west coast U.S. Loran-C chain meets the specifications published by the U.S. Coast Guard and shows the same daytime characteristics as those of the southeast U.S. Loran-C chain.

Significant low-frequency interference present in San Diego necessitates the use of notch filters to achieve satisfactory loran reception.

The loran service in the San Diego area is essentially unusable at night because of sky-wave interference.

The GDOP is about 7 north-south and 1.2 east-west for hyperbolic coordinate conversion. For circular conversion of three signals, it is about 1.2 both north-south and east-west.

REFERENCES

[1] *Specification of the Transmitted Loran-C Signal*, U.S. Coast Guard COMDTINTS M16562.4 (1981).

[2] "Observations of the Performance of the Southeast U.S. Loran-C Chain," in *Proc. Twelfth Annual Technical Symp.*, Wild Goose Assoc. (1983).

This work was supported by the Strategic Systems Program Office.

ISOLATING SOURCES OF ERRORS IN MODELS OF DYNAMIC SYSTEMS

J. C. Spall

An important step in the process of constructing a mathematical model of a system, such as the linear dynamic models used by APL to analyze the accuracy of advanced ballistic missile systems, is to study the model's validity. Although the model validation techniques currently available at the Laboratory are valuable in establishing the fidelity of the model under consideration, they are not especially suited to locating sources of errors in models that are ruled invalid. This article summarizes the error isolation methodology, a procedure that has been developed to locate misspecifications in dynamic models that are in state space form. Although the methodology was motivated by the ballistic missile system analysis problem, it could apply as well in other areas—such as biomedicine, geophysics, transportation, and economics—in which state space models are used.

BACKGROUND

When a model of a system is used to make an inference about the system itself, the integrity of the analysis depends, of course, on the fidelity of the model. Thus, an important step in the construction of a model of a dynamic system (such as the state space models being developed by APL to analyze advanced ballistic missile system prelaunch and boost phases) is a test of the model's validity after its parameter values have been specified. The test generally involves comparing actual system measurements with predicted output based on the model; the model is ruled invalid if those predictions are, in a statistical sense, too far from the system measurements. When a model is rejected, one faces the task of identifying the cause of the poor performance so that the model may be corrected. Aside from improving the model's predictive performance, isolating the source of the error may help the analyst to gain additional theoretical insight into the behavior of the system and may suggest that if the misspecified part of the model was estimated using a statistical technique (such as maximum likelihood), then one of the requisite assumptions of the technique was violated. The error isolation (EI) methodology is presented for locating sources of misspecifications in models of dynamic systems that are in linear state space form. Such models have been applied in the analysis of a wide variety of physical and social systems.

Two types of errors can occur in a state space model that has been ruled invalid: (a) the form (linearity and assumed order of the system) may be incorrect, or (b) the parameter values may be misspecified. It is assumed here that the model form is correct, so the methodology seeks errors in the parameters.

Traditionally, a form of error isolation has been performed by studying whether the specified values for the parameters in the model lie within approximate confidence intervals about corresponding estimates of the parameters from data. That approach is lacking in certain respects: (a) it is unable to examine parameters that have been either estimated nonstatistically or derived theoretically, and for which confidence intervals do not exist (e.g., the instrumentation parameters in a missile system model); (b) it does not conveniently account for interaction among parameters within a specified subset, particularly when some ofthe parameters have been estimated statistically and some have been determined otherwise; and (c) the confidence intervals, typically based on the inverse Fisher information matrix, are likely to be too narrow, possibly resulting in certain parameters being wrongly claimed as misspecified.

The model considered here has the following discrete time state space form:

$$x_k = \Phi_{k-1} x_{k-1} + w_{k-1}$$

$$z_k = H_k x_k + v_k, \quad k = 1,2, \ldots, n,$$

where, at time point k, x_k is the unobserved state of the system; z_k is the noisy measurement made of the state; Φ_k and H_k are appropriately dimensioned weighting matrices; and x_0, w_k, and v_k are random terms distributed $N(\mu, P_0)$, $N(q_k, Q_k)$, and $N(r_k, R_k)$, respectively. In the context of the API. advanced ballistic missile system model, the components of the measurement vector z_k are related to the position and velocity of the missile as measured by Global Positioning System satellites,[1] while the components of the state vector x_k include, for example, characteristics of the missile accelerometers and gyroscopes. The model parameters μ, P_0, and $\{\Phi_{k-1}, H_k, q_{k-1}, Q_{k-1}, r_k, R_k\}$ are assumed to be functions of an underlying set of parameters, $\theta_1, \theta_2, \ldots, \theta_m$ (i.e., $\mu = \mu(\theta_1, \ldots, \theta_m)$, $H_k = H_k(\theta_1, \ldots, \theta_m)$, etc., where the θ_i are parameter vectors that are candidates for misspecification. Letting $\theta_1^*, \theta_2^*, \ldots, \theta_m^*$ denote the set of specified values appearing in the invalid model for $\theta_1, \theta_2, \ldots, \theta_m$, we assume that one, and only one, θ_i^* is misspecified.

DISCUSSION

We now outline the basics of the EI methodology. Details can be found in Refs. 2 or 3. It is based on the well-known Bayes formula from probability and statistics. Using Bayes' rule, we can compute the probability that a given θ_i^* is not in error given a system observation z_k:

$$\phi_i(z_k) \equiv P(\theta_i^* \text{ correctly specified} \mid z_k). \qquad (1)$$

Thus, at time k, z_k provides evidence that θ_i^* is misspecified when $\phi_i(z_k)$ is low. More specifically, we will be interested in identifying which of $\phi_1(z_k), \ldots, \phi_m(z_k)$ is lowest since the θ_i^* associated with this curve is the most likely to be incorrectly specified. In this paper, we assume that z_k (but not necessarily x_k) is a scalar. Reference 3 addresses the multivariate z_k case. Figure 1 illustrates this idea for a case where $m = 3$; i.e., there are three candidates for misspecification. We see, for example, that if the observation z_k takes a value in the region labeled D_2, the observation provides evidence that θ_2^* is the parameter vector that is misspecified (the label D_2 denotes "detection region for θ_2").

Figure 2 presents the steps of the methodology. In box (a), we choose which parameters appearing in the invalid model are candidates for misspecification; i.e., we choose $\theta_1^*, \theta_2^*, \ldots, \theta_m^*$ and assign a Bayesian prior distribution to each θ_i that reflects any information available about the true value of θ_i. Next, in box (b), we determine the detection regions (the D_i) into which each of the observations $z_1, z_2, \ldots, z_n$ falls. If, for example, θ_i^* is the misspecified parameter vector, then the $z_1, z_2, \ldots, z_n$ will tend to land in the detection region D_i. Box (c) represents a formal mechanism for determining the one vector, say θ_{min}, in the set $\theta_1^*, \theta_2^*, \ldots, \theta_m^*$ that is most likely to be misspecified, given the sequence of detection regions into which each of the measurements fell. Details on this step may be found in Ref. 2; of more interest is the procedure represented by box (b), which we will now discuss.

The key aspect in the EI methodology is identifying the detection region into which each z_k falls. Since the idea behind locating those regions does not depend on the time index k, we can for convenience suppress that index and write z for z_k. As illustrated in Fig. 1, the D_i

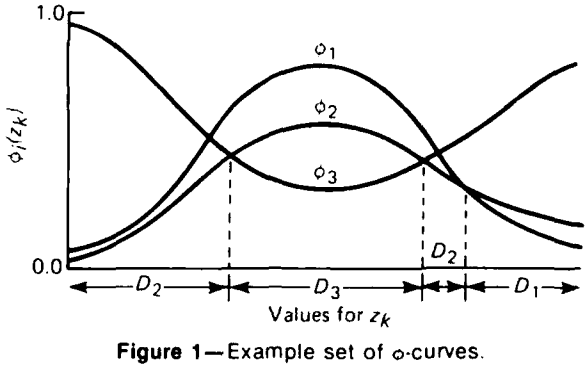

Figure 1—Example set of ϕ-curves.

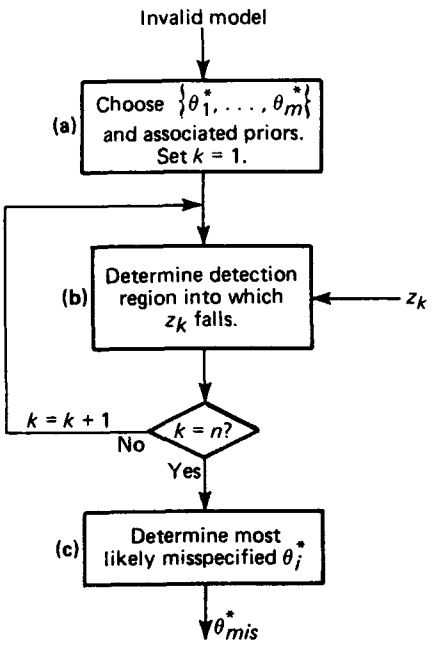

Figure 2—The steps in the EI methodology.

regions are determined by finding the roots of the equation

$$\phi_i(z) - \phi_j(z) = 0 \qquad (2)$$

for those indices i, j along the path corresponding to the lowest ϕ-curves. In Fig. 1, for example, we would be interested in finding the roots to $\phi_2(z) - \phi_3(z) = 0$, but we would not be interested in determining the roots to $\phi_1(z) - \phi_3(z) = 0$. Since it is rarely possible to solve Eq. 2 analytically, error isolation relies on a numerical procedure, stochastic approximation,[4] to find the roots. The stochastic approximation algorithm allows us to avoid the precise numerical integration usually associated with a Bayesian posterior probability such as $\phi_i(z)$ as given in Eq. 1; precise numerical integration can be computationally burdensome for multivariate integrals (as we have here) because the number of computations grows geometrically as a function of the order of the integral. Furthermore, unlike the usual Newton algorithm for finding the roots of an equation, stochastic approximation does not require derivative evaluations (which are not available here).

The basic idea behind the approach based on stochastic approximation to associating a detection region with z is as follows. At some point z_{min}, identify which ϕ-curve is lowest for all $z \in (-\infty, z_{min}]$. This can be done through knowledge of the behavior of the ϕ_i as $z \to \infty$.[5] Next, using stochastic approximation, we locate the first point at which this lowest curve intersects another curve as z moves in a positive direction along the real line (e.g., the first intersection of ϕ_2 and ϕ_3 in Fig. 1). We than proceed from that point until we identify the next point of intersection. The process is repeated until we identify the region into which the observation z falls. The input to the stochastic approximation algorithm is found by doing a crude numerical integration involving pseudorandom number generation so that the conditions of the algorithm are satisfied. The weighting of successive inputs in the algorithm, if properly chosen, damp out the errors in the approximate integration so that we get convergence to the true root. We are using crude numerical integration as a way to contain the computational burden of multivariate integration.

CONCLUSIONS

The EI methodology outlined in this article provides a way to isolate sources of errors in dynamic models that are in state space form. It is based on a form of Bayesian statistical analysis. One of its principal virtues is that the precise numerical integration usually needed to evaluate the posterior probability in a Bayesian setting is avoided. References 2, 3, and 5 discuss the methodology in significant detail, including aspects not mentioned here. For example, Ref. 2 presents a procedure, based on integer programming techniques, for controlling the probability of correctly detecting the misspecified parameter vector, and Ref. 3 presents a multivariate extension of the methodology and some results of a numerical study.

ACKNOWLEDGMENTS

M. I. Koch and J. L. Maryak have made significant contributions to the development of the EI methodology. In particular, the procedure based on integer programming and the numerical results mentioned in the Conclusions section were developed mainly by Dr. Koch.

REFERENCES

[1] T. Thompson and C. W. Meyrick, "The Satellite Missile Tracking Program," in *Developments in Science and Technology, Fiscal Year 1982*, JHU/APL DST-10.

[2] J. C. Spall, M. I. Koch, and J. L. Maryak, "On Detecting Sources of Parameter Errors in Invalid Linear Dynamic Models," in *Proc. Business and Economic Statistics Section, American Statistical Assoc.* (1984).

[3] J. C. Spall and M. I. Koch, "An Approach to Isolating Sources of Errors in Invalid State Space Models Based on Stochastic Approximation," in *Proc. American Control Conf.* (1985); also in JHU/APL PM-15865 (1984).

[4] H. J. Kushner and D. S. Clark, *Stochastic Approximation Methods for Constrained and Unconstrained Systems*, Springer-Verlag, New York (1978).

[5] J. C. Spall, *Characteristics of the Posterior Probability in the EI Methodology*, JHU/APL PSA-85-019 (1985).

This work was supported by the Strategic Systems Program Office.

A GENERAL COVARIANCE ANALYSIS PROGRAM FOR MISSILE LAUNCH AND IMPACT LOCATION SENSITIVITY ANALYSES

L. J. Levy, J. R. Vetter, T. L. Tomcsik, J. J. Gilligan, and S. A. Campbell

A generalized error covariance analysis program has been developed to evaluate the relative and geodetic survey accuracy of Deep Ocean Transponders configured in arrays for accurately measuring launch and impact locations of ballistic missiles in test firings. All the relevant error sources in the ship surveying process are modeled in a recursive Kalman filter suboptimal error analysis to allow for flexible sensitivity studies. The analysis has been used in a Deep Ocean Transponder presurvey scenario at Kwajalein Missile Range and Kwajalein Missile Range North in connection with Trident I/MX testing.

BACKGROUND

A transponder array survey is conducted to determine the latitude, longitude, and depth of each recoverable deep-ocean transponder (DOT) in a missile launch or impact array. The relative positions of the DOTs can be found acoustically by a ship passing over the array, interrogating the DOTs, and measuring the response times. The geodetic DOT positions are determined using external references (e.g., satellites such as the Navy Navigation Satellite System (NNSS)) or radio-navigation ranging stations, which locate the ship geodetically while it is maneuvering over the array (Fig. 1). The geodetic ship positions are translated into geodetic DOT positions by means of the relative acoustic measurements.

Batch least-squares techniques are used to analyze the DOT survey data. Those techniques do not model all the relevant errors inherent in the survey process, particularly systematic errors. The Missile Impact Location System Sensitivity Analysis III/General Covariance Analysis Program (MILSSA III/GCAP) was developed to evaluate the effect of neglecting relevant error sources in the survey process.

DISCUSSION

MILSSA III/GCAP is an error analysis that recursively approximates the propagation of errors in the batch least-squares survey technique. It does so by means of a variance-covariance analysis that models the errors associated with the acoustic travel-time measurements and the external geodetic measurements of the survey process. The covariance analysis, in particular, models the effect of various error sources on relative DOT positions. These include measurement biases—i.e., DOT position, watch

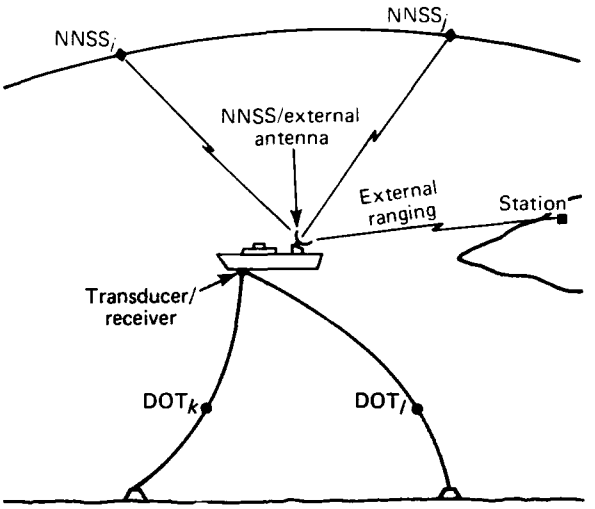

Figure 1—Geometry of MILSSA III/GCAP.

circle (the offset from vertical that a DOT makes on the end of its anchor tether), time delay, time synchronization, and velocity of sound errors—and state dynamic motion errors resulting from ship position, velocity, and attitude. It also models the effect of NNSS two-dimensional satellite fix errors on geodetic ship position and velocity (including geodetic height errors) and the effect of two- and three-dimensional external land-based position errors (for range/range and hyperbolic navigation) and transmitter timing errors on geodetic ship position. The proposed recursive analysis technique will only approximately model the error propagation in the actual batch processing survey algorithms. A complete batch processing analysis that would emulate all the iterations in the nested least-squares survey algorithms is beyond our scope at this time. However, the approximation is thought to be second order compared to the error-source and geometric-effects modeling.

The analysis is performed with a recursive covariance analysis that uses an optimal/suboptimal neglect-state Kalman filter. Variables that are estimated by the surveyor's algorithms become error estimate states for the Kalman filter. The variables or errors in variables that are neglected by the surveyor's algorithms become error neglect states for the filter. The neglect states usually represent unmodeled systematic errors. The "optimal" Kalman calculation computes Kalman gain matrices,

based on computations of the estimate-state covariance. The suboptimal Kalman covariance calculation uses the "optimally" generated gains to determine the effect of the neglected states on the uncertainties in the estimate states. A complete description of the model is given in Ref. 1.

RESULTS

A Kwajalein Missile Range presurvey scenario was used to test the analysis. It consisted of a single east-west pass of a survey ship over 10 DOTs in the lagoon of Kwajalein Atoll. Four geodetically fixed radio-navigation ground stations (external stations) on islands of the atoll were chosen. Transit navigation satellites provided geodetic fixes. The ship "pinged" the DOTs every 60 sec. If the external stations were providing geodetic fixes, they were received every 180 sec. If satellites were providing the geodetic fixes, they were received about every 90 min. Figure 2 illustrates the ship track, the 10 DOT positions, the 20 satellite fixes, and the scale of the test scenario.

All test runs modeled the collection of acoustic time measurements between the survey ship and the DOTs as the ship traversed the array. If the survey ship collected only acoustic time measurements, the test was termed an acoustic run (i.e., a relative survey). If the ship collected acoustic time measurements and geodetic fixes from satellites, it was termed a satellite run. If the geodetic fixes were from external stations, it was termed an external station run. Table 1 contains selected test results for runs of each type.

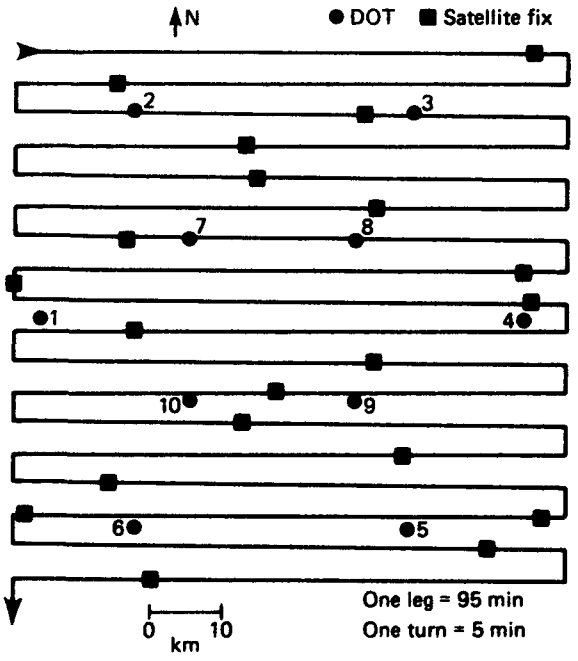

Figure 2—Geometry of the ship tracks and the DOT arrays.

In Table 1, three DOT position errors were picked for presentation. DOTS 2 and 6 were selected because they are at the beginning and end of the ship track and because they are in the outer ring. DOT 8 was chosen because it is in the middle of the ship track and in the inner ring. Ship position error, ship velocity error, sound velocity error, and DOT position error were estimated states for all the optimal runs in Table 1. For the suboptimal runs, the same states were estimated but the following were neglect states: watch circle error (all test runs), DOT timing delay error (all test runs), receiver time tag error (all test runs), transducer/antenna motion error (all test runs), satellite along-track error (satellite test runs), geodetic height error (satellite test runs), station fix error (external station test runs), and station range-measurement timing error (external station test runs).

Table 1—Selected MILSSA III/GCAP test runs.

Test Run	rss Horizontal DOT Position Error (ft)		
	DOT 2	DOT 6	DOT 8
Acoustic, optimal	5.5	11	5.5
Acoustic, suboptimal	17	20	17.5
Satellite, optimal	18	19	17
Satellite, suboptimal	25	25.5	24
External station, optimal	2	2.5	1.5
External station, suboptimal	18	18.5	18.5

The fact that optimal errors are smaller than suboptimal in all three types of test runs in Table 1 is consistent with covariance analysis theory. At Kwajalein Missile Range North (whose data set is very similar to the previous one), a survey conducted using the multipass technique[2] achieved an estimated DOT position accuracy of approximately 1.64 ft per axis, for the relative survey (equivalent to an acoustic test run). This gives a root sum squared (rss) horizontal DOT position error of approximately 2.32 ft. This error is close to the acoustic optimal errors for DOT 2 and DOT 8 in Table 1 and is reasonable because the surveyors disregard errors such as watch circle error (a neglect state that is included in the acoustic suboptimal test run). Also, in the acoustic optimal test run, only one east-west pass was made over the DOTs (fewer measurements than were used by the surveyors). DOT 6 has a larger position error because it does not come into range until later in the ship track; therefore, fewer correlations are available. More ship passes over the DOTs and different geometries tend to equalize the position errors.

At Kwajalein Missile Range North, using the multipass technique[2] with eight satellite passes and two pass-

es of the ship over the DOT array, the survey estimated that the composite DOT position error was 12.7 ft rss. The satellite suboptimal run in Table 1 using 20 satellite passes (none of which coincided with the 8 used in the multipass survey) and 1 east-west pass of the ship over the DOT array gives a composite DOT position error of 24.8 ft rss. The following results were noted:

1. The surveyors did not account for systematic errors (i.e., neglect states) such as watch circle error; therefore, the MILSSA III/GCAP errors will always be larger.
2. MILSSA III/GCAP modeled broadcast ephemeris satellite data, while the surveyors used precise ephemeris satellite data.
3. The north error (i.e., the y component) of DOTs in MILSSA III/GCAP satellite test runs will be reduced if test runs are conducted with a north-south ship pass over the DOT array.

At Kwajalein Missile Range North, Kentron International conducted the survey using external station measurements, although from different shore station positions than were modeled in MILSSA III/GCAP external station test runs. Kentron's composite DOT position error was 11.3 ft rss. The external station suboptimal results in Table 1 are approximately 18 ft. The difference is due to the inclusion of systematic errors in the external station test runs that are not included in Kentron's survey.

Individual neglect state errors (i.e., watch circle error, DOT timing delay error, etc.) were varied in different satellite suboptimal test runs to show the sensitivity of MILSSA III/GCAP to variations in individual errors. The variations in DOT position errors resulting from those test runs showed that its sensitivity to individual errors is consistent with the geometry and physics of the survey scenario.

In summary, MILSSA III/GCAP has proven to be an effective tool in analyzing the DOT's relative and geodetic survey accuracy and sensitivity to unmodeled error sources.

REFERENCES

[1] T. L. Tomcsik and J. J. Gilligan, *Missile Impact Location System Sensitivity Analysis III/General Covariance Analysis Program*, JHU/APL POR-5752 (1984).

[2] T. W. Jerardi and W. G. Innanen (APL) and B. D. Merritt (Defense Mapping Agency), *Kwajalein Test of a New Method of Open-Ocean Surveying*, JHU/APL POR-5649 (1983).

This work was supported by the Air Force MX Ballistic Missile Office.

A QUANTITATIVE DESCRIPTION OF THE TURBULENT BOUNDARY LAYER IN A SUPERSONIC ANNULAR FLOWFIELD

R. D. Stockbridge

A computational procedure has been developed for the calculation of all in-stream flow properties in a ducted supersonic flow where viscous effects are important. Experimental measurements of pitot pressures, wall pressure and temperature, and upstream plenum conditions are the input data. The procedure is distinguished by the fact that the mean flow and turbulent fluctuation results produced by it are theoretically consistent and are bounded by other experimental measurements for similar flow conditions. The procedure has been adopted for reducing test data for the combustor/inlet interaction tests in the Dual Combustion Ramjet Exploratory Development Program.

BACKGROUND

The Supersonic Combustion Ramjet (SCRAM) Propulsion Program at APL[1] demonstrated experimentally the importance of incorporating an isolator duct between the external flowfield of the air inlet and the supersonic combustor. The duct must be designed to capture completely the precombustion compression field that is positioned at the entrance to the combustor and upstream of it, thus isolating it from the the external compression field of the air inlet. It must also minimize total pressure loss as the supersonic airflow is ducted internally to the combustor.

Experimental data from the dual-combustion ramjet (DCR) exploratory development effort,[2] an outgrowth of the SCRAM program, have similarly demonstrated the need for an isolator duct to prevent undesirable combustor/inlet interactions. Accordingly, the goal of the combustor/inlet interaction (CII) experimental program is to describe the DCR isolator duct flowfield for a wide range of test conditions. The computational procedure described here will be used for that purpose.

DISCUSSION

Figure 1 is a schematic of the DCR CII test hardware currently being used to generate the experimental data to describe the isolator duct flowfield. The isolator duct has a 20.2-in.-long annulus with inner and outer radii of 3.1 and 4.2 in., respectively. The supersonic nozzle at the entrance to the duct expands cold air to Mach 2.4. In order to compute all of the flow properties at any point in the annular supersonic flow of the duct, two in-stream properties must be known.

The only in-stream property that is measured in the supersonic flow, the pitot pressure (p_t'), is measured at 21 radial positions in the 1.1-in. gap between the inner and outer walls for each of three axial positions in the annulus. It is not practical to measure independently another in-stream property (e.g., static pressure) in the existing experimental setup. The values for a second in-stream property must therefore be assumed throughout the annular flowfield if flow properties are to be computed. In addition to p_t', the only other experimental data that are available to aid in deducing the second in-stream property are static pressure measured on the inner and outer walls of the annulus, the total pressure and temperature in the plenum, and the wall temperature.

Four ways to determine the second in-stream property were investigated; in three of them the second property was chosen to be the static pressure; in the fourth it was the total pressure (p_t). The best procedure from among the four candidates evaluated is to derive a p_t

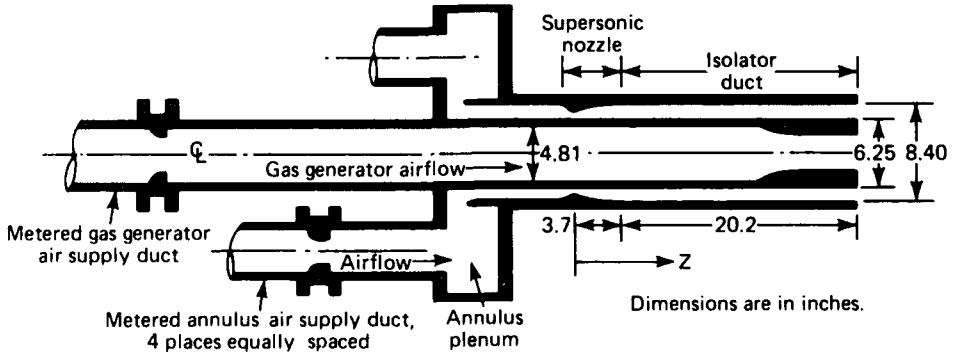

Figure 1—CII test hardware.

distribution that varies with both the radial (r) and axial (z) coordinates. This $p_t(r, z)$ distribution is designed to (a) conserve mass, (b) match the measured wall pressures, (c) ensure that the stagnation entropy never decreases in the flow direction, and (d) correctly model the effects of viscosity both in the center of the duct and next to the walls.

The procedure assumes a symmetric radial total pressure profile that is constant and equal to the plenum total pressure (p_{t_o}) over a central inviscid core at the center of the duct and is quadratic with respect to distance from the midpoint between the annular walls for the two wall regions (see Fig. 2). The quadratic curve fit allows three constraints to be imposed: zero slope at the junction of the quadratic with the central inviscid core segment, matching of the centerline total pressure, and matching of the wall pressure. The position of the junction point is determined iteratively to conserve mass. Figure 2 shows $p_t(r, z)$ for the three axial positions in the annular isolator duct for which pitot pressure measurements were made. The variable z is the distance in inches from the annular nozzle throat to the designated axial position. Figure 2 shows graphically the growth of the viscous wall region and the decay of the inviscid core as the flow progresses downstream.

The Mach number radial profile at each axial position in the CII isolator duct is established from the ratio of the measured pitot pressures and the calculated total pressures. In the inviscid core, the property gradients are zero and the local total pressure and temperature are equal to the plenum stagnation conditions. The velocity and static temperature are then calculated from the Crocco-Busemann equation[3] with a turbulent boundary layer recovery factor of 0.9.

The quantification of the viscous layer growth is the subject of Fig. 3, which presents, as a function of z, the boundary layer, displacement, momentum, and kinetic energy thicknesses. Boundary layer thickness measures the distance from either wall to the point where the local total pressure equals 99% of the plenum total pressure. This definition is recommended in Ref. 4 for turbulent supersonic flows because it removes the ambiguity that would arise if the velocity ratio were used and because it provides a common basis of comparison. It is also perfectly matched to the total pressure model used here. The other three thicknesses measure the deficit in mass flow, momentum, and kinetic energy in the boundary layer resulting from viscosity (which requires no slip at the wall). There was no change in these boundary layer results when the Reynolds number was varied from (37 to 58) $\times$ 10^6/ft. At the end of the constant area annular duct (z = 23.9 in.), the fractions of the total cross-sectional area (24.738 in^2) occupied by the various boundary layer thicknesses are 74, 13, 4.2, and 7.6%, respectively.

The above procedure for computing the in-stream flow properties in a ducted, supersonic flow where viscous effects are important has been verified by comparison with both theory and experimental data for similar flowfields. The results were consistent with respect to the magnitude of both the mean[5] and the turbulent fluctuation components[6] of the various flowfield properties of interest. Furthermore, the effort has shown that several alternative algorithms that model the in-stream static pressure rather than the total pressure were not as successful. Thus, $p_t(r, z)$ was shown to be the best variable to model, and the model presented was found to be consistent with all pertinent physical constraints.

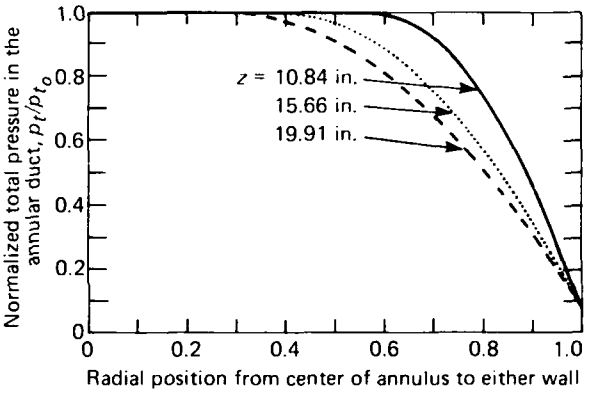

Figure 2—Assumed total pressure radial profiles in the CII duct, normalized with respect to the plenum total pressure and calculated to match the plenum and wall pressures and to conserve mass. Mach 2.4; Reynolds number (37 to 58) $\times$ 10^6/ft.

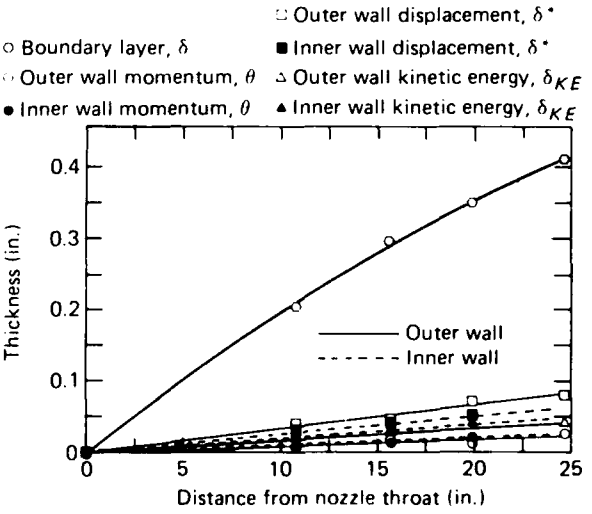

Figure 3—Boundary layer thicknesses along the annular walls in the CII duct for Mach 2.4 and Reynolds number (37 to 58) $\times$ 10^6/ft.

The application of this model along with the experimental data will provide design criteria to optimize the length of the isolator duct.

REFERENCES

[1] F. S. Billig, G. L. Dugger, and P. J. Waltrup, "Inlet-Combustor Interface Problems in Scramjet Engines," Third International Symp. on Airbreathing Engines, Munich (Mar 1976).

[2] P. P. Pandolfini et al., "Dual Combustion Ramjet Low Mach Number, High Altitude Connected-Pipe Combustor Tests," 1984 JANNAF Conf., New Orleans (Feb 7-9, 1984).

[3] F. M. White, *Viscous Fluid Flow*, McGraw Hill, New York, pp. 627-629 (1974).

[4] H. H. Fernholz and P. J. Finley, *A Critical Compilation of Compressible Turbulent Boundary Layer Data*, NATO Advisory Group for Aerospace Research and Development, Agardograph No. 223 (Jun 1977).

This work was supported by NAVSEASYSCOM. SEA-62R2.

NAVAL WARFARE ANALYSIS

INTRODUCTION

Analyses of naval warfare were first performed by APL during World War II when the Laboratory addressed the characteristics and optimum use of fire control directors. Since then, APL has continued to be involved in the analysis or assessment of Navy combat systems to investigate objectively and quantitatively how well current and future Navy systems will perform in battle.

Whereas in previous years naval warfare analysis was primarily directed toward the assessment of combat systems of individual ship types, emphasis today is on formulating concepts to improve the coordination of naval platforms of ships, aircraft, submarines, and satellites. This activity, called composite warfare analysis, is the combat use of maritime forces against enemy systems in the principal areas of antiair, antisurface, antisubmarine, and electronic warfare. Intrinsic to it are the attributes of force coordination among the warfare areas, including time and force position relationships, communications, combat system interfaces and interactions, tactics, doctrine, and training. By means of coordination, an attempt is made to achieve battle synergism among the warfare areas. Composite warfare analysis is being developed through efforts in the areas of surface warfare analysis, air warfare analysis, cruise missile analysis, technical intelligence, OPNAV studies, and analysis development.

The primary task in surface warfare is performance analysis with simulation and modeling of current and future surface combat systems covering surface-to-air missiles, combat systems, gun systems, electronic warfare, surveillance, and command/control systems. Pretest and posttest analysis and test and evaluation planning are included.

An example of work performed in the surface warfare analysis area is a methodology for developing doctrine that can be used to take advantage of the automatic control features of the Aegis combat system. Doctrine for three levels of hostile action were prepared using the methdology: the standard readiness set for peace time, the normal set for relatively limited hostile encounters, and the saturation set designed for a high density attack.

The effort in air warfare involves an analysis of the development and operational use of current and future air systems, including airborne surveillance and fire control systems, air-launched weapons like Phoenix and Harm, electronic warfare systems, and communication and data link systems. Emphasis is placed on enhancing air system performance in an environment of countermeasures and counter-countermeasures. For example, in order to optimize the jamming capability of the EF-111A tactical jamming aircraft, a Mission Data Generator computer program has been developed. It allows the EF-111A Electronic Warfare Officer to determine his jamming parameters for a given mission and also provides a way to examine various jammer configurations against a variety of threat scenarios.

The primary effort in the cruise missile area is the analysis of Harpoon and Tomahawk performance against hostile ships, patrol craft, and land targets. Current simulations have been upgraded to investigate the detailed effects of target cross section on missile performance and the capability of threat systems that use pulse Doppler radar to detect U.S. missiles.

In technical intelligence, the analysis is intended to provide a logical linking of technical information of foreign systems in the context of known physical and engineering limitations. The output of the analysis is a logical, consistent description of the item being investigated.

Work is performed for OPNAV on studies and analyses in support of wargaming and operational tactics. The wargaming effort includes the review, assessment, and development of algorithms and data. Tactics are developed and assessed in multiwarfare coordination and in individual warfare areas. To support these efforts, a Warfare Analysis Laboratory was developed in which open seminar technique games are played to support systems engineering and the assessment of naval forces and weapons systems.

Analysis development includes studies to enhance APL's capability for analyzing naval warfare. An example is the effort to specify a comprehensive set of principles for the development of scenarios to support technical evaluations. The principles identified also provide a basis for evaluating scenarios.

DEVELOPMENT OF GUIDELINES FOR THE USE OF AEGIS AUTOMATED DOCTRINE

J. G. Montanaro

A methodology for the construction and use of Aegis Combat System Command and Decision doctrine has been developed and evaluated in the APL Warfare Analysis Laboratory by means of naval warfare scenarios. The analysis findings provide guidelines for the effective use of the automated doctrine features aboard CG-47 class cruisers.

BACKGROUND

The automated control features of the Aegis Combat System bring new capabilities to the battle group for rapid threat evaluation and weapon response. Included are the automated features of the SPY-1A radar, Command and Decision (C&D) System doctrine management, Link 11 filters, the Aegis Display System, and the Weapons Control System. They provide the ship's command with a wide range of options for configuring the combat system to support battle group objectives. The task of the Aegis Mission Planning Analysis is to develop guidelines for the effective use of the automated features in a multiwarfare battle group environment. The first phase of the task examines the use of C&D System automated doctrine in that environment.

DISCUSSION

Command and Decision Doctrine

The Mk 1 C&D System aboard CG-47 class cruisers provides for the automated control of mission tasks through a concept called doctrine management, which allows the ship's command to develop a set of computer instructions to cause the C&D System to take certain actions when tracks meet certain specified criteria. The instructions are stored in the C&D System as doctrine statements. Sets of doctrine statements, when active, provide a level of automated response. Automation is required in order to obtain the combat system firepower and reaction time capabilities needed to cope with stressful threat conditions.

Track data originating from on-board radars, Link 11, and the identification friend or foe (IFF) system enter the C&D System track file. Link-11 filters in the C&D System can be used to control the classes of tracks that are to be transmitted on the link or accepted from the link. C&D System doctrine implements preplanned command decisions by initiating the specified actions. Specifically, doctrine can remove unwanted tracks from the track file, assign identity amplifications to unknown and friendly tracks, challenge tracks with IFF, alert operators, initiate engagements with appropriate weapons, and establish tight zones when tracks satisfy specified geometric, kinematic, and identification criteria. Tracks ordered for engagement by the C&D System are processed and engaged by the Weapons Control System.

The approach used to develop doctrine employment guidelines is illustrated in Fig. 1. The application of a proposed methodology for the construction and use of doctrine statements is evaluated by means of a warfare analysis process, which provides a way to refine the methodology and also provides doctrine "lessons learned" in a battle group environment. The methodology and the simulated operational experience provided by the warfare analysis process are combined with Fleet operational experience to develop guidelines for the use of Aegis Combat System doctrine.

Doctrine Employment Methodology

The proposed principles and procedures for constructing and using C&D doctrine are applicable in a wide variety of circumstances and are consistent with Naval

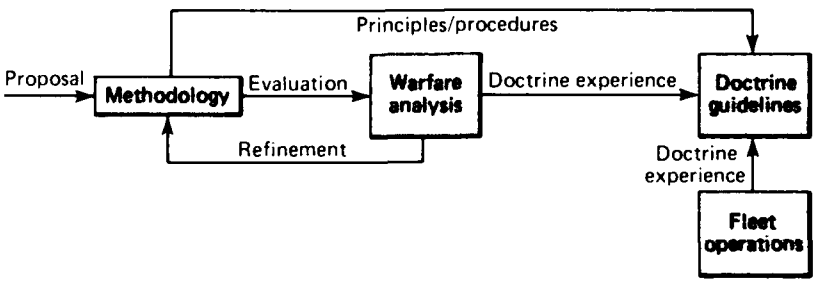

Figure 1—Development of doctrine guidelines.

tactics and procedures as specified in *Allied Tactical Procedures* and appropriate naval warfare publications. Within that context, the Composite Warfare Commander and his designated warfare commanders determine how they will use available forces to accomplish battle group objectives. The corresponding instructions and information are communicated to battle group units by means of force directives, which are issued prior to the start of an operation and are updated periodically as required.

As part of the premission planning process, doctrine for the control of the CG-47 C&D System is constructed to deal with expected and potential developments during the operation. The instruction and information required to construct the doctrine is provided primarily by written force directives such as OPORDERs and OPGENs. They include the concept of operations, rules of engagement, and own-ship tasking. Standard types of OPGENs that contain the required information have been identified.

Assumptions inherent in the proposed methodology include the following:

1. Doctrine is designed to meet the requirements of a particular operation.
2. Written directives provide the overall framework and specific parameters for the required doctrine.
3. The Aegis ship's command translates force directives into specific doctrine statements.
4. The activation of doctrine statement sets is based on coordination and control procedures, preplanned responses linked to reports and detections, and orders from the Composite Warfare Commander and his designated warfare commanders.

The overall doctrine construction process is illustrated in Fig. 2.

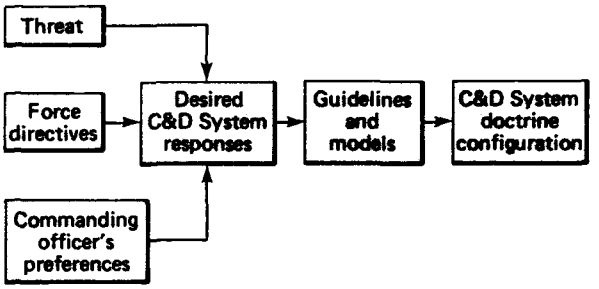

Figure 2—Methodology for doctrine construction.

Warfare Analysis

The proposed methodology for the construction and use of Aegis doctrine was evaluated by means of a warfare analysis procedure that uses an open seminar form of wargaming. Doctrine has been evaluated in two scenarios to date. The first involved a freedom-of-navigation exercise in international waters claimed by a third world country as sovereign territory. The second involved a preemptive attack by Soviet surface, subsurface, and air forces. Both encounters occur in the Mediterranean Sea in the 1985-1988 time frame.

Doctrine statements prepared for each operation are grouped into three sets, each designed to deal with a different level of hostility. The Standard Readiness set, intended for use in a peacetime situation, is characterized by the absence of weapon engagement statements. *Identification, IFF, and alert statements are used to assist in obtaining and maintaining a coherent air picture.*

The Normal set is designed to deal with a relatively limited hostile encounter, to be activated when such an encounter is imminent or in progress. That set of doctrine statements includes weapon engagement statements having a limited degree or automaticity, estimated to be sufficient for such an encounter. A substantial degree of manual control is retained in order to implement the rather restrictive rules of engagement in effect. Criteria for classifying targets as "assumed enemy" are biased toward avoiding the engagement of nonthreat tracks.

The Saturation set is designed to counter a high-density attack intended to saturate our force's air defenses. Such an attack is considered possible in the Mediterranean location. That set incorporates fully automated engagement modes and identification criteria biased toward engaging all but friendly tracks. Thus, combat system responses appropriate for a range of contingencies could be obtained by activating the corresponding doctrine statement set.

Specific parameters to define the various identification, IFF, alert, and weapon selection doctrine are derived from assigned areas of responsibility for surveillance, air intercept, area defense, and safety. The degree of engagement automation reflects the rules of engagement and prescribed coordination procedures among units and warfare commanders.

Doctrine sets prepared in accordance with the methodology were evaluated in the operational environment prescribed in the scenarios and evolving during the warfare analysis exercise. The exercise was conducted in the APL Warfare Analysis Laboratory, which provided database, computational, display, and records support. As the scenario progressed, doctrine statement responses to the track environment were examined and evaluated. Computer algorithms prepared for the investigation assisted in the process. Both during the exercise and in the subsequent analysis, the automated responses were evaluated for correctness and adequacy. Doctrine performance

was assessed in terms of the degree to which the doctrine provided the intended and desired responses. In a broader context, the compatibility of current force tactics with Aegis ship capabilities is also examined. In effect, all aspects of Aegis doctrine employment in the battle group environment are examined in order to maximize its effective use.

ANALYSIS FINDINGS

The findings provide a basis for developing doctrine employment guidelines and for defining C&D System design changes that can be incorporated into planned Aegis block upgrades. The simulated tactical experience also provides "lessons learned" that may be applicable to similar tactical situations. Issues raised from the analysis generally involve questions on how current force procedures might be modified to better accommodate and exploit Aegis ship capabilities. They identify areas that will require further investigation as Fleet capabilities and tactics evolve.

Overall, the efficacy of the proposed methodology for preparing and using Aegis doctrine was demonstrated. Over 30 findings and issues were identified by the analysis. The findings indicate that the effective application of Aegis doctrine requires a thorough knowledge of threat characteristics, own-weapons capabilities, Aegis combat system characteristics, the battle group concept of operations, and the role of the Aegis ship in supporting the battle groups objectives. Among the possible design improvements is one that recommends that criteria entries for range and bearing relative to a defined point be allowed so that fire zones, safety sectors, and corridors defined in force directives relative to force center may be modeled accurately by doctrine statements. Also, allowing inbound/outbound criteria to be specified relative to other units would provide a way to distinguish threat tracks from weapons fired by the units.

There are several findings that support the development of doctrine employment guidelines. The selected automation level for Standard Missile engagement should take into consideration weapons loadout, coordination with other ships, and engagement restrictions requiring operator decisions. The desired level of engagement automation can be obtained by using reduced-range-automatic and maximum-range-semiautomatic doctrine statements. When weapon engagement statements are activated by pushing a button, the safety measures provided by associated tight-zone statements can be obtained simultaneously only by preactivation of the tight-zone statements. The findings primarily address the methods and difficulties associated with implementing force orders and procedures within the scope of C&D System doctrine design.

This work was supported by NAVSEASYSCOM, PMS-400.

MISSION DATA GENERATOR FOR THE EF-111A TACTICAL JAMMING AIRCRAFT

G. S. Norcutt

A Mission Data Generator computer program has been developed to provide a resource management capability for the U.S. Air Force's EF-111A tactical jamming aircraft. Resource management is central to the mission planning process in preparing the EF-111A aircraft for its various jamming roles, including stand-off (barrier), close-in support, and penetration/escort. The program allows the EF-111A Electronic Warfare Officer to determine the jamming parameters for a given mission in a manner of minutes instead of days. It also provides a way to examine various jammer configurations against a variety of threat scenarios in order to determine optimum jammer loadout for the EF-111A.

BACKGROUND

The ALQ-99 Tactical Jamming Subsystem aboard the EF-111A includes up to 10 transmitters; each can generate several jamming spots and a variety of jamming

modulations. An Electronic Warfare Officer provides the Tactical Jamming Subsystem with data before each mission to tell it how to respond to the threat environment. Threat radars, including early warning, acquisition, and ground control intercept, may number in the hundreds (Fig. 1). The mission data instruct the Tactical Jamming Subsystem which frequencies to look for and which modulations to use when jamming is required.

The Electronic Warfare Officer must provide mission data for several EF-111A aircraft, accounting for mission type, threat parameter and location, changes, special priorities, and jammer availability.

Currently, APL produces for electronic combat squadrons the EF-111A Employment Guide document, which describes each threat radar and recommends the one-on-one jamming modulation to be used. In a moderate to heavy threat environment, the process of manually determining the mission data for a one-on-many jamming response can take the officer a matter of days to prepare. He must be very knowledgeable not only of the ALQ-99 Tactical Jamming Subsystem, but also of various threat peculiarities, and he must be able to perform his tasks anywhere the EF-111A may be deployed. The Mission Data Generator enables him to generate the necessary data very quickly and accurately. It also provides an analysis tool to investigate the effects of various possible solutions of jamming response against a changing threat scenario.

DISCUSSION

The Mission Data Generator computer program is written for the U.S. Air Force standard microcomputer (the Zenith Z-150). The computer's small size (desk top) allows it to be easily deployed with the squadron for on-site tactical use.

Figure 2 is a functional block diagram of the program. Threat radars for a given mission are entered in the form of a premade threat scenario data file, or they may be entered while "on line" with the generator. Threat scenario data include only the radar names and their locations. The generator contains a library of threat-radar data parameters and their respective one-on-one jamming modulations. The threat scenario is combined with the respective radar parameter data, mission geometry, and EF-111A jammer assets to derive a one-on-many jamming response solution.

The primary results of a program run are listings of mission data and of the desired transmitter load-out to be installed in the aircraft to counter the given threat scenario. Additional output information allows the operator to view a frequency plot in each band of the threats encountered, of the jamming response coverage, and of the receiver list coverage. Numerical parameters for each item that is plotted can be viewed easily.

The program evaluates the threat and determines the bands, the number of transmitters per band, and the appropriate modulations that are required to cover the threat. It also allows the operator to fix the transmitter load-out in advance or to fix some bands and let the processing vary the rest as needed.

The processing is strongly controlled by priority. On the basis of the mission role, the program handles different threat types with different priorities. Specific threats of special interest may be given a higher priority to ensure that ample jamming assets are assigned against them.

The high speed of the processing allows the operator to run the program many times to examine various

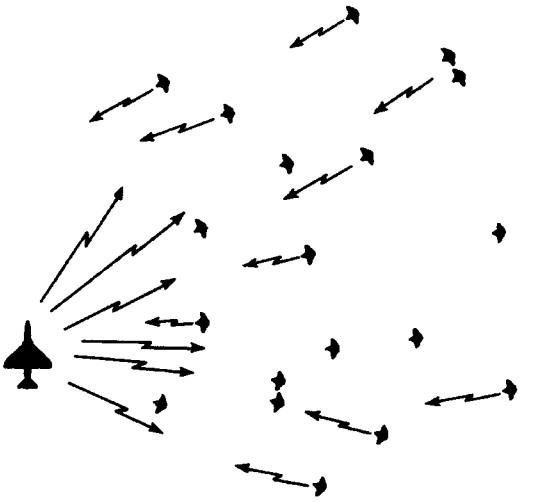

Figure 1—One EF-111A aircraft versus possibly hundreds of threat radars (early warning, acquisition, and ground control intercept).

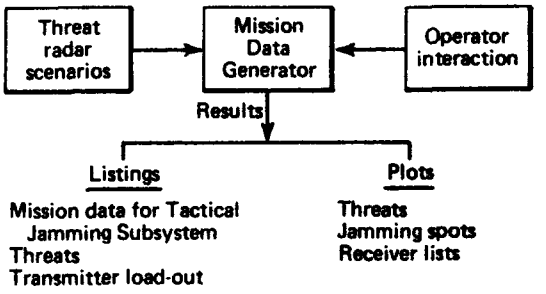

Figure 2—Functional block diagram of the Mission Data Generator.

aspects of different transmitter load-outs or jammer locations with respect to the threats. The recommended approach is to let the processing be fully automatic in selecting the required transmitter load-out for the first run and then to fix the load-out in a slightly different way for a rerun to evaluate the difference in jamming coverage.

During the processing, a hard copy record can be made of input and output data and of selections made during operator interaction.

The Mission Data Generator enhances the capability of the EF-111A electronic combat squadron by providing fast and accurate jamming mission data wherever the squadron is deployed.

This work was supported by the USAF Tactical Air Command.

PRINCIPLES FOR SCENARIO DEVELOPMENT AND EVALUATION

D. K. Pace

A relatively comprehensive set of principles for the development of scenarios to support technical evaluations has been specified. The application of those principles can improve the quality of scenarios used in a broad spectrum of both civilian and military analyses. The principles also provide a basis for evaluating scenarios.

BACKGROUND

The course given at APL on System Simulation and Modeling, for The Johns Hopkins University's Master of Science degree in Technical Management, contains a session on scenarios. Although scenarios are widely used in analyses, technical evaluations, and wargames and are recognized as having a major effect on their outcomes, "scenario development and evaluation remain an art without much discipline."[1] Thus, Dr. A. Kossiakoff, program chairman for the Technical Management Program, initiated a research project to produce a set of principles for the development and evaluation of scenarios to be used in technical evaluations and analyses.

Status

That research project produced an initial set of principles for scenario development and evaluation.[2] Those principles are now being reviewed (fall of 1984) by personnel at APL, OPNAV, Sandia and Los Alamos National Laboratories, Yale University, The Rand Corporation, the Naval Postgraduate School, and the Naval War College (which has begun to use them for the development of scenarios for wargames). Their general publication for scenario development, expected in the near future, will provide a first step in identifying and describing principles and procedures for scenario development and evaluation.

DISCUSSION

What Is a Scenario?

The term scenario originated in drama but now is used in artificial intelligence, wargaming, management gaming, and technical analyses. Connotations given to the term vary somewhat with the area of application, but in general a scenario is "a statement of assumptions about the operating environment of the particular system"[3] being studied, tested, or used. This is a broad definition. For example, it defines the collection of inputs for a computer simulation of a system in conjunction with the assumptions built into that simulation as a scenario. Consequently, it is apparent why a casual attitude toward the scenario is identical with a casual attitude toward the evaluation criteria used in analyzing a system. A system, in this definition of a scenario, may be as simple as a single item of equipment or as complex as a large military force or even an entire nation involved in a wargame analyzing global conflict.

Factors Affecting Scenarios

Scenarios have no generic value, at least as far as technical evaluations and analyses are concerned. They are only valuable as they support the objectives of an evaluation of the analysis of a system. Thus, the focus, scope, and character of a scenario will be shaped by the objectives of the technical evaluation, and its quality will be determined by how well it supports those objectives.

The personnel involved in scenario development are critical, yet few have had any formal training in the field. Such training is essentially nonexistent.[4] Scenario developers need access to (and influence with) both the decision maker for whom the technical evaluation is being done and the leader of the evaluation. Scenarists should be smart, well-trained, creative, familiar with models and analysis tools likely to be used in the evaluation, experienced in the area of the evaluation, good communicators, and patient enough to review and revise the scenario as often as needed; they also should possess good judgment, courage, and diplomatic perseverence.

Good scenarios are usually developed iteratively through several trial applications. They provide an adequate context for all persons involved in the evaluation to share a common view of the problem; are internally consistent, credible, and complete; and do not contain extraneous material. A clear and explicit definition of the objectives and scope of the technical evaluation is essential for developing a good scenario, as is a comprehensive analysis plan for the evaluation. Scenarios should be reviewed by experts, should undergo some form of validation, and should have adequate documentation.

Three types of parameters should be included in a scenario: (a) those required to support models, simulations, and other calculation procedures to be used in the evaluation, (b) those required logically by objectives of the technical evaluation, and (c) those required to provide an adequate context for the scenario. The parameter values should be within the bounds of logic (e.g., probabilities always less than or equal to one), physical laws, and technical feasibility. They should be relatively consistent (e.g., all *worst case* or all *nominal* conditions) except when the objectives of the technical evaluation dictate otherwise. Hidden assumptions must be searched out and stated explicitly.

The Impact of a Good Scenario

The relationship between a good (or bad) scenario and the outcome of a wargame or technical evaluation is unclear. Good analysts or game controllers/players can overcome scenario deficiencies. Likewise, a good scenario will not guarantee a quality technical evaluation. But application of the principles that produce a good scenario will facilitate a more insightful and better analysis, technical evaluation, or wargame. The effort required to develop a good scenario will be a substantial portion of the total analysis commitment in a technical evaluation and should be provided for in planning the total effort.

REFERENCES

[1] C. H. Builder, *Toward a Calculus of Scenarios,* The Rand Corporation N-1855-DNA (1983).

[2] D. K. Pace, "Scenarios for Technical Evaluations" (in process, 1984).

[3] S. Brown, "Scenarios in Systems Analysis," in *Systems Analysis and Policy Planning: Applications in Defense,* E. S. Quade and W. Boucher, eds., American Elsevier Publishing Co., New York (1968).

[4] G. D. Brewer and M. Shubek, *The War Game: A Critique of Military Problem Solving,* Harvard University Press, Cambridge, Mass. (1979).

This work was supported by The Johns Hopkins University Whiting School of Engineering.

SPACE SCIENCE AND TECHNOLOGY

INTRODUCTION

APL's involvement in space programs began in the postwar years when Aerobee and captured V-2 rockets carried Geiger tubes, magnetometers, and optical spectrometers high above the earth's surface. The flights provided the first high-altitude measurements of cosmic rays, the geomagnetic field, and atmospheric constituents. In 1946, a Laboratory camera aboard a V-2 rocket returned pictures of the earth from an altitude of 100 miles.

From these postwar beginnings, APL's activities in space expanded to include the conception, design, and development of the Navy Navigation Satellite System (Transit), starting in 1958, and other programs in basic space research and in space applications for Navy, DoD, and NASA sponsors. Currently the thrust of the Laboratory's space effort is organized into three broad areas: solar and space physics, space geophysics, and space applications.

The goal of APL's program in solar and space physics is to explain principles governing the energy flow between the sun and the earth. Of particular interest are charged particles and magnetic fields in interplanetary space and in the earth's magnetosphere. The NASA Active Magnetospheric Particle Tracer Explorer (AMPTE), launched on August 16, 1984, is providing information on how solar wind plasma enters the earth's magnetosphere. AMPTE consists of three spacecraft: the Charge Composition Explorer (CCE) (provided by APL), the Ion Release Module (provided by the Federal Republic of Germany), and a United Kingdom subsatellite.

An experiment that was developed for the International Solar Polar Mission (ISPM) has been successfully integrated into the European ISPM spacecraft. That spacecraft is scheduled for launch in 1986 and will make particle and field measurements as it orbits the sun's poles from 1989 to 1991. Particle and field instruments built by APL that are aboard the Voyager spacecraft and that were successfully used during the spacecraft's encounter with Jupiter will be used again when the spacecraft encounters Uranus. The Energetic Particle Detector was completed in 1983 for the NASA/Galileo (Jupiter Orbiter) Mission. The instrument has been integrated into the spacecraft, which will undergo final environmental testing in 1985.

Analysis continues of data from the HILAT (high latitude ionospheric research) satellite that APL launched in 1983 under sponsorship of the Defense Nuclear Agency and the Air Force Space Test Program. A follow-on to this mission, in the design phase, is known as the Polar Beacon/Auroral Research (Polar Bear) Satellite Program. The Hopkins Ultraviolet Telescope experiment is a collaborative effort with The Johns Hopkins University Physics Department to study the far ultraviolet spectrum of faint astronomical objects.

Major activities in space geophysics include radar altimeter programs and one satellite program, in addition to numerous research and engineering development efforts. The Navy is sponsoring the development of the Geosat Radar Altimeter and the supporting satellite, Geosat-A, which will obtain data for a preci-

sion determination of the geoid. NASA is sponsoring the development of an advanced technology demonstration model of the radar altimeter for the Topography Experiment for Ocean Circulation. Radar propagation research for several sponsors is under way as are activities involving use of the Seasat Synthetic Aperture Radar data products to perform ocean wave imaging and spectral studies.

Space applications encompass a wide range of programs, primarily for DoD and NASA. Among them is the Transit Program, which remains the nation's only fully operational worldwide satellite navigation system. Work on this program includes assisting the Navy Strategic Systems Projects Office and the Navy Astronautics Group in software development associated with the operation of the navigation system. It also involves technical assistance and review of the Transit spacecraft production contractor (RCA), selected participation in the in-orbit operation of the spacecraft, and modification and requalification of the Nova (the current Transit) spacecraft. Other Transit-related work includes developing precision time and frequency equipment, surveying test instrumentation locations, and developing and fabricating Doppler beacons. The Global Positioning System (GPS) is expected to be the eventual replacement for the Transit system. The Laboratory is engaged in work to provide the use of GPS for spacecraft navigation and missile tracking.

Twelve articles have been chosen for inclusion in this volume—eight related to solar and space physics, two to space geophysics, one to space applications, and one to all areas.

Of the eight articles in the solar and space physics area, five discuss the AMPTE/CCE spacecraft, the CCE attitude control and detection system, AMPTE postlaunch operations, the AMPTE science data center, and initial science results from the CCE medium energy particle analyzer. The sixth discusses completion of the Hopkins Ultraviolet Telescope, now undergoing final environmental test prior to delivery to NASA next March. The last two discuss investigations of safety issues related to the radioactive power systems to be used in the Galileo and other missions.

The two articles in the space geophysics area discuss upgrading of the APL Satellite Tracking Facility in readiness for the launch of Geosat-A next March, and study of the Synthetic Aperture Radar data obtained from the Seasat spacecraft.

In the space applications area, the Teflon coating of hydrogen maser storage bulbs is part of the continuing effort in support of precision time and frequency standards.

An article on reliability and quality assurance aspects of dual-in-line package mountings is applicable to all space-bound circuitry that uses such packages.

THE AMPTE CHARGE COMPOSITION EXPLORER SPACECRAFT

J. Dassoulas

On August 16, 1984, at 1048 EDT, the three AMPTE (Active Magnetospheric Particle Tracer Explorers) spacecraft (Charge Composition Explorer, Ion Release Module, and United Kingdom Satellite) were placed in orbit by a NASA launch vehicle. After a series of maneuvers, the satellites reached their final orbits within 17 hours following launch. All spacecraft subsystems and experiments were exercised prior to the opening of the solar wind release window (from September 3 to 28, 1984). The Charge Composition Explorer, designed and fabricated by APL for NASA, continues to perform flawlessly, meeting all of its expected performance requirements.

BACKGROUND

The AMPTE spacecraft will release and monitor tracer ions (lithium and barium) in the solar wind and within the distant magnetosphere. The objective is to study the access of solar wind ions to the magnetosphere and also the convective-diffusive transport and energizing of magnetospheric particles. The Charge Composition Explorer (CCE), with an apogee of about 8.8 R_e geocentric, is the primary platform for detection of the released ions.

DISCUSSION

CCE was designed to meet the mission requirements determined by the Science Working Team. The spacecraft carries five experiments, three of which (Hot Plasma Composition, Charge-Energy Mass, and Medium Energy Particle Analyzer) are devoted to comprehensive measurements of rare ionic species, while the Plasma Wave Experiment and the Magnetometer provide supporting plasma wave and field information.

Although there appeared to be abundant weight and volume available at the outset of the AMPTE Program, engineering realities quickly narrowed the margins, resulting in a lift-off weight of 242 kg. This was somewhat larger than anticipated but still within acceptable limits for the launch vehicle. Our first thoughts were to design a spacecraft based on past experience and to make use of the natural environment. Because the CCE would be required to perform several maneuvers before arriving at its final orbital position and then would have to be torqued to maintain solar panel orientation to the sun, a magnetic attitude control system was envisioned. It consisted of a spin/despin system and a torquing coil, with the magnetic reference to the earth's field provided by a triaxial vector magnetometer. As is often the case when a composite design is viewed, there was a power balance problem.

The diameter of the spacecraft was chosen to provide a torquing coil of such size that the current drawn would be minimized. As the detailed design evolved, we found that even this large coil would draw excessive current from a generously sized battery pack, thus putting us in a high-risk situation during the maneuvering phase of the mission. To remedy the situation, a cold-gas attitude control system was implemented. It provided spin, despin, and attitude orientation and became the primary system during the maneuvering phase, while the magnetic system was retained for use during the cruise (operational) phase. The cold-gas enabled us to perform attitude maneuvers rapidly and prior to the first apogee crossing after orbit insertion. It removed the possibility of power starvation during the portion of the trajectory in which the solar panels were stowed against the body of the spacecraft.

Another facet of the design was to place the instruments in locations on the spacecraft that would permit them clear fields of view, unobstructed by the solar panels or by other spacecraft appendages. All of the instruments and spacecraft electronics were mounted on a honeycomb deck, which was supported structurally by a center column and radial struts (Fig. 1). This provided a simple, lightweight structure compared to the weight of the components that it was to support. The center column was sized so that it could contain a solid propellant rocket motor that was used to change the inclination of the orbit plane. This motor was thermally isolated from the spacecraft to avoid excessive heat loss as a result of radiation.

The thermal design of the spacecraft consisted of multilayer blanket insulation installed over the body and four temperature-activated louvers mounted in critical locations to radiate or contain heat, as the case may be. The spacecraft had a viable thermal design in the launch mode when spin-stabilized with the solar panels and magnetometer stowed and also after maneuvering was completed and the spacecraft was on-station with the solar panels and magnetometer deployed. In the operational phase, the spacecraft is maintained between 10° and 30° of the earth-sun line, with radiators and louvers oriented away from the sun.

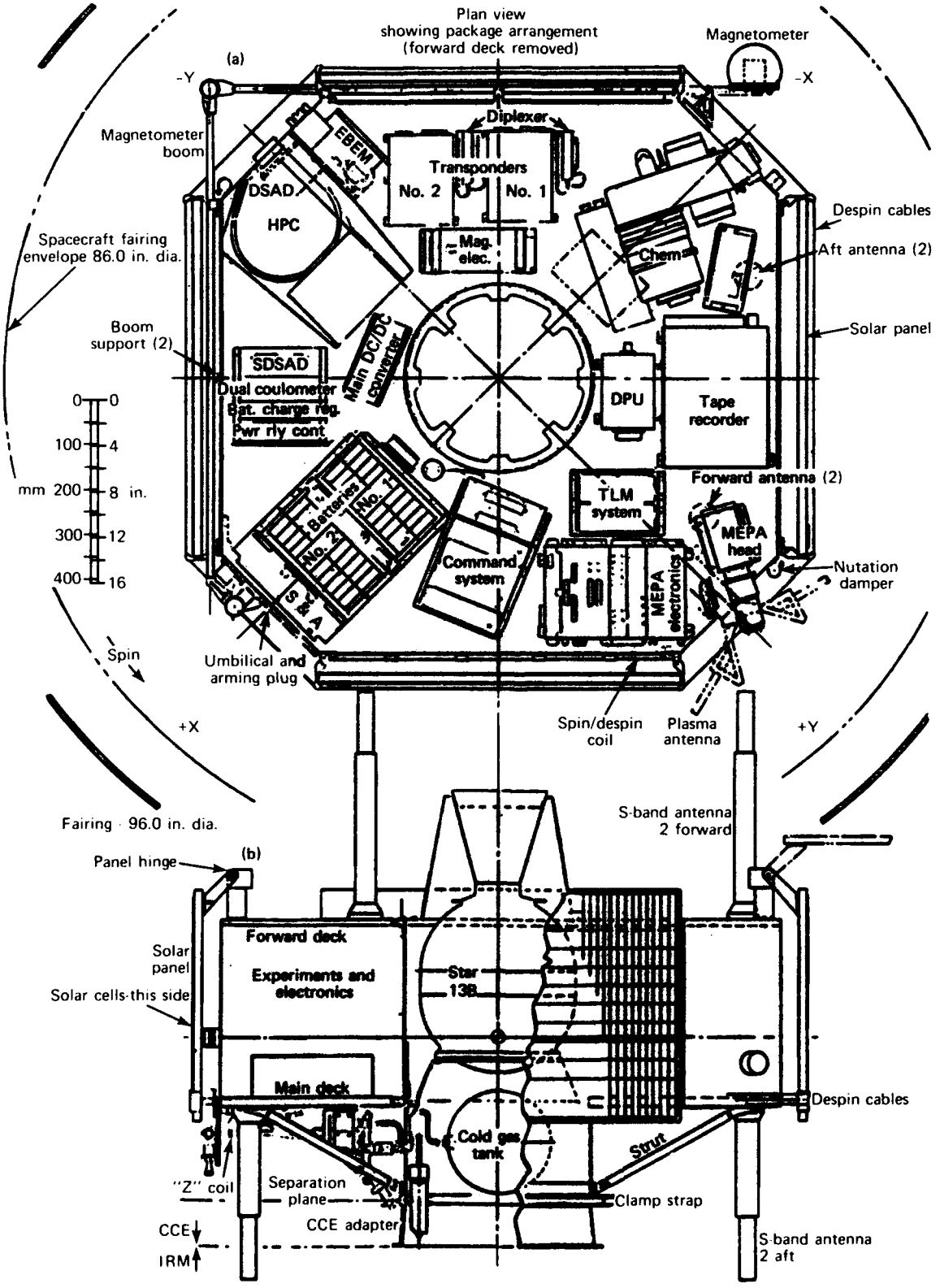

Figure 1—Package arrangement of the CCE spacecraft, (a) view from the top, and (b) view from the right side.

Communication with the spacecraft is accomplished through standard NASA S-band transponders and four antennas that may be RF-switched in pairs, depending on which side of the spacecraft is visible to the ground observing stations. Because of the amount of data required and possible priority problems concerned with arranging a schedule with the Deep Space Network, a tape recorder was carried on the spacecraft. The tape recorder "dumps" its data to an observing Deep Space Network station once per orbit. Real-time operations in addition to tape storage are carried out during canister release operations of the Ion Release Module (IRM). The real-time operating mode will be implemented if tape recorder malfunctions are encountered.

On August 16, 1984, at 10:48 EDT, the three spacecraft were injected into the elliptical transfer orbit by a single Delta 3924 launch vehicle. The initial orbit was within acceptable bounds. Approximately one hour and thirteen minutes after launch, the CCE separated from the other satellites. After verification of proper attitude and spin rate, the CCE executed a maneuver to place it in the proper attitude for firing the inclination change rocket. Its spin velocity was increased by firing the appropriate cold-gas jet prior to motor ignition. This increase in rotational energy was necessary to maintain spacecraft stability during the 16 sec burn of the inclination change rocket, which placed the CCE into an orbit of 1108 km perigee altitude, 49,684 km apogee altitude, an inclination of 4.8°, and a period of 15.66 hr, thus assuring fulfillment of the science requirements with respect to orbit characteristics. The AMPTE science mission can now begin. Post-launch operations are described in detail elsewhere in this volume.

ACKNOWLEDGMENTS

The author respectfully acknowledges the accomplishments and competence of the technical and administrative staff who placed AMPTE among the long line of outstanding achievements that have accrued since the launch of the first Transit, 25 years ago.

This work is supported by NASA.

COMPLETION OF THE CCE SATELLITE ATTITUDE CONTROL AND DETECTION SYSTEMS

F. F. Mobley, J. F. Smola, L. Scheer, W. A. Swartz, J. C. Ray, and J. D. Steinberg

The attitude control and detection systems for the CCE (Charge Composition Explorer) satellite were under active engineering development and testing at APL from 1981 until they were integrated with other satellite subsystems in early 1984. The satellite was launched successfully in August 1984. Post-launch performance of the satellite is discussed elsewhere in this volume.

BACKGROUND

The CCE attitude control system design, first considered in 1977, achieved attitude stabilization by spinning the satellite at 10 rpm and using magnetic coils to control the spin-axis orientation and spin rate. When a solid rocket for orbit inclination adjustment was later added to the design concept, the need arose to spin at about 100 rpm during firing of the inclination adjust rocket. Attitude maneuvering by magnetic coils at 100 rpm is very slow, so a cold-gas torquing system was added to the design to expedite the required maneuvers and spin rate changes. The attitude is determined by analyzing data from the Digital Solar Attitude Detector (DSAD) system and a three-axis vector magnetometer.

DISCUSSION

The attitude control system hardware consists of a Z magnetic torquing coil, an XY magnetic spin/despin

coil, two nutation dampers, a cold-gas torquing system, a digital sun sensor and thruster control system, a three-axis vector magnetometer, and a magnetometer boom. Figure 1 identifies these elements on the satellite configuration drawing.

The satellite is spin stabilized at 10 rpm except during firing of the inclination adjust rocket, when it is stabilized at 100 rpm. The two nutation dampers use small tungsten carbide spheres in nitrogen-filled tubes to damp nutations to near zero. The Z coil, turned on by command from the ground, interacts with the earth's magnetic field and precesses the Z axis in a predetermined direction. The angle between the Z axis and the sun line is maintained in the range of 10° to 30°.

The XY magnetic coil (not shown in the figure) is activated by the X magnetometer sensor to increase or decrease the spin rate.

The cold-gas torquing system has a pair of opposing nozzles in the XY plane to increase or decrease the spin rate upon command. A second pair of nozzles parallel to the Z axis may be operated singly or concurrently. These thrusters are repeatedly cycled on for one-fourth of a satellite revolution and off for three-fourths. Thus, a net torque perpendicular to the Z axis is produced that precesses the Z axis to the desired direction in space. The "phasing" of the "on" time is achieved by a command to the DSAD system. After the sun crossing, an 8-bit command word tells the DSAD system when to begin the maneuver thrusting. It is turned off one-fourth of a revolution later. This on/off process is repeated every revolution until a ground command is received to turn off the thrusters and stop the maneuver.

The propellant, Freon 14, is stored initially at 2800 psia, regulated to 50 psi, and exhausted through the thruster nozzles. It develops a specific impulse of 40 lb thrust per pound mass per second. The tank, regulator, and valves were supplied by Sterer, Inc. and integrated by APL into the CCE design.

The DSAD and maneuver thruster control systems consist of one electronics package and two sun sensors. They have the following functions:

1. Detect the sun crossing of the sun sensor azimuth and record the angle between the sun line and the satellite Z axis.
2. Generate 255 evenly spaced pulses between sun pulses for use by the scientific instruments in the azimuthal segregation of the data.
3. Upon command, turn on and off one or both of the cold-gas maneuver thrusters at a specific phase angle relative to the sun pulse.

Full redundancy is included in the sun sensor system. There are two sun sensors, and two identical electronic boards, one for each sensor. Only one system may be commanded on at any one time.

The three-axis vector magnetometer (which is used for attitude determination and scientific research) consists of a three-axis sensor at the end of an 8 ft boom and an electronics package with the following:

1. An analog electronics section that provides seven ranges of operation from ±65,500 to ±16 nT (1 nT = 10^{-5} gauss = 1 gamma),
2. A digital electronics section that converts three analog voltages to three 13-bit digital words and assembles the sampled data into a message of 200 bits containing five full vector samples to be read out every 0.62 sec,
3. Two AC filter and peak detector circuits to collect data from the magnetometer in the frequency range of 5 to 50 Hz,

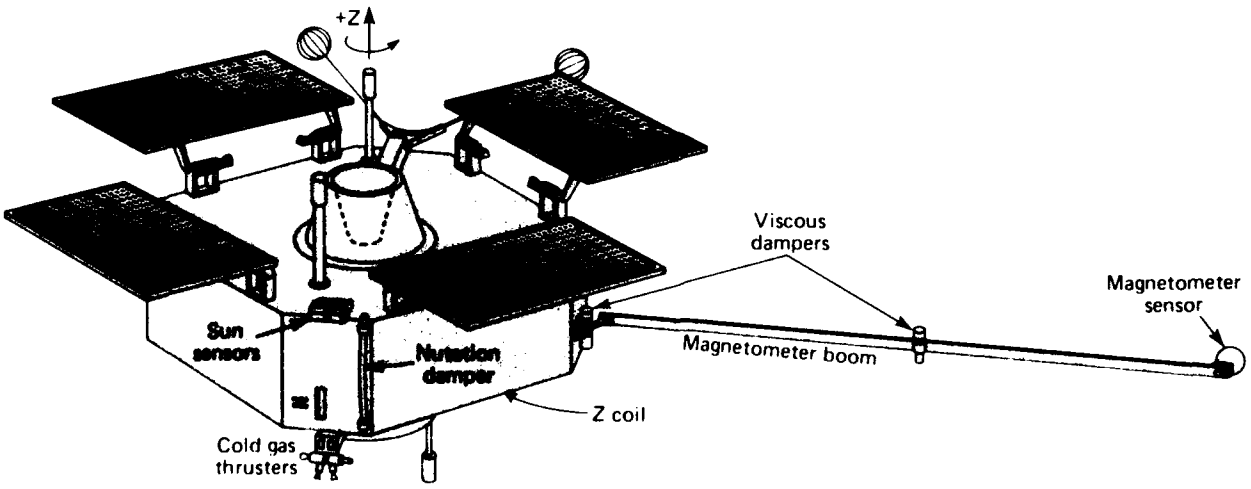

Figure 1—External components of the attitude control and detection systems of the CCE satellite.

4. Circuitry to amplify the X magnetometer analog voltage and drive the XY coil to change the satellite spin rate (upon command only),
5. Circuitry for the plasma wave detector instrument.

The magnetometer boom consists of two rigid links, each about 4 ft long, of a rectangular tube of aluminum alloy. The shoulder and elbow joints are spring-loaded to ensure positive torque at full extension; there also are viscous dampers to prevent excessive angular rates and loads during deployment.

CONCLUSION

All system elements were custom-designed for the requirements of the CCE mission and then were fabricated, tested, and integrated with the satellite. The performance in orbit is discussed in detail elsewhere in this volume. Briefly, all systems have performed in a completely successful fashion.

ACKNOWLEDGMENT

Assistance in the design of the vector magnetometer system was provided by Dr. Mario Acuna of Goddard Space Flight Center.

This work was supported by NASA Goddard Space Flight Center.

AMPTE POST-LAUNCH OPERATIONS

W. E. Radford and J. C. Ray

The Charge Composition Explorer spacecraft, launched on August 16, 1984, as part of the AMPTE (Active Magnetospheric Particle Tracer Explorers) project, was operated through a complicated series of attitude maneuvers, spin rate adjustments, and a solid rocket burn to change its orbital inclination. This is the first time that APL has carried out interactive, closed-loop, real-time maneuvering of a spacecraft.

BACKGROUND

AMPTE is a three-satellite project of the United States, the Federal Republic of Germany, and the United Kingdom. Its purpose is to use artificial injection of rare ionic species for the long-range tracing of mass transport into and through the magnetosphere.

The U.S. satellite, the Charge Composition Explorer (CCE), was designed and built by APL. It includes experiments from the University of Maryland, APL, and the Lockheed Corp. The experiments require that the orbit plane lie within 5° of the equatorial plane of the earth and that perigee be no less than 550 km and apogee 7.75 earth radii. However, the Delta 3924 launch vehicle could only achieve the required apogee and perigee at an orbital inclination of 28.7°. Therefore, the task was to change the inclination of the orbit from ≈28° to less than 5°. The two orbits are depicted in Fig. 1.

DISCUSSION

The CCE was equipped with a rocket motor, a sun sensor, a magnetometer, a delayed command system, and a cold gas torquing system that can be used both to change the satellite's spin rate and to maneuver the spin axis.

The inclination adjust rocket is a Thiokol Star-13-B, with 41 kg of propellant providing a velocity impulse of 525 m/sec. It is fired cross-orbit at apogee (Fig. 1) to change the inclination. After separating from the Delta rocket, the CCE is spinning at 60 rpm about a spin axis in the orbit plane. Before apogee is reached, the spin axis must be reoriented about 100° to the cross-orbit direction by means of the cold gas torquing system, which uses pulsed Freon thrusters to generate torques. The pulses are triggered after a specified delay after the

Figure 1—The CCE orbits before and after adjustment

sun sensor crosses the sun line. The specific delay word to achieve any desired torquing direction is computed on the ground and up-loaded into the spacecraft.

The inclination adjust rocket is fired at apogee, where the velocity is lowest, to maximize inclination change for the available velocity impulse. However, perigee altitude is also most sensitive to a change in velocity at apogee, and the rocket firing direction is critical in preventing lowering of the perigee and reentry. Attitude is determined by comparing sun sensor and magnetometer measurements to modeled values. The earth's magnetic field strength, and hence the accuracy of our model of its direction, decreases rapidly with altitude. Those considerations required that the reorientation maneuver be completed within about the first 30 min after injection (at perigee) in order to confirm that we had the correct attitude for rocket firing at first apogee.

To accomplish the maneuver, the system shown in Fig. 2 was evolved. Satellite telemetry data are collected at the Jet Propulsion Laboratory (JPL) from various worldwide ground stations and transmitted via the NASA communications network data line to the AMPTE Science Data Center VAX computer at APL. Real-time telemetry decommutation, attitude determination, and CRT display software were developed and tested thoroughly, so that the maneuver could be monitored. Adjustments to the torquing system's steering command word were determined by inspecting the CRT display, and the required commands were relayed to JPL controllers by voice telephone link. This "joy stick" approach permitted the confirmation and correction of the attitude essentially in real time, so that the maneuver could be completed and verified at low altitude.

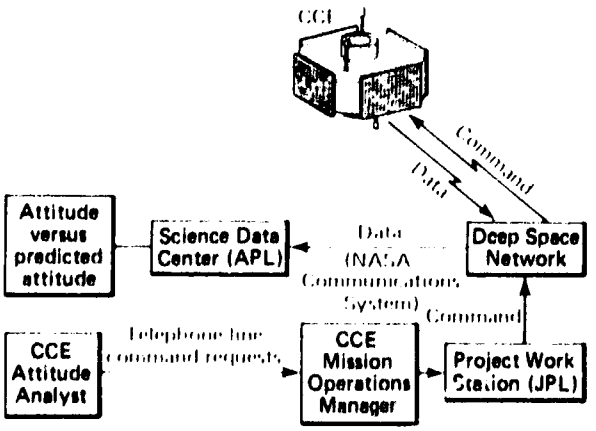

Figure 2—The flow of data and information during the attitude adjustment

The satellite was launched into orbit on August 16, 1984, from the Eastern Space and Missile Center on Cape Canaveral, Fla., at 1447:57 GMT. The first data after injection were obtained through the Goddard Space Tracking and Data Network station on Hawaii. The delayed command memory was read out and verified to have survived the launch environment without errors. It was also verified that the CCE had properly separated from the other two satellites. The spin rate was approximately 60 rpm, and the spin axis direction was nominal. The maneuver to reorient the CCE began at 1607 GMT, and the attitude of the satellite was displayed in real time (Fig. 3). By 1636 GMT, the spin axis orientation was proper, and the maneuvers were stopped. The spin rate was increased to 101 rpm using the cold gas torquing system from 1745 to 1756 GMT.

When the satellite approached apogee for the first time, the rocket was readied and fired at 2342 GMT. The inclination of the orbit was changed from 28.7° to 4.8° by this burn. About 10 min after the firing, the spin axis was maneuvered toward the sun in preparation for solar panel deployment. The first part of this maneuver was done at 100 rpm to achieve a favorable sun angle before deploying the solar panels and despinning by means of a "yo yo" release. When the desired sun angle (about 75°) was reached, the yo yos were released, the panels were deployed, and the spin rapidly dropped to about 14 rpm. At that spin rate, the remainder of the turn toward the sun took only about 3 min. When the final attitude

was achieved, the magnetometer boom was deployed, further reducing the spin rate to about 10.6 rpm. The rate was trimmed to about 10.2 rpm (nominal 10 ± 0.25) over the next few days.

By comparison of the orbital elements before and after the rocket firing, the actual direction of the velocity change resulting from the firing was determined to be less than 1° from the direction calculated in real time (Fig. 3). Prelaunch analyses had estimated a 1σ error of about 3° in the velocity change direction, so the interactive joy-stick maneuver was successful beyond our expectations.

The post-launch activity for the CCE spacecraft is unique in that:

1. The time to reorient the spacecraft and fire the rocket at first apogee was extremely short and required a near-perfect sequence of events.
2. This is the first time that APL has carried out interactive, closed-loop, real-time maneuvering of a spacecraft.
3. The satellite was built by APL, the control center was at JPL, the Science Data Center was at APL, and the project office was at NASA/Goddard Space Flight Center. These many organizational interfaces had to (and did) function perfectly from injection to first apogee. That may be a historic "first."

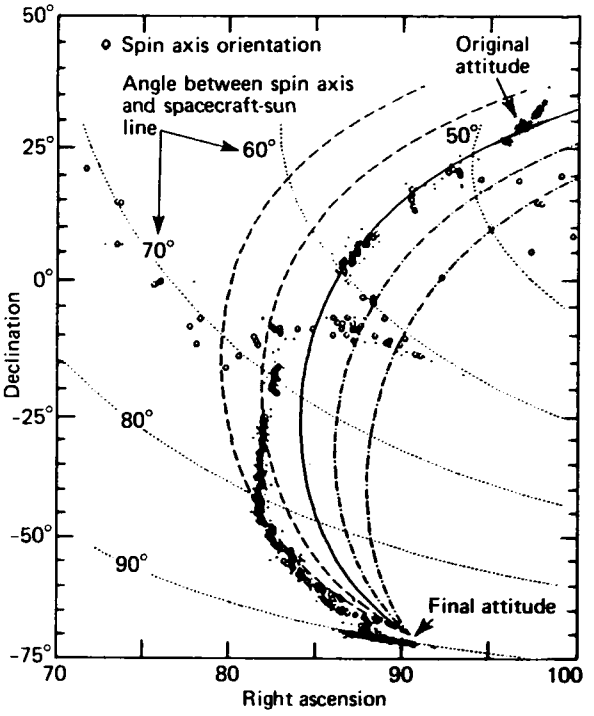

Figure 3—Actual data display during the first attitude maneuver.

This work was supported by NASA.

THE AMPTE CHARGE COMPOSITION EXPLORER SCIENCE DATA CENTER

B. B. Holland, H. K. Utterback, and S. R. Nylund

The Charge Composition Explorer Science Data Center at APL is dedicated exclusively to satisfying the computing needs of United States science investigators in their support of the Active Magnetospheric Particle Tracer Explorers (AMPTE) mission. That well-focused purpose has given the center its unique design, implementation, and operational characteristics.

BACKGROUND

The instrument complements on all three AMPTE spacecraft are dedicated to making unified measurements for certain scientific objectives. A concerted effort has been made to facilitate the analysis of those measurements by establishing a single science database for each spacecraft. The data reside in, and are distributed from, Science Data Centers in the United States, the Federal Republic of Germany, and the United Kingdom.[1]

The Charge Composition Explorer (CCE) carries five instruments: three charged particle measurement instruments, a plasma wave experiment, and a vector magnetometer. The measurements from the instruments form a unified set in that their spectra overlap or are mutually supportive. They are unique in certain aspects, such as data words and time/space synchronism, but require many common support services and ancillary data.

The major advantage enjoyed by a mission-dedicated data center is that, unlike a general-purpose computing facility that must deal with a broad (usually unknown) spectrum of programs and data sets, the total number, size, and types of programs and data sets that are to be handled can be estimated and can serve as design limits. Furthermore, the identification of common support services (e.g., file archiving, graphics production), processing steps (e.g., decommutation), and ancillary data sets allows the development of data center services to satisfy those particular needs.

DISCUSSION

Data

The CCE telemetry is simultaneously transmitted to NASA and stored on the spacecraft's magnetic tape recorder. The transmitted data are received by NASA's Deep Space Network during scheduled observation periods and are placed immediately on NASA Communications lines for direct communication to the Science Data Center. The recorded data are recovered about every eight hours by the Jet Propulsion Laboratory. The playbacks are concatenated and supplemented with real-time data to form as continuous a history as possible. The data are then placed on magnetic tape and mailed to the Science Data Center for processing.

Active phases of the mission require that data be processed in real time to allow experimenters to evaluate measurements and instrument responses. At other times, the recorder is the primary data source. The processing of recorded data places additional requirements on the system: (a) all recovered data are processed at least once, and additional processing is required, for example, when basic calibrations or software packages change; (b) hardcopy outputs (line plots, listings, color spectrograms) must be produced and distributed.

The spacecraft telemetry data must be sorted by instrument (decommutated) to re-form each instrument's original data stream. The data stream must be further decommutated to re-form the raw measurements, which are then calibrated and converted to engineering units. Those measurements are the primary contents of the master data file. In addition, the data are summarized in the form of time and, in some cases, spatial averages to form the pool files. These steps constitute the "first processing pass" on the data.

The pool file information is used both to scan data from individual instruments and to compare different instruments' data at times of interesting physical events. Color spectrograms (on 35-mm slides) and line plots of the pool files are produced and distributed to the experimenters to support that effort.

Ancillary information and services such as orbit ephemerides, spacecraft attitude, and time reconstruction are common to all instruments. The Science Data Center is responsible for generating, organizing, and storing all such files, thereby significantly reducing the problems that arise in directory updating, file purging, etc. when these tasks are performed by each user. This procedure also relieves the investigators of mundane, time-consuming tasks and increases the efficient use of the resources by reducing redundancy.

Design Concepts

The design of the processing structure and the choice of hardware in many ways reflect the exclusivity

of purpose, the well-defined computing mix, the (relatively) small group of users who share common goals, and the need to support both real-time and nonreal-time operations. All users have interactive access to the computing facility. Dedicated and dial-in telephone lines are provided for users at remote sites; local user terminals are connected directly to the computer.

Primary among the design concepts was that the initial processing steps (those required to take the data from raw form to the two major files in the system; see Fig. 1) would be performed by the Science Data Center staff. The two major files are:

1. The master data file, which consists of all the data in calibrated engineering units. The data are augmented with selected, higher level parameters that are generated normally as a part of the processing.
2. The pool file, which consists of (approximately) 6.4-min averages over the data.

The effect of this design feature is twofold. First, the initial processing is performed independently of the experimenters; although they supplied software packages for use in the processing, they do not control the execution of the process. Second, by design, the master data and pool files form the database against which all additional processing by the experimenters is run; that is, the later processes never see the "raw" data.

The second concept that had great influence on the design was that a single decommutation program be capable of processing both real-time and recorded data.

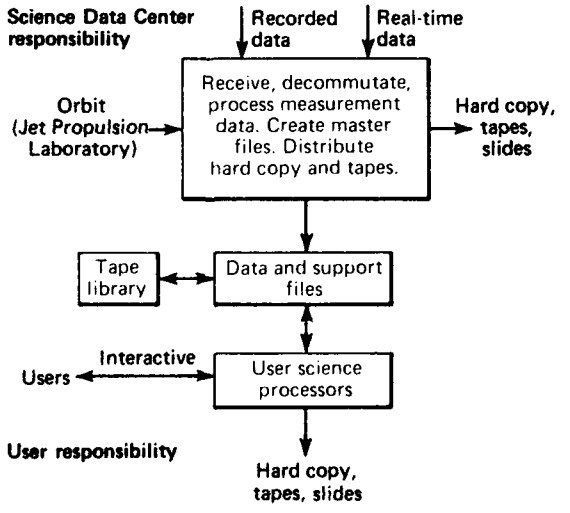

Figure 1—General processing structure showing the functions of the U.S. AMPTE Science Data Center. Note that users do not interact directly with the input data stream or with the tape library.

The distinction here is that real-time processing is driven by the arrival of the next block, and subprocesses must be completed before that arrival. Recorded data processing is driven by the completion of the subprocesses triggering the processing of the next block. The result is that the real-time bounds controlled the design of the timing and error-handling aspects of the decommutation program, especially the treatment of noisy, missing, or suspect data.

Hardware Configuration

The design of the Science Data Center has been optimized to provide as many services as possible within the bounds of available time and resources. We chose to target a facility where no more than half the resources would be consumed in performing the standard tasks associated with data collection and the processing necessary to provide a body of files containing clean, organized data and support information. This would leave adequate computing resources for detailed science analyses.

The hardware configuration is shown in Fig. 2. The central computer is a DEC VAX-11/780 with 4 megabytes of memory, approximately 1.5 gigabytes of disk, and three high-speed tape drives. There are three high-speed (9600 bits per second) and six low-speed (300 to 2400 bits per second) communications modems connecting the input data lines and user terminals to the computer. A PDP-11/34 is used as the communications receiver and preprocessor for the real-time telemetry data transmitted to the Science Data Center via the NASA Communications lines. Graphics are produced using a RAMTEK 9453 and an associated matrix camera. A user room houses the color monitors and terminals for the investigators' program development and scientific studies; it is also the science operations center during active phases of the mission.

OPERATIONS

The Science Data Center was operational at launch and supported the critical attitude maneuvers immediately after launch, followed by instrument turnon and checkout and finally by the two (active) solar wind releases. The operational demands occupied about 6 weeks of real-time data processing support. In addition, about a dozen days of recorder playback tapes were received and processed numerous times to support the inevitable software changes and early measurement and instrument anomaly investigations. The pressure of immediate and compelling questions probably can never be fully anticipated, nor can data volume, which inevitably is maximum in the early phases of any mission. Thus, a system cannot be optimally sized and at the same time accept such

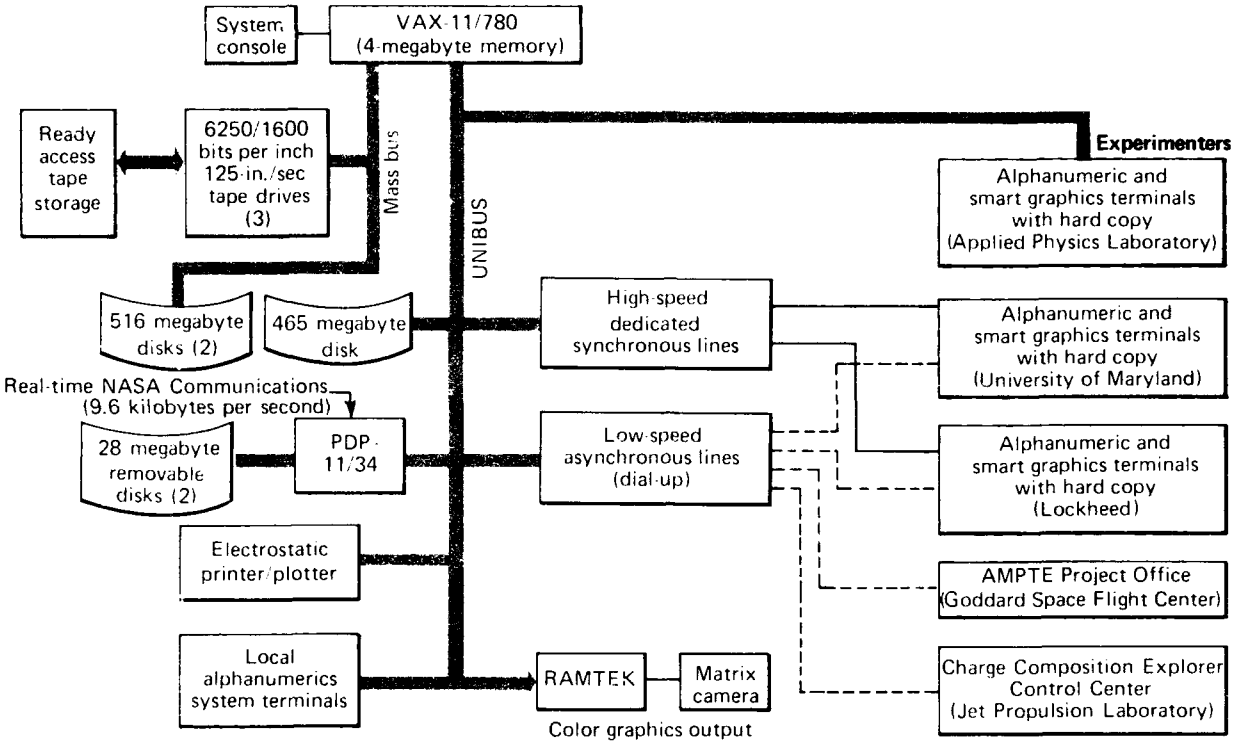

Figure 2—Block diagram of the hardware in the U.S. AMPTE Science Data Center and at the remote experimenter sites.

a flow rate without severe strain. That we have succeeded is a credit to the expertise and dedication of the Science Data Center staff.

ACKNOWLEDGMENTS

We would like to thank, in particular, J. Dassoulas of APL and G. Ousley, M. H. Acuna, R. Witt, R. Donnelly, and D. Margolies of NASA Goddard Space Flight Center for their support and encouragement. We also wish to acknowledge the major contributions to the Science Data Center development of: L. L. Pryor, B. J. Hook, H. Malcom, J. C. Ray, C. E. Williams, R. E. Gold, L. L. Suther, and R. W. McEntire, all of APL.

REFERENCE

1 S. M. Krimigis, G. Haerendel, R. W. McEntire, G. Paschmann, and D. A. Bryant, "The Active Magnetospheric Particle Tracer Explorers Program," *Johns Hopkins APL Tech. Dig.* **4**, 3-11 (1983).

This work was supported by the NASA Goddard Space Flight Center.

THE MEDIUM ENERGY PARTICLE ANALYZER ON THE AMPTE/CCE SPACECRAFT

R. W. McEntire, E. P. Keath, D. Fort, A. T. Y. Lui, and S. M. Krimigis

A new type of particle sensor has been developed and flown to measure the elemental composition of energetic ions in space. Particle time of flight and energy are measured to resolve the species present in the earth's magnetosphere and radiation belts over an energy range (greater than 10 keV per nucleon) not covered by any previous flight instrument.

BACKGROUND

The Active Magnetospheric Particle Tracer Explorers (AMPTE), launched in August 1984, comprise a three-spacecraft mission to study the entry of solar wind plasma into the earth's magnetosphere and to determine the elemental composition and dynamics of the natural energetic particle populations inside the magnetosphere. The American spacecraft of this three-nation mission is the Charge Composition Explorer (CCE), designed and built for NASA by APL. The Medium Energy Particle Analyzer (MEPA) is one of the three major CCE particles instruments; together, they can measure, for the first time, energetic particle fluxes and compositions over the broad range from thermal energies up to many millions of electron volts.

DISCUSSION

The design of MEPA was determined by the scientific requirements of the AMPTE mission, particularly the requirement for coverage of medium atomic mass nuclei (carbon and oxygen, for example) from energies of about 10 keV per nucleon upward, in order to provide coverage overlapping that of other instruments flown on the CCE. These nuclei can be rare and so a large geometric factor was necessary. At low energies, however, the large fluxes of protons (the most common species) could saturate the response of such an instrument. Thus, it was necessary to design a sensor with low efficiency for protons but high efficiency for the rarer, heavier nuclei. Those goals were achieved in MEPA by developing a technology to measure particle species that is new to space flight. Particle time of flight (and thus velocity) and total energy are measured to determine particle mass; the technique of measuring particle time of flight was designed to be able to discriminate against low-mass ions.

Particle Sensor

The MEPA instrument consists of a main electronics box and two particle detector heads: the time-of-flight head and the ion head. The time-of-flight head, the main MEPA particle sensor, is shown schematically in Fig. 1. It consists of a collimator containing a "sweeping" magnet to remove electrons from the incident energetic particle beam, followed by a thin-foil, solid-state-detector, time-of-flight telescope. A thin, lighttight front foil (32 $\mu g/cm^2$) is followed by a 10-cm time-of-flight path and a rear silicon-surface-barrier solid-state detector. Between these two elements is a very thin intermediate foil. Secondary electrons are emitted from each surface when an incident energetic ion traverses the first two foils and stops in the solid-state detector. These electrons are electrostatically focused onto microchannel plates (MCP) to provide timing pulses to measure the ion time of flight between the front and intermediate foils and the rear detector. Particle energy is measured in the rear detector. Incident ion velocity and energy are thus known, enabling us to determine the ion mass.

Electronics

Figure 2 is a block diagram of the MEPA electronics. The output pulses from the microchannel plates go into very fast, constant-fraction timing discriminators that produce sharp timing reference pulses (T1, T2, and T3) if the input pulse amplitude is above a preset level. Because the number of secondary electrons incident on each microchannel plate per incident ion is a function of ion energy and nuclear charge (fewer for high energy protons, many more for low-energy oxygen ions), the timing discriminators can be set by ground command to have a low efficiency for detecting protons (the most common species) but a high efficiency for detecting the heavier, rarer species.

Particle time of flight is measured, over a range from a few nanoseconds to 150 nsec, in two time-to-amplitude converters that output pulses proportional in amplitude to the time between T1 and T3 and between T2 and T3. To reject background, an event is considered valid only if T1, T2, and T3 occur within a 150-nsec coincidence interval, the two measured times of flight are consistent with each other, and an energy pulse is detected from the solid-state detector.

To prevent pileup in the solid-state detector channel because of overlapping pulses during high-count-rate periods, the shaping time constant of the preamplifier was chosen to be less than about 100 nsec. However, the subsequent electronics and hybrids cannot process such fast

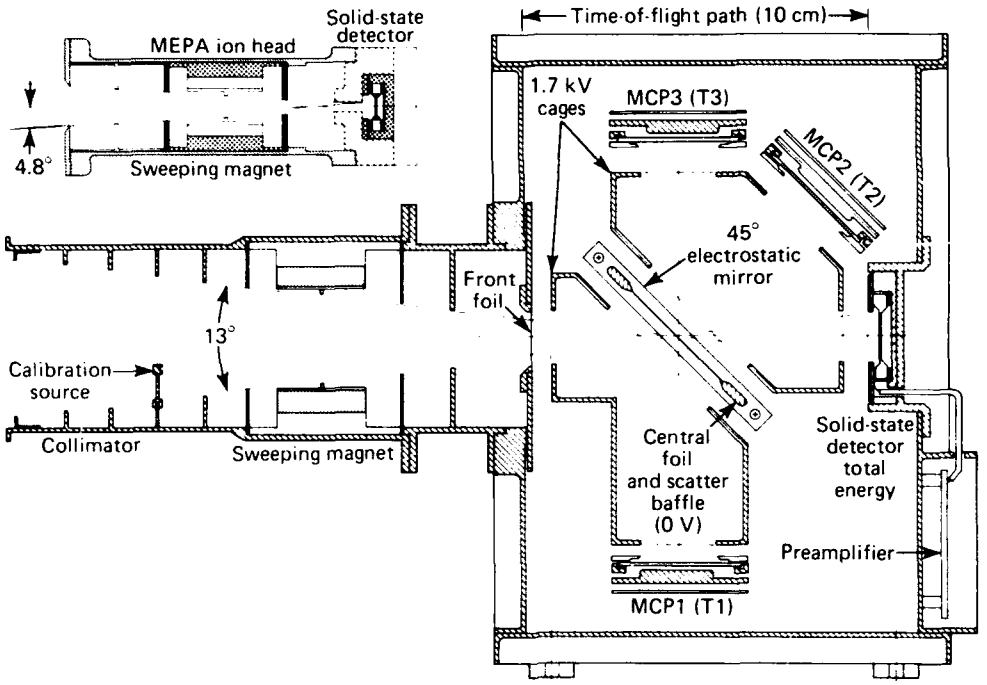

Figure 1—Cross-sectional views of the MEPA time-of-flight head and ion head. Ions incident on the time-of-flight head pass through the front and central foils and stop in the rear solid-state detector. Secondary electrons from the surface of the front foil and from the solid-state detector are accelerated into the 1.7 kV electrostatic cages, are reflected at the central electrostatic mirror, and are imaged onto MCP1 and MCP3, respectively. Electrons emitted from the central foil are accelerated directly onto MCP2.

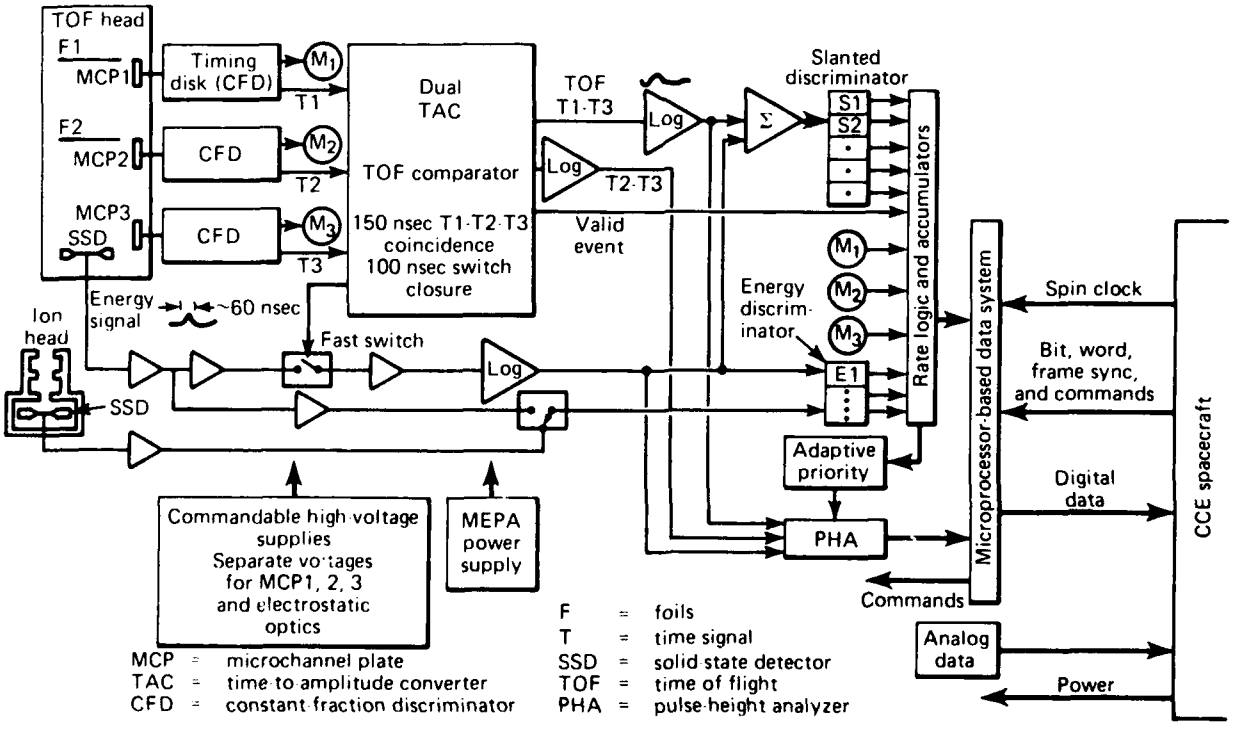

Figure 2—Functional block diagram of the MEPA instrument.

signals. A significant design innovation in MEPA is the introduction of a fast diode switch in the analog energy channel that closes for 100 nsec only when a T1-T2-T3 coincidence is detected. This passes the energy signal of the incident ion to the much slower electronics beyond, without allowing passage of the energy signals of events (background, most protons, etc.) that do not generate time-of-flight signals.

The energy versus time-of-flight space measured by MEPA is divided into 16 species channels covering the species or species groups of interest, in 32 angular sectors and several energy ranges each. In addition, all ions depositing ≥ 25 keV in the solid-state detector of the separate ion head (Fig. 1) are accumulated in 10 energy channels.

While the species channels provide high time and angular resolution data with moderate energy and species resolution, the most precise spectral and elemental resolution is obtained from 256-channel pulse-height analysis of the energy and time-of-flight signals for each event. Those signals, accumulated and processed on the ground, allow the accurate identification of even quite rare elements. Due to bit-rate limitations, only about five fully analyzed events can be transmitted per second.

The MEPA data system provides instrument command and control and processes all of the instrument data into a compressed and formatted output at 735 bits per second. The system is radiation-hardened CMOS (to save power), based on an 1802 microprocessor with 6000 bytes of stored program read-only memory and 12,000 bytes of user random-access memory. The normal spaceflight goals of redundancy and adaptability figured strongly in the MEPA design. Many of the unit subsystems can be reconfigured by command to adapt to unusual operating conditions or electrical problems, and the entire operating program resident in the read-only memory can, if necessary, be changed in flight by patches entered into the random-access memory.

STATUS

After a program of extensive testing and calibrations in the Laboratory and at a Van de Graaff ion accelerator facility, MEPA was installed on the CCE

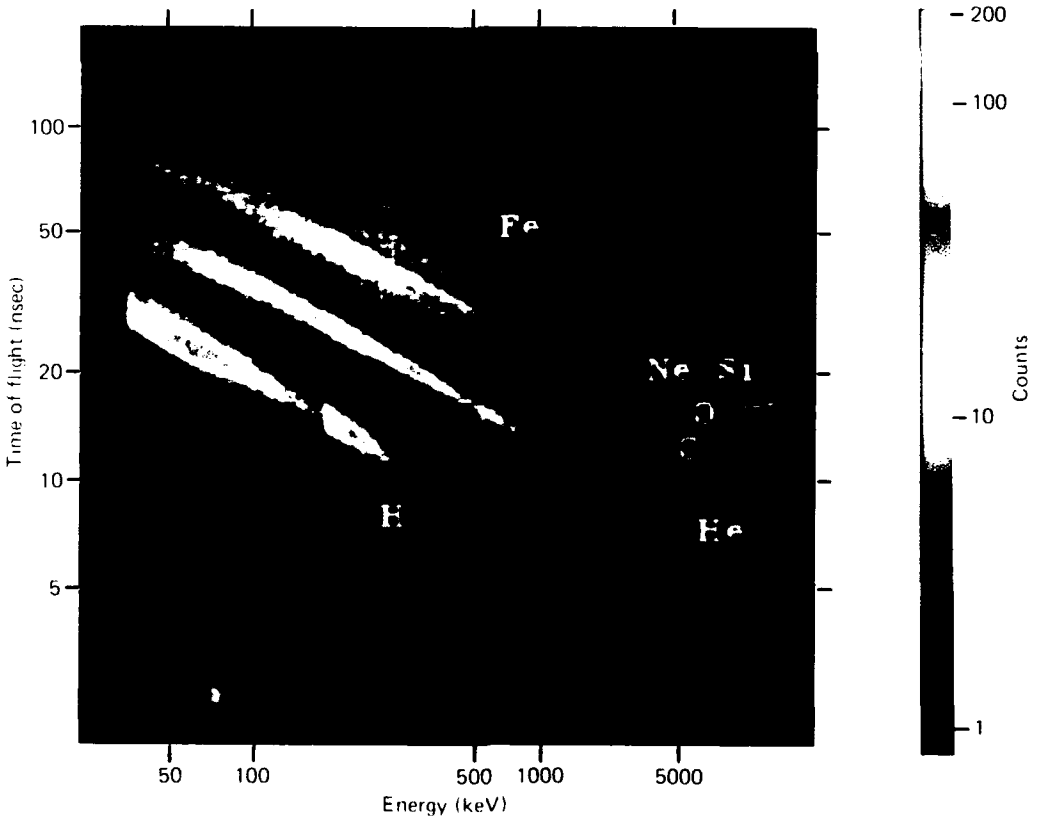

Figure 3—Flight pulse-height analysis matrix accumulated by MEPA, September 12, 1984, 21:19 to 23:31 UT (L = 5.15 to 7.76). Tracks of protons, helium, carbon, oxygen, the neon-silicon group, and iron can be seen. Jumps in intensity along the proton and helium tracks reflect energy boundaries in the priority system.

spacecraft and launched with the AMPTE mission on August 16, 1984. Data already received by the U.S. AMPTE Science Data Center at APL are very exciting and address a number of important scientific problems in magnetospheric physics. Figure 3, an example of MEPA pulse height analysis data, shows the clear separation of elements and groups of elements, including low energy fluxes of oxygen, the neon-through-silicon group, and iron, which was never before distinguished in the magnetosphere.

ACKNOWLEDGMENTS

The authors are deeply grateful to the following individuals for their efforts in the design, integration, and testing of the MEPA instrument: R. A. Reiter, R. Konigsberg, R. F. Cohn, A. Mattheiss, J. V. Burke, L. E. Brown, H. Malcom, H. G. Bolls, S. A. Gary, R. G. Martin, R. J. Counihan, B. J. Hook, J. W. Kohl, J. H. Crawford, J. A. Reier, and J. M. Roberts.

This work was supported by the National Aeronautics and Space Administration.

THE HOPKINS ULTRAVIOLET TELESCOPE

G. H. Fountain, L. C. Kohlenstein, and K. A. Potocki

The fabrication and assembly of the Hopkins Ultraviolet Telescope have been completed. The instrument is undergoing flight qualification testing preparatory to its delivery to the Kennedy Space Center for installation on the Shuttle and for use by NASA in the telescope's first mission, the observation of Halley's comet in 1986.

BACKGROUND

The Hopkins Ultraviolet Telescope (HUT) is designed for low-resolution spectrophotometry of faint astronomical objects at far-ultraviolet wavelengths (400 to 1850 Å), with special emphasis on the region between 1216 and 912 Å, the fundamental excitation states of the hydrogen atom. HUT is intended to supplement and complement the capabilities of the International Ultraviolet Explorer and the Space Telescope by extending spectrophotometric observations to objects somewhat fainter than those detectable by the International Ultraviolet Explorer and to shorter wavelengths (i.e., below 1200 Å) than are observable with it or the Space Telescope. HUT will be used to observe quasars, active galaxies, supernova remnants, hot white dwarf stars, and Halley's comet. It is one of four instruments to be flown as part of the Astro Missions aboard Space Shuttle. The Astro payload, which is being integrated by the Marshall Space Flight Center, is planned for flight on multiple missions in order to realize fully its scientific potential.

HUT is required to interact with an on-board astronomer designated the "payload specialist," a mission specialist who will control the Spacelab equipment supporting the Astro instruments, and a ground-based team who will monitor instrument performance in real time. To fulfill these rquirements, HUT has been designed to provide real-time spectra and pointing data and to allow adaptation to different targets and operating conditions.

DISCUSSION

Instrument Description

Astro payload constraints of geometry and heat dissipation required HUT to be partitioned into two modules, telescope and electronics. Both are mounted on the Spacelab Instrument Pointing System (IPS) along with the other three Astro instruments. The telescope module contains the optics and focal plane instrumentation, and the electronics module contains power conditioning and computer electronics.

Figure 1 illustrates the Astro payload on board Shuttle; IPS is shown orienting the instrument comple-

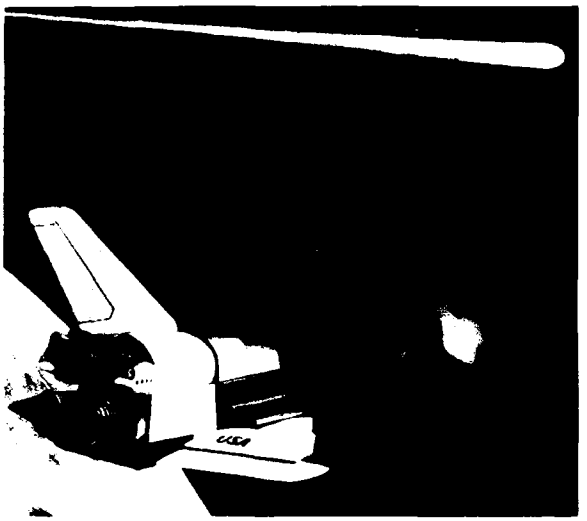

Figure 1—The Astro payload on board Shuttle. The Instrument Pointing System is orienting the instrument complement to observe Halley's comet.

ment to observe Halley's comet, one of the prime targets for the first flight. The instrument complement is attached to IPS by a cruciform structure that acts as an optical bench. That structure accommodates an instrument in each of its four quadrants as well as star cameras for attitude determination and an integrated radiator system, which holds several electronics packages including the electronics module. The IPS/instrument complement and Spacelab avionics (including computers, power conditioning and distribution systems, and mass storage devices) are mounted on two pallets that are attached directly to the Shuttle bay.

The payload and mission specialists operate and monitor the Astro instruments, which are located behind the commander/pilot console, from the aft flight deck by looking through two ports (shown in Fig. 1). The mission specialist controls IPS and performs other general Spacelab functions. The payload specialist controls the instruments by means of the Spacelab computers. The instruments can be tailored to changing conditions and observation opportunities with little time lost between the onset of an event and the execution of appropriate responses.

The telescope module is 1.0 m in diameter and 3.8 m long and weighs 697 kg. The instrument optics are housed inside an aluminum environental control canister that protects the optics from contamination during ground and launch operations and provides a thermally controlled, optically shielded environment during observations. The entrance aperture of the telescope is a door assembly that allows operating apertures of 5280, 50, or 1 cm^2 to be selected. Baffles within the environmental control canister and in a 1 m section forward of the door assembly provide protection from stray light. The telescope module is attached to the cruciform by three titanium feet to minimize mechanical distortions of the optical system.

The electronics module is 1.0 by 0.3 by 0.3 m and weighs 52 kg. All interfaces to the Spacelab avionics are conditioned by electronics within the module. Three DC/DC converters and an electromagnetic interference filter condition the primary power supplied by the Astro power distribution system. A command relay module distributes power from the primary power source and from the converters to the rest of HUT. A power inverter supplies 400-Hz, two-phase AC power to hysteresis synchronous motors in the telescope module. A heater control module regulates the temperature in the telescope and electronics modules. A spectrometer processor and a dedicated experiment processor condition the output of the focal plane instrumentation, control the subsystem functions, and format the system data for transmission to the on-board recorder and to the ground.

HUT is designed to operate highly interactively with both the payload specialist and the ground operations team. Information and commands flow via the Spacelab/Shuttle avionics to the ground and to the instrument. Figure 2 illustrates the major system interactions. Discrete and serial commands to HUT from the ground or the payload specialist are processed by the Spacelab experiment computer and are transmitted via the Spacelab Remote Acquisition Unit. Most discrete commands drive relays in the command relay module to switch primary power to subsystems within HUT. The serial commands, which are loaded into the dedicated experiment computer, provide configuration and timing information needed for the experiments. Discrete outputs, serial data, and video data are transmitted to the aft flight deck via the Remote Acquisition Unit and Shuttle video distribution system to allow the payload specialist to monitor the status of the instruments. A high-rate multiplexer data stream created by the dedicated experiment computer is used to transmit scientific, engineering, and video data to the ground. During the mission, telemetry ground support equipment located at Marshall Space Flight Center will analyze the data stream and display the information for use by the instrument science team in real time.

PROGRAM STATUS

The development phase of HUT was begun in October 1981. The program is a joint effort of The Johns Hopkins University Physics Department and APL. Dr. A. F. Davidsen of the Physics Department is the Principal Investigator. The Physics Department staff is planning the science mission and developing the spectrograph

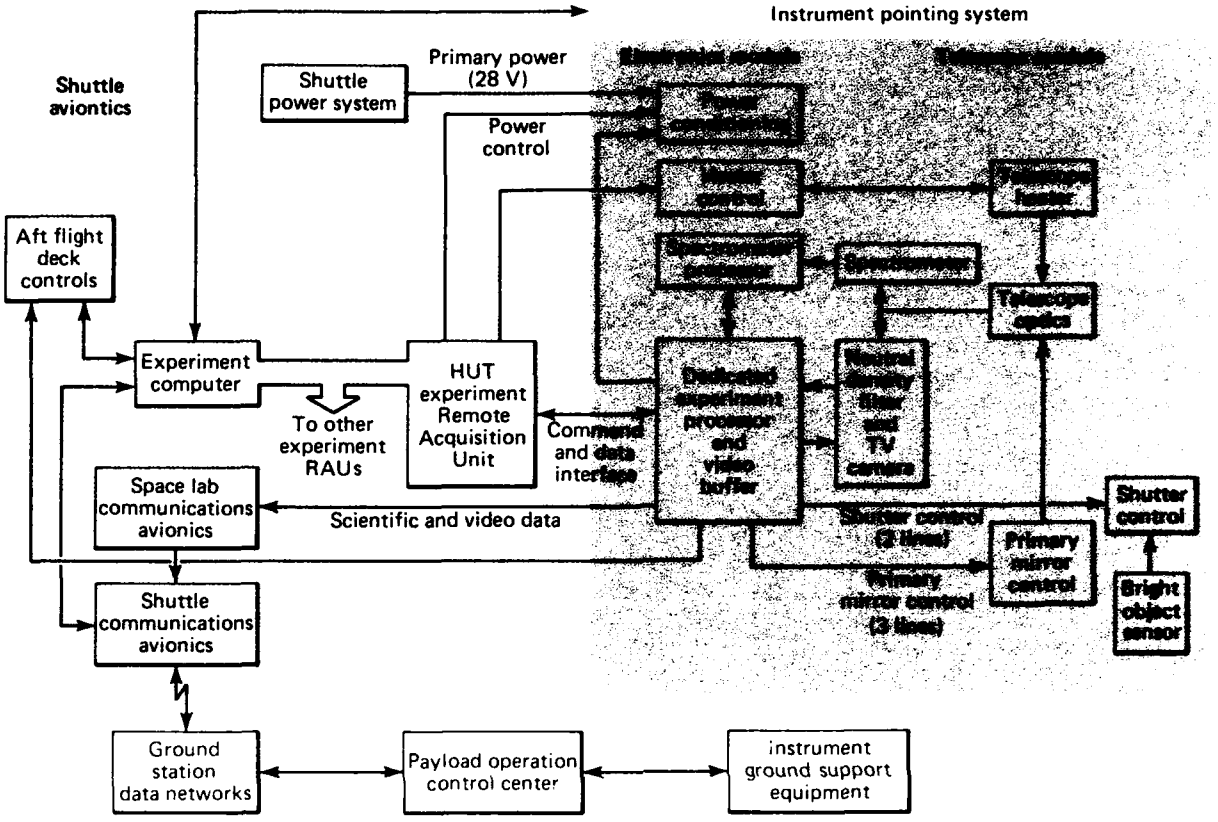

Figure 2—Block diagram of the Hopkins Ultraviolet Telescope.

and optics, and will perform the data analyses. APL is responsible for the design, analysis, fabrication, and qualification of the mechanical and electrical systems. A joint team is integrating and qualifying HUT for flight. The fabrication and assembly of both modules were completed in GFY 1984. Testing of the Electronics Module has been completed. Integration of the two modules is planned for November 1984. Instrument qualification will occur during the late fall and winter of 1984-1985. Delivery to Kennedy Space Center is planned for March 1985. HUT will be integrated with the other Astro instruments in 1985, and the first flight is scheduled for March 1986.

This work was supported by NASA under contract NAS 5-27000.

THERMOSTRUCTURAL RESPONSE OF THE GENERAL PURPOSE HEAT SOURCE TO REENTRY AERODYNAMIC HEATING

K. R. Waeber

A numerical model simulating the structural performance of the heat shield for a radioisotope heat source was formulated to qualify the heat source for spacecraft use. The heat shield was predicted to survive accidental reentry and breakup of the Galileo and Ulysses spacecraft—a launch safety requirement.

BACKGROUND

Since the launch of a Transit navigational satellite in 1961, nuclear power systems have been used in U.S. spacecraft to provide electricity for spacecraft communications, guidance, and instrumentation. The current nuclear power system, called the General Purpose Heat Source Radioisotope Thermoelectric Generator (GPHS-RTG), is being designed and built by General Electric under the auspices of the Department of Energy, Office of Special Nuclear Projects.

Radioisotope thermoelectric power generators are static systems that make electricity from the heat generated by the molecular ionization of plutonium 238. The radioactive plutonium fuel is encapsulated in cylindrically shaped iridium shells. The GPHS module (Fig. 1) consists of four fuel cylinders surrounded by graphitic parts that protect the plutonium fuel from adverse heating, impact, and ablation.

Environmental safety is a primary design requirement of the GPHS-RTG. Environmental safety during spacecraft launch is ensured by designing the power system to survive potential launch and reentry failures with the radioactive heat source intact.

Aerodynamic heating environments are known to create severe structural loading conditions for a heat source. APL has been asked to advise the Department of Energy on the reentry performance of the GPHS power system. In support of this task, an investigation was undertaken of the structural response of the heat source to the heating environment that would be encountered in the event of accidental reentry. The purpose of the investigation was to determine if the heat source would re-

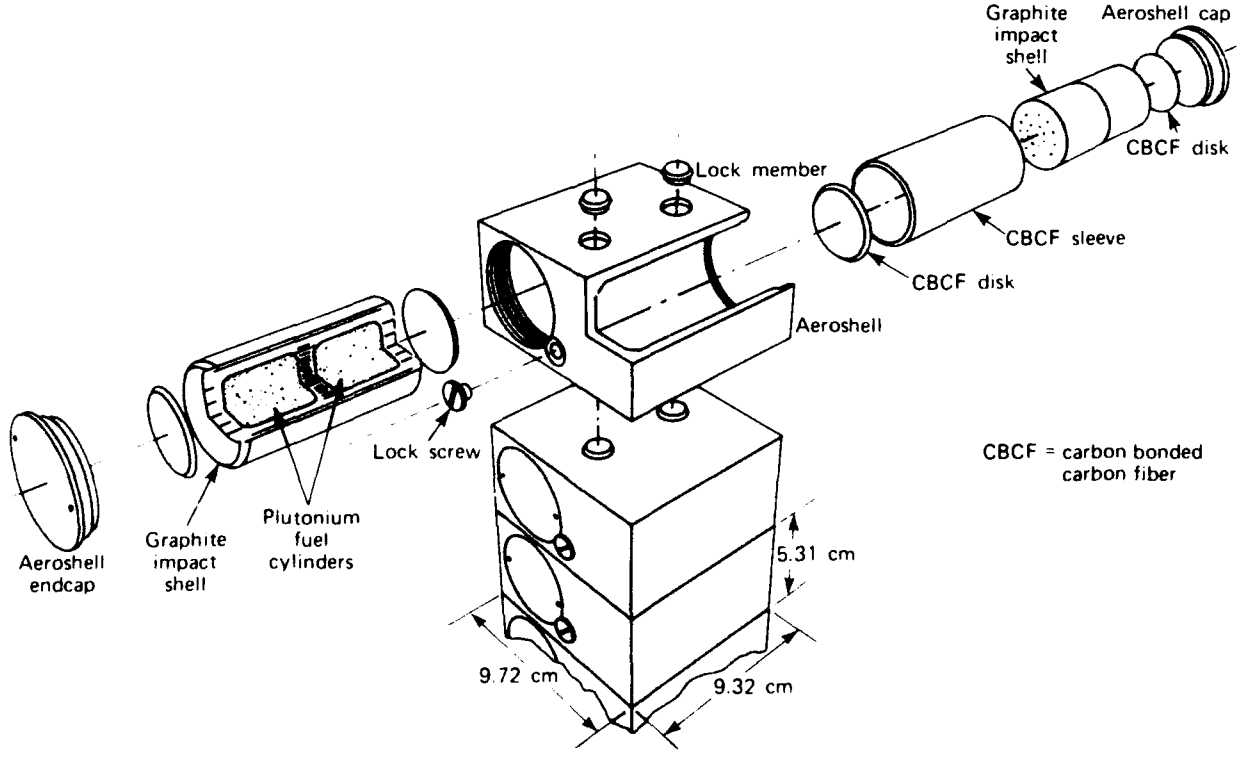

Figure 1—The General Purpose Heat Source.

main intact during reentry and breakup of the Galileo Jupiter probe and the Ulysses high heliographic latitude spacecraft.

DISCUSSION

A numerical model was formulated to simulate the thermostructural response of the heat source to reentry heating environments. Thermal stress failures of the heat source during steep-angle superorbital reentries of spacecraft carrying the nuclear power system were of primary interest. Steep angle reentries were chosen because they generate the highest heating rates, which, in turn, result in large thermal gradients and thermal stresses.

The prediction of the thermostructural response of the heat source was divided into two steps. The first step, determining the time of occurrence of the greatest thermal stress, was done by analyzing the heat source with an inexpensive numerical model of the structure at many timepoints in the reentry. The second step, determining if the heat source would fail at the time determined in step 1, was accomplished by calculating stresses in the heat source by means of a refined numerical model and comparing those stresses with the experimentally measured material strengths. The model used in step 1 is a planar slice of the heat source. In-plane and out-of-plane deformation responses are not coupled for the model, allowing a simpler and less expensive solution of the governing equations of elasticity. The model used in step 2, a complete three-dimensional representation of the heat source, gives accurate stress, strain, and displacement fields throughout the structure. Both models (Fig. 2) take advantage of loading and geometric symmetries by considering only one-fourth of the aeroshell. (The sudden heating of the heat source thermally shocks only the aeroshell, leaving the inner components at a lower temperature.)

Computer programs using the finite element method were chosen to solve the differential equations for the field variables of this solid mechanics problem. Stresses, strains, and displacements were computed in each of the elements in Fig. 2. The equations of elasticity were solved by minimizing the strain energy in each element. All calculations were based on linear elasticity, with an orthotropic constitutive model representing the aeroshell material.

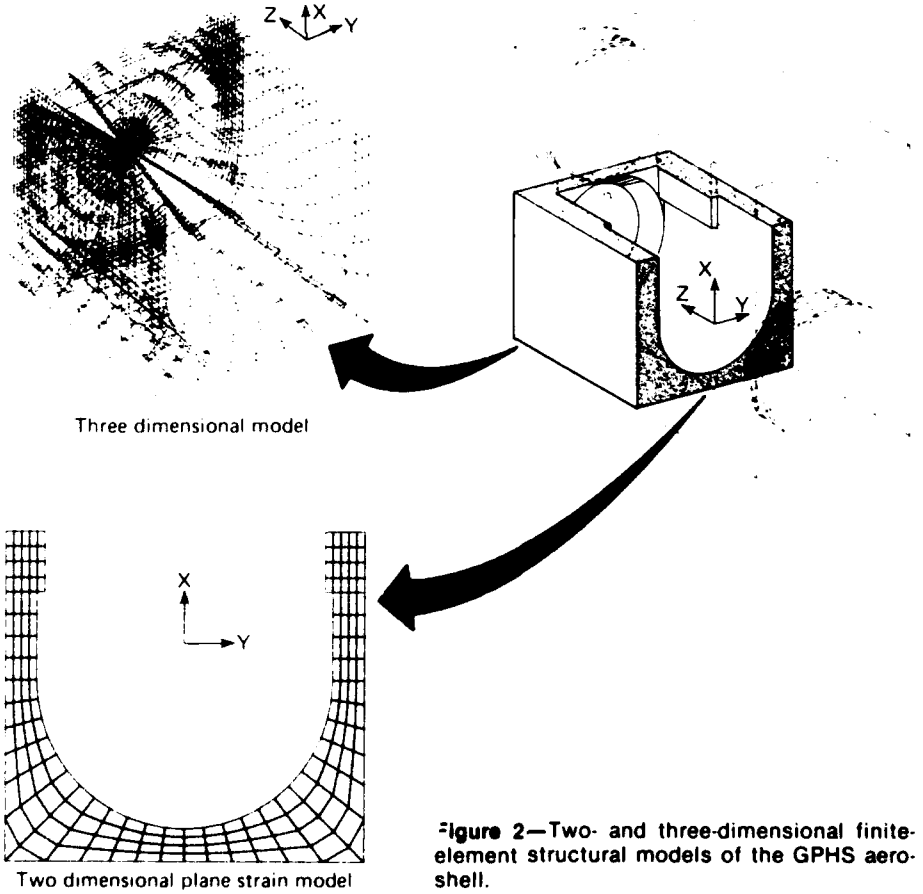

Figure 2—Two- and three-dimensional finite-element structural models of the GPHS aeroshell.

Results of Analysis

Results from step 1 indicate that maximum thermal stresses occur 3.0 sec after release of the heat source from the Galileo spacecraft and 1.4 sec after release from the Ulysses spacecraft. The time for peak stress was obtained by computing the von Mises equivalent stresses in each element in the two-dimensional model at a given time in the reentry. The largest equivalent stress was then plotted as a function of reentry time to determine the peak thermally induced equivalent stress occurring at any time in the reentry.

Results from step 2 indicate that the heat source will survive reentry and breakup of both spacecraft. Calculations from the three-dimensional model also reveal mechanisms of the aeroshell's structural behavior.

Figure 3 illustrates temperature, stress, and displacement fields in the GPHS aeroshell obtained from the three-dimensional model on the XY plane of model symmetry. Values are from Galileo reentry calculations. Figures 3a and 3b show that temperature gradients through the leading face wall are very large, causing thermal stresses to vary from highly compressive (-10,000 psi) on the outer surface to highly tensile (8000 psi) on the inner surface. The aeroshell wall that is leeward to the flow remains at a uniform temperature that is several thousand degrees less than that on the front face. Thermal stresses in this region are correspondingly small. The magnified plot of the deformed elements (Fig. 3c) shows that the hot leading face of the aeroshell expands much more than the cool trailing face does. Similar XY planar slices taken in the endcap region of the aeroshell indicate less deformation in those regions. Those sections are more rigid and resistant to thermal expansion so that the thermal stresses required to maintain compatibility and equilibrium of the structure are larger.

The largest thermal stresses occurred in the endcap region of the aeroshell. No peak stresses were found to exceed experimentally measured ultimate strengths of the material for either spacecraft reentry. The material strengths were greater than the calculated maximum thermal stresses by at least 40% for the postulated reentry of the Galileo spacecraft and by at least 10% for the Ulysses spacecraft.

Interagency Nuclear Safety Review Panel

Achievement of safety requirements, including reentry thermostructural survivability, is required before a nuclear power system can be approved for launch. The APL analysis is part of a review of the environmental impact of the GPHS-RTG performed by Department of Energy organizations for a panel composed of Department of Energy, Department of Defense, and NASA rep-

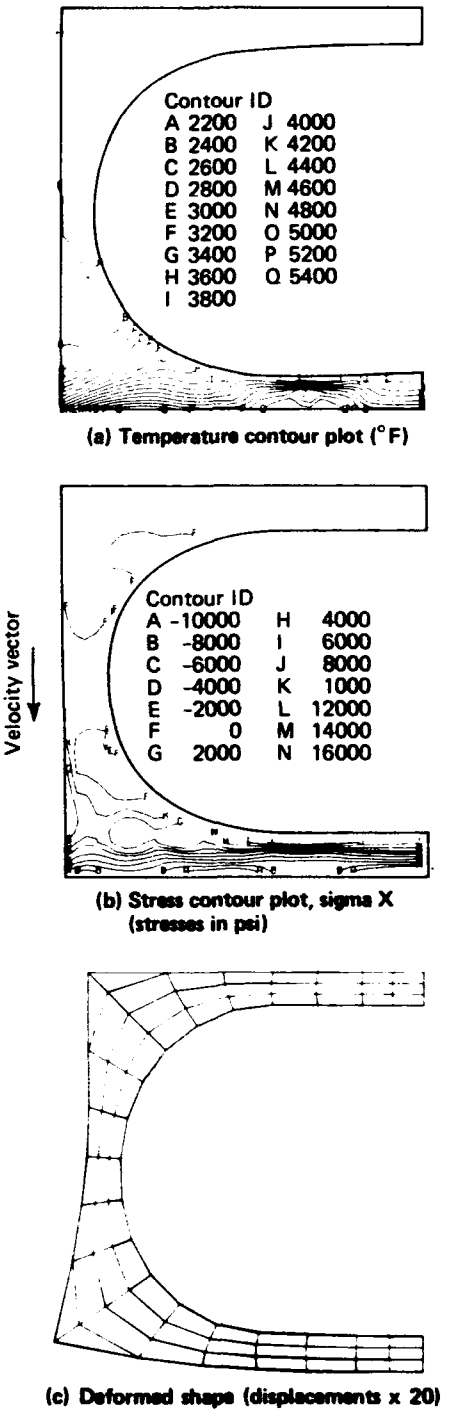

Figure 3—Temperature, stress, and displacement fields on the XY plane of symmetry of the three-dimensional finite-element model.

resentatives. Evaluation of the environmental safety of the nuclear-powered Galileo and Ulysses spacecraft involves reviewing the system contractor's nuclear safety analyses, supplemented by analyses performed by members of the panel.

The APL study was performed independently of those of the system contractor and serves as a check on the contractor's reentry thermostructural safety analysis. Accordingly, this analysis is a reference against which the independent review panel will assess the contractor's results.

This work was supported by the Department of Energy, Aerospace Nuclear Safety Program.

A THEORY OF CARBON ABLATION

L. W. Hunter

A theory has been developed that agrees well with extensive experimental data on the ablation rate of carbon in humid and dry air at temperatures from 1000 to 1800 K.

BACKGROUND

Radioactive power sources in the Galileo and Ulysses spacecraft are enclosed in carbon to protect them from aerodynamic heating during reentry. A theory of carbon ablation was needed for design calculations of the optimum thickness of the carbon.

DISCUSSION

Carbon has widespread application as a thermal insulator in high-temperature oxygen-containing environments. A spacecraft that reenters the earth's atmosphere experiences a high heat load because of atmospheric friction. The container for the radioactive material used for electrical power generation in some spacecraft must survive reentry; hence, those parts are usually encased in a carbon heat shield. During reentry, the carbon literally burns, at a rate depending on the speed. The design engineer is faced with the problem of calculating in advance the optimum thickness of the carbon so that some carbon will always remain to protect the underlying cargo, while keeping the weight of the spacecraft to a minimum. A similar situation occurs in ramjets where carbon combustors and nozzles are being designed to withstand the high temperatures of the combustor gases. A theory has been developed to predict the ablation of carbon in the reentry and combustor environments.[1]

To predict the burning rate of carbon, it is necessary to model the chemistry. Two sets of chemical reactions may be written to correspond to the two basic modes of burning—glowing and flaming.

Glowing combustion is the simpler one. The important chemical reaction is

$$2C(s) + O_2(g) \rightarrow 2CO(g) , \quad (1)$$

where s denotes solid and g denotes gas. This reaction sets up concentration and temperature profiles as shown qualitatively in Fig. 1a. Thus, the concentrations of O_2 and CO and the temperature T vary across a narrow boundary layer between values at the surface, where the reaction is occurring, and ambient values in the free stream. As indicated by the slopes of the concentration profiles, the O_2 diffuses toward the surface and the CO diffuses away. It is necessary to calculate the concentration profiles because the O_2 and CO carry chemical enthalpy to and from the surface, and this contributes to the net heat flux to the surface. In addition, the CO carries carbon from the surface, and so the mass flux of CO determines the ablation rate.

The chemical mechanism of flaming combustion involves two reactions coupled to form a feedback loop:

$$C(s) + CO_2(g) \rightarrow 2CO(g) , \quad (2)$$

$$2CO(g) + O_2(g) \rightarrow 2CO_2(g) . \quad (3)$$

The gas phase reaction, 3, generates CO_2, some of

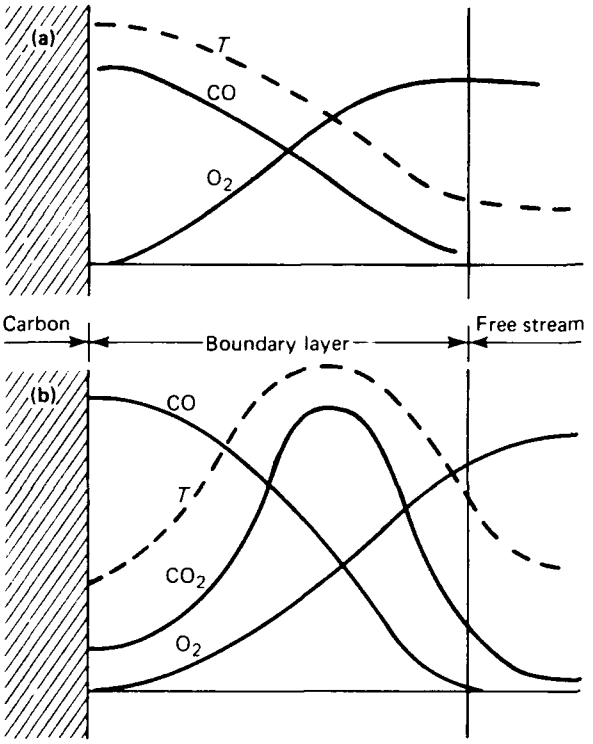

Figure 1—(a) Glowing and (b) flaming combustion of carbon. The composition and temperature profiles are shown near the surface.

which diffuses back to the surface where it reacts with carbon to supply the necessary CO. The profiles are shown qualitatively in Fig. 1b. Reaction 3 represents a flame. The heat released shows up in the maximum of the temperature profile.

The temperature and concentration profiles are governed by differential equations that describe conservation of heat and the mass of each species. An analysis of these equations shows that flaming combustion is possible only when the surface temperature is hot enough. At lower temperatures, the surface reaction is unable to generate CO fast enough to support a detached flame. It is also known that the oxidation of CO by reaction 3 is possible only when enough H_2O vapor is present, the H_2O being a catalyst for the reaction. As a first estimate, the relative humidty should exceed 0.1%. The humidity level in the atmosphere above 12 km altitude is lower than 0.1%; thus, a spacecraft reentering the earth's atmosphere cannot begin flaming combustion until it has fallen below 12 km.

The ablation rate of carbon has been measured[2,3] under conditions similar to those encountered during the subsonic portion of spacecraft reentry. That work provided an opportunity to test the theory derived in Ref. 1.

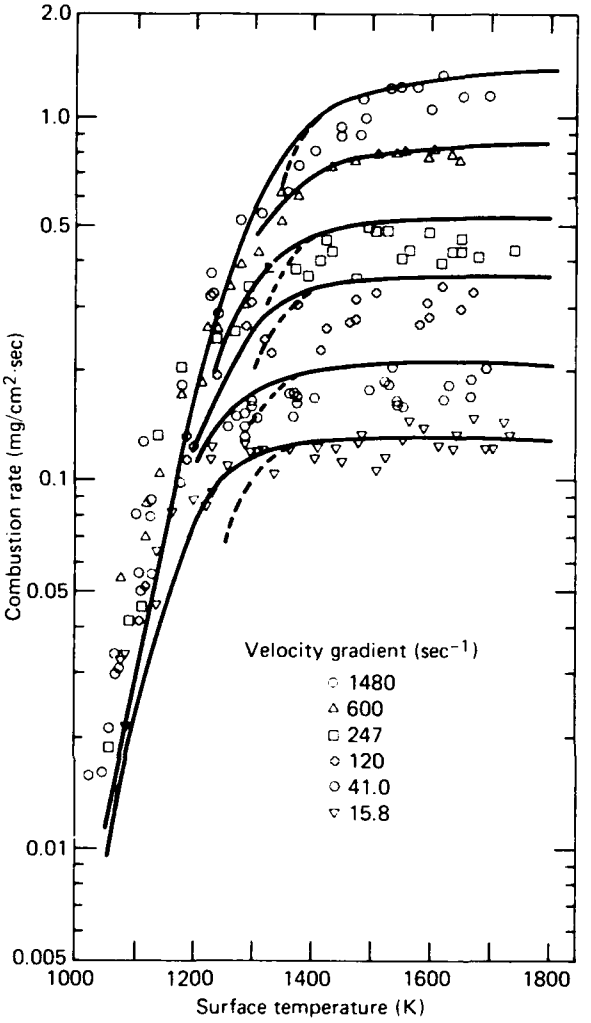

Figure 2—The ablation of carbon burning in air. Experimental points[2,3] are compared with calculations[1] for glowing combustion (solid lines) and flaming combustion (dashed lines). The oxygen mass concentration is 0.284 × 10^{-3}g•cm^{-3}.

Agreement was found to be quite good over the full range of experimental conditions.

Figure 2 shows typical experimental points[2] and superimposed calculations for glowing combustion (solid lines) and flaming combustion (dashed lines). The combustion rate of carbon depends on the surface temperature, the air composition, and the gradient of the air velocity distribution in the boundary layer next to the solid. In the case of spacecraft reentry, the velocity gradient reflects the size and speed of the reentry body. For example, a body having a radius of 30 cm and moving at terminal velocity in 20°C air at sea level experiences a velocity gradient of 1800 (cm•sec^{-1})cm^{-1}, that is, 1800

sec^{-1}. In general, the velocity gradient is proportional to velocity and inversely proportional to radius.[4]

At the higher temperatures shown, the ablation rates for flaming and glowing combustion are indistinguishable. As the temperature drops, the two rates begin to separate, but flaming stops before the difference gets very large. The humidity level in the experiments was large enough to permit flaming so that the predicted combustion rate follows the dashed curves at the high temperatures and the solid curves at the low temperatures. The predicted jump at the transition lies within the experimental scatter. However, in related experiments,[3] the humidity level was lowered to reduce the extent of flaming combustion. The ablation rate from 1200 to 1400 K was observed to increase in agreement with the theory.

The heat flux into burning carbon was also calculated. This information is needed as a boundary condition for the differential equations determining the in-depth temperatures. In addition, an examination of the heat flux leads to the conclusion that self-sustained steady combustion is not possible in either mechanism. Under these circumstances, the temperature of the reentry body tends to cool down toward ambient temperature until impact occurs.

The predicted conditions at impact are the most important applications of the theory to reentry safety problems. The calculated extent of ablation helps the designer choose the optimum thickness of the carbon heat shield.

ACKNOWLEDGMENT

The author wishes to thank J. C. Hagan and L. B. Weckesser for their encouragement and suggestions. In addition, the author benefited from helpful discussions with P. T. Brenza, D. W. Conn, R. W. Newman, and L. L. Perini.

REFERENCES

[1] L. W. Hunter, *The Ablation Rate of Burning Carbon and the In-Depth Heat Flux*, JHU/APL ANSP-260 (Jul 27, 1984).

[2] K. Matsui, A. Koyama, and K. Uehara, "Fluid-Mechanical Effects on the Combustion Rate of Solid Carbon," *Combust. Flame* **25**, 57 (1975).

[3] K. Matsui, H. Tsuji, and A. Makino, "The Effects of Water Vapor Concentration on the Rate of Combustion of an Artificial Graphite in Humid Air Flow," *Combust. Flame* **50**, 107 (1983).

[4] L. L. Perini, *Laminar Heat Transfer Distribution around Spheres and Cylinders in Subsonic-Supersonic Flow*, JHU/APL ANSP-098 (May 5, 1977).

This work was supported by the Department of Energy, Office of Special Nuclear Projects.

THE APL SATELLITE TRACKING FACILITY

E. F. Prozeller, W. C. Trimble, and L. M. DuBois

The APL Satellite Tracking Facility provides significant new capabilities resulting from the overhaul and upgrade of the Laboratory's 20-year-old navigation-satellite injection station. The modernization has included the incorporation of new, dual-redundant receiving and transmitting systems, a 5 m parabolic dish antenna (that works in concert with the overhauled 60 ft antenna), and new computers to link all the hardware, control the antennas, and provide for programmed control and status monitoring of the station. The facility will first serve as the single point of control for the Geosat-A spacecraft.

BACKGROUND

In the early 1960s, APL completed construction of the 60 ft parabolic dish antenna, which has become a Laboratory landmark, and began to operate a tracking station to receive data from and inject messages into the early Oscar navigation satellites. That station served as a prototype for the Navy Astronautics Group's satellite injection station at Pt. Magu, Calif., and continued to serve APL until the launch of the Nova-1 satellite in early 1981. The Navy's Geosat program, initiated in 1981, included the requirements for a primary ground station to command the satellite and receive and process the data and a backup station to take over in the event of a primary station outage. The Geosat program plan initially designated the APL station to serve as the primary Geosat station, a task requiring a relatively modest overhaul and upgrade; another undesignated station was to become the backup. Identifying a backup station to fulfill that function without seriously affecting operational commitments turned out to be very difficult, and it was decided to add redundant equipment to the APL station

to effectively make the facility serve as its own backup. As a result of that new requirement, the overhaul became a much more significant effort involving not only the complete refurbishment of the 60 ft antenna system,[1] but also the procurement of a 5 m dish antenna system and the development of computer-switchable, fully redundant transmitting and receiving systems.

Final testing of the new APL Satellite Tracking Facility was completed in August 1984, and the station is now ready for the Geosat-A launch.

DISCUSSION

The Satellite Tracking Facility is the ground station component that serves as the communication interface with the satellite and with the satellite-unique control center. It is a relatively general-purpose RF facility and has little dependence on the unique properties of any particular satellite. As a receiving station, it can be configured to receive and demodulate signals from VHF to S-band frequency with almost any conventional modulation format. As a transmitting station, it is presently limited to the VHF frequency range. A summary of its overall characteristics follows.

Antennas

1. 60 ft parabolic dish with 150 MHz, 400 MHz, and 1 to 3 GHz RF feeds. Both right-hand circular (RHC) and left-hand circular (LHC) polarizations available simultaneously for the 1 to 3 GHz feed. Receiving G/T (ratio of antenna gain to receiving system noise temperature) of 24 dB/K at 2200 MHz.
2. 5 m parabolic dish with 2200 to 2300 MHz and 1650 to 1750 MHz feeds. RHC or LHC polarization selectable. Receiving G/T of 14 dB/K at 2200 MHz. Dish steered by closed-loop autotrack of received signal.
3. Eight-turn axial-mode helix for command transmission at VHF. Gain of 12 dB.
4. Quad log-periodic antenna for receiving at 150 MHz and a short backfire antenna for receiving at 400 MHz. Both antennas provide LHC polarization and approximately 15 dB of gain.

Receiving/Demodulation

1. General-purpose modular telemetry receivers that can be configured for reception at VHF through S band and for demodulating AM, FM, or PM modulation.
2. General-purpose phase-shift-keyed demodulators and bit synchronizers capable of manual/computer control of frequencies and formats.

Computers

Two real-time control computers, one for steering the parabolic dish antennas and one for controlling the configuration and settings of the receiving/demodulating equipment.

Transmitters

Two 1-kW VHF transmitters with self-contained AM modulators capable of up to 5 kHz modulation rate.

Frequency/Time

A fully redundant UTC timing system providing IRIG-B and NASA time signals phase-locked to the APL hydrogen maser standard.

Elements of the Facility

The Satellite Tracking Facility is divided into 10 major systems (Fig. 1). Three antennas provide the RF interface to the satellite. The primary antenna is the 60 ft parabolic dish, which can transmit at VHF while simultaneously receiving over a number of frequency bands. High receiving sensitivity has been obtained over the 1 to 3 GHz band by placing redundant, high-gain, low-noise amplifiers at the dish feed point. The secondary antennas consist of the 5 m parabolic dish and an eight-turn axial-mode helix. The antenna steering computer system (ASCS) consists of the hardware and software required to provide the steering information for each antenna. Because the 60 ft antenna is positioned by means of an open-loop pointing system, it must be provided line-of-site angles as a function of time throughout the pass. On the other hand, the 5 m system contains a four-quadrant monopulse feed system that allows angle-tracking loops to be closed once the satellite signal has come within the beam. The ASCS provides the acquisition angles for the 5 m antenna as well as time printouts for manually positioning the helix antenna pedestal. The orbital elements from which the pointing data are derived are obtained by special processing at APL of predicted satellite parameters obtained from the Naval Space Surveillance Network. The ASCS can be programmed to drive the dish antennas through 100 satellite passes without operator intervention, a feature that should help minimize the cost of satellite operations.

All timing signals used by the facility and provided to the individual satellite control centers (referred to as "users") are generated by the station Time and Frequency System (TFS), which contains two oscillator/clock systems operating in parallel; time signals are distribut-

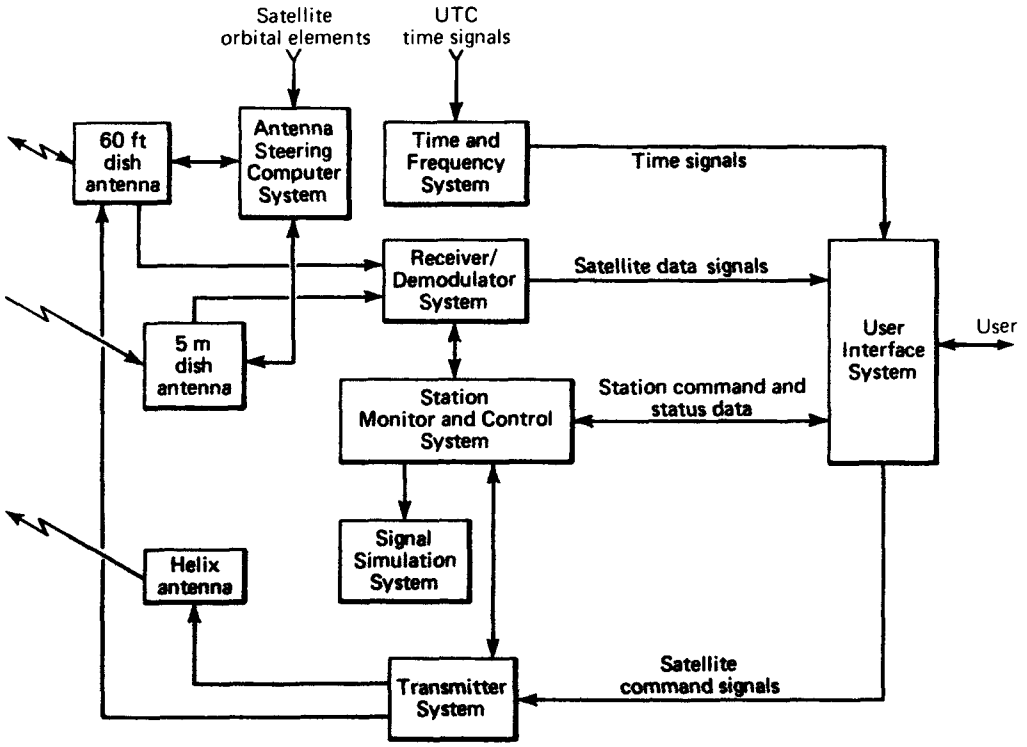

Figure 1—Block diagram of the Satellite Tracking Facility.

ed within the station and to the user from one system, and the second system is available if an outage occurs. The TFS has battery backup power for up to 2 hr if station power is interrupted.

The RF signals from the two dishes are routed over low-loss cables to the Receiver/Demodulator System in the operations room. This system comprises two independent receiving channels, each containing a phase-locked receiver, a phase-shift-keyed demodulator, and two bit synchronizers. By means of changeable plug-in units and frequency settings, a wide range of signals can be tracked and demodulated. For Geosat, the two channels will be connected separately to each dish output to recover two independent sets of data; however, the Receiver/Demodulator System contains electronic switching that allows cross-strapping of the receiving equipment in case of an outage. It is also possible to configure the receiving channels to process the LHC and RHC 60-ft feed outputs separately in a diversity reception mode.

The Satellite Tracking Facility also contains two transmitters although only one is keyed at a time; the other is powered in standby condition. The transmitter system incorporates RF switches that allow either of the two transmitters to be connected to either of the two uplink antennas, the primary 60 ft dish, or the helix.

An S-band RF signal simulation system has been incorporated to emulate the Geosat signal structure and to allow complete end-to-end receiving system checkout to be performed as a function of signal level. The RF signal can be either hardwired into the feeds of the two receiving antennas or radiated to them from a special test antenna. The simulator contains read-only memories that are programmed to generate the Geosat data patterns. The Geosat ground station operational plan calls for the demonstration of ground station readiness prior to each pass. This will be accomplished by commanding turn-on of the simulator from the Geosat control center and by recovering the data patterns and comparing them to the known transmitted patterns. Readiness testing of the transmitters will also be performed; however, instead of test data being recovered, power and percent modulation parameters will be detected and used to evaluate readiness.

A key part of the new station consists of the Station Monitor and Control System (SMACS). The heart of SMACS is a desk-top computer interfaced to the receiving and transmitting equipment as well as to the signal simulator. This computer provides the single point within the facility from which all the equipment can be controlled and monitored. Highly user-friendly, menu-driven software allows the operator to observe and reconfigure the station's equipment, change equipment settings

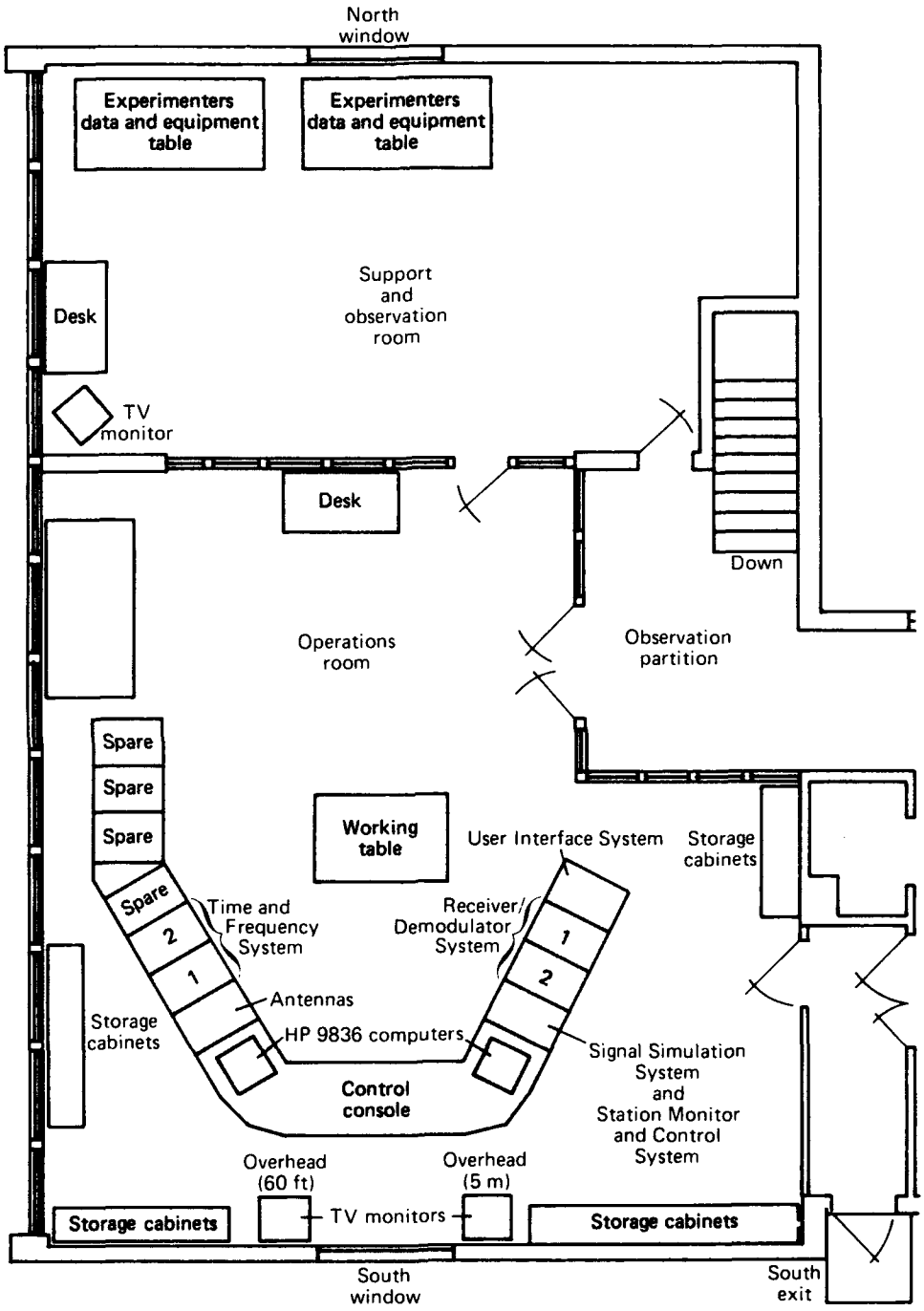

Figure 2—The operations area.

(e.g., frequencies and modes), and monitor and log the real-time performance of the equipment during a satellite pass by observing received signal levels, the demodulator lock status, transmitter power, and modulation index. SMACS also interfaces the user's control center by means of an RS232 link that allows the facility to be monitored and controlled remotely from the user's computer. By means of the SMACS link and by programming of the antenna steering computer, it should be possible to fully automate operations during a satellite pass. The goal for the Geosat operation is that the facility will be unattended outside of regular working hours for the final 18-month period of routine experimental data gathering.

The floor plan of the operations area is shown in Fig. 2. The operations room contains all the hardware except the transmitters, which are located in a separate room for safety and RFI reasons. The equipment is arranged in two rows of racks that are joined by a master console containing the two computers. The console faces a window view of the 60 ft dish. The operations room is separated from the adjoining support and observation room by glass partitions. Beside providing a visitor's observation area, the latter room also is a temporary control and data center for satellite programs for which the facility is only used for short-term operations immediately following launch (such as HILAT in the summer of 1983 and Polar Bear planned for the fall of 1986). A window in the north wall of the support and observation room presents a view of the 5 m dish on the roof of another building.

Test and Evaluation

Testing of the facility was completed in August 1984, and the station was accepted as fulfilling the requirements of the Geosat program. Formal testing was carried out starting in January as the systems were integrated (integration tests) and at the overall station level in conjunction with the Geosat control center and the spacecraft (compatibility tests) in early spring and late summer.

Two of the principal integration tests were Landsat tracking and downlink margin verification tests. The first test involved tracking the S-band signals from the Landsat-D satellite, which has an orbit and signal structure similar to those of Geosat, in order to determine the pointing accuracies of the two dishes in conjunction with the steering computer software and the Navy Space Surveillance element processing. The test demonstrated that the goal of 0.1° maximum pointing error for the 60 ft dish and the proper positioning, acquisition, and autotracking of the 5 m antenna had been achieved.

The data recovery margins achievable with the downlink equipment were verified using the signal simulator. The signal lines were hardwired to the 60 ft downlink at the antenna outputs, and the levels were adjusted over the full range of values expected to be received from Geosat. In the case of the 5 m dish, the signals were passed through the antenna feed and referenced to the known power spectral density at the 60 ft dish. The bit error rates in the recovered data were measured as a function of the signal levels expected from the two downlink antennas, and the margins were determined as the differences between the minimum expected level from Geosat and the signal levels required to achieve a bit error rate of 1×10^{-6}. The test results indicated margins of 10 dB for the 60 ft dish and 5 dB for the 5 m dish—exceeding the Geosat program requirements of 6 and 3 dB, respectively.

When the integration tests were completed, the facility was connected to the Geosat control center for a series of spacecraft compatibility tests. The facility served as an "RF pipe" between the control center equipment and the satellite. The S-band signal lines were hardwired directly from the spacecraft transmitters to the downlinks, and the demodulated data were delivered to the Geosat control room for processing. The transmitters were modulated by command signals generated in the control room, and the resulting RF signal was cabled directly to the spacecraft command receivers. This series of tests proved the compatibility of the spacecraft uplink and downlink signal structures with the facility. The series also demonstrated control and monitoring of the equipment from the Geosat control room.

ACKNOWLEDGMENT

The upgrade of the Satellite Tracking Facility resulted from the contributions of many people. The authors would like specifically to acknowledge the following individuals who were intimately involved in the design, development, and fabrication of the systems: R. S. Bokulic, F. A. Burnham, A. A. Chacos, M. W. Ganz, R. J. Heins, R. K. Huebschman, J. J. Neary, R. A. Reiter, R. Sunderland, and R. R. Yost.

REFERENCES

[1] R. L. Konigsberg, V. F. Neradka, and T. M. Rankin, "Upgrade of the APL 60-ft Dish Antenna Control System," in *Developments in Science and Technology, Fiscal Year 1983*, JHU/APL DST-11.

This work was supported by the Office of Naval Research.

AMPLITUDE DISTRIBUTIONS FOR SEASAT SAR AND SKYLAB DATA WITH STATISTICS FOR CLASSIFICATION AND CORRELATION

D. G. Tilley

Scenes of Nantucket Island made by the Seasat synthetic aperture radar (SAR) and Skylab have been mapped to the same scale and orientation for comparison of their reflectance distributions and for classification of terrain. Rayleigh and Poisson statistics are used in random Monte Carlo computer simulations to model the intensity distributions of the reflectance data. Two-dimensional autocorrelation functions for SAR and optical data individually and an amplitude-normalized cross correlation are computed with fast Fourier transform methods.

BACKGROUND

A Gaussian probability distribution is often used to model the statistical properties of reflectance variations that are observed in an optical image. Radar cross section data exhibit Rayleigh statistics that are the bandwidth-limited equivalent of Gaussian noise.[1] For Doppler imaging radars, the Poisson probability distribution[2] characterizes the detection of electromagnetic chirps during the time interval required to form a synthetic aperture. Thus, it is convenient to represent the SAR reflectance for a given picture element (pixel) as a Rayleigh sum over the surface distribution of scatterers weighted by a Poisson probability for detection within a finite time period.

As microwave and optical sensors proliferate in space, large quantities of pictorial data are amassed at ground stations, and many applications require that multisensor scenes be referenced to the same map projection. The accuracy of the spatial registration can be evaluated with cross correlations that may also reveal differences in the radiometric response of the sensors to the same geographic features.

DISCUSSION

Empirical Models

The passive optical sensors aboard Skylab in 1976 provided an incoherent measurement of scene reflectance. A mean-to-standard deviation ratio of 4.1 was measured for the uniformly textured Skylab segment south of Nantucket Island identified by the square overlay in Fig. 1. The SAR obtained primarily an incoherent measurement of scene reflectance. However, the amplitude distribu-

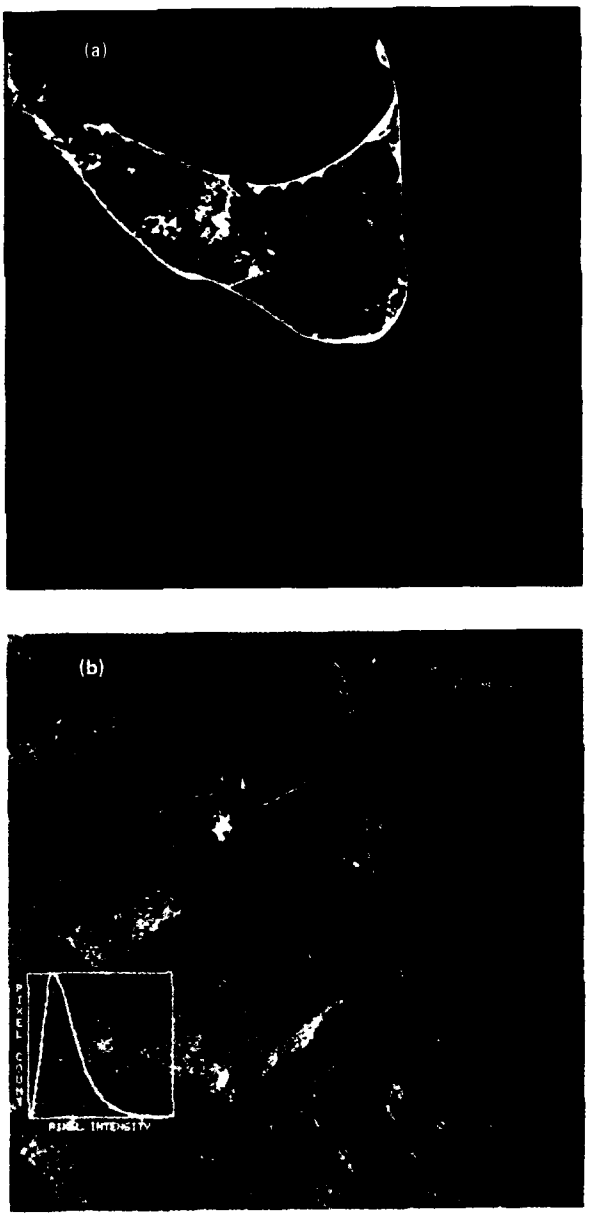

Figure 1—(a) Gray-scaled color separation produced by digitally scanning a monochromatic light beam and photometer over a photograph of Nantucket Island recorded originally by a Skylab camera in August 1976. (b) Scene of Nantucket Island obtained by Seasat SAR in September 1978.

tion is skewed toward higher reflectance values with a lower mean-to-standard deviation ratio, 0.91, than that found with the Skylab sensors. This increase in the signal variance relative to the mean is generally attributed to coherent scattering from randomly correlated surface waves. The effect alone is not enough to produce the observed variance, so a statistical model was needed to describe the noise imposed on a signal fading at the edges of a finite observation period.

The SAR intensity for a given pixel can be represented[3] by a product of the Rayleigh and Poisson distribution functions:

$$\sigma_{p,N} = A_{p,N} \left| \sum_{n}^{N} (\cos \phi_n + i \sin \phi_n) \right|^2 , \quad (1)$$

where

$$\text{Prob}\,(A_{p,N}) = \frac{e^{-(Np)}\,(Np)^A}{A!} , \quad (2)$$

$$A = 1, 2, 3, \ldots N ;$$

and

$$\text{Prob}\,(\phi_n) = \pi/N , \quad (3)$$

$$n = 1, 2, 3, \ldots N .$$

The Poisson amplitudes $A_{p,N}$ are proportional to the number N of chirps backscattered within a resolution element of the sensor and to the probability p of detection within the integration time of the processor. Coherent Rayleigh noise is reduced as N becomes large,[4] and the Poisson distribution approaches a Gaussian distribution for large values of Np. Therefore, the discrete Rayleigh-Poisson model approaches the continuous Gaussian distribution for large N.

A Rayleigh-Poisson simulation of the Skylab optical data is shown in Fig. 2. The solid black graph in Fig. 2a depicts the pixel intensity distribution for the green color component of the Skylab Nantucket scene. The data are in good agreement with the simulation produced from Eq. 1 with $N = 40$ and $p = 0.25$. Figure 2b is a Monte Carlo simulation of the SAR data segment. The solid black graph represents the pixel intensity distribution for the actual SAR data that are modeled well by Eq. 1 with $N = 11$ and $p = 0.36$. In both cases, the three white curves represent a composite Rayleigh-Poisson simulation, the Rayleigh component ($A_{p,N} = 1$), and the Poisson component ($\phi_n = 0$).

Image Processing

The Skylab image of Nantucket Island was received as a color print that was photographically reduced to an 8 × 10 in. color negative and then converted to digital image data with the 50 μm aperture and green filter of the Optronics Model P-1700 photodensitometer. A pipelined processor, the Comtal Vision One/20, was used to apply a two-dimensional interpolation, reducing the effective resolution of the Skylab database to 50 m per pixel pair.

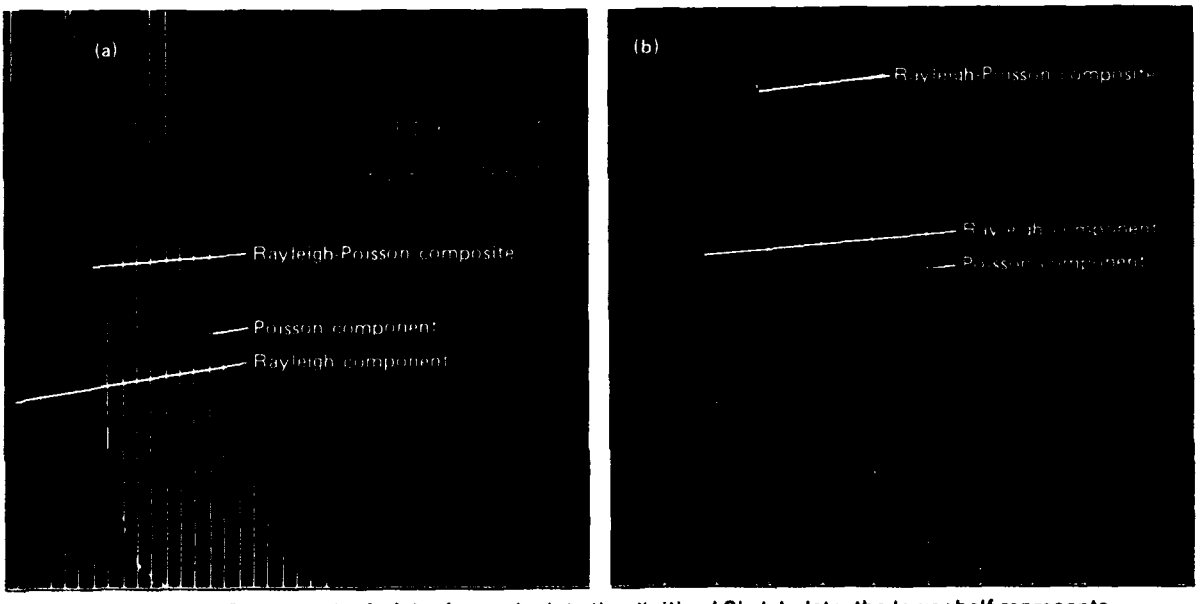

Figure 2—(a) The upper half of the frame depicts the digitized Skylab data; the lower half represents the Rayleigh-Poisson simulation computed from tables of random numbers. (b) The upper half of the frame depicts the Seasat SAR data characterized by a standard deviation equal to its mean; the lower half represents the Monte Carlo simulation based on Rayleigh-Poisson statistics.

The Seasat SAR image was compressed by pixel averaging, reducing the image resolution to 50 m per pixel pair. A geometric correction[5] was applied to map the slant range coordinate to ground range, using pixel replication and deletion to stretch the near range and to compress the far range portions of the image. The computer software developed in Fortran 77 for this range coordinate correction applied a numerical integration to a kinematic differential equation to determine which image lines would be replicated and which would be deleted. A second geometric correction was applied to remove azimuth skew introduced by the earth's rotation.

Since the sign of the Seasat-Skylab correlation is strongly influenced by the tilt orientation of the surface scatterers, this remote sensor combination is particularly effective for the classification of terrain. A cumulative scatter plot can be developed by counting the pixels that occur for each combination of Seasat and Skylab intensities. For this scene, three major classes of terrain (ocean, land, and sand) were defined on the basis of the scatter plot. Minor classes with pixel counts so low that they did not appear in the scatter plot were discovered by a more exhaustive interrogation of the multisensor imagery. Regions exhibiting either high or low multisensor cross correlations were scrutinized in order to discover and define two other terrain classes as high-profile and flat reflectors. The town of Nantucket and its airfield to the south, respectively, are the best examples of those classes.

Seasat-Skylab Correlations

The Skylab and Seasat segments enclosed by white rectangles in Fig. 1 were subjected individually to digital autocorrelation algorithms. The convolution theorem was used to define autocorrelation as a Fourier transformation followed by the Fourier inversion of a complex conjugate (*) product:

$$C(x,y) = \iint \hat{I}(k,K)\cdot\hat{I}(k,K)^* \, e^{ikx}e^{iKy} \, dk \, dK \, . \quad (4)$$

The Fourier transform, $\hat{I}(k,K)$, and the Fourier inversion were computed with fast Fourier transform algorithms[6] applied to 512 × 512 pixel databases.

The autocorrelation of the Skylab data in Fig. 3a falls off by 9 dB within three pixels and is symmetric with regard to the vertical and horizontal coordinates. The horizontal stripe indicates that the pixels are correlated at a low level within image lines as scanned with the photographic digitizer. This is not surprising because the digitizer is recalibrated for each rotation of the drum (i.e., for each image line).

Figure 3b shows the SAR autocorrelation function computed with four-look data at 25 m resolution ac-

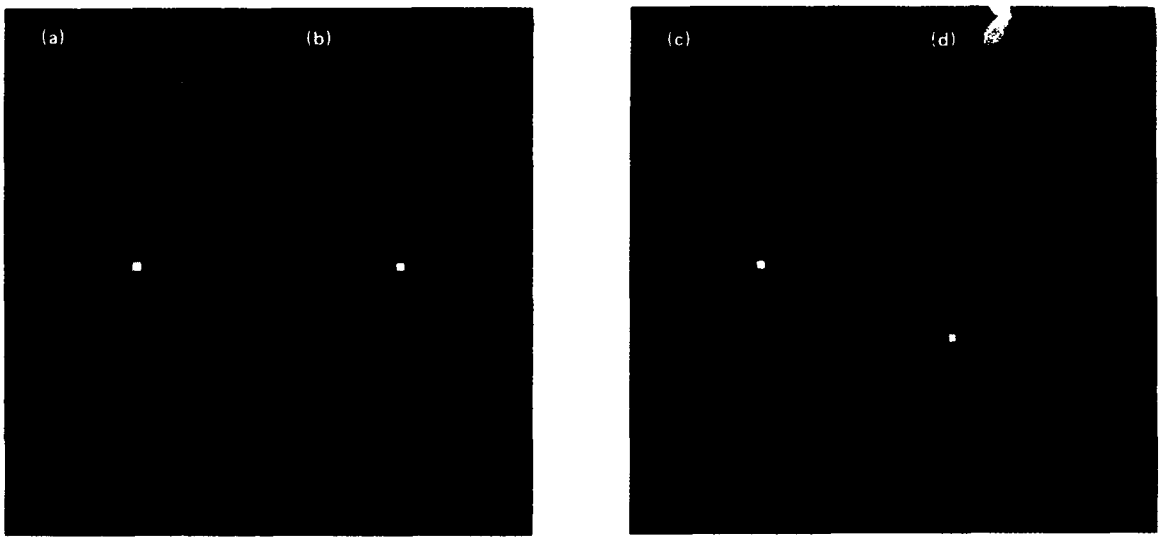

Figure 3—(a) The autocorrelation function for the digital data created by a photometric scan of the Skylab color print shows a strong central peak. (b) The autocorrelation function for the four-look Seasat SAR data falls off to a gray level typical of random correlations within 25 m in range and 50 m in azimuth. (c) The cross correlation for the red and green Skylab color separations falls off by 5 dB within one pixel, representing 50 m on Nantucket Island. (d) The cross correlation of the Skylab green separation with the Seasat SAR image confirms that both positive (white) and negative (black) correlations exist.

quired in 1980 from the digital correlator at the Jet Propulsion Laboratory. The correlation falls off by 17 dB within two and four pixels for the range and azimuth coordinates, respectively. The correlation also shows a periodic component at a correlation distance of about 100 m and at 25° from the vertical. This is evidence of the wind-streaked seas that can be observed along the southern coast of Nantucket.

A cross correlation of the two Nantucket images was computed with fast Fourier transform methods on a PDP-11/70 computer to determine how well features in the scenes had been mapped to identical ground coordinates. Prior to the application of the Fourier transforms, the mean pixel intensity was subtracted from each of the two images so that opposite deviations from their means for a common feature would contribute negatively to the cross correlation. After the computations were applied to each image, the complex cross product was formed in the spectral domain and was amplitude normalized so that well-registered, low-intensity features would contribute equally with well-registered, high-intensity features. The Seasat-Skylab cross correlation was then obtained by Fourier inversion of the amplitude-normalized cross spectrum:

$$C_{12}(x,y) = \iint \frac{\hat{I}_1(k,K)\cdot\hat{I}_2(k,K)^*}{|\hat{I}_1(k,K)|\,|\hat{I}_2(k,K)|} e^{ikx}e^{iKy}\,dk\,dK\,. \tag{5}$$

This same procedure was also applied to the red and green color separations of the Skylab image in order to obtain a reference cross correlation for two images that are identical geometrically.

The cross correlation of the Skylab green and blue color separations is shown in Fig. 3c as a test of the repositioning accuracy of the Optronics P-1700 photodigitizer and as a reference for the Skylab-Seasat correlation. Note in Fig. 3d that positively correlated features in the multisensor scenes are registered to within two pixels horizontally and three pixels vertically (e.g., 100 and 150 m, respectively).

SUMMARY

The pixel intensity distributions for the uniform Nantucket seas as recorded by the Seasat SAR and Skylab camera may be modeled well by Rayleigh-Poisson statistics. The skewing of the reflectance distribution with a low mean-to-standard deviation ratio can be simulated in random computer trials by a proper choice of N and p.

The classification of terrain features appearing in the Nantucket imagery has demonstrated that scene interpretation is enhanced by combining the information returned by sensors that penetrate to different depths and respond selectively to different textures.

Cross correlation of the Seasat and Skylab scenes shows both positive and negative correlations, depending on the characteristic length scales of the rough surfaces. The sand beach was found to be a diffuse surface for optical wavelengths but a specular surface for the L-band SAR. The two-dimensional cross correlation also demonstrated that documented geometric corrections could be applied to an unrectified SAR data product for a mapping of the Seasat image to the Skylab standard projection.

ACKNOWLEDGMENTS

The author appreciates the guidance provided by J. R. Apel, R. C. Beal, and J. P. Randolph. The computer programming contributed by W. E. Snelling was very helpful as was the word processing contributed by J. S. Greene.

REFERENCES

[1] R. G. Reeves, *Manual of Remote Sensing*, American Society of Photogrammetry, Falls Church, Va., pp. 421-423 (1975).

[2] M. D. Srinath and P. K. Rajasekaran, *Statistical Signal Processing*, Wiley and Sons, New York, pp. 28-29 (1979).

[3] D. G. Tilley, "Amplitude Distributions for Seasat SAR and Skylab Data with Statistics for Classification and Correlation," *Electromagn. Soc. J.* (in press).

[4] R. K. Raney, "Wave Orbital Velocity, Fade and SAR Response to Azimuth Waves," *IEEE J. Oceanic Eng.* **OE-6**, 140-146 (Oct 1981).

[5] J. C. Curlander and S. N. Pang, "Geometric Registration and Rectification of Spaceborne SAR Imagery," presented at International Geoscience and Remote Sensing Symp., Munich (Jun 1-4, 1982).

[6] D. Fraser, "Optimized Mass Storage FFT Program," in *Programs for Digital Signal Processing*, IEEE Press, New York (1979).

This work was supported by NAVSEASYSCOM.

TEFLON COATING OF HYDROGEN MASER STORAGE BULBS

J. A. Weiner, H. K. Charles, Jr., and D. O. Shapiro

The Microelectronics Group at APL has developed an improved process for the Teflon coating of quartz storage bulbs used in the NASA Research hydrogen maser systems built in the APL Space Department. Techniques established for inspection and acceptance testing of the incoming bulbs and the Teflon source material, and for the cleaning, coating, and thermal-processing sequences, give acceptable coatings routinely. Scanning electron microscopy is used to determine the particle size distribution in the Teflon dispersion used in the coating process and to characterize the final coating. Seven of the 15 operational hydrogen maser systems built by APL are currently using bulbs coated in APL's microelectronics facility. Several other bulbs will be used for experimental purposes or as spares for delivered systems.

BACKGROUND

The hydrogen maser is a precision standard for time and frequency. Hydrogen molecules are dissociated into atoms which are then "sorted" by their electronic state so that only those in the higher energy state are admitted to the storage bulb. A microwave cavity around the bulb is tuned to the characteristic frequency of atomic hydrogen, 1420 MHz. The induced oscillation of the hydrogen atoms at their resonant frequency results in maser amplification. The pressure in the bulb is maintained at about 5×10^{-7} Torr, and the average storage time is typically 0.6 sec.[1] Under those conditions, and with a typical storage bulb (Fig. 1), the average atom experiences over 10,000 wall collisions. Because of the large number of interactions, the power intensity and bandwidth of the output signal are largely fixed by the chemistry of the material that makes up the storage vessel wall.[2] In addition to minimizing interactions with the atomic hydrogen, the storage vessel must provide mechanical stability and microwave transparency.

For over 20 years, the interiors of quartz storage bulbs have been coated to minimize losses resulting from those interactions. Coatings that have been evaluated include paraffin waxes, polyethylene, graphite, inorganic salts,[3] and several commercial fluorinated polymers, such as Teflon TFE and Teflon FEP (trade marks of E. I. du Pont de Nemours, Inc.). Teflon FEP has been nearly universally adopted because it has consistently caused the smallest perturbation in the detected frequency, i.e., the smallest wall shift.[4] It is procured as an aqueous dispersion consisting of 0.2 μm Teflon particles, a wetting agent (Triton® X-100), and ammonium hydroxide (which is added as a fungicide and a colloid stabilization agent).[5]

APL delivers complete hydrogen maser systems in an integrated rack-mounted package to the NASA/Goddard Space Flight Center. APL also services existing systems returned for periodic refurbishing or unanticipated difficulties, often including the production of suitably coated storage bulbs to replace damaged or broken bulbs and the recoating of bulbs found to have worn or contaminated coatings. The coating technique development at APL has cast considerable light on the causes of the variability seen by past researchers in this field.[2-4]

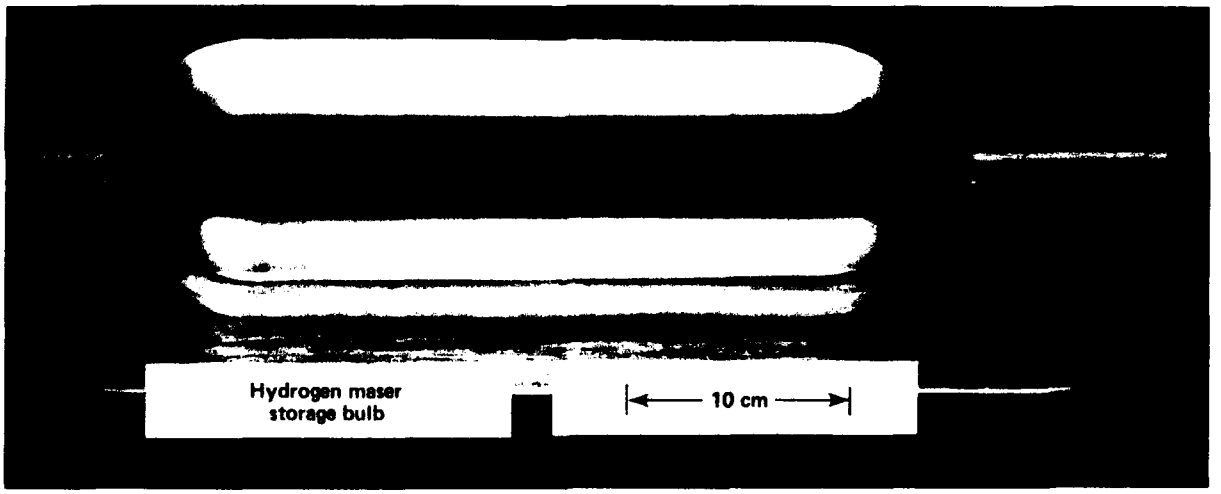

Figure 1—NASA Research hydrogen maser storage bulb.

DISCUSSION

The processes involved in coating the interior of a quartz storage bulb include: quality assurance testing and inspection of the bulb and the Teflon dispersion materials, cleaning and pretreating the surface of the bulb, coating the bulb with the dispersion, baking the bulb to fuse the dispersion particles into a continuous film, and inspecting and testing the coating. A review of the literature indicated a wide variety of procedures for cleaning, coating, and baking the bulbs.

Several cleaning methods have been found to be suitable. The cleaning is intended to remove material that could diffuse through the coating to the Teflon/hydrogen interface and to provide a clean surface that will be wetted uniformly by the dispersion. The baking of the wet coating varies from laboratory to laboratory to meet the manufacturer's minimum recommendations. The cleaning and baking procedures adopted in our laboratory are discussed below. The entire sequence is diagrammed in Fig. 2. The wetting test indicated in the flow chart involved placing 10 ml of high-purity water into the bulb and rolling it around until it had touched all areas of the bulb. If droplets adhered to the surface, the coating was unacceptable and another layer had to be applied.

The work can be divided into three subtasks: material inspection and quality assurance testing; bulb cleaning; and bulb coating, firing, and reprocessing. The first was of major concern because of difficulties found to be due to lot-to-lot variations in the Teflon dispersion. This has been reported both in the literature and during private communications with other bulb-coating facilities.[2-4] The cleaning of the bulb was critical because of the high level of surface purity required at the Teflon/hydrogen discharge interface. The ability to produce uniform, adherent, and continuous films of Teflon was a strong function of the techniques used for coating, firing, and reprocessing.

Material Inspection and Quality Assurance Testing

Early experiences with the Teflon dispersion showed that different lots of material received from Du Pont had different chemical and physical properties. Facilities, expertise, and procedures were developed to ana-

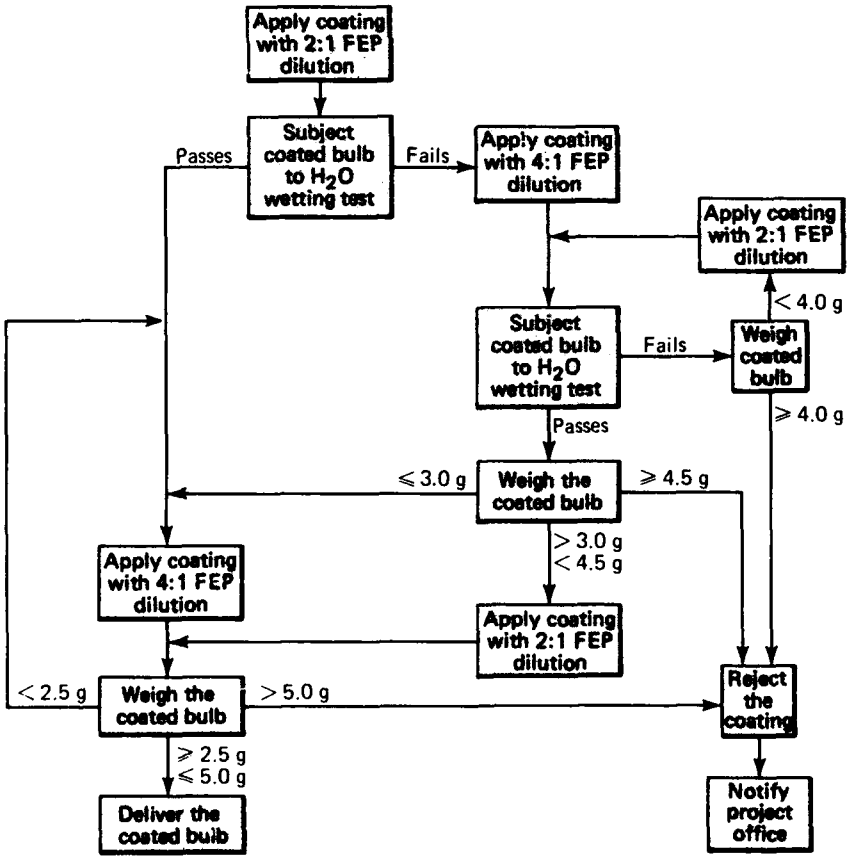

Figure 2—Processing sequence for Teflon coating of hydrogen maser bulbs.

lyze the incoming batches of Teflon FEP dispersion quantitatively for specific gravity, pH, viscosity, surface tension, percentage of surfactant, percentage of solids, particle size distribution, and iron content. The specific gravity is a measure of the total amount of nonaqueous material (surfactant plus Teflon). The pH indicates the amount of ammonium hydroxide. Viscosity indicates the thickness of the wet layer left on the walls of the quartz vessel. Surface tension and percentage of surfactant indicate the ability of the dispersion to wet a surface. (This is particularly important during multiple coating operations, where the surface to be wetted is already a continuous film of Teflon.) The percentage of solids (amount of Teflon dispersion per milliliter) affects the thickness of the final coating, assuming that the same thickness of wet coating is applied.

The FEP particle size distribution is significant because the material tends to agglomerate with age, forming particles too large to fuse properly during baking (see Fig. 3). The need to monitor the iron content of the dispersion became apparent when a red precipitate (iron oxide) was found floating on the surface of one batch of material. Du Pont has indicated that there have been instances over the years when iron was leached out of the processing equipment and precipitated by the ammonium hydroxide in the solution.

Many quartz bulbs were found to have defects in the glass that hindered the achievement of a uniform coating. A common defect was extraneous particles fused into the interior surface of the bulb. The particles interfered with the flow of the Teflon dispersion away from that area and caused thickness inhomogeneities and subsequent film failure during coating. Another common defect was irregularities and ripples in the joints between the entry tube and the body of the bulb. This problem was pandemic and was solved only through extensive hands-on experience at applying the dispersion.

Cleaning

The procedure for cleaning the bulbs prior to coating is outlined in Table 1. It was based on our prior experience in cleaning critical biological implants and spacecraft hardware and electronics.

If the coating was not performed on the day the bulb was first cleaned, the cleaning procedure was restarted at step 5. Whenever the bulb was not being "wet" processed, either the open end of the bulb was wrapped with clean aluminum foil or the bulb was purged continuously with dry nitrogen.

Coating, Baking, and Reprocessing

Preliminary experiments using Pyrex test tubes revealed that if the Teflon dispersion was used at the concentration supplied by Du Pont, the resulting film was too thick to fuse properly during baking, and it would craze extensively. If the dispersion was diluted with pure water, wetting the inside of a bulb that had already received a coating of Teflon was difficult. Instead, a stock solution was used for dilution that contained ammonium hydroxide and the wetting agent in the same concentrations as in the dispersion.

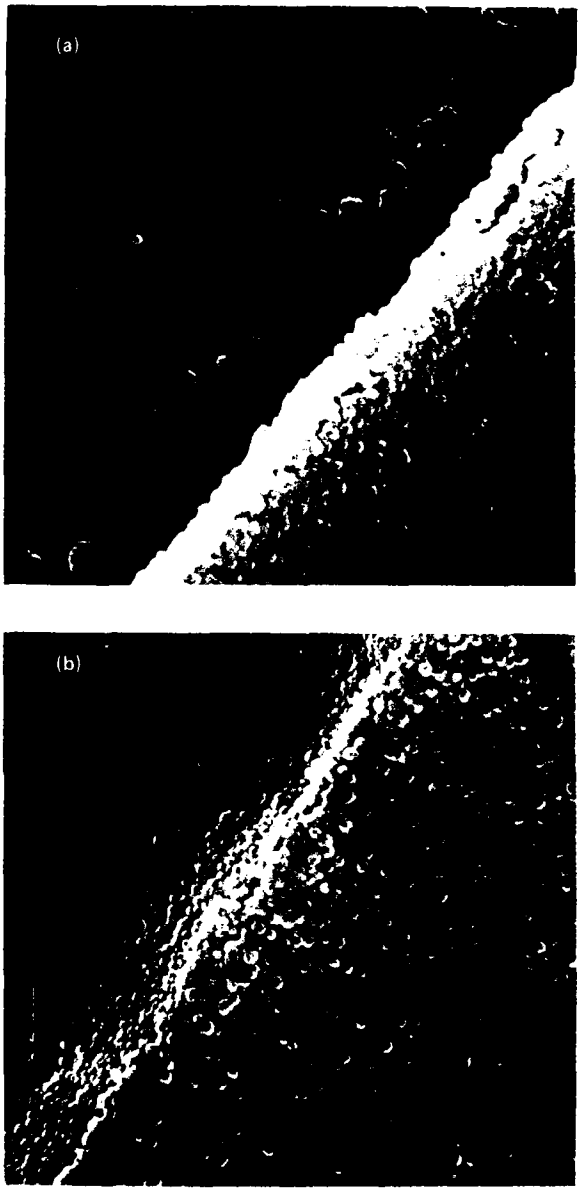

Figure 3—Teflon particles before (a) and after (b) filtration. Magnification is × 10,000.

The process of wetting the inside of the bulb with the diluted dispersion is the most critical aspect of the entire coating procedure. The technique finally adopted

Table 1—Procedure for cleaning bulbs before coating.

Step	Procedure	Comment
1	Wash bulb	Warm deionized water + commercial detergent
2	Rinse bulb	Running deionized water at 2 gal/min for 20 min
3	Dry bulb	Blow interior dry with high purity nitrogen
4	Inspect	Document chips, occlusions, etc.
5-7	Repeat steps 1-3	
8	Methanol boil	Fill three-quarters full with electronic grade methanol
9	Dry bulb	As in step 3
10	Hydrofluoric acid etch	250 ml of 10% electronic grade hydrofluoric acid for 10 min
11-12	Repeat steps 2-3	Wrap in aluminum foil

is to add the diluted dispersion to the bulb, holding it horizontally and gently rotating it around its long axis while occasionally tilting it $\pm 15°$ until all points are wetted by the dispersion. The bulb is then held vertically so that the excess liquid can drain out the open end. The top of the bulb is tilted off axis about 15° and rotated around a vertical line passing through the open end once every 30 sec. In this way, no puddles of liquid are allowed to accumulate in the irregularities at the bulb-to-neck joint.

When the drainage rate decreases to one drop every 15 sec, the bulb is placed on a stand and dry nitrogen is blown up into it until the film has a translucent appearance, indicating it is dry. The coating is then inspected for defects (crazing, missed spots, striations, foreign material, etc.).

The firing of the bulb is a two-step process. The wetting agent in the dispersion is oxidized at 290°C. That temperature must be maintained long enough to let the wetting agent diffuse through the thickness of the film to the surface, where it can react with oxygen in the air. The temperature is then increased to 390°C, where the 0.2 μm Teflon particles immediately fuse into a continuous film. During the entire time the bulb is in the oven, high purity air at a flow rate of 1.5 liters/min is admitted into the bulb.

Because of the limited thickness that can be obtained in a single coating without causing crazing, each bulb receives several coatings in order to achieve the required thickness.[5] The coating and baking are repeated until the thickness and nonwetting requirements are satisfied.

It was occasionally necessary to strip an existing coating. Since no chemical etchant will remove the Teflon film, several alternatives have been developed. One is to scratch the surface of the film and then lift it off by etching the quartz substrate with hydrofluoric acid solution. This works well but may severely etch the quartz. Another way is to heat the bulb to a temperature high enough to decompose the Teflon. Here, again, the quartz tends to be etched by the fluorine gases generated and by the high temperature (over 500°C). Both methods have been used to strip bulbs returned from field use and bulbs unsuccessfully coated in-house. However, because of the hazards and the appreciable number of man-hours required, we prefer to start with a new bulb whenever possible.

REFERENCES

[1] L. Rueger, "Characteristics of the NASA Research Hydrogen Maser," *J. Inst. Electron. Telecommun. Eng.* **27**, 493-500 (1981).

[2] P. W. Zitzewitz and N. F. Ramsey, "Studies of the Wall Shift in the Hydrogen Maser," *Phys. Rev. A* **3**, 51-61 (1971).

[3] H. M. Goldenberg, D. Kleppner, and N. F. Ramsey, "Atomic Beam Resonance Experiments with Stored Beams," *Phys. Rev.* **123**, 530-537 (1961); F. Walls (NBS) (private communication).

[4] J. Vanier and R. Larouche, "A Comparison of the Wall Shift in TFE and FEP Teflon Coatings in the Hydrogen Maser," *Metrologia* **14**, 31-37 (1978).

[5] J. F. Lontz and W. B. Happoldt, Jr., "Teflon Tetrafluoroethylene Resin Dispersion," *Ind. Eng. Chem.* **44**, 1800-1805 (1952).

This work was supported by the National Aeronautics and Space Administration.

DUAL-IN-LINE-PACKAGE MOUNTING FOR SPACE APPLICATIONS

R. H. Maurer and O. M. Uy

Two experiments were carried out to determine the most reliable way to mount dual-in-line packages on welded wire boards as well as the preferred fabrication process for the boards in order to maintain electrical design flexibility while producing reliable space hardware. The best configuration is the soldered one with conformal coating to damp the amplitude of vibration in order to prevent lead breakage and with vented socket pins to ensure good solder joints. Unvented socket pins can be soldered reliably when extra flux is used in a lengthened soldering process. This permits a conformal coating on the wiring side of the board before the component side is soldered, thus minimizing handling damage to welded wire joints and maximizing component design flexibility. The unvented socket pin technique will be implemented for one-of-a-kind designs using stitchweld technology to increase electronic packaging density in present and future APL space programs. The vented socket pin technique can be implemented for systems in which the design has been frozen and many replicates are to be manufactured (for example, an avionics application).

BACKGROUND

We investigated all aspects of high-density electronic packaging using dual-in-line integrated circuits mounted on printed circuit boards to manufacture more powerful and faster microprocessor systems for space use. The recommendation was made that dual-in-line packages (DIPs) should be soldered into vented socket pins for greater electrical reliability, perhaps thereby compromising mechanical reliability. We therefore designed a controlled factorial experiment to evaluate DIP mounting techniques, both with and without solder.

We also determined that DIPs could be soldered into unvented socket pins, a preferred technique because the wiring side of the board could be conformally coated and thereby protected before work was done on the component side. The second part of the experiment was designed to study that technique.

DISCUSSION

To develop a reliable process for high-density electronic packaging, several tools were used:

1. A controlled factorial experiment was designed (Table 1) to determine the importance and interactions of the various factors.
2. A sufficiently large sample size was used so that statistically valid conclusions could be drawn at a high confidence level (95% in this case).
3. A sensitive electrical parameter—low voltage level contact resistance—was chosen in order to measure responses quantitatively.
4. Appropriate laboratory environmental tests were used to simulate spacecraft launch and life.

Table 1—Test matrix for the controlled factorial experiment (the numbers represent the DIP designation).

Solder	Perimeter	Conformal Coating				No Conformal Coating			
		Solithane Bumper		No Solithane Bumper		Solithane Bumper		No Solithane Bumper	
		Pkg. RTV	No Pkg. RTV	Pkg. RTV	No Pkg. RTV	Pkg. RTV	No Pkg. RTV	Pkg. RTV	No Pkg. RTV
No	Inner	7 39	5 37	3 35	1 33	23 55	21 53	19 51	17 49
No	Outer	15 47	13 45	11 43	9 41	31 63	29 61	27 59	25 57
Yes	Inner	8 40	6 38	4 36	2 34	24 56	22 54	20 52	18 50
Yes	Outer	16 48	14 46	12 44	10 42	32 64	30 62	28 60	26 58

The Controlled Factorial Experiment

Table 1 shows the test matrix for the first experiment. Although traditional philosophy says to vary only one factor at a time while holding all others constant, that thinking is often counterproductive for engineering experiments, particularly when a process is being optimized. The main effect in process optimization may be the result of interaction between two or more factors, not an individual factor. Five factors and their interactions were studied in the first experiment:

1. Solder—Both soldered and unsoldered electrical joints between the DIP lead and the socket pin;
2. RTV support of the body of the DIP—Samples with and without package RTV (a tradename for a group of silicone rubber compounds) to determine the difference that this additional mechanical support would make (see Fig. 1);
3. Solithane bumpers on the DIP leads—Samples with and without Solithane bumpers to determine their effect on excluding conformal coating from unsoldered electrical joints and on providing additional mechanical support (Fig. 1);
4. Conformal coating—Samples with and without conformal coating to study the actual flight board (conformal coated) versus the prototype design board in which no conformal coating was used and soldered DIP legs broke;
5. Board position—Samples mounted taking into consideration their positions on the board with respect to the board stiffeners and the distance from the center of each half of the board (Fig. 2) (denoted inner and outer perimeters in Table 1).

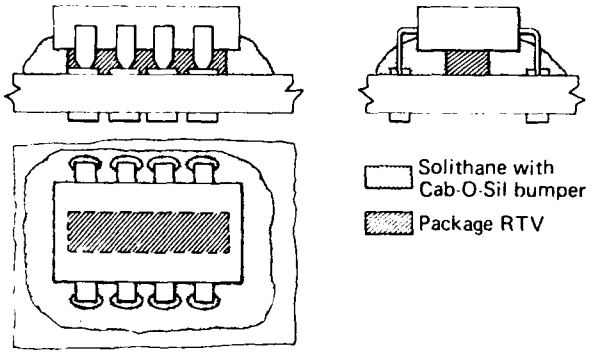

Figure 1—Mounting of a standard DIP with a Solithane bumper and package RTV.

The second part of the experiment addressed the following factors:

1. Vented versus nonvented socket pin. The vent allows trapped gases formed during soldering to escape from the socket pin away from the solder joint.
2. Extra solder flux versus core solder flux only. Additional flux ensures better joints and greater coverage in nonvented socket pins.
3. Conformal coating on the component side of the board. This may only be significant during vibration since it is applied after soldering has been completed.
4. Conformal coating on the wiring side of the board before and after soldering. This makes no difference to nonvented socket pins but af-

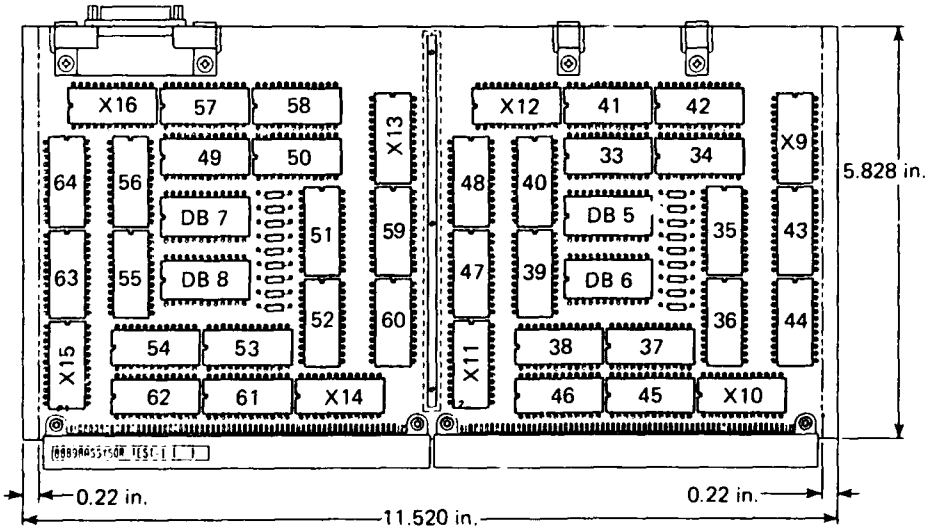

Figure 2—Layout of test board used in the first experiment. Numbers 33 through 64 are standard DIPs.

fects vented ones because coating the wiring side before working on the component side can contaminate the socket pin electrical interfaces.

5. Use of a dummy DIP during conformal coating of the wiring side. This may affect vented socket pins because good contact at the interfaces during conformal coating tends to prevent the coating from contaminating the most critical area of the socket pin. Dummy DIPs are removed after the conformal coating has been completed, and the test DIPs are then soldered in. Half of the board positions had no dummy DIPs because they were coated after soldering; one-fourth had none and were coated before soldering.

Large Sample Size

Figure 2 shows the layout of one test board. Each standard DIP has 24 pins, yielding 24 contact resistance measurements between DIP legs and socket pins; 1536 such contact resistances were monitored during the first experiment. The second experiment used 16 pin DIPs; 477 contact resistances were monitored (some were not monitored because of inadvertent grounding). Generally, one would like to replicate individual combinations of factors to avoid accidental bias effects. Furthermore, when statistics that evaluate comparisons among mean values or variances of different groups become asymptotic as the number of degrees of freedom increases, it is best to choose a sample size at or above the asymptotic number. This allows enough degrees of freedom to make the experimental error in an analysis of variance reasonably small without requiring an impractical number of samples.

Choice of a Sensitive Electrical Parameter

The DIP leg/socket pin electrical joint was examined visually and the contact resistance was also measured to determine degradation other than a broken leg. Contact resistance measurements, particularly useful in evaluating changes in unsoldered electrical joints, were made using the four-probe technique. The power supply was adjusted so that the short-circuit test current was 100 mA, and the open circuit voltage was limited to 200 mV. That kind of measurement is not truly a dry circuit technique since 50 mV is considered an upper limit for a dry circuit. However, it was the lowest voltage that could be used to obtain stable resistance readings over some of the higher impedance paths, and it is conservative compared to the actual 5 V circuitry in spacecraft applications. Low-level voltage measurement techniques have the advantage of not breaking down contaminating films being formed by environmental testing. Oxide and sulfide films formed in electrical joints that are not truly gas tight (often the objective to be proved or disproved) are usually several hundred angstroms thick and can be broken down by a few volts.

Laboratory Environmental Tests

Sometimes the tests to be run in the laboratory are obvious, such as the soldering and conformal coating sequences. Vibration can also be simulated at the board level by using a power frequency spectrum that is a few decibels above that to be experienced during spacecraft launch. To simulate spacecraft life, we chose a temperature cycling test: 100 cycles from -65° to +150°C with

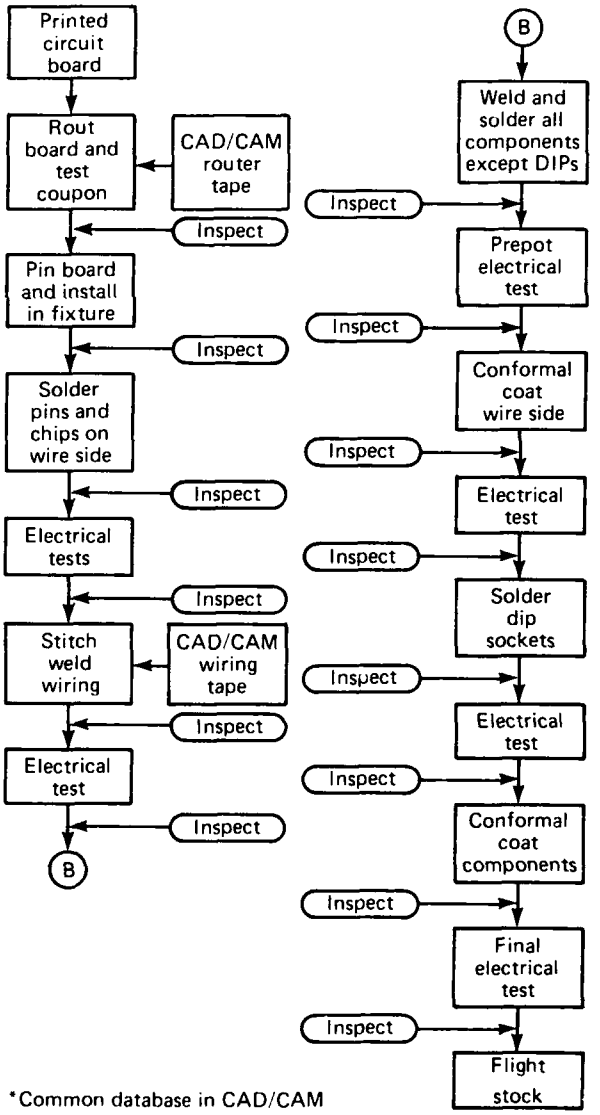

*Common database in CAD/CAM

Figure 3—Manufacturing flow chart using unvented socket pins.

15-min dwell periods at each extreme. The dwell period must be long enough for the test board to reach temperature equilibrium. Even though life testing has traditionally been done using only elevated temperature (the Arrhenius technique), the spacecraft environment usually involves continuous temperature cycling. Although there is no accelerated aging associated with extremely low temperatures, we know from experience that such temperatures can create a concentration of stresses, especially at joints or interfaces.

Details of the test sequence and the statistical analysis of the contact resistance data and of the visual inspections for mechanical DIP leg breakage can be found in Ref. 1.

CONCLUSIONS

For a one-of-a-kind design, use conformal coating of the wire side of the board before soldering into unvented socket pins and use extra flux in a lengthened soldering process. If vented socket pins must be used, plug dummy DIPs into those sockets to protect the electrical contact area during conformal coating of the wiring side; when flight DIPs are soldered into the vented socket pins, use extra flux.

For a frozen design to be manufactured many times, solder into vented socket pins before conformal coating of either side of the printed circuit board.

Figure 3 shows the manufacturing flow chart using unvented socket pins that we developed as a result of our experiments.

REFERENCE

[1] R. H. Maurer and O. M. Uy, "Dual-in-Line-Package Mounting for Space Applications," in *Proc. 34th Electronic Components Conf.*, pp. 498-510 (May 1984).

This work was supported by NASA and the Department of the Navy.

OCEAN SCIENCE AND TECHNOLOGY

INTRODUCTION

In a very broad sense, the field of ocean science and technology (OS&T) may be viewed as a special subset of the entire subject of the environment. As reported in this volume, however, OS&T is presented separately (see also the Environmental Science and Technology Section), a treatment that is consistent both with the relative magnitude of the effort at APL and with the differences in objectives between "pure" environmental research and the more "directed" nature of OS&T. Even so, the distinction becomes blurred at times, for even the most hardware-intensive technological project often has its roots in the fields of basic research.

The selected examples of OS&T work that follow serve to highlight the wide diversity of Laboratory efforts in this field. Despite their variety, however, they all embody a central, invariant theme: the conception, development, and application of new tools and techniques for characterizing and using ocean properties and processes in ways that contribute toward reaping a benefit from the sea or surmounting an obstacle posed by it.

METEOROLOGICAL BUOY AND TOWER FOR REAL-TIME WIND MEASUREMENTS IN DELAWARE BAY

S. J. Seymour, D. C. Wenstrand, M. J. Jose, and J. H. Meyer

APL has developed a meteorological station consisting of a buoy and a 10-m tower and has deployed the system at Brandywine Shoals in Delaware Bay. Wind speed and direction are sensed at heights of 2 and 4 m on the buoy and 4 and 10 m on the tower. The data, which are telemetered to the National Ocean Service, Rockville, Md., are critical inputs to a real-time numerical water-current model of Delaware Bay.

BACKGROUND

The National Ocean Service Circulation Survey Program is developing, with APL recommendations, a new approach to predicting currents in United States harbors and estuaries to aid commercial and recreational navigators. Survey vessels and mechanical current meters for determining currents will be replaced by numerical models and strategically placed monitoring stations. The APL meteorological instrumentation is a prototype of the measurement system that will be used in conjunction with numerical models to provide more frequent, higher quality, and more economic service to the public in the new National Ocean Service program.

DISCUSSION

The Delaware Bay and River were the sites chosen to demonstrate the capability and value of total circulation models in providing predictions of currents and water levels. From June to September 1984, a real-time measurement and modeling system was designed and built by a team consisting of the National Ocean Service, APL, and Science Applications, Inc. APL was responsible for the measurements of wind speed and direction.

The instrumentation in Delaware Bay consisted of four water-level measuring stations, a meteorological buoy and tower, and a Remote Acoustic Doppler System for the measurement of water velocity profiles. As shown in Fig. 1, the data were transmitted in real time to Rockville for validation and assimilation into a National Ocean Service two-dimensional numerical model for predictions of current and into an extrapolated National Weather Service model for predictions of wind. Several small minicomputers acquired and preprocessed the data; then, after model calculations on a Cyber 205, they were used to access the model predictions and generate various products, including 36-hr predictions of currents and water levels.

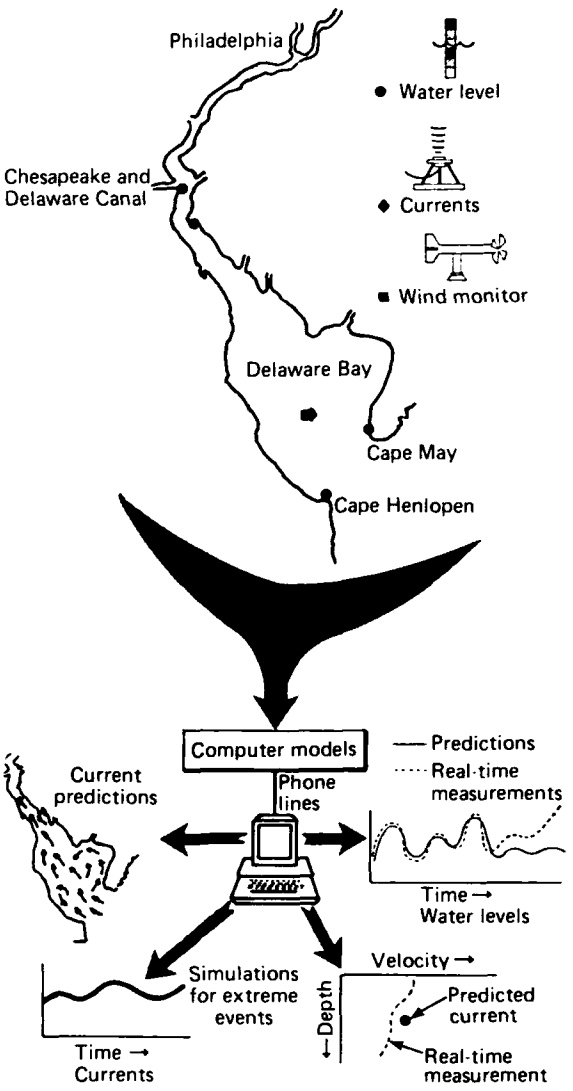

Figure 1—The real-time measurement system.

The APL meteorological station was deployed to measure wind stress (force per unit area) on the surface of the water. This meteorological forcing information was used in combination with the tidal forcing information to drive the numerical model of Delaware Bay. Wind velocity measurements at three heights (2, 4, and 10 m) were obtained in order to calculate boundary layer properties including mean speed profile, surface roughness scale, wind stress, and friction velocity.

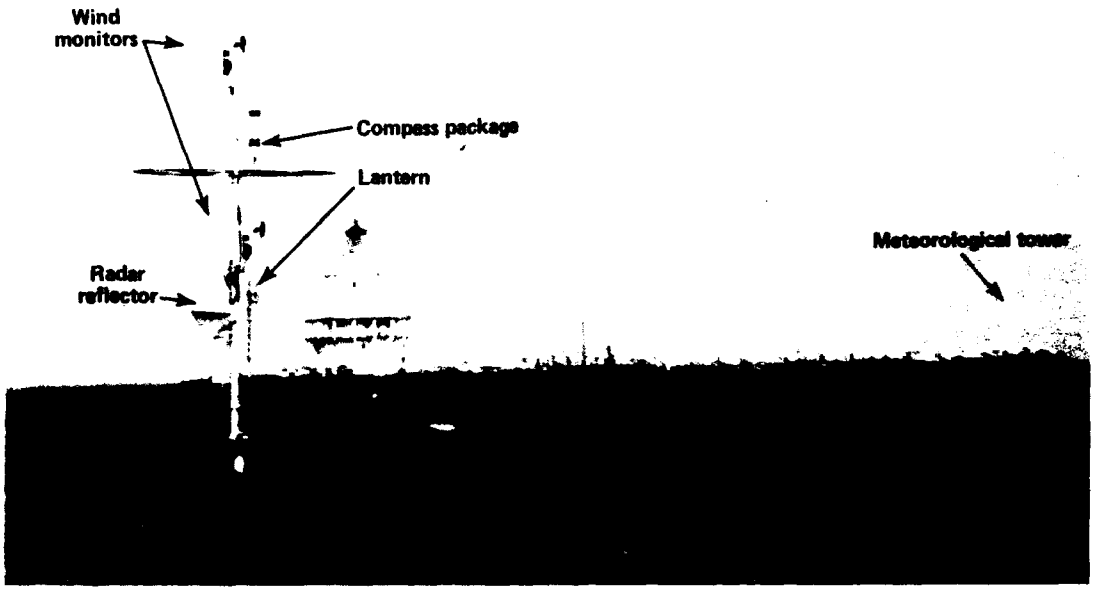

Figure 2—The meteorological buoy and tower.

Instrumentation

The meteorological buoy developed by APL consists of a 24-in. spherical foam float with 12 ft of 2 in. chain leading to a single-point slack mooring for easy buoy deployment and recovery. The 14-ft buoy mast holds two R. M. Young wind monitors at heights of 2 and 4 m to measure wind speed (±2%) and direction (±5°). Two Anderaa compasses on the mast measure buoy orientation. The mast also has a radar reflector and a warning lantern.

The buoy, which was deployed 2000 ft from Brandywine Shoals in central Delaware Bay, is shown in Fig. 2. Figure 3 is a schematic of the installation. The wind data were transmitted by underwater cable to the lighthouse at Brandywine Shoals for transmission to Rockville.

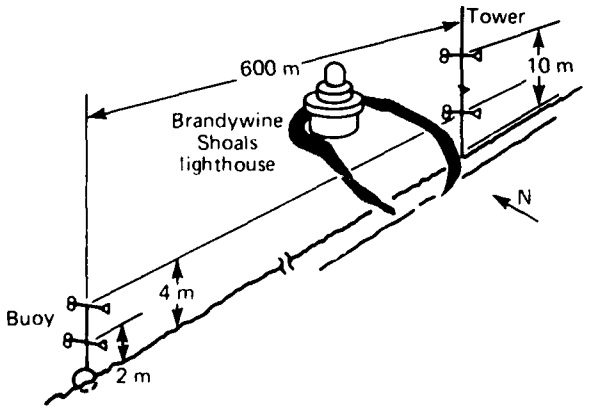

Figure 3—Schematic of the buoy and tower installation.

The buoy electronics package consists of power and signal conditioning circuits for the two Anderaa compasses (primary and backup) and the two wind speed and direction sensors. Individual signals are transmitted as currents by underwater conductors to the lighthouse where they are current-to-voltage converted, filtered, digitized, and telemetered every 6 min to the NOAA Cyber 205 computer that runs the Delaware Bay numerical model.

Two other wind monitors are supported by a 10-m-high, guyed-aluminum-truss tower located on the rocks at the lighthouse site. One monitor is 4 m high and the other 10 m. A signal cable runs from the tower to the lighthouse, where the information is recorded and transmitted to shore.

The instrumentation performed well in the marine environment, and high-quality data were obtained throughout the 2-month period during which the numerical model was being demonstrated. The system is expected to operate continuously for many months.

Data Analysis

Figure 4 shows a 14-day set of wind speed data from the four buoy and tower sensors. Evident from the figure is the clear tendency for wind speed to increase with height in the boundary layer, as would be expected from the so-called law of the wall:

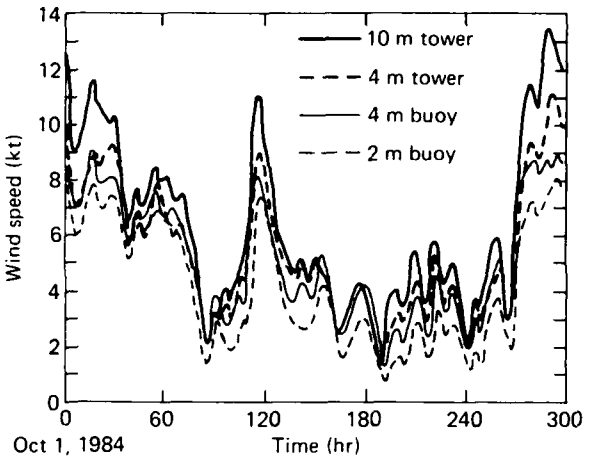

Figure 4—Wind speed data from the four measurement stations.

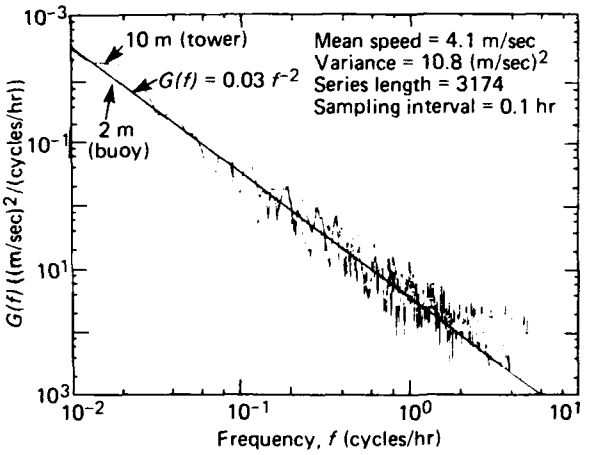

Figure 5—Autospectra of wind speed for the four measurement stations.

$$\frac{u}{u_*} = \frac{1}{k} \ln \frac{z}{z_0} \quad ,$$

where u is the wind speed at height z, u_* is the friction velocity, z_0 is the surface roughness scale height, and k is the van Karman constant approximately equal to 0.4. From this relation and from the wind speed data at the three heights, z_0 and u_* can be obtained. u_* is related to the wind stress, τ, by

$$u_* = \sqrt{\tau/\rho} \quad ,$$

where ρ is the air density.

As is evident in Fig. 4, the wind speeds were highly correlated between the upper and lower sensors at each location, showing correlation coefficients of 0.99. Between the buoy and the tower, correlations dropped slightly to 0.96.

Figure 5 shows the autospectra of wind speed for the four sensors, each spectrum showing an f^{-2} dependence. Owing to this rapid falloff in wind spectral density, relatively little variance is lost by low-pass filtering the wind-speed/time series at a low frequency. For example, if the data are filtered at 0.2 cycle per hour, the variance removed corresponds to an rms velocity of only 0.3 m/sec. Thus, these results would indicate that it is probably not necessary to take samples of average wind speed more frequently than every 1 to 2 hr to calculate the effects of wind stress over the estuary.

Future analysis of this data set will be directed at determining how to construct wind stress measurement stations for other estuaries. Issues such as how many sensors are necessary, their heights, and sampling rates will be addressed.

SUMMARY

The prototype real-time harbor monitoring system is currently operating in Delaware Bay. Second only to tidal effects, meteorological effects are significant in accurately predicting the currents in this commercially important estuary. More accurate and less costly data on currents and water levels will now be available to ensure safe ship transits, to maintain a clean environment, and to use the estuary resources more effectively. The technology and experience gained in this project will be applied to new systems nationwide.

This work was supported by the NOAA National Ocean Service.

ACOUSTIC SURFACE DUCT CHARACTERIZATION IN THE NORTHEAST ATLANTIC OCEAN AND THE NORWEGIAN SEA

P. G. Fuechsel and C. H. Sinex

APL has developed a unique way to characterize the open-ocean acoustic environment based on the cutoff frequency of acoustic surface ducts. The results are presented as contour maps of the probability of trapping 400-, 200-, and 60-Hz acoustic energy in the northeast Atlantic Ocean and the Norwegian Sea month by month.

DISCUSSION

An acoustic surface duct occurs when the sound velocity increases with depth below the surface. When a shallow noise source operates in a duct, acoustic energy can be trapped in the duct and can propagate for long distances. The lowest frequency that is trapped depends in part on the depth of the duct. Because duct formation is related to the vertical temperature gradient, the duct depth has a distinct annual cycle. In the winter, strong storms and large heat losses from the upper ocean create deep ducts (200 to 400 m) that trap relatively low frequencies (below 400 Hz). In the summer, heat gain in the upper ocean results in shallow ducts (50 to 100 m), with a corresponding increase in the lowest frequency trapped. Duct depth is also influenced by ocean currents and ocean bottom contours as measured by bathymetry, both of which are strongly dependent on geographic location.

Duct depth has been the traditional criterion for analyzing acoustic propagation in surface ducts. However, it has two major limitations. First, many of the historical depth/temperature profiles do not extend deep enough to reach the bottom of the duct. Second, duct depth alone does not adequately characterize the duct. The lowest frequency trapped by a duct depends on both duct depth and duct strength (i.e., total sound-speed gradient across the duct).

Those problems can be minimized by characterizing ducts in terms of the probability of trapping a discrete frequency in a duct. That probability is determined by computing the cutoff frequency as a function of depth for a given sound velocity profile. The cutoff frequency is obtained using the Wentzel, Kramers, Brillouin (WKB) method, which leads to an integral along the profile.[1,2]

The minimum trapping probability in a given area is obtained by organizing data into files containing depth/temperature profiles in a grid 3° in longitude by 3° in latitude. The cutoff frequency for each profile is computed and compared with the frequency of interest. The trapping probability is the ratio of (a) the number of profiles exhibiting a cutoff frequency equal to or lower than the frequency of interest, to (b) the total number of profiles in the grid. Some profiles that showed strong ducting conditions did not meet this criterion because they were not sampled deep enough. Hence, the computed ratio represented a minimum trapping probability.

RESULTS

Examples of the plotted trapping contours for 400 Hz are shown in Figs. 1 and 2 for the months of May and September, respectively. Several features of acoustic surface ducts in the northeast Atlantic Ocean and the Norwegian Sea can be identified from the figures. The more significant duct characteristics are as follows:

1. As late as May, much of the region traps 400-Hz energy with a trapping probability of 40% or greater.
2. The spatial variability of the probability of 400-Hz trapping is clearly evident, with trapping probabilities generally increasing with higher latitudes. The 100% trapping probability in the waters off the western coast of Norway is noteworthy.

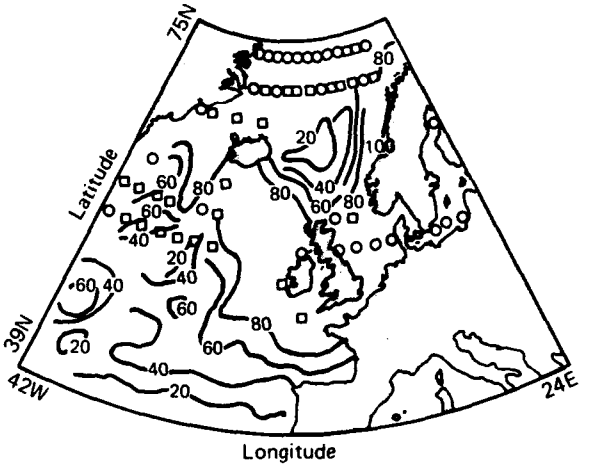

Frequency	400 Hz	o = No data in grid
Month	May	□ = Less than 10 profiles in grid
Max. analysis depth	240 m	
Grid size	3° x 3°	
Source depth	50 m	
Mode	2	

Figure 1—Minimum trapping probability contours (in percent) for a 400-Hz noise source in a surface duct in May.

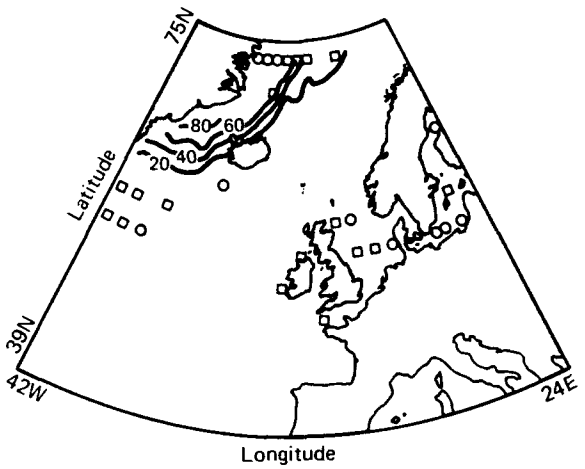

Frequency	400 Hz	o = No data in grid
Month	September	□ = Less than 10 profiles
Max. analysis depth	240 m	in grid
Grid size	3° x 3°	
Source depth	50 m	
Mode	2	

Figure 2—Minimum trapping probability contours (in percent) for a 400-Hz noise source in a surface duct in September.

3. In late summer (September), the region of high 400-Hz ducting probability has decreased markedly and is confined to the area east of Greenland.
4. Areas that show low probabilities of trapping 400-Hz signals may have shallower ducts that can trap frequencies greater than 400 Hz with high probability, but those higher frequencies were not considered in the analysis.

As a general rule, the probability of trapping 200-Hz signals is about 20% lower than the probability of trapping 400-Hz signals for the regions and seasons examined (viz., 40% compared with 60%). The effect of variations in source depth on trapping probabilities for 200-Hz energy was also investigated. It was found that changes in source depth between 15 and 100 m caused no significant difference in trapping probability.

The 60-Hz signal results are treated separately in this analysis because the very limited quantity of adequate deep historical data confines temporal characterization to the area west of Spain and Ireland—an area influenced by the Mediterranean outflow. The seasonal trends for that area can be summarized as follows. During winter, the area exhibits deep ducting conditions (duct depths exceeding 500 m) with a greater than 60% probability of trapping 60-Hz energy. With surface heating in spring and early summer, the probability gradually declines to 20%. However, as late as July, localized areas west of Ireland can still exhibit a 60% probability. During the rest of the summer, the probability of trapping remains at less than 20%, with a slow increase in the fall to 20 to 40%. Other areas such as the Reykjanes Basin may also have deep ducting conditions, but adequate deep data are currently not available to assess them.

REFERENCES

[1] R. J. Urick, *Principles of Underwater Sound for Engineers*, McGraw-Hill, New York, p. 125 (1961).

[2] D. E. Kerr, *Propagation of Short Radio Waves* 13, MIT Radiation Laboratory Series, McGraw-Hill, New York, p. 72 (1951).

This work was supported by the Department of the Navy.

AN INSTRUMENTED, UNDULATING, TOWED VEHICLE FOR OCEANOGRAPHIC MEASUREMENTS

C. V. Nelson, P. E. Panneton, L. M. Burns, and C. W. Anderson

An instrumented, undulating, towed vehicle for measuring oceanographic parameters within the upper 100 m of the ocean has been designed, fabricated, and tested at sea. The system provides a unique capability for measuring vertical and horizontal variations of ocean parameters.

BACKGROUND

The measurement of vertical and horizontal variations of upper ocean parameters is important for addressing scientific issues of interest to oceanographers and the Navy. Obtaining such data from a series of vertical profiles made at discrete locations is generally unsatisfactory if the ocean parameters change rapidly in time or space. Data can be obtained more efficiently by placing sensors on a platform that can execute depth excursions while being towed behind a surface ship. A new design was proposed by APL in 1981[1] that doubled the profiling rate of previous undulating systems.[2,3] That system, which is a towed paravane, is instrumented with environmental sensors and can make rapid and controlled depth excursions in the upper ocean. The vehicle, its computer control system, and several sensors were designed and built by APL. The data acquisition system and other sensors were procured commercially. The design of the vehicle's shape is based on data provided by the David Taylor Naval Ship Research and Development Center (DTNSRDC).

The vehicle, its computer control system, and its sensor data acquisition system were designed and built at APL. Some of the other instruments were also designed at APL; others were procured commercially.

DISCUSSION

The undulating, towed vehicle is constructed around a center strongback to which five pressure vessels are attached. Four pressure vessels house the vehicle's instrumentation and oceanographic instruments; the fifth contains a motor for a control vane that causes the vehicle to change depth. Molded syntactic foam covering the pressure vessels and the strongback provides buoyancy and streamlining. Two fixed biwings produce dynamic lift. The vehicle (Fig. 1) is 1.67 m long and 0.34 m in diameter; it has a wingspan of 1.4 m and a mass of 141 kg. An electromechanical tow cable connects the vehicle to the shipboard control and data acquisition electronics.

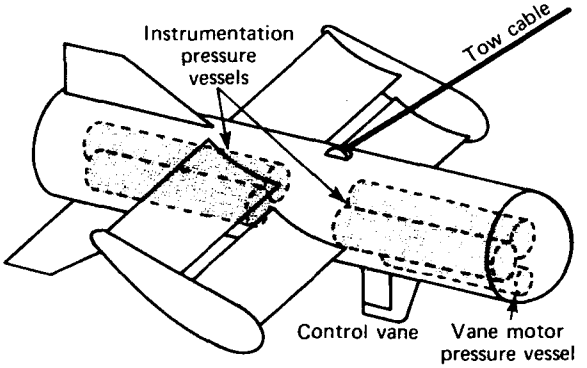

Figure 1—The instrumented, undulating, towed vehicle.

System Operation

The vehicle roll angle is altered by a bottom-mounted control vane. With a fixed cable length, roll motions change the direction of the wings' dynamic lift, causing the vehicle to rise as it moves to one side of the tow ship. The profiling trajectory is shown in Fig. 2. If the ocean is laterally homogeneous over the scope of the tow cable (typically 100 m or less), measurements made over this trajectory will accurately reflect local vertical variations.

Vertical profiling maneuvers are controlled by a digital closed-loop feedback system consisting of a topside HP 9816 computer and a vehicle-mounted microcomputer. The on-board microcomputer senses the vehicle roll and depth and transmits that information to the topside computer. The system operator provides the desired profiling sequence to the HP 9816, which computes the proper control signals and transmits them to the microcomputer. Analog control signals are then generated and supplied to the vane motor. The HP 9816 also displays the vehicle's depth history, roll angle, and control status parameters. Data for post-test analysis are recorded on magnetic tape.

The vehicle is presently instrumented to measure temperature, depth, conductivity, chlorophyll-*a* concentration, and the optical beam attenuation coefficient. An on-board, 16-channel, 16-bit data acquisition system collects the sensor data at a 12 Hz rate and transmits them to a deck unit. The deck unit buffers the data and sends

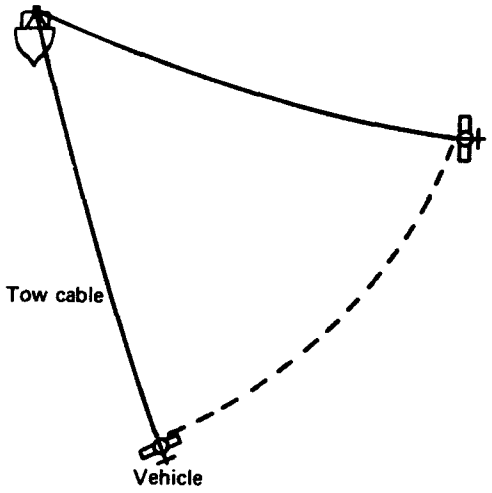

Figure 2—The profiling trajectory.

them to an HP 9826 computer for processing and display. Ship navigation data are also collected and together with all other data are recorded on a 9-track tape recorder. Figure 3 is a simplified block diagram of the complete system.

System Performance

Computer simulations were performed on the vehicle design to verify the profiling technique and to obtain numerical values for the control system's variables. Validation of the simulation program was made using profiling sea test data from a smaller paravane.[4] Towing stability was then verified at speeds up to 12 kt in a tow tank at DTNSRDC.

A field test of the towed vehicle system was conducted in July 1984 off the Florida coast. The vehicle was towed at 8 kt while executing depth variations from 100 to 15 m. Maximum ascent and descent rates were 5 and 2.5 m/sec, respectively. Typical cycling times were 2.5 min.

CONCLUSION

A rapidly profiling towed vehicle has proven to be an excellent platform for studying horizontal and vertical variations of ocean parameters. It offers the following advantages:

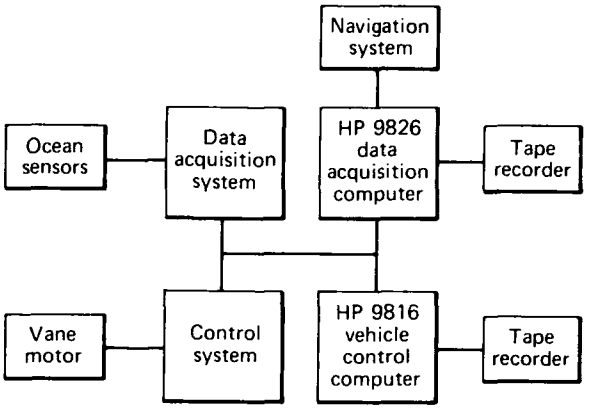

Figure 3—Block diagram of the measurement system.

1. It can profile vertically at faster rates than can existing platforms of similar size and payload capacity.
2. Operator control and data acquisition flexibility are significantly enhanced by using a computer-driven control system.

While designed for use with specific ocean instruments, the vehicle should be readily adaptable to carry other instruments for a variety of oceanographic investigations.

REFERENCES

[1] C. W. Anderson, "Surface-Operated Controlled-Depth Paravane," *Developments in Science and Technology, Fiscal Year 1981*, JHU/APL DST-9.

[2] J. G. Dessureault, " 'Batfish,' A Depth Controllable Towed Body for Collecting Oceanographic Data," *Ocean Eng.* 3, (1976).

[3] R. Knutson and R. Singleton, "Operating and Hydrodynamic Evaluations of a Controlled Depth Towed Depressor Designed to House a Conductivity, Temperature, Depth (CTD) Instrument System," David Taylor Naval Ship Research and Development Center, DTNSRDC-81/012 (Mar 1981).

[4] C. W. Anderson, "Surface-Operated Profiling Paravane," Oceans '84 Conf., Washington (10-12 Sep 1984).

This work was supported by the Office of the Secretary of the Navy, OP-21.

DOPPLER SONAR ERROR PROPAGATION AND TRACK CORRECTION

D. W. Jourdan

The technique of estimating a vessel's speed over the ground by measuring the Doppler frequency shift of an acoustic pulse reflected from the bottom has been used successfully by the oceanographic community for many years. Despite the history of success of the Doppler sonar navigation system to date, improvements in marine technology and more stringent operational requirements have placed new demands on system accuracy. This study addresses the expected performance of a typical Doppler sonar navigation system, identifies error sources contributing to degraded accuracy, and develops a method by which significant improvements may be achieved in using the system for precision oceanographic survey operations.

BACKGROUND

The effective conduct of oceanographic survey operations presents two separate but related navigation problems: (a) determination of the absolute geodetic location of the ship, and (b) determination of the location of the ship relative to all other points in the local area over which the survey is conducted. The accuracy requirements of the second problem are generally more stringent because correlation of the collected data will be impossible if one is uncertain about where the data were obtained. Because geodetic positioning data (such as from navigation satellites) are generally not available with sufficient frequency or accuracy for relative positioning, an accurate dead-reckoning device, such as Doppler sonar, must be used.* Operational experience has demonstrated that, over a period of time, large enough errors may develop in the Doppler navigation system so as to seriously degrade the precision of local navigation. The objective of this study was to identify sources of error within and external to the system, develop a model that describes the effects of those errors for given system parameters, and provide a method by which the model may be applied in order to estimate the appropriate corrections to the relative ship's track. The system model and the method of application are singularly significant because a definitive model of error growth in the Doppler sonar navigation system that could be used to estimate corrections to ship tracks had not previously existed.

*The Global Positioning System has recently been placed in operation and is currently capable of providing accurate navigation for short periods of time each day. Coverage and accuracy will be improved through the rest of the decade; by 1989, the system is expected to provide extremely accurate, continuous geodetic position. However, it may not be usable in certain operations such as the navigation of towed vehicles. Another accurate geodetic positioning system is LONARS (loran navigation receiving system), but it is only available in certain very limited areas of the ocean. Other systems, such as inertial devices, do not have the required accuracy.

DISCUSSION

System Description

The basic concept of a Doppler sonar navigation system is that an acoustic pulse generated by a ship, after reflection by the ocean bottom and return to the ship, undergoes a change in frequency (Doppler shift) that is related to the velocity of the ship with respect to the bottom. The frequency shift may be measured by the system and used to determine accurately the ship's motion over the earth. A typical system consists of a transducer assembly that forms the acoustic pulse into the proper beam configuration and receives the reflected pulse, a receiver/transmitter that provides the input signal to the transducers and accepts the return signal for processing, a processor that measures the frequency shift and computes a velocity signal, and a display for position and velocity readout. The processor requires a ship's heading reference (usually external to the system) so that ship motion may be resolved properly into motion over the earth in a north-oriented coordinate system. In order to measure both horizontal velocity components of the ship and to minimize the effect of vertical velocity, pitch, and roll, three or four distinct acoustic beams are generally used; Fig. 1 shows a typical four-beam system.

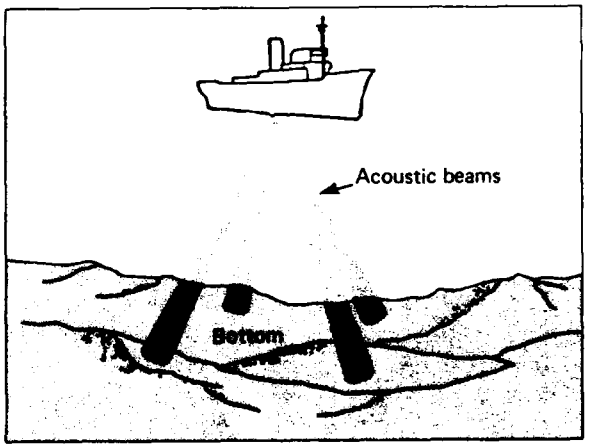

Figure 1—A typical Doppler sonar navigation system.

Under ideal conditions, the Doppler navigation system described above may provide exceptional navigation accuracy. Assuming that the system is carefully aligned and adjusted and is provided with accurate heading and sound velocity reference sources, errors of less than 0.5% of the distance traveled may be expected. However, usual operating conditions act to degrade performance so that errors of 2 or 3% of the distance traveled typically have been observed.

Error Sources

The first step in the study was to identify the causes of error in the typical system, based on theory of operation and on past observations of system performance. Research revealed that Doppler system errors arise from three sources: effects of the medium through which the acoustic signals must pass, processing of signals, and transformation of velocity signals into north-oriented coordinate system components. Medium effects include reflection of acoustic pulses from the water column (reverberation) and random acoustic noise. Errors in processing include those in scaling approximations, velocity of sound measurements, frequency shift measurements, the base frequency setting, and the smoothing and sampling of data. Transformation errors include misalignment of the transducer assembly, errors in the heading reference, and earth meridian convergence effects.

Once the error sources had been identified, the thrust of the study turned to the analysis of each effect in order to determine a useful mathematical expression of its impact on the net Doppler velocity error. The result was a collection of equations relating the net velocity error to functions of measurable quantities (such as sound velocity, ship's heading, and ship's altitude) and various unknown error parameters. Where appropriate, both random and bias error parameters were included so that each could be treated separately. The next step was to group the equations into a logical framework, or model, showing how each contributes to the total error.

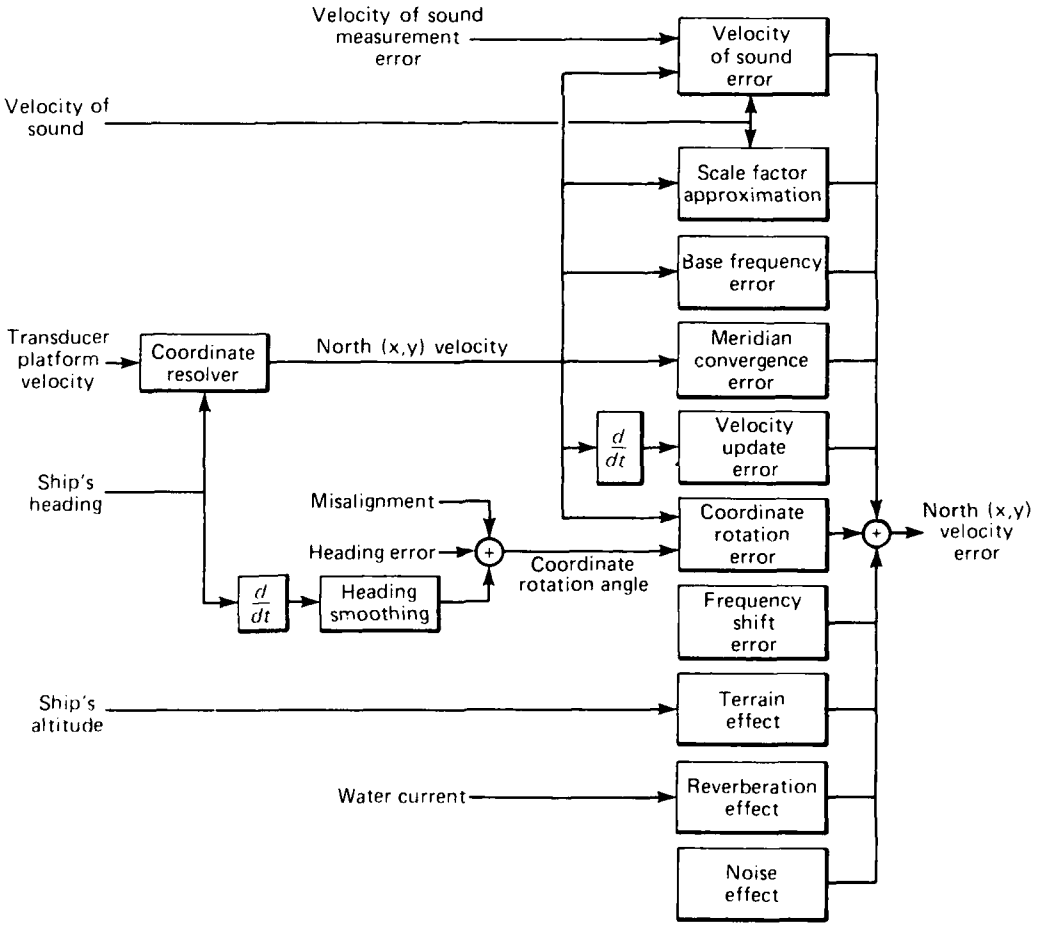

Figure 2—Flow diagram of the velocity error model.

System Model

The system error model as conceived in this study may be represented by a flow diagram (Fig. 2). In the illustration, measurements of input quantities are shown on the left. Processes that occur within the system to produce errors or intermediate quantities are shown in boxes; error sources external to the system are unboxed. (These processes and error sources may be represented mathematically by functions of various error parameters.) The net velocity error in the north (x,y) coordinate system, obtained after summing all error sources, is represented by the quantity at the far right.

The flow diagram represents a comprehensive model of Doppler system error growth. Although, in practice, many of the error parameters (particularly the random ones) are not known precisely, estimates may be made of individual terms or collections of like terms based on test data, performance history, and real-time measurements. The estimates may then be used to compute velocity and position corrections during all periods of operation, resulting in improved navigation accuracy.

Application and Significance

The study of the propagation of Doppler sonar navigation error has provided a framework for significant improvements in the precision of oceanographic survey operations. The concepts advanced by the study have been applied to the analysis of test data in a number of ways. First, knowledge of the expected behavior of Doppler errors has improved the ability to evaluate system performance and has helped to place such evaluations on a better quantitative footing. Second, computer software has been developed that provides estimates of some error terms in the model and applies those estimates to track data, yielding improved track accuracy. Finally, corrected Doppler data have been used as a velocity reference for other navigation systems, including inertial systems and satellite positioning systems. Further improvements are possible through the use of established estimating techniques (such as the Kalman filter), ultimately allowing continuous, real-time corrections to be applied to navigation data.

This work was supported by the Department of the Navy.

BIOMEDICAL SCIENCE AND ENGINEERING

INTRODUCTION

The collaborative biomedical program between APL and the Johns Hopkins Medical Institutions (JHMI) formally began in 1965. The program brings together the expertise in medical and biological sciences found at JHMI with that in the physical sciences, engineering, and mathematics found at APL, in order to solve significant problems in biomedical science and health-care delivery. From the beginning, the collaboration has received strong support from the University's leadership and encouragement from the Navy, APL's major DoD sponsor. The strength of the collaboration is evidenced by the joint appointments made within the two University divisions: 18 members of the APL staff have appointments at the Medical School, and 17 members of the medical faculty have Principal Professional Staff appointments at APL.

Currently, there are 31 active projects in ophthalmology, neurosensory research and instrumentation development, cardiovascular systems, patient monitoring, therapy and rehabilitation, clinical information systems, and clinical engineering. Thirty-nine APL physical scientists and engineers are working in collaboration with biomedical scientists and clinicians from 13 JHMI departments on those projects. The results of their research and development are published in the peer-reviewed scientific and medical literature. Since the program's inception, over 390 papers have been published, and there have been even more than that number of published abstracts and presentations at major scientific and medical meetings.

The articles presented in this section give an indication of the scope of the work done in the collaborative biomedical program. The effort ranges from studies of fundamental biological mechanisms to the development of practical and useful devices for research as well as for improvements in patient care.

COMMUNICATIONS BETWEEN PERIPHERAL NERVE FIBERS

R. A. Meyer (APL) and S. N. Raja and J. N. Campbell (JHMI)

Heretofore, neuronal interactions have been presumed to occur only within the central nervous system and ganglia of the autonomic nervous system. The finding described here of coupling between unmyelinated peripheral nerve fibers indicates that interactions occur in the peripheral nervous system.

BACKGROUND

It has been generally assumed that somatosensory nerve fibers have no connection with one another outside the central nervous system. However, crosstalk between nerve fibers, presumably resulting from electrical coupling, has been observed following nerve injury.[1] This prompted us to examine whether similar interfiber interactions might occur in normal peripheral nerves. As will be described below, we found that bidirectional coupling of action potential activity occurs between unmyelinated fibers in the normal peripheral nerve of monkey. The site of coupling is near the cutaneous nociceptive receptor associated with one of the fibers. This coupling could be due to an electrical synapse and could provide the basis for the flare associated with the axon reflex.

METHODS

Monkeys were anesthetized, paralyzed to eliminate artifacts caused by muscle twitching, and mechanically ventilated. Recordings from single fibers in the peripheral nerve were obtained from finely teased nerve strands using standard techniques.[2] The strands were cut proximally so that only centripetally directed action potentials were recorded (Fig. 1a). Tripolar stimulating electrodes were placed on the parent nerve proximal (PSE) and distal (DSE) to the recording site and were insulated from surrounding tissue with plastic. The preparation was bathed in mineral oil. Action potentials recorded at the recording electrode (RE) in response to PSE stimulation indicated coupling of action potential activity between nerve fibers.

RESULTS

Coupling was observed in 33 instances. In each case, it was between two unmyelinated fibers. Coupling between more than two fibers was not observed. In the example shown in Fig. 1, PSE stimulation resulted in an action potential at a latency of 280 msec. Action potential collision techniques[3] were used to verify that this action potential was due to coupling of action potential activity between two peripheral nerve fibers. Collision techniques were also used to demonstrate that the action potentials could propagate in either direction across the coupling site (bidirectional coupling).

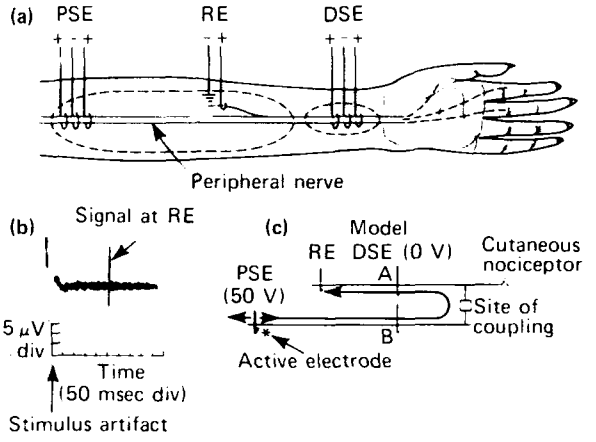

Figure 1—Demonstration of action potential coupling between unmyelinated fibers in the normal peripheral nerve of the monkey. (a) Location of recording electrode (RE), proximal stimulating electrode (PSE), and distal stimulating electrode (DSE). (b) Electrical stimulation at the PSE resulted in an action potential at the RE after a latency of 280 msec (arrow points to action potential). (c) Model to explain the observation. The action potential reached the RE via coupling between fibers A and B.

In 15 cases, we tested for a cutaneous receptor with an action potential whose shape was the same as that observed for the coupled pair. In 13 cases, a receptor was identified and, in each instance, classified as a nociceptor (i.e., a receptor that responds to noxious stimuli and therefore is thought to signal pain) based on a monotonically increasing response to high-intensity mechanical and heat stimuli.[4] Two lines of evidence corroborated the conclusion that the cutaneous receptor was associated with the coupled action potential produced by PSE stimulation. Mechanical stimulation of the receptive field, but not of the surrounding skin, resulted in an increase in the latency of the coupled action potential from PSE stimulation (Fig. 2a). Electrical stimulation at the PSE resulted in a subsequent decrease in response of the receptor to heat stimuli (Fig. 2b).

The intracutaneous injection of a local anesthetic into the receptive field of seven fiber pairs abolished the coupled responses for about 40 minutes. These results suggest that the site of coupling was at or near the receptive

field. As further support of this hypothesis, the measured distance from the RE to the receptive field corresponded to the distance to the coupling site computed from collision data.

We found coupling in about 3% of the unmyelinated fibers tested. The true incidence of coupling is likely to be higher as the demonstration of coupling in this preparation depends on the chance that one of the coupled fibers occurs in the parent nerve and the other occurs in the teased strand from which the recording is obtained. It seems likely that coupled fibers would tend to remain in close proximity throughout their course in the peripheral nerve and, therefore, would not often be teased apart.

DISCUSSION

Although several different mechanisms could explain the observed coupling, perhaps the most exciting possibility is that a bidirectional synapse (either chemical or electrical) occurs between unmyelinated nerve fibers near the cutaneous receptor. Bidirectional chemical synapses have been reported in invertebrates but not in mammals.[6] Electrotonic coupling between cells in the nervous system has been reported both for vertebrates and invertebrates[7] and is thought to be associated with gap junctions. There is some evidence that gap junctions may occur in tooth pulp where coupling between myelinated fibers has been reported.[8]

The function of this interaction is not clear. One noteworthy possibility is that it provides a basis for the flare response (Fig. 3). Following a cutaneous injury such as a cut or burn, the area surrounding the injury becomes red because of vasodilation. The reddening or flare occurs only if the peripheral nerve serving the area is intact, and thus the flare is neurogenic. It is thought that the activation of nociceptors leads to antidromic invasion of unstimulated branches of the receptor, resulting in the release of vasodilating substances. Although free nerve endings have been observed in the dermis and around capillaries, no axonal connection between these endings has been described. Our finding of coupling involving nociceptors suggests that these two types of free nerve endings could be coupled.

Another explanation of the interaction is that sympathetic efferents are coupled to nociceptors. This idea is of interest in view of the occasional occurrence of certain chronic pain states such as causalgia or reflex sympathetic dystrophy—pain states that are marked by excessive sympathetic activity in the affected region. Further experiments will be needed to determine the true incidence of coupling and its functional significance.

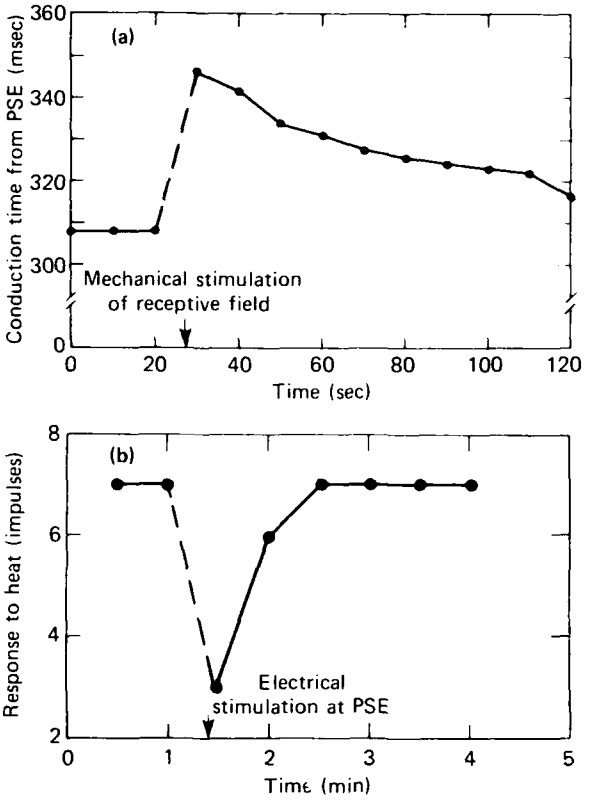

Figure 2—Evidence that a cutaneous nociceptor is associated with the coupled fiber. (a) PSE stimulation every 10 sec resulted in an action potential at the RE after a latency of 308 msec. The latency increased substantially following mechanical stimulation of the receptive field with a stiff nylon probe (35 g, 0.57 mm diameter) immediately preceding trial 4. The mechanical stimulation evoked 32 action potentials. (b) Using a laser thermal stimulator,[5] 1-sec heat stimuli at 47°C were applied to the receptive field every 30 sec, resulting in a response of seven action potentials per stimulus. Three seconds before the heat stimulus of trial 3, the PSE was stimulated at 50 Hz for 1.5 sec at a strength sufficient to elicit the coupled action potential. The response to heat was suppressed for two trials.

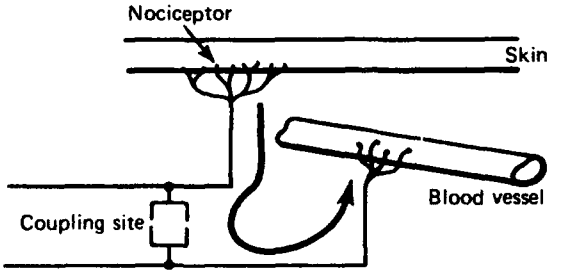

Figure 3—The observed interaction could explain the flare that occurs following a cutaneous injury. Action potentials originating from the cutaneous nociceptor couple to nerve fibers that have their endings near capillaries, resulting in vasodilation.

ACKNOWLEDGMENT

We are thankful for the contributions of R. Burke and J. Aryanpur of the Johns Hopkins Medical School.

REFERENCES

[1] R. A. Meyer, S. N. Raja, J. N. Campbell, S. E. Mackinnon, and A. L. Dellon, "Neural Activity Originating from a Neuroma in the Baboon," *Brain Res.* (in press).

[2] J. N. Campbell and R. A. Meyer, "Sensitization of Unmyelinated Nociceptive Afferents in the Monkey Varies with Skin Type," *J. Neurophysiol.* **49**, 98-110 (1983).

[3] R. A. Meyer, S. N. Raja, and J. N. Campbell, "Coupling of Action Potential Activity between Unmyelinated Fibers in the Peripheral Nerve of Monkey," *Science* (in press).

[4] R. A. Meyer and J. N. Campbell, "Myelinated Nociceptive Afferents Account for the Hyperalgesia that Follows a Burn to the Hand," *Science* **213**, 1527-1529 (1981).

[5] R. A. Meyer, R. E. Walker, and V. B. Mountcastle, "A Laser Stimulator for the Study of Cutaneous Thermal and Pain Sensations," *IEEE Trans. Biomed. Eng.* **23**, 54-60 (1976).

[6] P. A. V. Anderson and W. E. Schwab, "Action Potential in Neurons of Motor Nerve Net Cyanea (Coelenterata)," *J. Neurophysiol.* **50**, 671-683 (1983).

[7] F. E. Dudek, R. D. Andrew, B. A. MacVica, R. W. Snow, and C. P. Taylor, "Recent Evidence and Possible Significance of Gap Junctions and Electrotonic Synapses in the Mammalian Brain," in *Basic Mechanisms of Neuronal Hyperexcitability*, H. H. Jasper and N. M. VanGelder, eds., Liss, New York, pp. 31-73 (1983).

[8] B. Matthews and G. R. Holland, "Coupling between Nerves in Teeth," *Brain Res.* **98**, 354-358 (1975).

This work was supported by National Institutes of Health grants NS-14447 and NS-00519 and by Independent R&D.

INDIVIDUAL DIFFERENCES IN SENSITIVITY TO TRANSIENT ELECTRIC SHOCK

J. P. Reilly (APL) and W. D. Larkin (University of Maryland)

One hundred twenty-four subjects were tested in a procedure designed to measure sensitivity to transient electric shock and to assess individual characteristics accounting for sensitivity differences. Of the subject variables examined, body size was the most significant correlate of sensitivity.

BACKGROUND

The electric field from a high voltage transmission line can induce potentials up to several thousand volts in nearby conducting objects that are electrically insulated from ground. For example, an automobile, with its insulating tires, may satisfy the conditions necessary for large induced potentials. A person who contacts such an object may receive a transient electric shock, similar to the capacitive discharge encountered with a "carpet spark."

Industry and regulatory groups would like to understand human sensitivity to these transient electric shocks in order to specify rational equipment or environmental safeguards in electric field environments. Two such groups have sponsored research at APL on transient electric shock: the Maryland Department of Natural Resources Power Plant Siting Program and the Canadian Electrical Association. The objective of the research is to define human sensory reactions to the transient electric currents that can be induced by high-voltage electric fields in order to help reduce the possibility of unacceptable public or occupational exposures.

There is no single quantitative scale that can be used to describe electrical sensitivity. Rather, there are many parameters related to the method of applying the stimulus and a variety of subjective and physiological variables that must be considered. Some of the variables we studied systematically in our research are related to the subject (e.g., where the stimulus is applied), the stimulus (e.g., current magnitude and waveshape), the method of applying the stimulus (e.g., the masking effects of touch), and the electrode/subject interface (e.g., skin hydration).

Even if all the known variables are controlled or accounted for, we still observe significant variations in sensitivity from one person to another. In order to describe those variations, part of our research included a large-sample study involving many subjects.

A complete account of our research is contained in three annual reports.[1-3] This article briefly summarizes some results from the large-sample study.

DISCUSSION

The purpose of the large-sample study was to assess how electrocutaneous sensitivity varies in adult populations and to examine possible bases for differences among individuals. The 124 subjects tested in a procedure designed to measure cutaneous sensitivity to capacitive discharges included 25 college women, 24 college men, 25 female office workers, and 50 male maintenance workers (plumbers, carpenters, and electricians).

Stimulation to the fingertip was provided when subjects tapped an electrode connected to a charged capacitor. Stimulation to the arm was provided by capacitive discharges to an electrode held in contact with the skin. Using standard psychophysical paradigms adapted for our purpose, we determined threshold voltages for detection and annoyance with stimulation to the fingertip and forearm. In this article, we will confine our discussion to sensitivity of the fingertip with discharges from a 200 pF capacitor, although other conditions were also evaluated in the study.

A wide variety of nonsensory measurements were also taken for each individual in an attempt to account for individual differences (occupation, sex, age, height, weight, skin temperature, finger or forearm diameter, skin hardness, prior degree of physical activity, and prior experience with electric shock).

Figure 1 illustrates the statistical distribution of thresholds for perception and annoyance using 200 pF discharges to the fingertip. The data follow a lognormal distribution, with significant differences in sensitivity between men and women. A further breakdown by categories showed that the college women did not differ significantly from the office women, and maintenance workers had higher thresholds than any other subgroup.

It might seem that there is a component related to sex and occupation that partially accounts for individual sensitivity differences. However, a multivariate statistical analysis revealed that, of all the individual attributes measured, only body size is significantly correlated with sensitivity. The apparent sex and occupation differences are, in fact, artifacts of an underlying body-size dependency: women in our sample group tended to be smaller than men, and maintenance workers were larger than college men. To our knowledge, there has been no previous research calling attention to body size as a correlate for electrical sensitivity.

Of the various body-size related variables that we measured, weight is probably the most easily determined in practical situations. A regression equation based on body weight was determined:

$$V = \alpha e^{\beta W} , \qquad (1)$$

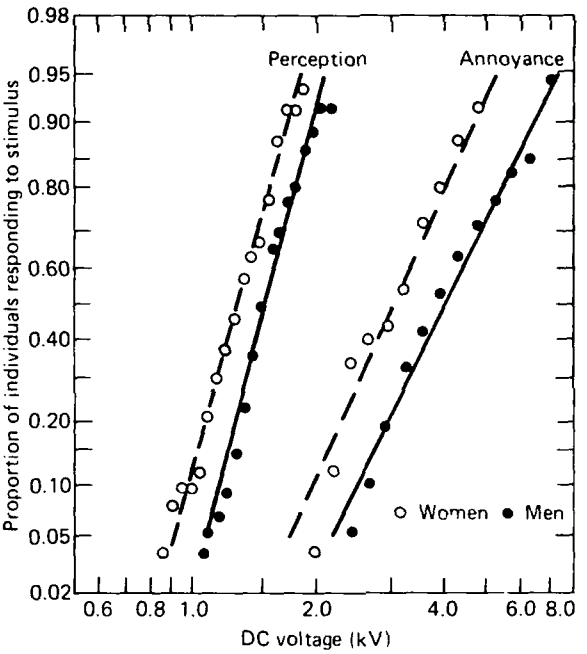

Figure 1—Cumulative probability that a 200 pF capacitive discharge to the fingertip will be perceived or rated "definitely annoying" (combined samples of 74 men and 50 women) (positive polarity discharges).

where V is the median perception or annoyance voltage, W is the subject's weight (in pounds), and α and β are empirical parameters. Values for α and β that apply to discharges from a 200 pF capacitor are given in Table 1. Statistical variations about the median follow the lognormal distribution, with a 90th percentile value at a factor of approximately 1.5 times the median and a 10th percentile at approximately 0.7 times the median.

Table 1—Parameter estimates relating body weight to sensitivity of the fingertip (200 pF capacitive discharges).

Parameter	Perception	Annoyance
α	971	1904
β	0.0024	0.0042

Table 2 expresses weight-dependent thresholds for 200 pF discharges, based on Eq. 1, using the parameters of Table 1. Over a 4:1 weight variation, perception thresholds vary by 1.4:1 and annoyance thresholds by 1.9:1. As a result, the threshold-to-annoyance multiples vary somewhat over the weight classes.

The extrapolation of Eq. 1 to light body weights may be used as a guide in order to estimate sensitivity levels of children. We urge caution, however, because

there has not been empirical verification that the body weight relationship is valid for children.

Table 2—Thresholds for various body weight classes (discharges to the finger from 200 pF capacitor).

Weight (lb)	Perception (V)	Annoyance (V)	Threshold-to-Annoyance Multiple
50	1095	2349	2.15
100	1234	2898	2.45
150	1392	3575	2.57
200	1569	4411	2.81

ACKNOWLEDGMENTS

We wish to acknowledge the other members of the research team: M. J. Flynn, V. T. Freeman, and R. J. Taylor of APL and L. B. Kittler of the University of Maryland, Department of Psychology.

REFERENCES

[1] J. P. Reilly, W. D. Larkin, R. J. Taylor, and V. T. Freeman, *Human Reactions to Transient Electric Currents—Annual Report, July 1981-July 1982*, JHU/APL CPE-8203 (1982).

[2] J. P. Reilly, W. D. Larkin, R. J. Taylor, V. T. Freeman, and L. B. Kittler, *Human Reactions to Transient Electric Currents—Annual Report, July 1982-June 1983*, JHU/APL CPE-8305 (1983).

[3] J. P. Reilly, W. D. Larkin, L. B. Kittler, and V. T. Freeman, *Human Reactions to Transient Electric Currents—Annual Report, July 1983-June 1984*, JHU/APL CPE-8313 (1984).

This work was supported by the State of Maryland, Department of Natural Resources, and by the Canadian Electrical Association.

A NEW SUTURELESS METHOD FOR THE ANASTOMOSIS OF BLOOD VESSELS

J. J. Wozniak

When large numbers of battle casualties arrive at a field hospital, the requisite skills, facilities, and time may not be available to perform all necessary, but not necessarily critical, end-to-end vascular anastomoses with sutures. A sutureless concept was proposed in which the proximal and distal ends of a severed vessel are everted over ferrules and the everted ends are held together with a biocompatible, low-temperature, heat-shrinkable sleeve. Two essential elements in the sutureless concept—a surgical vascular everting instrument and the heat-shrinkable sleeve—have been developed, and a demonstration of the sutureless technique has been accomplished on one laboratory animal. Personnel from APL, the Johns Hopkins Medical Institutions, and the University of Maryland, representing talents in the disciplines of engineering, vascular surgery, and polymer science, joined forces to work on this project.[1]

BACKGROUND

Anastomosis of blood vessels was successfully performed by Alexis Carrel in the early 1900s;[2] however, it was not until after World War II, in Korea and Vietnam,[3] that the techniques of vascular surgery and the training of its practitioners were developed to the point where vascular surgery became standard practice for major trauma. In the case of wounds of the extremities, this resulted in a tremendous increase of personnel able to return to duty who, in earlier years, would have undergone amputation. Two key problems in vascular surgery that must be faced when dealing with large numbers of combat casualties are the availability of surgeons skilled in needed techniques and the amount of time required to perform each surgical procedure.

DISCUSSION

Figure 1 shows the steps involved in the sutureless anastomosis technique. Figure 1a shows the severed vessel, which characteristically constricts and retracts because of the smooth muscular structure (media) within the vessel wall. In the first step, temporary clips are ap-

plied to the transectioned vessel, and the lumen is irrigated with saline. The vessel diameter is sized, and ferrules are selected that approximately match the outside diameter of the vessel.

Each vessel end is then everted over a ferrule (Fig. 1b). A prototype instrument to perform the vascular eversion has been developed. Everting fully opens the vessel and ensures continuous intimal contact, which is vital to prevent thrombosis formation after the anastomosis is completed.

In the next step, a sleeve fabricated from a low-temperature, heat-shrinkable, biocompatible polymer is placed on one of the vessel ends. The two ends are brought together, and the sleeve is centered over the junction (Fig. 1c). The sleeve is heated with a jet of warm saline. Heat causes the sleeve to contract and assume the local contour of the everted vessel (Fig. 1d).

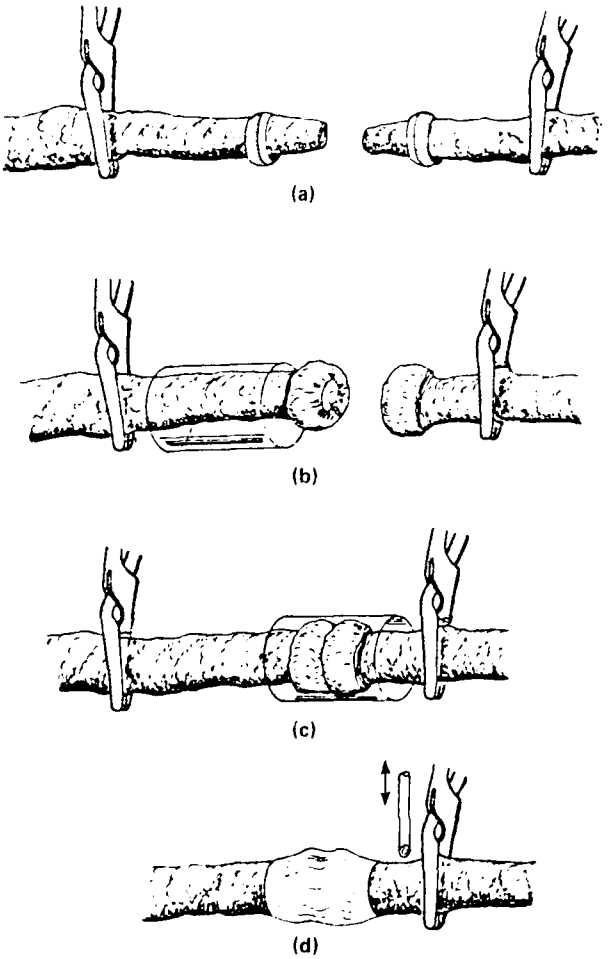

Figure 1—The steps in the sutureless vascular anastomosis technique.

In the completion sequence, the proximal clip is removed (Fig. 1d), and a hypodermic needle is inserted into the vessel lumen to relieve entrapped air. When a steady flow of blood through the hypodermic needle is achieved, the needle and distal clip are removed.

Vascular Everting Instrument

For the sutureless anastomosis technique to be an alternative to sutures, an effective way had to be developed to evert each vessel end over a ferrule. Two essential requirements for the everting instrument are minimal damage and minimal displacement of the endothelial cells lining the lumen and flexibility for one instrument to evert vessels having a range of lumen dimensions.

A prototype everting instrument was developed earlier;[1] it used an iris-diaphragm mechanism to flare the leading edge of the artery and a miniature balloon inflated within the lumen to accomplish the everting action.

While bench tests demonstrated the instrument on arteries possessing moderate to high elasticity, it could not be made to function reliably on arteries with lesser compliance expected in clinical applications. As a result, a new instrument was developed (Fig. 2) that again uses the iris-diaphragm principle to flare the leading edge of the artery, but uses a separate special curved forceps to complete the everting action.

Heat-Shrinkable Sleeve

Inducing "elastic memory" in a polymer by irradiation was selected as the most promising technology for developing the sleeve. Two candidate polymers, polyethylene oxide (PEO) and synthetic trans-1,4 polyisoprene (TPIP), have undergone extensive radiation chemistry and sleeve processing experimentation. This work was per-

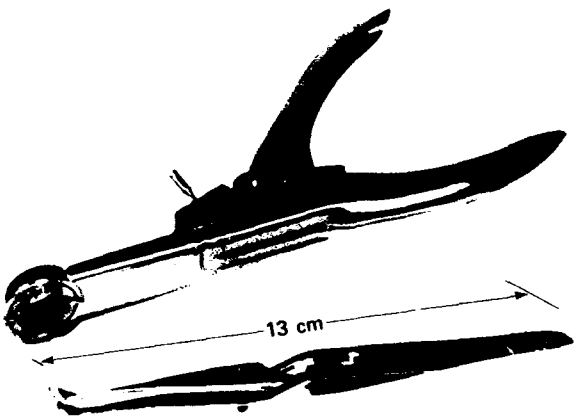

Figure 2—The new everting instrument.

formed at the University of Maryland Laboratory for Radiation and Polymer Science and was reported earlier.[1]

PEO, which satisfied the mechanical, biocompatibility, and shrink-temperature requirements, could not be made hydrophobic. It tended to swell and become very slippery when placed in water. Synthetic TPIP met the mechanical and shrink-temperature requirements and is unaffected by water, but its biocompatibility was unknown.

Under subcontract to APL, the Materials Science Toxicology Laboratory at the University of Tennessee performed an acute toxicity screening program on crosslinked TPIP. The test program included direct contact of the material on tissue culture (mammalian cell), intramuscular implantation (in rabbits), and multiple tests with extracts of the material. Reference 4 provides the test program protocol.

The material evaluation report[5] concluded that radiation-crosslinked synthetic TPIP has an extremely low potential toxic liability. In fact, TPIP received a toxicity figure of merit rating similar to those of silicone and polycarbonate, which are frequently used in implants.

In-Vivo Demonstration

One in-vivo demonstration of the sutureless anastomosis technique was conducted on a 25 kg male mongrel dog. Under sterile conditions, the left carotid artery was isolated and exposed in the neck. Clips were applied, and the carotid artery (3 to 4 mm lumen) was transected. The artery sections were irrigated with heparinized saline.

The sutureless procedure took approximately 5 min to complete. Ferrules fabricated from polycarbonate were used in this experiment. A jet of warm (130°F) sterile saline, applied for a few seconds with a squeeze-type wash bottle, was used to contract the sleeve. Cold saline, applied in a similar manner, "locked" the sleeve in its contracted state. Good pulsations were observed on release of the vascular clips. A small amount of blood emerged from the intima junction when the clips were first removed; however, no bleeding occurred from the site of the anastomosis itself. Figure 3 is a photograph of the anastomosed artery. Antibiotics were administered postoperatively. Anticoagulants were not required. Angiograms taken 5 and 21 days after the anastomosis was performed showed good blood flow although slight stenosis was present. The stenosis is believed to result from the use of undersized ferrules (the ferrule's inside diameter was smaller than the artery's outside diameter). After the twenty-first day the site was reopened, the artery was ligated, and the anastomosed section was removed. The excised vessel was fixed in formalin.

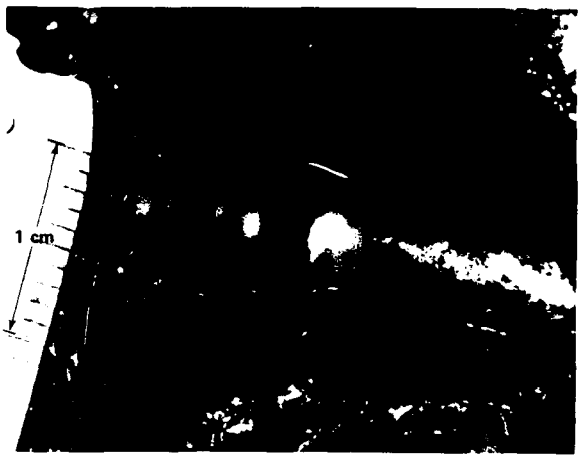

Figure 3—An anastomosed artery using the sutureless technique.

Subsequently, the anastomosed artery was embedded in paraffin and sectioned. Histological examination showed that the artery was patent, without any adherent thrombus, and that a continuum of endothelium had occurred. The time was insufficient to observe significant medial regrowth.

Future plans call for the development of absorbable ferrules to avoid chronic stenosis, sleeve processing refinements to enhance intima-to-intima contact, and extensive animal implant tests.

ACKNOWLEDGMENT

The author wishes to acknowledge the contributions of J. Silverman and H. C. Yang of the University of Maryland, M. H. Epstein of the Johns Hopkins Medical Institutions, and R. W. Flower and D. E. Walters of APL.

REFERENCES

[1] J. J. Wozniak, "Sutureless Vascular Anastomosis System," in *Developments in Science and Technology, Fiscal Year 1983*, JHU/APL DST-11.

[2] C. Sabiston, ed., *Davis-Christopher Textbook for Surgery: The Biological Basis of Modern Surgical Practice* **11**, W. B. Saunders, Co., Philadelphia (1977).

[3] N. M. Rich, J. H. Baugh, and C. W. Hughes, "Acute Arterial Injuries in Vietnam: 1,000 Cases," *J. Trauma* **10**, 359-369 (May 1970).

[4] J. Autian, *Toxicological Evaluation of Biomaterials: Primary Acute Toxicity Screening Program, Artificial Organs* **1**, pp. 53-60 (1977).

[5] J. Autian, "Report on Toxicity of Synthetic Trans-1,4 Polyisoprene under Project Number PT 0.1921" (private correspondence), the University of Tennessee Materials Science Toxicology Laboratory (Feb 1, 1984).

This work was supported by the Naval Medical R&D Command and Independent R&D.

ARTERIAL RESPONSE TO HEMODYNAMIC SHEAR STRESS

M. H. Friedman, O. J. Deters, and C. B. Bargeron (APL), G. M. Hutchins (JHMI), and F. F. Mark (APL)

Fluid mechanical measurements have been made by laser Doppler anemometry in 10 flow-through casts of human aortic bifurcations. The thickness of the inner lining of the arterial wall (the intima, where arteriosclerosis begins) was measured at corresponding sites in the original vessels. Correlation of the fluid dynamic and morphologic measurements suggests a nonlinear relationship between wall shear and intimal thickening. A model of the vascular response to hemodynamic shear stress has been developed to explain this relationship and fits the results quite well. The model offers an explanation of the role of hemodynamics in the pathogenesis of arterial disease.

BACKGROUND

There is a considerable body of indirect evidence, largely based on the pattern of the disease, that hemodynamic factors are at least partially responsible for the initial formation of atherosclerotic lesions. However, the most important of these factors have not been identified, and much remains to be learned about the response of the vascular wall to its hemodynamic environment. The purpose of the research is to advance knowledge in this area through a unique protocol that offers the possibility of identifying features of the arterial flow that are associated with early atherosclerotic changes in human arteries, while providing a database that will be used to examine the interaction between the flow field and the vessel wall.

DISCUSSION

We have investigated the morphological response of the arterial wall to extremes of shear stress and other hemodynamic phenomena, using the aortic bifurcation as a test segment. Values of the hemodynamic variables were derived from laser Doppler anemometer measurements of pulsatile velocities in rigid transparent casts of the vessels.

The flow through the casts consisted of a steady component generated by an adjustable metering pump and a pulsatile component produced by a cam-driven piston pump. The flow system was designed to produce a flow wave typical of the in vivo flow at the aortic bifurcation. The mean flow rate and pulse frequency of the system were adjusted so that fluid mechanical scaling was achieved. The flow wave in each cast was computed from the time-varying velocity at the inlet centerline; in all casts, the flow partitioned approximately equally between the two daughter arteries.

Our studies failed to demonstrate extensive separation or any turbulence at the aortic bifurcation.[1] Weak transient eddies have been observed on occasion but only in diastole.[2] Consequently, major emphasis has been directed toward the relationship between interfacial shear and vascular morphology.

Interfacial shear values are derived from measurements of the pulsatile velocity close to the walls of the cast. The velocity measurements were made primarily in the plane of the bifurcation. At such sites, the effects of secondary flow are small since the plane of the bifurcation is an approximate plane of symmetry. Velocity measurements were made at sites whose distance from the wall varied from 0.4 to 0.9 mm. At these proximities to the wall, and in the absence of strong secondary flows, the fluid velocity vector is approximately parallel to the wall and in the plane of the bifurcation. Approximate shear rates were derived at each site by dividing the measured velocities by the perpendicular distance from the measurement site to the wall. Close to the wall, the velocity varies nearly linearly with distance from the wall. Measurements were made in 10 casts; the number of measurement sites varied from 12 to 23.

The in vivo blood flow in the experimental arterial specimens was not known, and the flow wave used in the experiments varied somewhat from one cast to another. The effects of these variations were reduced by normalizing the shear rates. Normalized shear rates were obtained by dividing each experimental shear rate by the average of the measured shear rates in that cast.

Linear regressions between intimal thickness and normalized shear rate were performed for each vessel as an initial step in the analysis of the experimental data. The variation of the slopes of the correlations with mean intimal thickness suggested that sites exposed to high shear thicken quickly to a modest value and slowly thereafter, while the intimal thickness at sites exposed to low shear rises more slowly initially but ultimately reaches higher values.

A simplified model has been devised that reproduces this behavior. The basic assumptions of the model are:

1. A blood-borne substance diffuses into an intimal compartment in which its concentration

is fixed; its permeability depends linearly on shear rate.

2. The substance is catabolized in the intima or otherwise removed via a first-order rate process; the rate constant varies exponentially with reciprocal shear rate, i.e., as an activation process.
3. The substance accumulates in the intima according to the difference between the rate at which it enters and the rate at which it is destroyed or lost. This accumulation causes the intima to thicken.

A nonlinear estimation routine was used to fit the model to the experimental data. The correlations were performed using three shear measures—maximum, mean, and "pulse"[3] shear rates—and no constraints were placed on the magnitude or sign of any of the parameters of the model. The correlation based on maximum shear rate provided the best fit to the experimental data, but it was not significantly better than the correlations based on mean and pulse shear rate. The standard error of estimate of the correlation was 105 μm. A plot of the correlation is given in Fig. 1.

The model provides a simplified description of intimal thickening that is based on physical processes for which there is experimental evidence. Of course, the mechanism of time-dependent wall thickening is more complex than this, involving additional processes not included in the model. While the analysis is incomplete, it offers insights into the phenomenology of intimal thickening under shear and suggests mechanisms that explain this behavior. The most significant of these are the concept that relative thickening rates under low and high shear stress can change with age and its explanation in terms of competing shear-dependent processes.

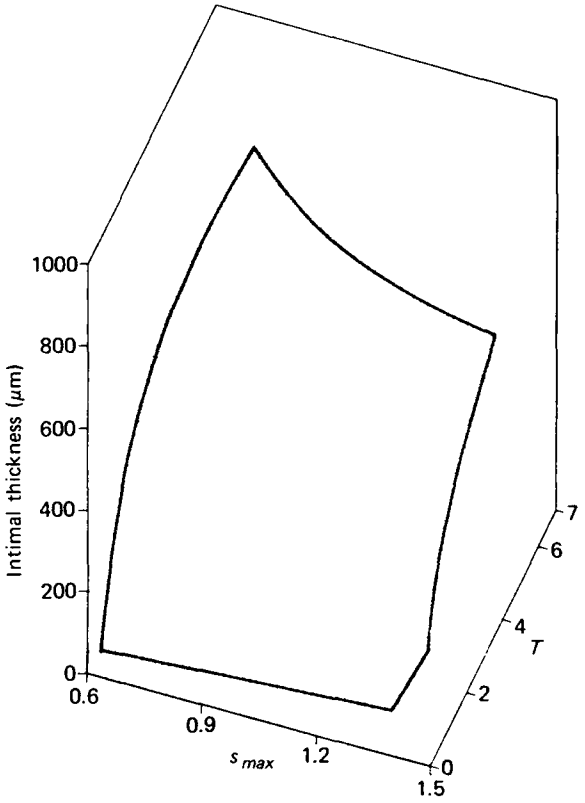

Figure 1—Correlation of intimal thickness with nondimensional time, T, and normalized maximum shear rate, s_{max}. The region in the s_{max} - T space within which the correlation applies is indicated by heavy lines; the rest of the surface is included to provide a better sense of its shape. Nondimensional time is defined by $T = r_o t$, where r_o is the removal rate constant at $s_{max} = 1$ and t is physical time.

REFERENCES

[1] M. H. Friedman, C. B. Bargeron, G. M. Hutchins, F. F. Mark, and O. J. Deters, "Hemodynamic Measurements in Human Arterial Casts, and Their Correlation with Histology and Luminal Area," *J. Biomech. Eng.* **102**, 247-251 (1980).

[2] F. F. Mark, C. B. Bargeron, O. J. Deters, G. M. Hutchins, and M. H. Friedman, "Velocity Measurements of Pulsatile Flow through a Cast of an Asymmetric Human Aortic Bifurcation," in *1981 Biomechanics Symp.*, W. C. Van Buskirk and S. L.-Y. Woo, eds., American Society of Mechanical Engineers, New York, pp. 47-50 (1981).

[3] M. H. Friedman, G. M. Hutchins, C. B. Bargeron, O. J. Deters, and F. F. Mark, "Correlation between Intimal Thickness and Fluid Shear in Human Arteries," *Atherosclerosis* **39**, 425-436 (1981).

This work was supported by the National Institutes of Health and Independent R&D.

THREE-DIMENSIONAL IMAGING OF THE HUMAN HEART BY ECHOCARDIOGRAPHY

W. H. Guier (APL) and J. L. Weiss (JHMI)

Scanning two-dimensional echocardiography provides visualization and analysis of sections through the beating heart. By combining many such sections with data on the relative position and angulation of the echo probe, a three-dimensional (3D) view of the heart at any chosen time can be synthesized. In collaboration with the Johns Hopkins Medical Institutions, the method has been implemented for clinical trials. Candidates for total heart transplantation are examined by echocardiography prior to surgery, and the heart's shape and weight are estimated from the synthesized 3D image. The diseased heart, after being replaced by the transplant, is weighed and compared with that predicted from the 3D echocardiographic data. The error of the weight predicted from echo reconstructions was 5.7% rms for the five transplants studied to date. If confirmed with continued studies, this accuracy will be sufficient for clinical applications.

BACKGROUND

The quantification of the size, shape, and motion of the diseased human heart has been a goal of cardiology from its beginning. Ultrasound, being completely noninvasive, has long been a valuable way to do this. At present, 2D scanning echocardiography can provide moving images of beating heart walls, opening and closing of heart valves, blood clots, tumors, etc. during an outpatient visit. Continuing improvements in resolution and discrimination between neighboring soft tissues have resulted in 2D echocardiography becoming an established clinical specialty area.

Immediately after demonstrating that a 2D visualization of the beating heart could yield clinically useful information on the heart's functional state and the nature and extent of its disease, APL and JHMI collaborated in quantitating that information.[1-4] Among several related efforts was the attempt to develop a way to combine multiple quantitated 2D echo images into a synthesized 3D image of the left ventricle, the main pumping chamber of the heart. This Johns Hopkins group is now one of our investigative groups in the United States vigorously pursuing this goal. The Hopkins team achieved a working system for in vitro echo subjects in the spring of 1982.[5] In 1984, the Hopkins group was the first of the four groups to achieve clinical validation in humans. This is a report of the earliest of these human trials to validate the method in diseased hearts.

RESULTS

The direct and unequivocal clinical validation of this method of 3D reconstruction of the beating heart results from the opportunity of the present clinical team to contribute to the clinical program of heart transplantation at JHMI.[6] Multiple 2D echo views with probe position and angulation data are taken during routine clinical testing of heart transplant candidates. The pretransplant 2D echos of patients who undergo heart transplantation within 3 weeks of the echo study are contoured and are entered with the probe position and angulation data into the APL central computer for 3D analysis. The estimated volume of the muscle mass of the left ventricle from the 3D echo is then compared with the directly weighed left ventricular mass of the patient's explanted heart after removal of the atria, valves, and right ventricular free wall. The results for the first three patients are shown in Table 1.[6]

Table 1—Results of validation for the first three patients.

Patient	Echo Left-Ventricular Mass (g)	True Left-Ventricular Weight (g)	Error (%)
1	442	422	+4.7
2	506	473	+7.0
3	190	180	+5.6
Mean	379 ± 167	358 ± 157	+5.8 ± 1.2
Total rms error			5.8

Tests on two more patients have now been completed. The combined error of all five patients is 2.5 ± 5.1%, or a total rms error of 5.7%.

DISCUSSION

Figure 1 is a schematic diagram of the 3D echo system; Fig. 2 shows the clinical setup when "echoing" a patient. Attached to the 2D scanning echo probe are three spark gaps that produce a sharp noise spike each time they are fired by the electronics. An acoustic receiver array of four microphones receives the spikes from the spark gaps, and the electronics measures the travel time of the noise spikes over the 12 geometric paths (three transmitters to four receivers). The 12 range values are redundant with respect to the absolute position and orientation of the echocardiographic probe; after proper calibration in vitro, they can be used to determine the

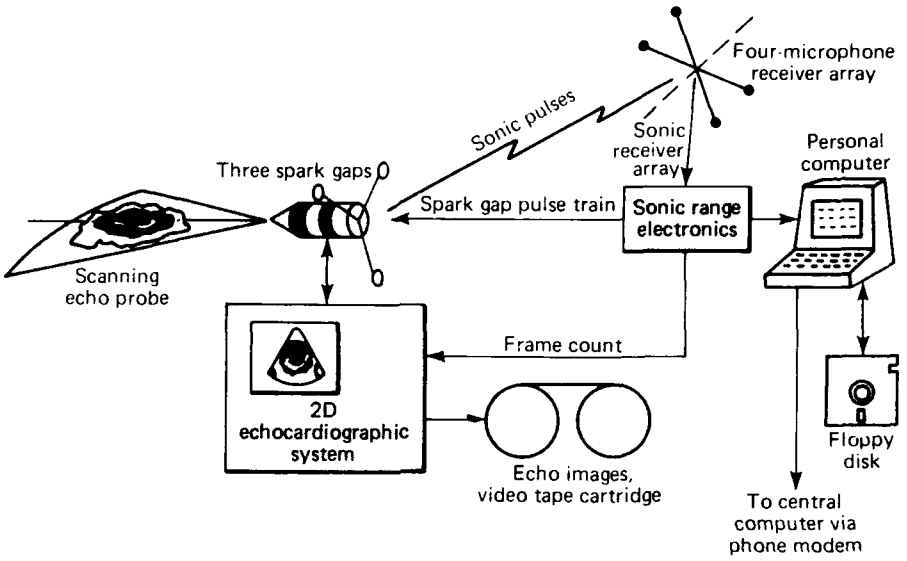

Figure 1—The 3D echocardiographic system and the sonic range data subsystem.

Figure 2—Clinical setup when "echoing" a patient.

absolute position of a sharply imaged small object to about ⅓ mm rms. This array of 12 ranges is recorded four times per second along with a video frame count so that associated with any 2D echo image are the 12 range values. The position and orientation of the video images that are chosen to be used for the 3D image reconstruction are then computed from the range values determined by the video field count.

Figure 3 corresponds to end diastole, the time of maximum expansion just prior to the contraction that forces the blood through the arteries. Figure 3a shows a stereo pair generated by a graphics terminal; each 2D contour for the inside surface (endocardium) of the left ventricle represents one "loop" in the stereo 3D figure. Interpolation between these meshed loops yields in 3D the inferred endocardial surface and, for example, the volume of the cavity it encloses. The same inference performed on the outside surface yields the size, shape, and volume of the epicardial surface. Clearly, these inferences can be performed anytime within the cardiac cycle.

Figure 3b shows a stereo pair of the inferred 3D surfaces, outlined in this case along slices through the heart muscle—much like cutting a half melon into "orange slices." The difference between the areas enclosed by the inside and the outside surfaces is the muscle volume of the left ventricle. That computed volume, multiplied by the muscle density, is the mass measured in the explanted heart. It is tabulated in Table 1. In addition to affording a direct comparison for validation, this muscle mass also is of clinical interest in certain types of heart disease and, therefore, is itself an example of the clinical potential of the technique.

ACKNOWLEDGMENT

We wish to acknowledge the participation of J. G. Chubbuck of APL and M. D. McGaughey, M. J. Hausknecht, A. Herskowitz, and B. Walters of JHMI on the clinical team.

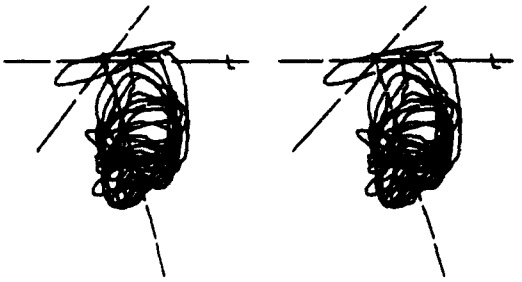

(a) Original oblique views for endocardial surface

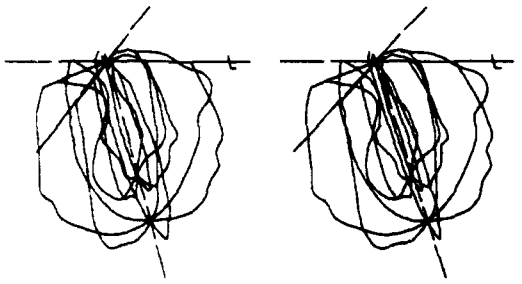

(b) Alternate (odd-numbered) slices for endocardial and epicardial surfaces

Figure 3—Stereo views of 3D reconstruction. The figures can be viewed with a standard stereo map viewer using lenses. With practice, they can be viewed by focusing the eyes at infinity so that each eye sees only one view. It may be helpful to place a vertical white card between the two sides so that each eye sees only its intended view.

REFERENCES

[1] J. B. Garrison, J. L. Weiss, M. L. Maughan, O. M. Tuch, W. H. Guier, and N. J. Fortuin, "Quantifying Regional Wall Motion and Thickening in Two-Dimensional Echocardiography with Computer-Aided Contouring System," in *Computers in Cardiology*, IEEE, Long Beach, Calif., pp. 25-35 (1977).

[2] A. N. Lieberman, J. L. Weiss, B. I. Jugdutt, L. C. Becker, B. H. Bulkley, J. B. Garrison, C. A. Kallman, and M. L. Weisfeldt, "Two-Dimensional Echocardiography and Infarct Size: Relationship of Wall Motion and Thickening to the Extent of Myocardial Infarction in the Dog," *Circulation* **63**, 739-746 (1981).

[3] J. L. Weiss, "Quantitative Two-Dimensional Echocardiography in Coronary Artery Disease," in *Echocardiography*, M. Nijhoff, ed., H. Rijsterborgh, The Hague.

[4] J. L. Weiss, R. E. Jenkins, and J. B. Garrison, "An Automated High-Speed Contouring System for Two-Dimensional Echocardiography" (abstract), *Clin. Res.* **28**, 22A (1980).

[5] W. H. Guier, J. T. Massey, W. Schneider, J. L. Weiss, and J. G. Chubbuck, "The Use of PC's for On-Line Data Processing in Medical and Clinical Research," in *Proc. 7th Hawaii International Conf. on System Sciences* **II**, B. Schriver, T. M. Walker, T. R. Cousins, and R. H. Sprague, eds. (1984).

[6] M. D. McGaughey, W. H. Guier, M. J. Hausknecht, A. Herskowitz, B. Walters, and J. L. Weiss, "Three-Dimensional Echo Reconstruction of the Left Ventricle in Cardiac Transplant Patients" (AHA abstract), *Circulation* (in press).

This work was supported by the National Institutes of Health and the F. T. McClure Fellowship for 1982-1984.

ENVIRONMENTAL SCIENCE AND TECHNOLOGY

INTRODUCTION

The Laboratory's interest in the environment and programmatic involvement with it are matters of some years' standing. Notable among such matters are, first, the properties and processes of the oceans in areas of interest to the naval and maritime communities and, second, a variety of aspects of the Chesapeake Bay. APL has also extended the scope of its environmental work to other fields of investigation. An example of this extension is the worldwide characterization of certain atmospheric properties in terms that enable predictions of anomalous propagation of radar-frequency energy. Another example of atmosphere-related work is computer modeling of the behavior of the plume from a power plant cooling tower.

The growing concern over the health—indeed, the very survival—of the Chesapeake Bay has led the Laboratory into new and diverse endeavors and into new cooperative efforts with other elements of the academic and scientific communities as well. The coalition between the Laboratory and the Chesapeake Bay Institute to investigate some of the seemingly vital factors that influence the propagation and survival of commercially and recreationally important species of Bay life is an example of the recent impetus given to efforts to improve the Bay.

The Ocean Science and Technology Section of this volume also includes reports of work directly related to the ocean environment.

A REFRACTION ANALYSIS SYSTEM FOR THE METEOROLOGICAL ASSESSMENT OF ANOMALOUS PROPAGATION

J. P. Skura, H. W. Ko, and J. H. Meyer

APL personnel have developed an automated computer code to convert large volumes of basic meteorological data measured by radiosondes into refractivity units. The statistical summary of atmospheric ducting, superrefraction, and subrefraction is implemented for thousands of radiosonde launches at numerous stations. The summaries are given in 20 different formats for selectable height intervals. The system provides detailed statistical analyses while retaining the details of refractivity structure, such as refractive layer thickness and refractivity gradient.

BACKGROUND

The World Meteorological Organization routinely launches radiosondes at least twice a day from stations worldwide. All data from these launches, recorded in absolute values, are being retained. Quality control marks are provided for the basic meteorological parameters, such as temperature. However, the data are not checked for accuracy.

The APL Refractivity Analysis System (RAS) is a computer software package that first checks for bad or missing data and then checks for accuracy and for consistency with accepted meteorological lapse rates. From these certified good data, the vertical refraction profile is calculated in terms of the radio refractivity. The statistics are then calculated monthly for selectable height intervals, yielding percent of occurrences and gradient strengths for each type of propagation cataloged at each station by day, by hour, and by height.

DISCUSSION

Atmospheric parameters measured by radiosonde devices include pressure, ambient temperature, dewpoint temperature depression, wind speed, and wind direction. The RAS accepts and uses these data to generate a detailed description of the index of refraction in terms of the commonly used refractivity unit, N, and the modified refractivity unit, M. The vertical gradient of the refractivity describes the ability of the atmosphere to support various types of electromagnetic wave propagation. The major types of propagation are given as standard (rays propagate normally), subrefraction (rays are abnormally bent upward), superrefraction (rays are abnormally bent downward with a radius of curvature approximately equal to the earth's radius), and ducting or trapping (rays are abnormally bent downward with a radius of curvature much less than that of the earth). Figure 1 defines the gradient regimes for each type of propagation.

The RAS basically comprises three programs. The first reads in the meteorological data, checks for bad or missing data, and checks for accuracy and for consistency with accepted meteorological lapse rates. From these certified good data, the relative humidity and refractivity are calculated. The new set of vertical refraction profiles is now ready for analysis.

The second program in RAS produces the statistics on a month's data for a given site. The height increments above the site where the statistics are to be calculated are specified by the user in order to obtain as fine a profile structure as may be necessary. The vertical refraction profiles for a site are read in, and the gradient for each level in the profile is calculated and then classified as to the type of propagation it will support. Linear interpolations are then performed on the data to obtain the gradients and type of propagation for the height structure specified by the user. The counters for the occurrence of each type of propagation for the given height increments are updated to calculate the percent occurrence. Next, the mean gradient of each type of each height increment and the mean profile are updated. The daily

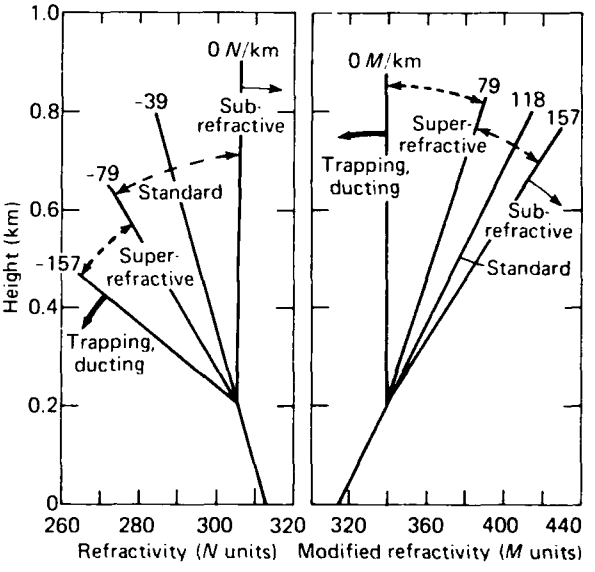

Figure 1—N and M gradients and refractive effects.

Table 1—Statistical output for the Bangkok site (Apr 1982, 1200 GMT).

Height (m)	Ducting		Superrefraction		Subrefraction	
	Percent Occurrence	Mean Strength	Percent Occurrence	Mean Strength	Percent Occurrence	Mean Strength
33	7	-65	43	-33	7	52
67	7	-65	43	-33	7	52
100	7	-65	40	-34	7	52
133	7	-65	37	-34	7	52
167	7	-65	37	-34	7	52
200	7	-65	37	-34	7	52
233	7	-65	33	-34	7	52
267	3	-71	33	-34	0	–
300	0	–	30	-34	0	–
333	0	–	30	-34	0	–

Note: Strengths are expressed in N per thousand feet.

counters that keep track of the presence or absence of a given type on any day are then updated. Finally, information on each type of propagation that exists in the profile is extracted, and that information (top of layer, thickness of layer, type of propagation, and strength of layer) is used to update the average information on layer types. The process is repeated for each profile for a particular month. When the month is finished, all the statistical data are written into a data file for later access.

The third part of the RAS is a program to output the statistical data onto paper in easy-to-read format. Examples of some of the outputs are shown in Table 1 and Fig. 2.

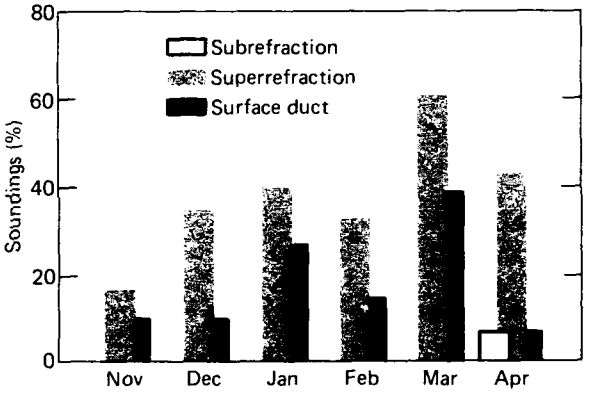

Figure 2—Example of anomalous propagation at the Bangkok site (1200 GMT).

SUMMARY

The RAS code is the first one capable of the computerized characterization of worldwide electromagnetic propagation conditions that has been developed to be available for unrestricted use. Its capability extends from the surface up to 30,000 ft in any altitude increments desired, and it can accommodate any meteorological data set that is comparable in format with the one used by the World Meteorological Organization. When the code is applied, the occurrence of subrefraction, superrefraction, and ducting conditions at specific locations or worldwide can be described quantitatively in terms that permit the evaluation of the performance aspects of communications, sensing, and ranging systems that depend on (or can be hindered by) anomalous electromagnetic propagation.

ACKNOWLEDGMENTS

The authors would like to thank K. A. Kostoff and D. A. Roberts for their participation in processing the meteorological data tapes obtained from various contributors.

This work was supported by the Air Force Electronic Systems Division.

COOLING TOWER PLUME AND DRIFT MODEL FOR ENVIRONMENTAL IMPACT STUDIES

E. A. Davis

A computer model of cooling tower vapor plumes and saline drift emissions has been developed in conjunction with power plant siting studies. The model has been used to make estimates of environmental impacts such as visible plumes, fog and ice enhancement, and deposition of salt on soils, crops, and structures in the vicinity of a power plant.

BACKGROUND

The model is an outgrowth of earlier work done at APL. The present form of the model, the computer program, is a direct result of two projects: (a) the Chalk Point Cooling Tower project (1978-1979), jointly sponsored by the Power Plant Siting Program of the State of Maryland, the Electric Power Research Institute, the U.S. Department of Energy, the Environmental Protection Agency, and the Potomac Electric Power Company; and (b) the Vienna Siting Study (1979-1980), performed for the Maryland Power Plant Siting Program as part of its work in connection with the application of the Delmarva Lighting and Power Company to expand its generating facilities at Vienna, Md. The model was completed and delivered to the State of Maryland in 1984 and is documented in Ref. 1. It is briefly referred to as the APL plume and drift (APLPAD) model.

DISCUSSION

Modeling Concept

The model represents the performance of a single tower in flat terrain. Multiple towers are analyzed by using the model to obtain results for the individual towers and then processing them to obtain the desired combined results; e.g., total salt deposition is found by adding the individual results after making the appropriate coordinate transformation to a common deposition grid.

The internal characteristics of the cooling tower are not modeled. Vapor plume and drift emission characteristics are either direct inputs or are computed from simple relations derived from previous analyses. The model then simulates plume and drift behavior through the use of appropriate analytic algorithms that represent the various physical phenomena that are involved.

Figure 1 illustrates the modeling concept. The saturated vapor plume exits the tower with a velocity and temperature that depend on the ambient atmospheric conditions and the cooling range of the tower. The buoyant plume rises and grows with the entrainment of ambient air until it reaches its final rise point. Beyond that point, it disperses as a Gaussian plume that is visible as long as the air on its centerline remains saturated. Exceptions to this modeling concept can occur under certain ambient conditions, such as high winds or low-level atmospheric temperature inversions (which can prevent normal plume rise). The model detects those conditions and responds appropriately.

The drift modeling concept has four components: rise, breakaway, evaporation, and deposition. Drift droplets entrained in the buoyant flow are carried out of the tower. They fall at a rate that depends on their size and mass. As long as the plume rise rate exceeds their fall velocity, the droplets are rising with respect to the ground. At some downwind distance, the plume rise rate equals the fall rate of droplets of a given size, and they break away to fall free of the vapor plume. As they fall, they are transported by ambient winds. During those processes, the droplets may shrink in size by evaporation and thus reduce their fall rate. Also, they may increase in size by condensation, depending on the conditions of the surrounding air in which they are moving. As the droplets are transported, they disperse because of the turbulent motion of the atmosphere. Eventually they strike the ground and are deposited.

The model simulates the trajectory of only selected droplet sizes called size classes or "bins." All droplets exiting the tower are assigned to one of the bins for modeling. The dispersion of droplets about the central trajectory of a class is assumed to be normally distributed, as is shown in Fig. 1.

The computations are done using these concepts for each meteorological record in the database. The results, such as salt deposition at selected ground locations around the tower, are written to data files for later analysis and tabulation.

Model Features

The focus of the model is on its use in assessing the effects of cooling tower air emissions. Since thousands of cases must be considered (e.g., hourly meteorological conditions over several years), the modeling algorithms are reasonably simple and efficient in execution. The approach of APLPAD has been to assemble various al-

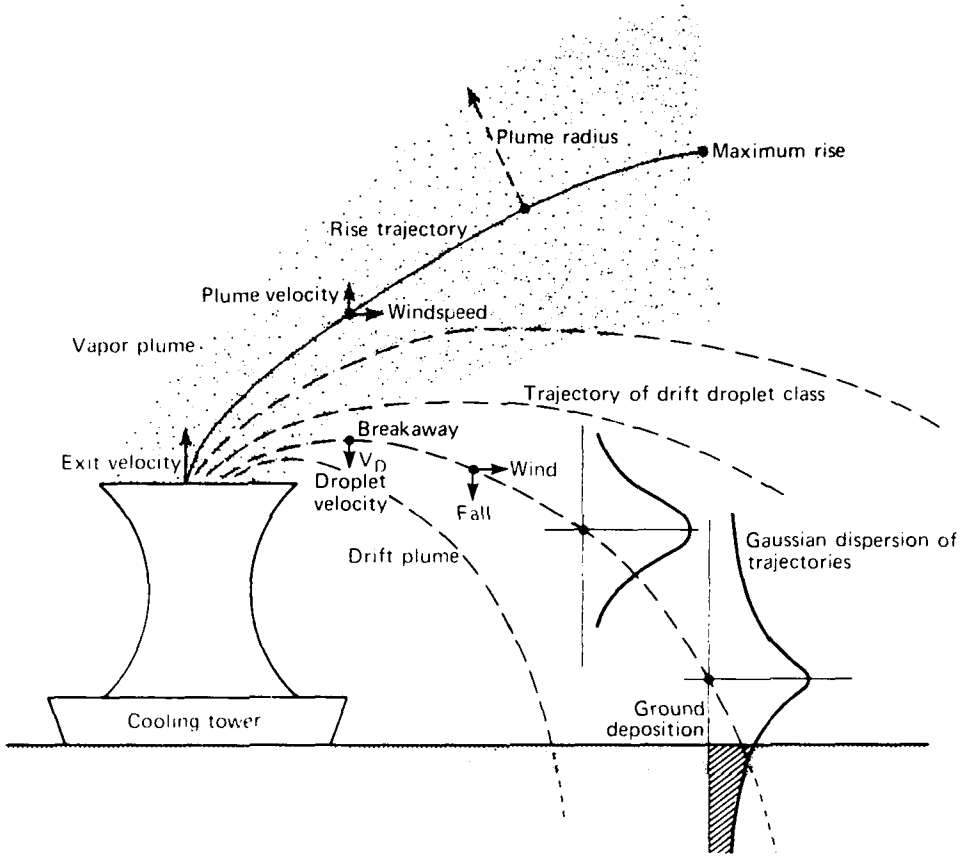

Figure 1—Essential features of the APL plume and drift model.

gorithms representing the important physical processes—each being only as detailed as necessary to maintain a proper overall balance in the modeling representation of reality. Control options are provided in the code so that various levels of detail can be selected for the various submodels. Also, several parameters can be adjusted so that the model can be tuned to field data and validated against other more detailed models of individual physical processes.

During model development, a logical modeling structure has been maintained so that new processes and environmental impacts peculiar to a specific application can be readily incorporated. The configuration has been controlled by a systematic structure of code blocks. All modifications are made by substituting entire blocks of new code, previously checked out, rather than by making line-by-line changes at scattered locations in the code. This procedure allows duplicates of the model at different locations to be maintained in an identical, known configuration.

The model is written in IBM Fortran (H Extended) and has been run at APL on the IBM 3033 using the multiple virtual system operating system. The code includes enough commentary so that it is self-explanatory. All inputs are defaulted, and an imbedded test case is provided so that the model can be run and an example output obtained without user action. Debugging facilities are provided so that more details of the model computations can be seen if needed.

The efficient use of computer resources was an overriding consideration during model development to allow its use in studies with large meteorological databases and to support sensitivity/configuration analyses in connection with siting studies. Efficiency is achieved by avoiding unnecessary computations, following good coding practices, using simplified algorithms, and categorizing meteorological cases so that duplications are not recomputed. The unique scheme devised to order these cases for consideration can decrease by 70% the number of cases to be computed when using a 10-year hourly database (87,672 cases).

Model Validation

The need for model validation is evident from work by others, which shows that various salt deposition

models using the same inputs can give predictions that differ by as much as two orders of magnitude.

The APLPAD model has been validated by tuning its internal parameters to obtain reasonable agreement with field data and by comparing its predictions with those of other models. The field data used were obtained by APL on a natural draft tower in the Chalk Point Cooling Tower Project and on a mechanical draft tower at PEPCO's Benning Road generating station in Washington, D.C. The data have been used to tune the rise predictions of the plume submodel and to validate the drift deposition submodel.

The primary objective of the validation program has been to establish confidence in the APLPAD model as a tool for predicting salt deposition under various conditions. The results indicate that the model probably overpredicts salt deposition for the natural draft tower and should provide conservative estimates of salt deposition effects. These results and a comparison of this model with others indicate that it reasonably represents the physical processes involved and provides predictions in reasonable agreement (a factor of two) with other models.

Model Use

The APLPAD model is a working tool to support analyses; new features are added to meet the needs of current studies. Figure 2 shows its role in the analysis process. As indicated, it is only one tool in the process. Other models and processing programs are used to prepare inputs and process outputs.

Since APLPAD has been used at APL as part of an on-line computing environment, the tendency has been to write plume and drift results to data files and then to process them with interactive programs to obtain the desired results. For example, the visible plume length for each meteorological record is written to a file and later that file is processed to obtain distributions of lengths. Only the results for the deposition of salt from saline drift are done in a "production" mode to provide finished tables.

ACKNOWLEDGMENTS

There have been many contributions to the development of the APLPAD model, both its earlier version

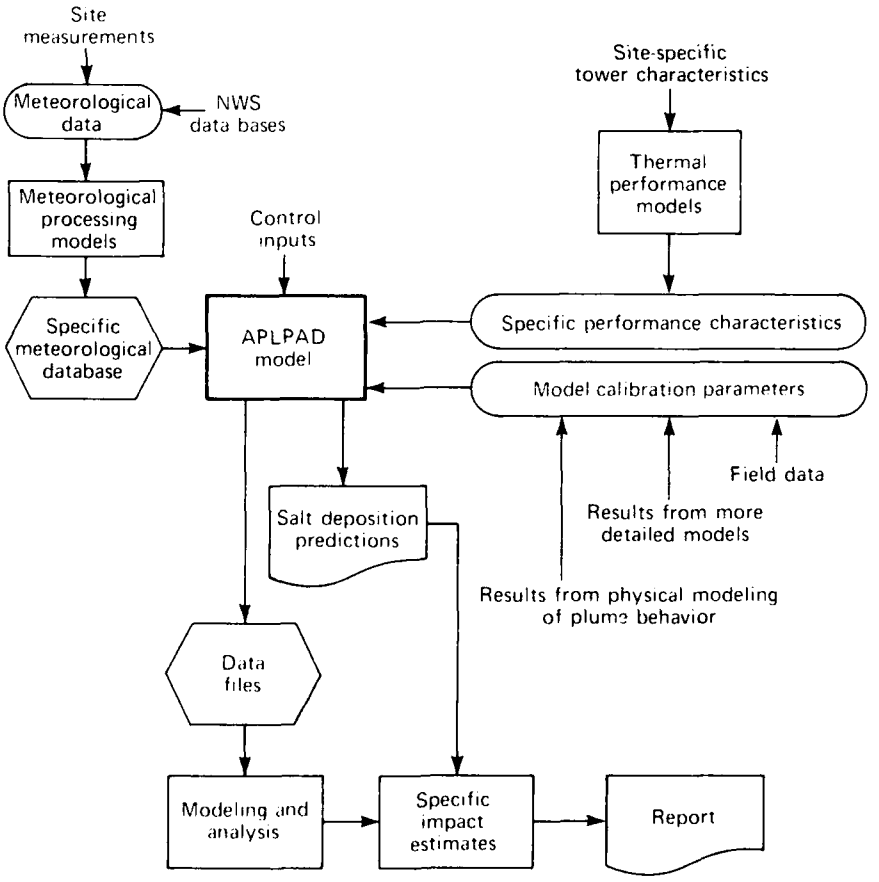

Figure 2—The APLPAD model as part of the analysis process.

and the current one. T. W. Eagles, L. C. Kohlenstein, J. A. Kagan, W. D. Stanbro, and J. H. Meyer were instrumental in creating the early version of the model. M. L. Moon, as a leader in the Chalk Point Cooling Tower Project, provided the impetus for the current version. E. M. Portner, as Project Engineer for the Vienna Siting Study, vigorously supported model improvement for use in that study. W. D. Stanbro provided a better subroutine to compute drift water droplet evaporation. J. J. Lentz provided a computer program to analyze the thermal performance of cooling towers. V. T. Freeman was very helpful in bringing the model code to its current state and in applying it to the impact analyses done for the Vienna Siting Study.

REFERENCE

[1] E. A. Davis, *Cooling Tower Plume and Drift Model: Description and User's Guide*, JHU/APL PPSE T-25 (Apr 1984).

This work was supported by the Maryland Power Plant Siting Program.

FIELD ASSESSMENT OF STRIPED BASS LARVAL SURVIVAL CORRELATED WITH CONTAMINANTS AND WATER QUALITY PARAMETERS

L. W. Hall, Jr.

In-situ field studies have identified some primary factors responsible for striped bass (Morone saxatilis) *larval mortality in the Nanticoke River on the Eastern Shore of Chesapeake Bay. The factors that were reported to cause that mortality were low pH conditions, high aluminum concentrations, and the presence of soft (low alkalinity) fresh water. The data have provided insight on one possible reason for the fact that striped bass stocks are declining on the east coast of the United States.*

BACKGROUND

The population of striped bass has been declining on both the Atlantic and the Pacific coasts in recent years because of the reduced production of dominant year classes. Factors influencing the survival of this species during the first 60 days of life will ultimately determine the abundance of striped bass stocks.[1] The factors or combinations of factors that have been implicated in affecting the survival of striped bass eggs and larvae are fishing pressure, predation, disease, stream flow, food availability, entrainment and impingement by power plants, and chemical contaminants.[2]

Research in the area of contaminant effects has provided documentation that organic and inorganic contaminants inhibit the survival of the early life stages of striped bass.[3,4] Evaluations of contaminant effects have been conducted primarily in the laboratory. Those studies

have provided essential documentation; however, we need to develop a useful approach for evaluating contaminant effects in the natural environment if key questions addressing the decline of the striped bass are to be answered.

Most of the striped bass migrating along the Atlantic coast are spawned in tributaries of Chesapeake Bay.[5,6] Estimates based on recent investigations of meristic, morphometric, and biochemical characteristics have indicated that approximately 90% of the coastal striped bass stock harvest originate in Chesapeake Bay.[7] The most important spawning areas in the Maryland area of the Bay are the Nanticoke River, Choptank River, Potomac River, and Upper Chesapeake Bay.[8] However, documentation is lacking on the survival of the early developmental stages of striped bass in those spawning habitats in conjunction with extensive contaminant and water quality monitoring.

The objective of this study was to evaluate the survival of the prolarvae (about 1 day old) in their natural spawning habitat (the Nanticoke River near Vienna, Md.) by using in-situ environmental test chambers. Extensive chemical analyses of both organic and inorganic contaminants and background water quality were made daily so that the correlations could be analyzed.

DISCUSSION

General Methods

The basic features of the in-situ environmental test chambers (68 liter volume) and the rafts for housing the chambers are shown in Figs. 1 and 2. One-day-old striped bass larvae were cultured from fertilized, water-hardened, striped bass eggs obtained from the Dennis Wildlife Center in Bonneau, S.C. The eggs were hatched in contaminant-free control water in McDonald hatching jars in a field station in Vienna.

Approximately 24 hr after hatching, 500 larvae were tested in replicate in the test chambers at three Nanticoke River locations and in two control tanks in the laboratory (one of 0 to 1 part per thousand salinity and the other of 2 to 3 parts per thousand salinity). The three locations represented approximately 5.5 mi of striped bass spawning habitat. Mortality observations were taken every 24 hr during each of two 96-hr experiments. Subsampling procedures (100 ml volume) were used to evaluate the larval survival.

Analytical and Water Quality Procedures

A Masterflex composite sampler with a peristatic pump was used to collect the 24-hr composite aqueous samples at 15-min intervals. The organic and inorganic contaminants that were measured from each sample are

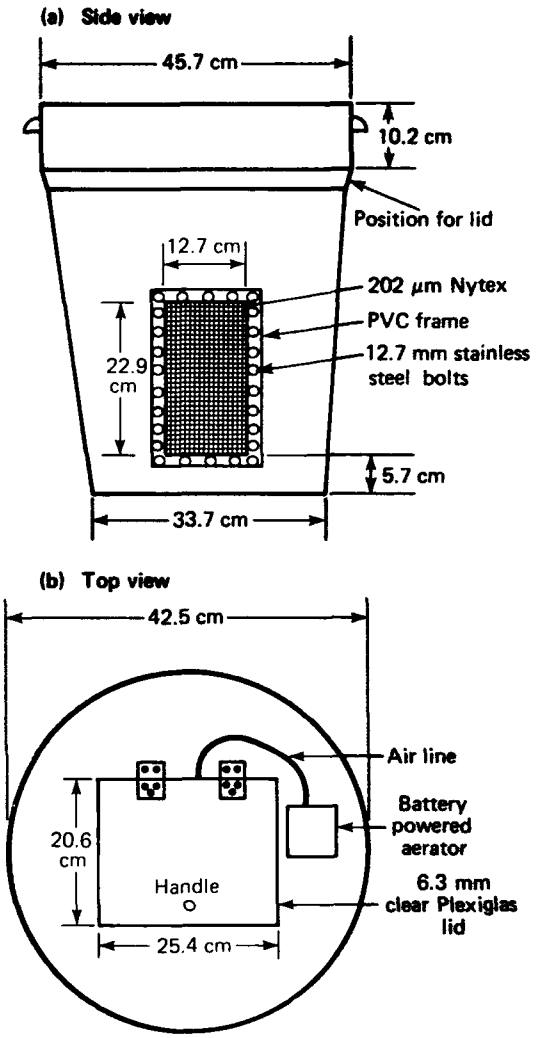

Figure 1—Side and top views of the in-situ test chambers.

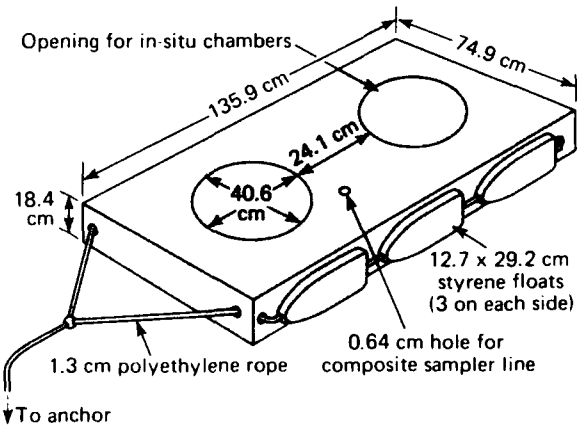

Figure 2—Raft used to house the test chambers in the river.

reported in Table 1. The following water quality parameters were also evaluated daily: temperature, salinity, dissolved oxygen, pH, conductivity, and hardness. Ammonia, nitrate, and orthophosphate levels, the precipitation, and the air temperature were also reported during each experiment.

Table 1—Organic and inorganic contaminants reported during each experiment.

Contaminant	Detection Limit
Aluminum	2 μg/l
Arsenic	1 μg/l
Cadmium	0.2 μg/l
Chromium	1 μg/l
Copper	1 μg/l
Lead	1 μg/l
Selenium	1 μg/l
Zinc	5 μg/l
Toxaphene	42 ng/l
Aroclor 1248	8 ng/l
Aroclor 1254	11 ng/l
Aroclor 1260	14 ng/l
Chlordane	6 ng/l
DDE	2 ng/l
Fluorene	40 ng/l
Phenanthrene	40 ng/l
Fluoranthene	40 ng/l
Perylene	40 ng/l
Anthracene	40 ng/l
Pyrene	40 ng/l
Chrysene + benz (o) anthracene	80 ng/l

Data Interpretation

Data from the experiments demonstrated that the survival of striped bass larvae was less than 10% after 96 hr of exposure to Nanticoke River water at all stations. The survival of both sets of controls was greater than 75%. Three basic categories have been assessed as possible causes of the mortality: organic contaminants, inorganic contaminants, and water quality parameters. The data suggest that the organic contaminants that were evaluated in this river system can be eliminated as a contributing factor. Of the eight inorganic contaminants that were measured, aluminum was the only trace metal that appeared in high, potentially toxic concentrations. Total unfiltered aluminum concentrations ranging from 0.48 to 4.1 mg/l were reported during both experiments. A mean concentration of 0.12 mg/l of aluminum was found in nine filtered river water samples taken during the second experiment. Previous investigators have reported that 0.1 to 0.2 mg/l of inorganic aluminum (aluminum fluoride, aluminum hydroxide complexes, and free aluminum) was highly toxic to fish fry.[9]

The potential toxicity of aluminum to striped bass prolarvae cannot be evaluated without considering the Nanticoke River pH of about 6.3. Although such pH conditions are not extremely acidic, they represent a potentially stressful condition for the striped bass prolarvae. Recent studies completed at the Columbia National Fisheries Research Laboratory have reported that a pH of 6.5 is toxic to 19-day-old striped bass after 7 days of exposure.[10] They also reported that a pH of 6.5 plus the addition of 0.1 mg/l of aluminum caused 100% mortality to 19-day-old striped bass after 5 days of exposure. The pH reported in the Nanticoke River probably was a stressful condition that contributed to the mortality.

The in-situ studies were conducted concurrently with on-site laboratory studies by the Columbia National Fisheries Research Laboratory.[10] A 24-hr composite of habitat water from all three stations and the same control water were used in both the in-situ and the on-site studies. Larvae at the same life stage experienced a cumulative mortality in the on-site tests similar to that reported for the in-situ experiments. Greater than 80% mortality for the prolarvae was reported after 4 days of exposure to river water from all three sample sites during both experiments.[10] This rigorously designed test confirmed that habitat water was extremely toxic to prolarval striped bass after 4 days of exposure.

The precipitation that occurred during both of these experiments probably affected the high aluminum and low pH conditions in the river. Precipitation of 3.27 cm fell during the first experiment, 1.95 cm during the second; this may have been an adverse factor because it causes a sudden increase in the mobilization of aluminum and a decrease in pH. The abrupt changes in the conditions may have been as critical a factor as the underlying condition. The spring precipitation also changed the low-salinity conditions that can exist in this soft Eastern-Shore river water. During dry spring periods, the low salinity found in the lower regions on the Nanticoke River striped bass spawning area can be an asset in enhancing survival of the prolarvae. Burton[11] reported that low-salinity conditions significantly increased the survival of striped bass prolarvae in soft fresh water. Therefore, the lack of significant salinity (less than 1 part per thousand) at any of the study sites, including the downstream station, was another factor that may have affected the survival rate.

It is not possible from the present study to isolate a single factor as a cause for the mortality. The factors that were influential in causing mortality were low pH conditions, high aluminum concentrations, and the presence of soft freshwater. Any one of the three factors or the interaction of all three may be responsible. The important information obtained from this study is that high larval mortality was documented in a prime striped bass spawning habitat during the optimum spawning period. The data represent documented adverse conditions found in only one spawning habitat; extrapolation to other

Chesapeake Bay river systems would not be warranted if different water quality conditions were present.

REFERENCES

[1] D. T. Westin and B. A. Rogers, *Synopsis of Biological Data on the Striped Bass,* Morone saxatilis (*Walbaum*), University of Rhode Island Marine Technical Report 67, Kingston (1978).

[2] P. M. Mehrle, *Summary of Striped Bass Contaminant Investigations at CNFRL,* Summary Report, U.S. Fish and Wildlife Service, Columbia National Fisheries Research Laboratory, Columbia, Mo. (1982).

[3] Columbia National Fisheries Research Laboratory, *Impacts of Contaminants on Early Life Stages of Striped Bass,* U.S. Fish and Wildlife Service, Columbia, Mo. (1983).

[4] L. W. Hall, L. O. Horseman, and S. Zeger, "Effects of Multiple Organic and Inorganic Contaminants on Fertilization, Hatching Success and Prolarval Survival of Striped Bass, *Morone saxatilis,*" *Arch. Environ. Contam. Toxicol.* **13**, 723-729 (1984).

[5] L. C. Kohlenstein, "On the Proportion of Chesapeake Bay Stock of Striped Bass that Migrates into the Coastal Fishery," *Trans. Am. Fish. Soc.* **110**, 168-179 (1981).

[6] R. J. Kernehan, M. R. Headrick, and R. E. Smith, "Early Life History of Striped Bass in the Chesapeake and Delaware Canal and Vicinity," *Trans. Am. Fish. Soc.* **110**, 137-150 (1981).

[7] T. J. Berggren and J. T. Lieberman, *Relative Contribution of Hudson, Chesapeake and Roanoke Striped Bass,* Morone saxatilis, *Stocks to the Atlantic Coast Fishery,* U.S. Fish and Wildlife Service Bulletin 76, 335-345 (1978).

[8] L. C. Kohlenstein, *Aspects of the Population Dynamics of Striped Bass* (Morone saxatilis) *Spawning in Maryland Tributaries of the Chesapeake Bay,* JHU PPSE T-14 (1980).

[9] J. Baker and C. Schofield, "Aluminum Toxicity to Fish as Related to Acid Precipitation and Adirondack Surface Water Quality," in *Proc. of the International Conf. on the Ecological Impact of Acid Precipitation, Acid Precipitation Effects on Forest and Fish Projects,* D. Drahlos and A. Tollan, eds., pp. 292-293 (1980).

[10] P. M. Mehrle, D. Buckler, S. Finger, and L. Ludke, *Impact of Contaminants on Striped Bass,* Interim Report, U.S. Fish and Wildlife Service, Columbia National Fisheries Research Laboratory, Columbia, Mo. (1984).

[11] D. T. Burton, *An Evaluation of the Potential Toxicity of Treated Bleached Kraft Mill Effluent to the Early Life Stages of Striped Bass,* Morone saxatilis, JHU/APL CPE-8204 (1982).

This work was supported by the U.S. Fish and Wildlife Service.

FUNDAMENTAL RESEARCH

INTRODUCTION

APL has long supported fundamental research, recognizing its importance in keeping the Laboratory in the mainstream of new developments in basic science and technology. Much of the basic research conducted at APL is done in the Research Center, which was formally established in 1947. Its objectives are "to carry on basic research supporting present and potential mission areas of the Laboratory, to establish the Laboratory as a contributor to basic science, to provide research techniques and technical consulting for solving problems critical to Laboratory programs, and to serve as an entry for new talent and scientific information into the Laboratory." Since its inception, the Research Center has spawned new programs that are now carried out in other units of the Laboratory. Most notable are the programs of the Space Department and the Biomedical Research Program.

Today, the Milton S. Eisenhower Research Center comprises 52 staff members organized into four groups. Research is reported in the professional scientific literature; typically, 60 papers are published each year. The reports in this section represent work in areas of traditional strength in the Research Center—photochemistry and theoretical quantum chemistry—as well as a new area of work, artificial intelligence.

MAGNETOPHOTOSELECTIVE PHOTOLYSIS OF FREE RADICALS

F. J. Adrian, J. Bohandy, and B. F. Kim

Magnetophotoselection—polarized light photolysis that results in partial orientation of a paramagnetic product or reactant with respect to an external magnetic field—has been observed for the first time in a spin-doublet free radical. Such observations in photochemical reactions that produce or decompose free radicals can determine the optical transition moment of the photochemical transition. The optical transition moment is unknown for most free radical reactions and is important for determining the reaction mechanism.

BACKGROUND

A new program to investigate materials important in semiconductor devices has been initiated. Specific topics include laser microchemistry and the effects of electromagnetic radiation on materials and processes of interest in solid-state electronics. The study of radiation-induced defects is relevant because the properties of some devices can be degraded by exposure to ionizing radiation. This article discusses the observation of magnetophotoselection in a defect that can be produced in silicon dioxide (SiO_2), an insulating material used in metal-oxide semiconducting devices.

SUMMARY

Some types of high-purity fused silica contain approximately 1200 ppm of silicon-bound hydroxyl species (≡Si-OH). Ionizing radiation dissociates the OH bond, yielding hydrogen atoms that are highly reactive and, in this case, react with trace carbon monoxide (CO) impurities to form the formyl (HCO) radical. Because fused silica is amorphous, the resulting electron spin resonance (ESR) spectrum of the HCO radical is that of a randomly oriented paramagnetic species, usually called a powder spectrum. The characteristic feature of powder spectra is a series of sharp lines that correspond to radicals oriented in such a way that a magnetic axis of the paramagnetic species is approximately parallel to the external magnetic field.

The location of the magnetic axes of the planar HCO radical is shown in Fig. 1. The HCO radical has optical transitions with an anisotropic transition dipole moment. If the result of optical excitation of the radical is either a reaction or a reorientation of the radical, then excitation with polarized light will lead to a nonuniform distribution of the radicals. This effect will manifest itself by a change in the powder spectrum and can provide another way to study the structure and dynamics of the radical. Fused silica satisfies the requirement that the optical quality of the sample must be good enough that the exciting light is not depolarized by scattering; it turns out to be a system in which this magnetophotoselective photolysis can be observed.[1]

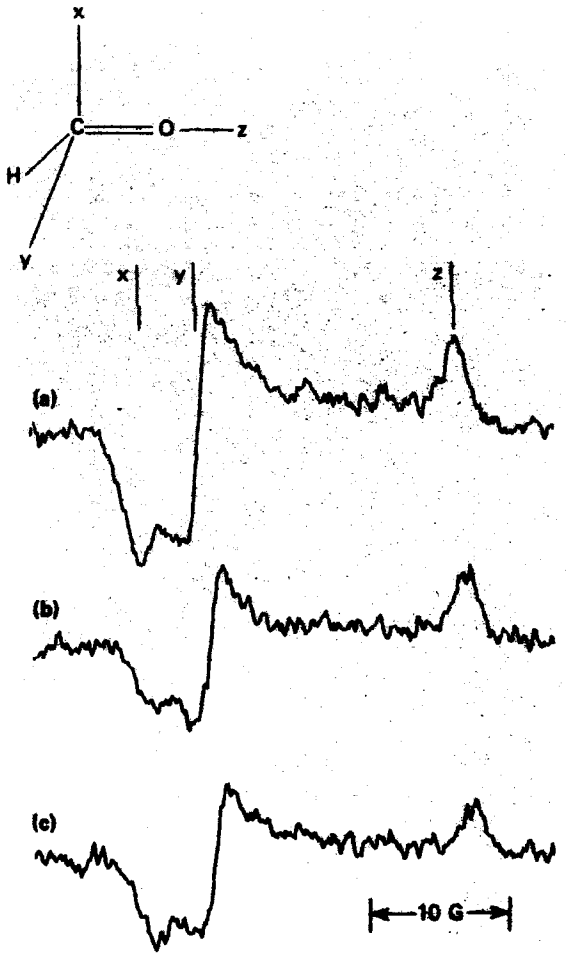

Figure 1—Effect of polarized light photolysis with $E_0 \| H_{DC}$ on the ESR spectrum of HCO in Suprasil 1 fused silica: (a) unphotolyzed high-field line, (b) after photolysis, and (c) effect of rotating the photolyzed sample 90° about the axis perpendicular to both H_{DC} and the direction of the photolyzing light. The approximate location of the principal axes of the g-tensor relative to the HCO molecule is also shown.

A 4 mm rod of Suprasil 1 fused silica was X-irradiated for 30 min at room temperature. It was then transferred to an Air Products Helitran variable temperature system located in an ESR cavity having slots through which the sample could be irradiated with polarized light, using a 200 W high-pressure mercury lamp and a Glan prism.

At 77 K, the ESR spectrum of the HCO radical consists of two powder patterns separated by the proton hyperfine splitting (hfs). At lower temperatures and lower microwave power, all three components of the high-field hfs line are resolved (Fig. 1a). Irradiation of the sample for 8 min using light polarized with the electric vector ($\mathbf{E}_0$) parallel to the external magnetic field ($\mathbf{H}_{DC}$) and with the wavelength, λ, greater than 500 nm (in the optical absorption band of the HCO radical) produced the spectrum shown in Fig. 1b. One sees a nonuniform decrease in the intensities of the three components (thus the term magnetophotoselective) with the x-component decreasing the most and the z-component decreasing the least. A convenient check for a nonuniform orientational distribution of radicals is to rotate the sample 90° about an axis perpendicular to the magnetic field. A uniform distribution would give the same ESR spectrum, whereas the actual spectrum, shown in Fig. 1c, has the x-component increasing in intensity and the y- and z-components decreasing.

These results show that the largest component of the optical transition dipole moment is along the x axis, which is known from analysis of the ESR spectrum to be perpendicular to the molecular plane. This result is consistent with theory, which predicts that the dipole moment for the lowest-energy optical transition in a rigid HCO molecule is perpendicular to the molecular plane. The observed small decay of the z-component of the spectrum can be explained by partial depolarization of the exciting light by scattering inside the microwave cavity. The decrease of the y-component, which is intermediate between those of the x- and z-components and which also should be zero in a nonrotating radical, indicates that the radical is not rigidly fixed in the silica host but executes a torsional oscillation about the z (C=O bond) axis, thereby enabling the y molecular axis to "steal" optical transition intensity from the x axis.

The effect of magnetophotoselection on ESR powder patterns can be calculated by modifying the random distribution function of the radicals so as to account for the orientationally selective photolysis.[1] A computer simulation of the effect of polarized light on the high-field HCO line, assuming that the photoexcitation either decomposes the radical or transforms it into a nonparamagnetic species, agrees well with experimental spectra.

Magnetophotoselection was also observed in the HCO radical trapped in a CO matrix at 13 K.[2] HCO was formed by irradiating a CO matrix containing 1% hydrogen iodide (HI) with ultraviolet light and photodissociating the HI to produce H atoms, which then reacted with the CO matrix to form HCO. Photolysis of the sample with polarized light decreased the intensity of the x principal-axis component of the high-field line while increasing the y- and z-components, as in fused silica. However, in this case the total integrated intensity of the HCO ESR spectrum is unchanged by visible light photolysis, so the line shape changes are completely the result of the magnetophotoselective transfer of intensity between radical orientations.

In this system, thermally activated reorientation of the HCO radical could be detected. This was done by first noting that the total intensity of the post-photolysis spectrum should be orientation independent; therefore, any change in the spectrum upon a 90° rotation of the sample gives a measure of the orientation anisotropy. By monitoring this anisotropy as a function of temperature, it was determined that the x-y anisotropy disappeared around 25 K but that the remaining (x,y)-z anisotropy persisted to approximately 40 K.

In conclusion, it has been shown that the detection of the magnetophotoselective photolysis of free radicals has much potential for investigating the structure, photochemistry, and photodynamics of free radicals.

ACKNOWLEDGMENT

The authors are indebted to P. R. Zarriello for his capable assistance with these experiments.

REFERENCES

[1] J. Bohandy, B. F. Kim, and F. J. Adrian, "Magnetophotoselective Photolysis of the Formyl Radical in Fused Silica," *Chem. Phys. Lett.* **104**, 413-417 (1984).

[2] F. J. Adrian, J. Bohandy, and B. F. Kim, "ESR Studies of the Formyl Radical in a CO Matrix: Magnetophotoselective Photolysis and Thermally Activated Rotations," *J. Chem. Phys.* (in press).

This work was supported by Independent R&D.

THEORY OF INDIRECT ELECTRON-NUCLEAR HYPERFINE INTERACTIONS OF HOLE CENTERS IN IONIC CRYSTALS AND MOLECULES

F. J. Adrian and A. N. Jette

A theory has been developed and applied to explain transferred metallic-cation electron-nuclear magnetic hyperfine interactions for a number of important ionic defects in solids and ionic molecules where more usual and direct methods predict that these interactions vanish. The problem has been solved by an indirect mechanism relying on a purely quantum mechanical phenomenon termed spin polarization (a consequence of the Pauli exclusion principle).

BACKGROUND

Many of the defects introduced into materials, either during their preparation or by environmental stresses such as exposure to actinic or ionizing radiation, are paramagnetic. Examples of such defects whose paramagnetism is due to an unpaired electron spin are (a) an electron trapped by a vacancy or a molecular complex in a crystalline lattice and (b) neutral or ionic molecular fragments (radicals) resulting from radiation-induced dissociation of stable molecules. Electron spin resonance and electron-nuclear double resonance spectroscopies are powerful methods for the identification and structural characterization of the paramagnetic defects. The basic election spin resonance transition between parallel and antiparallel orientations of the electron spin magnetic moment in an external magnetic field has superimposed on it a great deal of structural information, the most important being the hyperfine structure (hfs) splittings resulting from magnetic interactions between the unpaired electron and the magnetic moments of various nuclei in the defect and its neighbors. In many cases, molecular structure theory as applied to electron-nuclear hyperfine interactions is vital to the full utilization of the raw experimental hfs data; for example, the comparison of experiments with hfs splittings calculated for various models can determine the structure of the defect. The need for theory is especially critical in some cases, such as the case of several trapped hole centers in oxides containing Al^{+3} ions, either as a constituent as in Al_2O_3 or as an impurity,[1] and the case of the free radicals $Na(C=CH_2)$ and NaO_2.[2]

For both cases of defect centers in solids and the ionic molecules, the experimental hfs interactions show two distinct peculiarities: the isotropic hyperfine constant (hfc), denoted A, is large and negative (with the exception of $Na(C=CH_2)$ where the sign was not determined); and the value of the anisotropic hfc, denoted $B_{\|}$, is much smaller than one would expect from the classical dipole-dipole interaction between the unpaired electron and the magnetic cation nuclei. The common electronic configuration for all these centers (Fig. 1) is that the Al^{+3} (or Na^{+} as the case may be) cation is in a nodal plane of the unpaired O^{-} p orbital (the C^{-} p orbital in $Na(C=CH_2)$), so that there is zero overlap between it and the Al^{+3} (Na^{+}) ion cores and, consequently, no directly transferred isotropic hfc. The sign of the transferred hfc resulting from this direct interaction is necessarily positive.

The explanation of the foregoing difficulty is well known, at least in principle, and involves an indirect mechanism called exchange polarization.[3] Exchange polarization, a consequence of the Pauli exclusion principle, is a purely quantum mechanical phenomenon without a classical analog. It involves the fact that the interactions between the unpaired electron and all the other electrons in filled orbitals (i.e., paired with one electron having spin "up" and the other electron having spin "down") are partly spin dependent. Consequently, the electron orbitals that are perfectly paired in the zeroth approximation become slightly unpaired because they interact differently with the unpaired electron; this effect introduces a small amount of unpaired electron density into these orbitals. Some of the filled orbitals do not have a zero density at the cation nuclei (i.e., the cation nuclei are not situated on a nodal plane of these orbitals) and, consequently, there exists a nonzero hfs interaction, called an "indirect" hfs interaction, that is negative.

However, calculation of the hfs resulting from this method is quite difficult because the spin polarization of

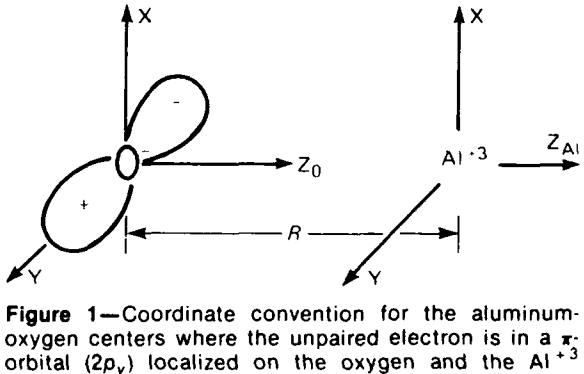

Figure 1—Coordinate convention for the aluminum-oxygen centers where the unpaired electron is in a π-orbital ($2p_y$) localized on the oxygen and the Al^{+3} nucleus is on the nodal plane of this orbital.

closed-shell or lone-pair orbitals by an unpaired electron in another orbital must be determined by the admixture of various excited electronic states into the zeroth-order approximation to the ground-state wave function. Virtually nothing is known about these excited state functions; even worse, the expansion requires a very large number of excited states to describe the spin polarization adequately. Here, we shall outline a semiempirical treatment of the spin polarization mechanism of transferred hfcs of metal ion ligands (neighbors) that is simple enough to be applied to a wide variety of paramagnetic systems.

DISCUSSION

As a point of departure, consider the O^-–Al^{+3} system illustrated in Fig. 1; it consists of an unpaired electron (hole) in a π-orbital ($2p_y$) localized on the oxygen interacting with a neighboring Al^{+3} cation that is on the z axis. Because the Al^{+3} nucleus is on the nodal plane of the unpaired electron, $\langle\psi_0|\mathbf{H}_{hfs}|\psi_0\rangle = 0$, where ψ_0 is the zeroth-order ground-state wave function of this many-electron system, and $\mathbf{H}_{hfs}$ is the electron-nuclear magnetic hyperfine interaction. However, if this zeroth-order wave function is spin polarized by the coulomb interaction between the unpaired electron and the paired electrons, the polarized many-electron wave function can be written as

$$\psi_0^{(n)} = \psi_0 + \sum (E_0 - E_n)^{-1}\langle\psi_n|\mathbf{H}_c|\psi_0\rangle\psi_n \quad ,$$

$$n = \text{excited states} \quad ,$$

where $-(E_0 - E_n)$ is the excitation energy from the ground to the nth excited electronic state, ψ_n, and $\mathbf{H}_c$ is the electron-electron coulomb interaction, i.e.,

$$\mathbf{H}_c = e^2 \sum_{\mu>\nu} (1/r_{\mu\nu}) \quad .$$

This wave function gives a nonzero hfs interaction:

$$2\sum \langle\psi_0|\mathbf{H}_c|\psi_n\rangle\langle\psi_n|\mathbf{H}_{hfs}|\psi_0\rangle/(E_0 - E_n) \quad ,$$

$$n = \text{excited states} \quad ,$$

to first order in $\mathbf{H}_c$. The problem of summing over the many excited states, E_n, can be overcome if the excitation energies of the various excited states in the sum are close enough together that they may be replaced by a single "average" excitation energy. This "average energy approximation," together with the fact that the electronic states that describe the wave function are a complete set, can be used to reduce the sum over all excited states to an expression involving only the zeroth-order ground-state wave function. If we replace $E_0 - E_n$ by an average excitation energy, ΔE, and complete the sum over the states by adding the ψ_0 state (which contributes nothing in this case since $\langle\psi_0|\mathbf{H}_{hfs}|\psi_0\rangle = 0$), we get

$$\frac{2}{\Delta E}\sum \langle\psi_0|\mathbf{H}_c|\psi_n\rangle\langle\psi_n|\mathbf{H}_{hfs}|\psi_0\rangle$$

$$n = \text{all states}$$

$$= \frac{2}{\Delta E}\langle\psi_0|\mathbf{H}_c\mathbf{H}_{hfs}|\psi_0\rangle \quad .$$

This last result, which gives the hfs interaction in terms of the ground-state wave function only, is obtained from standard formulas for matrix products, provided that the ψ_n form a complete set of states.

Unfortunately, as it stands, this procedure is of limited utility in the present problem because there is a wide variety of excited states whose excitation energies are too dissimilar to be described by a single average excitation energy. In some cases (and the method appears to be quite general), the problem has been overcome by subdividing the various excited states into groups according to symmetry, the type of orbital excited, etc., so that the excitation energies of states within a group can be represented by an average excitation energy. Thus, the hfs interaction resulting from each group of excited states can be calculated individually, using the average excitation energy approximation and the individual completeness of a group of states of a particular symmetry or orbital type.

In the O^-–Al^{+3} system, for example, two groups of excited states correspond, respectively, to (a) spin polarization of the Al^{+3} closed shells and (b) spin polarization of the lone pair of σ ($2p_z$) orbitals of the O^- ion. Although the first class of states would seem to give the largest Al^{+3} hfs because the polarized orbitals are localized on the Al^{+3} nucleus and hence have a very large density at the Al^{+3} nucleus, their contribution is actually small because of their distance from the unpaired electron on O^- and because of the very large excitation energies of the Al^{+3} orbitals. Thus, the calculated hfs, which is in good agreement with experiment for reasonable values of the O^-–Al^{+3} distance, comes from the spin polarization of the O^- lone pair $\sigma(2p_z)$ orbitals combined with the transfer of the unpaired electron density in these orbitals to the Al^{+3} orbitals via their mutual overlap.

This theory has been applied to interpret the election spin resonance and election-nuclear double resonance measurements of the Al^{+3} transferred hfcs in Na-β-

alumina, α-$Al^{+3}O_3$:Mg^{++}, GeO_2, and SiO_2, where Al^{+3} exists as an impurity in the latter two crystals. In all cases, negative isotropic hfcs and small anisotropic hfcs were measured. The theory explains the major features of the hfcs of these defect centers in which Al^{+3} is in the nodal plane of the unpaired oxygen p-orbital. A rather precise O^{-}–Al^{+3} distance can be derived from this analysis and from the experimental isotropic hfcs when the electrostatic contribution to the average excitation energy of oxygen is known approximately. Since A depends exponentially on this distance, the estimate is rather good despite uncertainties in the average excitation energies. On the other hand, with an estimate of the bond length and the experimental value for the isotropic hfc, one can get an approximate electrostatic crystal field, which is often difficult to obtain. The theoretical values for $B_{\|}$ are less reliable because they are the differences of a fairly large number of terms of comparable magnitude. The theory reflects the experimental findings of nearly the same value of $B_{\|}$ for a wide range of O^{-}–Al^{+3} distances, and it explains the strong reduction compared to a pure classical dipole-dipole interaction. For the $Na^{+}(C^{-}-CH_2)$ and NaO_2 molecules, the calculated isotropic hfcs are in good agreement with the experimental values.

In summary, the present method, although admittedly approximate and empirical, offers a simple and reasonably accurate way to calculate metal-atom transferred hfcs resulting from the spin-polarization mechanism. Given the difficulty of calculating spin-polarization hfcs by ab initio and more refined methods, the present method is a useful approach to this problem.

ACKNOWLEDGMENT

It is a pleasure to acknowledge the many important contributions to this work by J. M. Spaeth of the University of Paderborn, Federal Republic of Germany, and the stimulation he provided, without which it would not have been completed.

REFERENCES

[1] F. J. Adrian, A. N. Jette, and J. M. Spaeth, "Theory of Indirect Hyperfine Interactions of Oxygen Aluminum Defects in Ionic Crystals" (submitted to *Phys. Rev.*).

[2] F. J. Adrian and A. N. Jette, "Semiempirical Model of the Exchange Polarization Mechanism of Transferred Hyperfine Interactions in Ionic Radicals," *J. Chem. Phys.* **81**, 2415-2419 (Sep 1, 1984).

[3] R. E. Watson and A. J. Freeman, *Hyperfine Interactions*, Academic Press, New York, pp. 53-94 (1967).

This work was supported by Independent R&D.

A PARADIGM FOR OBJECT RECOGNITION

B. F. Kim, J. Bohandy, and V. G. Sigillito

A paradigm for object recognition has been devised that has characteristics important in the development of a general robotic machine vision system.

BACKGROUND

Future generations of automata will play essential roles in civilian and military systems. Intelligent robots will not only decrease risks to humans in dangerous environments, but will also provide designers and planners with system concepts that are presently unavailable. The realization of such robotic machines will require machine vision systems with capabilities comparable to those of human vision. The results described here are significant because they contribute to the development of concepts required for the realization of a general robotic machine vision system.

DISCUSSION

A recognition paradigm is described here that has several characteristics thought to be important in the development of a general machine vision system. A principal feature of this paradigm is that it learns to recognize objects by seeing them instead of requiring that explicit models or rules be programmed into the computer. A vision system based on this principle would be able to in

terpret visual scenes falling within its realm of previous experience. Such is also the case in human vision.

The system described here has been simulated in a LISP program called Recognize. A hierarchy of symbolic images of monotonically decreasing size is generated, the last of which yields an interpretation of the original image. At each level, the symbolic image is interpreted by comparison with elements of a memory associated with that level, and a new image is generated for interpretation recursively in the next level. The scheme is illustrated in Fig. 1.

At a given level, the image is partitioned into an array of subarrays. Each subarray in the partitioned image is compared with the elements in the memory for that level by a matching routine. A unique symbol associated with each memory element is called its "name." If a subarray matches a particular memory element, the name of the element becomes the "value" of that subarray. If no matching memory element is found, one that matches is created and is placed in the memory. A new symbol is assigned as the name of the new memory element and also as the value of the subarray. In Fig. 1, the indicated subarray has been given the value *S1*. Each subarray is interpreted in this way, the result being a new image whose "pixel" elements are the values assigned to the subarrays. The new image is then interpreted recursively in the next level.

The last level is the liaison between the output of the system and other possible components of a larger intelligent system. In our immediate case, the system is part of a research project on machine vision, and the communication is with a human by means of a computer terminal. In the last level, the name of each memory element is a description or name of an object or pattern in the original image (first level) that was to be recognized. If a memory element matches the image in this level, the name of the element is displayed on the terminal screen. If no match is found, the system asks what the object is. A memory element that matches the image is stored in memory, and the name of the element is a description entered from the terminal keyboard. The object will then be recognized by the system in future encounters.

The hierarchically distributed memory consists of a stack at each level that is compared sequentially with subarrays at that level. When a match is found, the memory element that was successfully matched is placed at the top of the stack. If no match is achieved, a memory element that matches the subarray is created and is placed at the top of the stack, while the last element of the stack is discarded. This leads to the property that the system most quickly recognizes objects it has seen recently, and it may forget or lose its ability to recognize objects that are not reinforced by usage. This property is also characteristic of biological vision systems.

Each memory element is a list of symbols of length equal to the number of pixels in the subarray. The matching function converts the subarrays into lists that are compared directly with the memory elements, as indicated in Fig. 2. Although the figure indicates an exact match (essentially a template match) between a subarray and a memory element, an exact match requirement may not be advantageous in all cases. A partial match in the first level, for example, would alleviate noise problems in interpretations at that level.

CONCLUSION

The recognition paradigm described here is a module that will be part of a larger machine vision system. The larger system is envisioned to contain a number of functional modules that will evolve in the course of development of the system as a whole. Although our main interest at the moment is in further development of a vision paradigm, our results might at some point be ap-

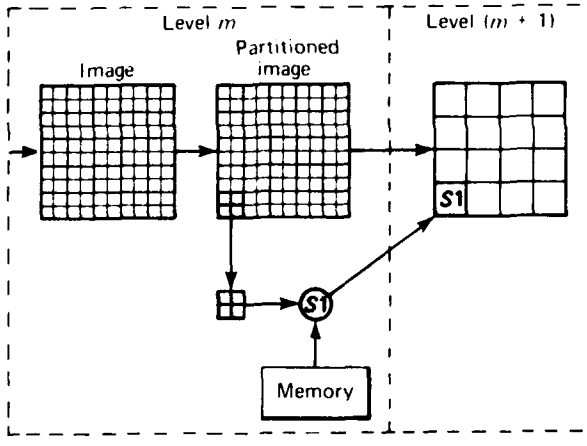

Figure 1 — Two adjacent levels in the Recognize program.

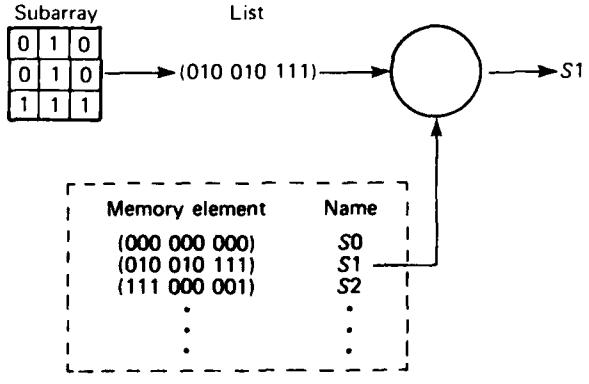

Figure 2 — Matching the content of a subarray with memory.

plicable to particular vision problems. In that event, the paradigm or some extension of it could be implemented in a more efficient software code or in a highly parallel hardware architecture. A hierarchical structure using cellular arrays[1] would seem to be a natural implementation using present computer technology.

ACKNOWLEDGMENT

We wish to thank Raymond E. Sterner for his kind assistance in providing us with digital images.

REFERENCE

[1] A Rosenfeld, "Parellel Image Processing Using Cellular Arrays," *IEEE Comput. Mag.* **16**, 14-20 (1983).

This work was supported by Independent R&D.

PATENTS

PATENTS ACTIVITIES

The APL Patents Office is responsible for ensuring compliance with contract and grant requirements relative to patent and data rights, as imposed by the various governmental agencies that sponsor work at the Laboratory. In addition to preparing formal disclosures of inventions for the appropriate sponsors, the Patents Office prepares and prosecutes patent applications on behalf of both the University and the Department of the Navy.

The following lists indicate the invention disclosures submitted to sponsors, the patent applications prepared and filed in the United States Patent Office, and the previously filed applications that were successfully prosecuted to issuance as patents, during fiscal year 1983.

INVENTION DISCLOSURES

G. L. Boyer and R. W. Proue—*Three-Dimensional Radar Centroid Processor*

A. Brandt—*Hydrodynamic Flowfield Imaging*

G. B. Bush—*Isolating Platform for Satellites*

G. B. Bush—*Proof Mass Sensor for GRM Satellite*

H. C. Davey and H. H. Knapp—*An All Solid-State ECM Test Set*

G. F. Emch—*Endarcholator*

G. H. Fountain—*Patient ECG Recording Control of the Automatic Implantable Defibrillator*

A. B. Fraser and G. J. Farrugia—*Conductivity Sensor*

D. P. Gentilucci, L. L. Hanson, and A. L. Newman—*Method for Programming Printed Circuit Boards*

S. E. Grenleski—*Ramjet Combustor for Vehicle Launched from Various Platforms*

S. E. Grenleski, A. T. Hayes, and R. F. Krupa—*Water-Cooled Spherical Pressure Probe for Use in High-Temperature Flows*

S. E. Grenleski and J. L. Keirsey—*Torpedo Tube Vehicle Ramjet Combustor*

M. L. Hill—*Erectable Rigid Delta Wing Airplane*

M. L. Hill—*SYMDEL 3 Expendable Drone*

A. S. Hughes, W. E. Snelling, and T. R. Hocker—*Array Processor Application for Emulation of the Terrier CWAT Radar*

D. A. Kitchin and A. B. Fraser—*A Distributed Intelligent Oceanographic Data Acquisition System for Towed Sensor Arrays*

M. A. Konodi—*Onboard Ship Control Trainer for Trident Submarines*

J. A. Krill—*Air Inlet for Internal Cooling of Overmoded Waveguide*

J. A. Krill and D. G. Grant—*A System for Sensing Radar Holes and Ducts Using Satellites*

J. A. Krill and W. H. Zinger—*Design for Overmoded Waveguide and Bend*

J. H. Kuck—*Automatic Attenuator for Sonobuoys*

P. E. Lakomy—*A Phase Shifter Control Method for Reducing Phased Array Antenna Gain Modulations*

D. G. Lee, Jr.—*Mouth Switch Keyboard Emulator System*

J. S. Lombardo, H. M. Grady, D. N. Qualkinbush, and S. J. Kundin—*A Paravane System for Compensation of Aperture Distortion in Towed Arrays*

J. H. Loveless—*Bite Controller for Robotic Arm*

F. T. Marcellino—*Microscope Rotating Stage*

F. T. Marcellino—*Vise Jaws for Delidding Integrated Circuits*

D. L. Mitchell and M. C. Heidkamp—*A Software Translator for the National Semi-Conductor IMP-16C Microprocessor*

M. R. Newcomer—*A Method of Remotely Piloted Vehicle (RPV) Station Keeping Using Range Measurements*

R. S. Potember and T. O. Poehler—*Multistate Optical Switching and Memory Using an Amphoteric Organic Charge Transfer Material*

R. A. Quinnel and C. A. Twigg—*Videotape Digital Data Recovery System*

T. M. Rankin—*RAM Pseudo Gyro*

R. E. Rouse—*A Dynamic Phase Correction System for Paralleling RF Amplifiers*

R. E. Rouse—*Magnetron Filament Voltage Regulator*

F. W. Schenkel, B. S. Ogorzalek, and C.-I. Meng—*Satellite Auroral/Ionospheric UV Imager*

W. Seamone and J. H. Loveless—*Prosthetic Elbow with a Motor-Driven Release Mechanism*

W. E. Snelling and J. E. Penn—*2's Complement Digital Multiplier Implemented in NMOS Semiconductor Technology*

H. M. South—*Digital Recording and Processing Systems for Hydrophone Arrays*

G. M. Starken, J. Cavin, R. A. Quinnel, C. A. Twigg, and D. P. Crawford—*Tape-X-Digital Data Formatter for Data Storage via Video Recorder*

W. I. Sternberger, S. Cooper, W. K. Weber, and G. A. Starstrom—*Temperature Compensated Thermistor Anemometer*

G. A. Sullins—*Electric-Motor Driven Fuel Pump with Ram-Air Turbine Driven Boost*

R. R. Talbott—*New Fiber Optic Computer Channel Using Existing STANAG-4153 Components in a Novel Way*

L. W. Taylor—*Self-Referencing Visual Power Supply Monitor*

M. E. Thomas and H. W. Ko—*A Method of Characterizing Surface Ducts from Radar Clutter Measurements*

R. E. Thurber, R. J. Prengaman, J. Phipps, and R. Rzemien—*Coherent Radar Digital Data Collector and Sampling Technique for Noncoherent Transmitter Radars*

J. T. Turner—*Improved Method of Welding Electronic Parts*

R. Turner—*A Method for Generating and Measuring Gas Bubbles Utilizing Lasers*

L. A. Twigg and K. J. Mach—*A Die and Substrate Solder-Attach Station*

L. A. Twigg and K. J. Mach—*Microelectronic Component Replacement Station*

E. E. Westerfield—*Transdigitizer for Relaying of Signals from GPS Satellites*

J. J. Wozniak—*Data Processing System for the Evaluation of the Underwater Flight Dynamics of Missiles*

T. Wyatt—*Proportional Control Thrusting for Spacecraft*

PATENT APPLICATIONS

G. F. Emch—*Power Independent Real-Time Clock*

J. C. Firman, R. E. Rouse, and W. H. Zinger—*Solid State Modulator for Microwave Power Tubes*

R. E. Fischell—*Single Valve Diaphragm Pump with Decreased Sensitivity to Ambient Conditions*

R. E. Fischell, A. L. Newman, H. B. Riblet, and W. R. Powell—*An Improved Apparatus for Inhibiting Self-Injurious Behavior (SIB) in Patients*

R. E. Fischell, A. C. Sadilek, and W. Swift—*Method for Clearing a Gas Bubble from a Positive Displacement Pump Contained within a Fluid Dispensing System*

C. A. Keller—*Fluid Level Measuring Device with Linear, High Resolution Output*

R. A. Makofski, J. T. Massey, F. F. Mark, F. B. Weiskopf, Jr., W. H. Guier, P. C. Walsh, and F. F. Marshall—*Means and Method for Noninvasive Fragmentation of Body Concretions*

J. G. Parker and W. D. Stanbro—*An Improved Electro-optical Device for Monitoring Instantaneous Singlet Oxygen Concentration Produced during Photoradiation Using Pulsed Excitation and Time Domain Signal Processing*

J. G. Parker and W. D. Stanbro—*Electro-optical Device for Monitoring Instantaneous Singlet Oxygen Concentration Produced during Photoradiation Therapy Using a CW Excitation Source*

R. S. Potember and T. O. Poehler—*Multistate Optical Switching and Memory Using an Amphoteric Organic Charge Transfer Material*

W. Seamone and J. H. Loveless—*Prosthetic Elbow with a Motor-Driven Release Mechanism*

W. Swift and R. E. Fischell—*Passive Filling Device*

C. W. Webster and R. K. Stilwell—*Technique for Impedance Matching Bifilar Helix Antenna*

PATENTS ISSUED

A. B. Fraser—*Frequency Encoding Closed Loop Circuit with Transducer,* No. 4,408,169

P. H. Gilbert—*Phase Demodulator Utilizing a Frequency Divider, Synchronous Filter, and Phase Comparator,* No. 4,419,630

R. E. Fischell—*A Low Susceptibility Proof Mass for a Single Axis Drag Compensation System,* No. 4,422,330

J. H. Loveless—*Motorized Wheel Chair,* No. 4,422,515

W. H. Avery—*Open Cycle OTEC Plant,* No. 4,430,861

R. E. Fischell, G. H. Fountain, and C. M. Blackburn—*Self-Injurious Behavior Inhibiting System,* No. 4,440,160

C. A. Keller—*Fluid Level Measuring Device with Linear, High Resolution Output,* No. 4,443,699

E. P. Irzinski—*A Coaxial Waveguide Commutation Feed Network for Use with a Scanning Circular Phased Array Antenna,* No. 4,446,463

S. A. Kahn, R. L. Stewart, and S. G. Tolchin—*Local Area Communication Network,* No. 4,451,827

W. O. Wilkinson and D. W. Rabenhorst—*High Speed Imaging Television System,* No. 4,453,182

J. C. Murphy and L. C. Aamodt—*Optical Beam Deflection Thermal Imaging,* No. 4,468,136

J. J. Wozniak—*Sutureless Vascular Anastomosis Means and Methods,* No. 4,470,415

PUBLICATIONS AND PRESENTATIONS

PUBLICATIONS

L. C. Aamodt and J. C. Murphy, "Generalized Saturation Criteria for Photothermal Measurements," *J. Phys. (Paris)* **C6**, 115-119 (1983).

M. H. Acuna and J. K. Alexander (NASA), R. A. Brown (Space Telescope Science Inst.), T. W. Hill (Rice Univ.), S. M. Krimigis (APL), L. J. Lanzerotti (Bell Labs.), and G. L. Siscoe (Univ. California, Los Angeles), "Physics of the Jovian and Saturnian Magnetospheres: Highlights of a Conference Held at the Applied Physics Laboratory The Johns Hopkins University, October 22-24, 1981," *Space Sci. Rev.* **35**, 269-292 (1983).

F. J. Adrian and A. N. Jette, "Semiempirical Model of the Exchange Polarization Mechanism of Transferred Hyperfine Interactions in Ionic Radicals," *J. Chem. Phys.* **81**, 2415-2419 (1984).

F. J. Adrian and A. N. Jette, "Semiempirical Valence Bond Model of Hyperfine Interactions and Bonding in RbO and CsO," *J. Chem Phys.* **81**, 2411-2414 (1984).

J. R. Apel, "Remote Measurement of the Ocean—An Overview," in *Remote Sensing Applications in Marine Science Technology*, D. Reidel Pub. Co., Dordrecht, Holland (1983).

J. R. Apel, "A Survey of Some Recent Scientific Results from the SEASAT Altimeter," in *Satellite Microwave Remote Sensing*, Ellis Horwood Ltd., Chichester, England (1983).

J. R. Apel (APL) and J. R. Holbrook (Pacific Marine Environmental Lab.), "Internal Solitary Waves in the Sulu Sea," *Johns Hopkins APL Tech. Dig.* **4**, 267-275 (1983).

T. P. Armstrong, M. T. Paonessa, and E. V. Bell II (Univ. Kansas) and S. M. Krimigis (APL), "Voyager Observations of Saturnian Ion and Electron Phase Space Densities," *J. Geophys. Res.* **88**, 8893-8904 (1983).

W. D. Ashcraft (Rockwell International Corp.) and H. M. South (APL), "Architecture and Control of a Distributed Signal Processor," in *Proc. IEEE International Conf. on Acoustics, Speech, and Signal Processing*, pp. 44.8.1-44.8.4 (1984).

W. H. Avery, "Methanol from Ocean Thermal Energy," *Johns Hopkins APL Tech. Dig.* **5**, 159-166 (1984).

W. H. Avery, "OTEC Methanol: A New Approach," Chap. 2 in *The Emerging Marine Economy of the Pacific*, C. Gopalakrishnan, ed., Butterworth Pub., Stonehan, Mass. (1984).

W. H. Avery and D. Richards (APL) and W. G. Niemeyer and J. D. Shoemaker (Brown and Root Development Inc.), "OTEC Energy via Methanol Production," in *18th Intersociety Energy Conversion Engineering Conf. Record*, pp. 346-354 (1983).

A. E. Baitis, T. A. Applebee, and T. M. McNamara, "Human Factors Considerations Applied to Operations of the FFG-8 and Lamps Mk III," *Naval Eng. J.* **96**, 191-199 (1984).

C. B. Bargeron, A. N. Jette, and B. H. Nall, "Electron Current Image Diffraction from Crystal Surfaces at Low Energies," *Johns Hopkins APL Tech. Dig.* **5**, 51-55 (1984).

C. B. Bargeron, B. H. Nall, and A. N. Jette, "Low-Energy Electron Current Image Diffraction (CID) of the Basal Plane of Titanium," *Surf. Sci.* **139**, 219-230 (1984).

D. A. Batchelor, *Energetic Electrons in Impulsive Solar Flares*, NASA TM 86102 (1984).

D. A. Batchelor (APL), A. O. Benz (ETH, Zurich), and H. J. Wiehl (Univ. Bern), "Decimetric Gyrosynchrotron Emission during a Solar Flare," *Astrophys. J.* **280**, 879-883 (1984).

W. G. Bath and F. R. Castella, "Detection Performance of a Noncoherent MTI," in *Proc. IEEE National Radar Conf.*, pp. 74-78 (1984).

W. G. Bath, E. W. David, and J. T. Miller, "Development and Testing of the Gridlock Demonstration System," in *Record, 30th Tri-Service Radar Symp.*, Environmental Research Inst. of Michigan, pp. 1-10 (1984).

R. C. Beal, "Spectrasat: A Concept for the Collection of Global Directional Wave Spectra," in *Proc. URSI Commission F Symp. and Workshop, Frontiers of Remote Sensing of the Oceans and Troposphere from Air and Space Platforms*, NASA Conf. Pub. 2303, pp. 19-28 (1984).

R. C. Beal, T. W. Gerling, and D. E. Irvine, "The Potential of SAR Directional Spectra in Operational Wave Forecasting," in *Proc. 1983 International Geoscience and Remote Sensing Symp.*, pp. 3.1-3.6 (1983).

P. M. Bischoff and S. D. Wajer (Wilmer Ophthalmological Inst.), and R. W. Flower (APL), "Scanning Electron Microscopic Studies of the Hyaloid Vascular System in Newborn Mice Exposed to O_2 and CO_2," *Graefe's Arch. Clin. Exp. Ophthalmol.* **220**, 257-263 (1983).

H. D. Black and A. Eisner, "Correcting Satellite Doppler Data for Tropospheric Effects," *J. Geophys. Res.* **89**, 2616-2626 (1984).

B. I. Blum, "Bits, Bytes, Words, and Numbers," *M.D. Comput.* **1**(2), 59-64 (1984).

B. I. Blum, "Designing Systems to Facilitate Maintenance," *Conference Notebook, 2nd National Conf. on EDP Software Maintenance*, DPMA (1984).

B. I. Blum, "A Computer Glossary," *Johns Hopkins APL Tech. Dig.* **5**, 218-224 (1984).

B. I. Blum, "A Dynamic, Nonlinear Document," *MUMPS Users' Group Q.* **14**, 80-87 (1984).

B. I. Blum, "A Framework for Medical Information Science," in *ACM SIGCSE Bull.* **16**, pp. 207-210 (1984).

B. I. Blum, "An Integrated Data Base for Patient Care," in *Proc. AAMSI Congress-84*, pp. 417-422 (1984).

B. I. Blum, "Information Systems for Patient Care," in *Information Systems for Patient Care*, B. I. Blum, ed., Springer-Verlag, New York, pp. 3-19 (1984).

B. I. Blum, "Models and Languages for a Specific Application Class," in *Proc. International Workshop on Models and Languages for Software Specification and Design*, pp. 68-69 (1984).

B. I. Blum, "Three Paradigms for Developing Information Systems," In *Proc. International Conf. on Software Engineering*, pp. 534-543 (1984).

B. I. Blum, "Understanding Computer Basics," *M.D. Comput.* **1**(1), 59-65 (1984).

B. I. Blum, "Understanding the Software Paradox," in *Proc. 23rd Annual Technical Symp.*, Washington, D.C. Chapter ACM (1984).

B. I. Blum, "A Workstation for Information Systems Development," in *Proc. IEEE Computer Soc. International Computer and Applications Conf.*, pp. 116-120 (1983).

B. I. Blum (APL) and E. E. McColligan (JHMI), "Evaluation of Ambulatory Care Systems," in *Proc. AAMSI Congress-84*, pp. 15-17 (1984).

B. I. Blum (APL) and R. E. Miller and R. E. Lenhard, Jr. (JHMI), "Distributed Laboratory Data Processing in a Large Hospital: The Johns Hopkins Experience," in *Computerization and Automation, 1, Informatics in Health Facilities*, M. Rubin, ed., CRC Press, Boca Raton, Fla., pp. 47-57 (1984).

S. Bockstahler-Brandt and L. Kassoff, "Evolution of an Historical Oceanographic Data Base," in *Proc. Digital Equipment Computer User's Soc. Symp.*, pp. 35-37 (1984).

J. Bohandy, B. F. Kim, and F. J. Adrian, "Magnetophotoselective Photolysis of the Formyl Radical in Fused Silica," *Chem. Phys. Lett.* **104**, 413-417 (1984).

W. Börsch-Supan (Johannes Gutenberg-Universität) and L. W. Hunter and J. R. Kuttler (APL), "Endothermic Gasification of a Solid by Thermal Radiation Absorbed in Depth," *Int. J. Heat Mass Transfer* **27**, 1171-1182 (1984).

C. A. Boyles, *Acoustic Waveguides: Applications to Oceanic Science*, John Wiley & Sons, New York (1984).

D. Brocklebank, "APL—The Language," *Johns Hopkins APL Tech. Dig.* **5**, 280-283 (1984).

W. E. Buchanan, "Microcomputers and the Handicapped—Extensions of the Johns Hopkins Search," *Johns Hopkins APL Tech. Dig.* **5**, 261-265 (1984).

D. T. Burton (APL) and J. F. Garey (Marine Biocontrol Corp.), "Macrofouling in Power Plant Service Water Systems," *Trans. Am. Nucl. Soc.* **46**, 698-699 (1984).

D. T. Burton, L. W. Hall, Jr., R. J. Klauda, and S. L. Margrey, "Effects of Treated Bleached Kraft Mill Effluent on Eggs and Prolarvae of Striped Bass (*Morone saxatilis*)," *Water Resour. Bull.* **19**, 869-879 (1983).

D. T. Burton, L. B. Richardson, and R. J. Taylor, "Control of Colonial Hydroid Macrofouling by Free-Field Ultrasonic Radiation," *Science* **223**, 1410-1411 (1984).

P. F. Bythrow, T. A. Potemra, and L. J. Zanetti, "Variation of the Auroral Birkeland Current Pattern Associated with the North-South Component of the IMF," in *Magnetospheric Currents*, T. A. Potemra, ed., *Geophys. Monogr. Am. Geophys. Union* **28**, pp. 131-136 (1984).

M. Candidi (National Research Council, Italy) and C.-I. Meng (APL), "Nearly Simultaneous Observations of the Conjugate Polar Cusp Regions," *Planet. Space Sci.* **32**, 41-46 (1984).

F. R. Castella and R. E. Thurber, "Experimental Results for a Coherent Radar Digital Data Collector," in *Proc. International Conf. on Radar*, pp. 455-460 (1984).

J. F. Carbary and S. M. Krimigis (APL) and W.-H. Ip (Max-Planck Inst. Aeronomie), "Energetic Particle Microsignatures of Saturn's Satellites," *J. Geophys. Res.* **88**, 8947-8958 (1983).

J. F. Carbary, B. H. Mauk, and S. M. Krimigis, "Corotation Anisotropies in Saturn's Magnetosphere," *J. Geophys. Res.* **88**, 8937-8946 (1983).

J. R. Champion, "Enhancing Word Processing Productivity with an Optical Character Reader," *Top. Health Rec. Manage.* **4**, 47 (1983).

H. K. Charles, Jr., and G. V. Clatterbaugh, "Ball Bond Shearing—A Complement to the Wire Bond Pull Test," *Int. J. Hybrid Microelectron.* **6**, 171 (1983).

H. K. Charles, Jr., and G. D. Wagner, "The Application of Ceramic Chip Carriers in High Reliability Environments," in *Proc. 3rd International Microelectronics Conf.* (1984).

H. K. Charles, Jr., and G. D. Wagner, "Verification of Hybrid Wire Bonds: Ball Shear versus the Traditional Pull Test," in *Proc. 3rd International Microelectronics Conf.* (1984).

H. K. Charles, Jr., and J. A. Weiner, "Capacitor End Cap Testing and Analysis," in *Proc. 1984 Capacitor and Resistor Technology Symp.* (1984).

H. K. Charles, Jr., J. A. Weiner, R. C. Benson, and E. S. Dettmer, "Residual Gas and Surface Analytical Techniques for Epoxy Characterization," in *Proc. 1984 International Reliability Physics Symp.* (1984).

A. F. Cheng, "Adiabatic Theory in Rapidly Rotating Magnetospheres," *J. Geophys. Res.* **89**, 5453-5459 (1984).

A. F. Cheng, "Escape of Sulfur and Oxygen from Io," *J. Geophys. Res.* **89**, 3939-3944 (1984).

A. F. Cheng, "The Millisecond Pulsar," *Ann. N.Y. Acad. Sci.* **422**, 182-185 (1984).

A. F. Cheng (APL), C. G. Lanzerotti (Bell Labs.), M. T. Paonessa (APL), and T. P. Armstrong (Univ. Kansas), "Longitudinal Asymmetry in the Io Plasma Torus," *Eos*, **64**, 795 (1983).

A. F. Cheng and M. T. Paonessa (APL), C. G. Maclennan and L. J. Lanzerotti (Bell Labs.), and T. P. Armstrong (Univ. Kansas), "Longitudinal Asymmetry in the Io Plasma Torus," *J. Geophys. Res.* **89**, 3005-3010 (1984).

W. T. Citrin and K. A. Skrivseth, "New Threat Upgrade Combat System, Overview and Test Results," in *Record, 30th Tri-Service Radar Symp.*, Environmental Research Inst. of Michigan, pp. 89-96 (1984).

G. V. Clatterbaugh, J. A. Weiner, and H. K. Charles, Jr., "Gold-Aluminum Intermetallics: Ball Bond Shear Testing and Thin Film Reaction Couples," in *Proc. 34th Electronic Components Conf.* (1984).

R. J. Costlow, "Frequency (Standard) Combines Selector," in *Proc. 37th Annual Frequency Control Symp.* (1983).

A. J. Cote, Jr., "Speech Images on the IBM PC," *Byte* **8**, 402-407 (1983).

S. F. Czajkowski and J. S. J. Peri, "Strategic Communications Network Performance Evaluation Model," *Johns Hopkins APL Tech. Dig.* **5**, 22-27 (1984).

R. B. Decker, "Formation of Shock-Spike Events at Quasi-Perpendicular Shocks, *J. Geophys. Res.* **88**, 9959-9973 (1983).

R. B. Decker and S. M. Krimigis (APL) and D. Venkatesan (Univ. Calgary), "Estimate of Cosmic-Ray Latitudinal Gradient in 1981-1982," *Astrophys. J.* **278**, L119-L122 (1984).

R. B. Decker (APL), L. Vlahos (Univ. Maryland), and A. T. Y. Lui (APL), "Predictions of Lithium Interactions with Earth's Bow Shock in the Presence of Wave Activity," *J. Geophys. Res.* **89**, 7331-7337 (1984).

C. de Jager and A. Boelee (Lab. Space Research, Utrecht) and D. M. Rust (APL), "Spatial Development of X-Ray Emission during the Impulsive Phase of a Solar Flare," *Solar Phys.* **92**, 245-258 (1984).

O. J. Deters, F. F. Mark, and C. B. Bargeron (APL), G. M. Hutchins (JHMI), and M. H. Friedman (APL), "Comparison of Steady and Pulsatile Flow near the Ventral and Dorsal Walls of Casts of Human Aortic Bifurcations," *J. Biomech. Eng.* **106**, 79-82 (1984).

O. J. Deters and F. F. Mark (APL), G. M. Hutchins (JHMI), and C. B. Bargeron and M. H. Friedman (APL), "Secondary Flows in Aortic Bifurcations," in *Proc. 36th Annual Conf. on Engineering in Medicine and Biology*, p. 191 (1983).

E. S. Dettmer, H. K. Charles, Jr., R. C. Benson, B. H. Nall, F. G. Satkiewicz, C. B. Bargeron, and T. E. Phillips, "Epoxy Characterization and Testing Using Mechanical, Electrical, and Surface Analysis Techniques," *Int. J. Hybrid Microelectron.* **6**, 375-386 (1983).

E. B. Dodson and D. E. Irvine, "Investigation of Gulf Stream Ring Detection with Spaceborne Altimeter Using Mean Sea Height, Wave Height, and Radar Cross Section," in *Proc. International Geoscience and Remote Sensing Symp.*, p. TA-3 (1983).

D. D. Duncan and D. E. Larch, "Lateral Coherence of Aerosol-Scattered Laser Radiation," *Opt. Lett.* **9**, 1-3 (1984).

G. L. Dugger, L. L. Perini, D. Richards, and F. C. Paddison, "The Potential for a Hybrid Geothermal-Ocean Thermal Energy Conversion (GEOTEC) Power Plant Installation at Adak Island, Alaska," in *18th Intersociety Energy Conversion Engineering Conf. Record*, pp. 355-363 (1983).

L. W. Ehrlich, "The Ad-Hoc SOR Method: A Local Relaxation Scheme," in *Elliptic Problem Solvers* **II**, Academic Press, New York, pp. 257-269 (1984).

T. J. Emge and D. O. Cowan (JHU), A. N. Bloch (Exxon), and T. J. Kistenmacher (APL), "On the Crystal Structure of the Organic Charge-Transfer Salt Derived from Hexamethylenetetraselenafulvalene (HMTSF) and Tetrafluoro-7, 7, 8, 8-Tetracyano-p-Quinodimethane ($TCNQF_4$), HMTSF-$TCNQF_4$," *Mol. Cryst. Liq. Cryst.* **95**, 191-207 (1983).

M. J. Engebretson (Augsburg College), L. J. Cahill, Jr. (Univ. Minnesota), T. A. Potemra and L. J. Zanetti (APL), R. L. Arnoldy (Univ. New Hampshire), S. B. Mende (Lockheed), and T. J. Rosenberg (Univ. Maryland), "On the Relationship between Morning Sector Irregular Magnetic Pulsations and Field Aligned Currents," *J. Geophys. Res.* **89**, 1602-1612 (1984).

J. A. Fave (EA Eng., Sci., & Tech.) and D. T. Burton (APL), "Toxicity of Chlorine to Aquatic Life and Its Impact on the Environment," in *Proc. 1984 Water Pollution Control Federation Conf., Wastewater Disinfection—The Pros and Cons,* pp. 1-24 (1984).

R. E. Fischell, W. E. Radford, A. F. Hogrefe, C. A. Blackburn, and K. H. Sanders (APL), C. D. Saudek (JHMI), W. G. Webster, W. G. Swift, and W. B. Mayfield (Parker-Hannifin Corp.), and P. Lord (Pacesetter Systems, Inc.), "A Programmable Implantable Medication System (PIMS) for the Treatment of Diabetes," in *Proc. 4th Congress, International Soc. for Artificial Organs* (1984).

R. E. Fischell and W. E. Radford (APL) and C. D. Saudek (JHH), "Programmable Implantable Medication System: Application to Diabetes," *Med. Electron.* **14** (6), 114-119 (1983).

R. W. Flower, "A Mechanism for Oxygen Damage to the Immature Retinal Vasculature," in *Oxygen Transport to Tissue* V, D. W. Lubbers et al., eds., Plenum Pub., pp. 671-687 (1984).

R. W. Flower, "Indomethacin and Retrolental Fibroplasia," *J. Pediatr.* **104**, 326 (1984).

R. W. Flower (APL) and D. S. McLeod, S. D. Wajer, G. S. Sendi, P. G. Egner, and N. H. Dubin (JHMI), "Prostaglandins as Mediators of Vasotonia in the Immature Retina," *Pediatrics* **73**, 440-444 (1984).

S. N. Foner and R. L. Hudson, "Energy Transfer and Catalytic Decomposition of Ammonia on Rhenium at High Temperatures," *J. Chem. Phys.* **80**, 4013-4019 (1984).

S. N. Foner and R. L. Hudson, "On Energy Transfer and Catalytic Reaction of 1-Butene on Platinum," *J. Chem. Phys.* **80**, 503-507 (1984).

S. N. Foner and R. L. Hudson, "Suprathermal Vibrational Excitation of Hydrogen Molecules by Heated Rhenium," *Chem. Phys. Lett.* **104**, 504-509 (1984).

S. N. Foner and R. L. Hudson, "Vibrationally Excited Nitrogen Molecules Formed in the Catalytic Decomposition of Ammonia on Platinum," *J. Chem. Phys.* **80**, 518-523 (1984).

D. W. Fox and J. R. Kuttler, "Sloshing Frequencies," *J. Appl. Math. Phys. (ZAMP)* **34**, 668-696 (1983).

J. D. Franson and K. A. Potocki, "An Experimental Test of the Quantum Theory," *Johns Hopkins APL Tech. Dig.* **5**, 305-308 (1984).

R. K. Frazer, "Rain Erosion Tests of Full-Size Slip Cast Fused Silica Radomes at M3.5 and M4.8," in *Proc. 17th Symp. on Electromagnetic Windows,* H. L. Bassett, ed., pp. 215-219 (1984).

M. H. Friedman, O. J. Deters, F. F. Mark, and C. B. Bargeron, "Geometric Effects on the Hemodynamic Environment of the Arterial Wall: A Basis for Geometric Risk Factors?" in *Proc. 1982 Heidelberg Meeting on Fluid Dynamics as a Localizing Factor in Atherogenesis,* Springer-Verlag, Heidelberg, pp. 71-78 (1983).

M. H. Friedman and L. W. Ehrlich, "Estimation of Wall Shear in Aortic Bifurcations from Fluid Dynamic Computations," in *Proc. 4th International Conf. on Mechanics in Medicine and Biology,* pp. 119-122 (1984).

A. D. Goldfinger, R. C. Beal, F. M. Monaldo, and D. G. Tilley, "Tracking Ocean Wave Spectrum from SAR Images," in *Proc. URSI Commission F Symp. and Workshop, Frontiers of Remote Sensing of the Oceans and Troposphere from Air and Space Platforms,* NASA Conf. Pub. 2303, pp. 159-168 (1984).

J. Goldhirsh, "Comparison of Simultaneous Radiometer and Radar Derived Slant Path Attenuation Statistics at 28.56 GHz," in *Proc. Joint Meeting of the IEEE Geoscience and Remote Sensing Society and URSI/USNC Commission F,* p. 15 (1983).

J. Goldhirsh, "Radar Modeling of Space Diversity Associated with Slant Path Rain Attenuation at Variable Frequencies, Path Angles, and Drop Size Distributions," *Synopses of Papers Submitted for Presentation at International URSI Commission F. Symp.,* pp. 437-455 (1983).

J. Goldhirsh, "Rain Cell Size Statistics as a Function of Rain Rate for Attenuation Modeling," *IEEE Trans. Antennas Propag.* **AP-31**, 799-801 (1983).

J. Goldhirsh, "Slant Path Rain Attenuation and Path Diversity Statistics Obtained through Radar Modeling of Rain Structure," *IEEE Trans. Antennas Propag.* **AP-32**, 54-60 (1984).

J. Goldhirsh, "Yearly Variations of Rain-Rate Statistics at Wallops Island and Their Impact on Modeled Slant Path Attenuation Distributions," *IEEE Trans. Antennas Propag.* **AP-31**, 918-921 (1983).

J. Goldhirsh and F. Monaldo, "Altimeter Height Measurement Errors Introduced by the Presence of Variable Cloud and Rain Attenuation," in *Proc. URSI Commission F Symp. and Workshop, Frontiers of Remote Sensing of the Oceans and Troposphere from Air and Space Platforms,* NASA Conf. Pub. 2303, pp. 287-296 (1984).

J. Goldhirsh and F. Monaldo, "Improved Resolution Rain Measurements from Spaceborne Radar Altimeters," in *Proc. URSI Commission F. Symp. and Workshop, Frontiers of Remote Sensing of the Oceans and Troposphere from Air and Space Platforms,* NASA Conf. Pub. 2303, pp. 297-306 (1984).

W. L. Goodfellow, Jr., and D. T. Burton (APL) and K. E. Cooper (Rutgers Univ.), "Effect of Picric and Picramic Acids on Growth of Rainbow Trout (*Salmo gairdneri*) and American Oysters (*Crassostrea virginica*)," *Chemosphere* **12**, 1259-1268 (1983).

S. H. Gordon, W. J. Graham, D. Hudson, and J. A. Mazie, "Laser Radar for Shipboard Point Defense," in *Proc. Meeting of the IRIS Specialty Group on Active Systems,* Environmental Research Inst. of Michigan 165000-9-X, pp. 341-364 (1984).

E. P. Gray, R. W. Hart, and R. A. Farrell, "The Structure of the Internal Wave Mach Front Generated by a Point Source Moving in a Stratified Fluid," *Phys. Fluids* **26**, 2919-2931 (1983).

M. E. Greenspan, "Effects of Oblique Double Layers on Upgoing Ion Pitch Angle and Gyrophase," *J. Geophys. Res.* **89**, 2842-2848 (1984).

R. A. Greenwald and K. B. Baker (APL) and J. P. Villain (Univ. Toulon), "Initial Studies of Small-Scale F Region Irregularities at Very High Latitudes," *Radio Sci.* **18**, 1122-1132 (1983).

M. D. Griffin, "Calculation of Inviscid Air Capture and Additive Drag for 3-D Supersonic Inlet Flows," in *Computational Methods for Ramjets, 1983 JPM Specialist Session,* pp. 41-50 (1983).

M. D. Griffin, F. S. Billig, and M. E. White, "Applications of Computational Techniques in the Design of Ramjet Engines," in *Proc. 16th International Aeronautics Congress, 6th International Symp. on Air Breathing Engines,* pp. 215-228 (1983).

M. D. Griffin, T. E. Strikwerda, and D. G. Grant, "The Space Telescope Alternate Fine Guidance Sensor," in *Proc. AIAA Guidance and Control Conf.,* pp. 143-153 (1984).

R. R. Guenther and N. K. Brown, "A Player Support System for an Interactive Theater-Level War Game," *Johns Hopkins APL Tech. Dig.* **5**, 19-21 (1984).

T. C. Guo, and W. W. Guo, "A Transient-State Theory of Dielectric Relaxation and the Curie-von Schweidler Law," *J. Phys. C: Solid State Phys.* **16**, 1955-1960 (1983).

T. C. Guo and W. W. Guo, "A Transient-State Theory of Dielectric Relaxation and a Proposal for an Experimental Verification of the Distributions of Relaxation Times," *Dielectrics Soc. 1983 Meeting on the Physics of Dielectric Solids* (1983).

T. C. Guo and W. W. Guo (APL) and L. E. Larsen (Walter Reed Inst. Research) "Medical Microwave Imagery: An In-

verse Scattering Approach," in *Proc. 8th International Symp. on Infrared and Millimeter Waves*, IEEE Pub. 83CH1917-4 (1983).

T. C. Guo and W. W. Guo (APL) and L. E. Larsen (Walter Reed Inst. Research), "Comment on 'Microwave Diffraction Tomography for Biomedical Applications'," *IEEE Trans. Microwave Theory Tech.* **32**, 473-474 (1984).

T. C. Guo and W. W. Guo (APL) and L. E. Larsen and J. H. Jacobi (Walter Reed Inst. Research), "An After-Field Effect of the Distribution of Relaxation Times and a Transient-State Theory of Dielectric Relaxations," in *Proc. 1st International Conf. on Conduction and Breakdown in Solid Dielectrics*, p. 448 (1983).

C. Gurgiolo (Southwest Res. Inst.), G. K. Parks (Univ. Washington), and B. H. Mauk (APL), "Upstream Gyrophase Bunched Ions: A Mechanism for Creation at the Bow Shock and the Growth of Velocity Space Structure through Gyrophase Mixing," *J. Geophys. Res.* **88**, 9093 (1983).

L. W. Hall, Jr., D. T. Burton, W. C. Graves, and S. L. Margrey, "Avoidance Responses of Estuarine Fish Exposed to Heated-Dechlorinated Power Plant Effluents," *Environ. Sci. Tech.* **18**, 561-566 (1984).

L. W. Hall, Jr., D. T. Burton, W. C. Graves, and S. L. Margrey, "Behavioral Modification of Estuarine Fish Exposed to Sulfur Dioxide," *J. Toxicol. Environ. Health* **13**, 969-978 (1984).

L. W. Hall, Jr., S. L. Margrey, D. T. Burton, and W. C. Graves, "Avoidance Behavior of Juvenile Striped Bass, *Morone saxatilis*, Subjected to Simultaneous Chlorine and Elevated Temperature Conditions," *Arch. Environ. Contam. Toxicol.* **12**, 715-720 (1983).

L. W. Hall, Jr., and A. E. Pinkney (APL), S. Zeger (JHU), and D. T. Burton and M. J. Lenkevich (APL), "Behavioral Responses of Two Estuarine Fish Species Subjected to bis (tri-n-Butyltin) Oxide," *Water Resour. Bull.* **20**, 235-239 (1984).

G. D. Halushynsky and J. K. Beam, "A Concept for Navy Command and Control in the Year 2000," *Johns Hopkins APL Tech. Dig.* **5**, 9-18 (1984).

B. W. Hamill, "Visual Perception of Structured Symbols," *Johns Hopkins APL Tech. Dig.* **5**, 167-171 (1984).

R. F. Henrick (APL) and J. R. Brannan, D. B. Warner, and G. P.Forney (Clemson Univ.), "The Uniform WKB Modal Approach to Pulsed and Broadband Propagation," *J. Acoust. Soc. Am.* **74**, 1464-1473 (1983).

R. E. Hicks, H. K. Charles, Jr., G. D. Wagner, and B. M. Romenesko, "Trends in Medical Electronics Using Surface Mounted Components and Hybrids," *Int. J. Hybrid Microelectron.* **6**, 283-289 (1983); also *Solid State Technol.* **26** (12), 145-150 (1983).

M. L. Hill, "A Closed Course Distance Record for Powered Radio-Controlled Aeromodels," *Johns Hopkins APL Tech. Dig.* **5**, 172-183 (1984).

M. L. Hill, "Fabrication Methods: Autopilots and Guidance Techniques," *Unmanned Syst.* **2**, 20-24 (1984).

L. W. Hirst, C. Aner, H. Abbey, and J. Cohn (JHMI) and H. Kues (APL), "Quantitative Analysis of Wide-Field Endothelial Specular Photomicrographs," *Am. J. Ophthalmol.* **97**, 488-495 (1984).

B. B. Holland, "The AMPTE Charge Composition Explorer Science Data Center," *Johns Hopkins APL Tech. Dig.* **5**, 274-276 (1984).

E. D. Holm and E. E. Westerfield, "A GPS Fast Acquisition Receiver," in *NTC '83—IEEE National Telesystems Conf. Record*, pp. 214-218 (1983).

R. H. Holzworth (Univ. California) and C.-I. Meng (APL), "Polar Cap Motions with Varying Interplanetary Magnetic Field," *Planet. Space Sci.* **32**, 25-29 (1984).

R. E. Huffman (Air Force Geophysics Lab.) and C.-I. Meng (APL), "Ultraviolet Imaging of Sunlit Auroras from HILAT," *Johns Hopkins APL Tech. Dig.* **5**, 138-142 (1984).

L. W. Hunter and J. R. Kuttler, "Cooling of a Slab with Thermal Contraction and Progressive Loss of Contact with a Cold Surface," *J. Heat Transfer* **105**, 936-938 (1983).

T. Iijima (Univ. Tokyo) and T. A. Potemra, L. J. Zanetti, and P. F. Bythrow (APL), "Large-Scale Birkeland Currents in the Dayside Polar Region during Strongly Northward IMF: A New Birkeland Current System," *J. Geophys. Res.* **89**, 7441-7452 (1984).

J. O. Jenkins, J. P. Randolph, D. G. Tilley, and C. A. Waters, "The APL Image Processing Laboratory," *Johns Hopkins APL Tech. Dig.* **5**, 59-78 (1984).

R. E. Jenkins, "A Demonstration of the Value of Spacecraft Computers," *Johns Hopkins APL Tech. Dig.* **5**, 225-237 (1984).

A. N. Jette, B. H. Nall, and C. B. Bargeron, "Low Energy Electron Channeling Observed by Current Image Diffraction (CID)," *J. Vac. Sci. Technol.* **2**, 978-982 (1984).

S. C. Jones (APL) and V. J. DiLosa (NASA/Goddard), "Computer Model for a Waveguide Replay Link," in *NTC '83—National Telesystems Conf. Record*, pp. 30-31 (1983).

R. I. Joseph (JHU) and M. E. Thomas and K. R. Allen (APL), "Magnetic Field and Field Gradient Corrections within a Nonconducting Sensor Enclosure in a Conducting Fluid—Part I: Potential Flow," *IEEE Trans. Geosci. Remote Sensing* **GE-21**, 409-416 (1983).

R. I. Joseph (JHU) and M. E. Thomas (APL), "Magnetic Field and Field Gradient Corrections within a Nonconducting Sensor Enclosure in a Conducting Fluid—Part II: Vorticity," *IEEE Trans. Geosci. Remote Sensing* **GE-22**, 159-165 (1984).

Y. Kamide (Kyoto Sangyo Univ.), R. M. Robinson (SRI International), S.-I. Akasofu (Univ. Alaska), and T. A. Potemra (APL), "Aurora and Electrojet Configuration in the Early Morning Sector," *J. Geophys. Res.* **89**, 389-393 (1984).

W. C. Keller (NRL) and B. L. Gotwols (APL), "Two-Dimensional Optical Measurement of Wave Slope," *Appl. Opt.* **22**, 3476-3478 (1983).

T. J. Kistenmacher, "Anion Size and the Structural Properties of $(TMTSF)_2X$ Salts: Intracolumnar Effects," *Solid State Commun.* **51**, 275-279 (1984).

T. J. Kistenmacher, "Cavity Size versus Anion Size in $(TMTSF)_2X$ Salts: Possible Implications for the Uniqueness of $(TMTSF)_2ClO_4$," *Solid State Commun.* **50**, 729-733 (1984).

H. W. Ko, J. W. Sari, M. E. Thomas, P. J. Herchenroeder, and P. J. Martone, "Anomalous Propagation and Radar Coverage through Inhomogeneous Atmospheres," in *AGARD Conf. Proc.* No. CP-346, pp. 25-1 to 25-14 (1984).

S. Koslov, "Bridging the Gap," in *Nonlinear Electrodynamics in Biological Systems*, W. R. Adey and A. F. Lawrence, eds., Plenum Pub. Co., New York, pp. 585-598 (1984).

A. Kossiakoff, P. L. Hazan, and M. V. Panyan, "Microcomputer-Based Individually Managed Instruction for the Handicapped," *Johns Hopkins APL Tech. Dig.* **5**, 245-260 (1984).

S. M. Krimigis, J. F. Carbary, and E. P. Keath (APL), T. P. Armstrong (Univ. Kansas), L. J. Lanzerotti (Bell Labs.), and G. Gloeckler (Univ. Maryland), "General Characteristics of Hot Plasma and Energetic Particles in the Saturnian Magnetosphere: Results from the Voyager Spacecraft," *J. Geophys. Res.* **88**, 8871-8892 (1983).

J. R. Kuttler, "A New Method for Calculating TE and TM Cutoff Frequencies of Uniform Waveguides with Lunar or Eccentric Annular Cross Section," *IEEE Trans. Microwave Theory Tech.* **32**, 348-354 (1984).

J. R. Kuttler and V. G. Sigillito, "Eigenvalues of the Laplacian in Two Dimensions," *SIAM Rev.* **26**, 163-193 (1984).

J. R. Kuttler and V. G. Sigillito, "Sloshing of Liquids in Cylindrical Tanks," *Am. Inst. Aeronaut. Astronaut.* **22**, 309-311 (1984).

L. J. Lanzerotti (Bell Labs.), R. E. Gold (APL), K. A. Anderson (Univ. California, Berkeley), T. P. Armstrong (Univ. Kansas), S. M. Krimigis (APL), R. P. Lin (Univ. California, Berkeley), M. Pick (Observatoire de Paris), E. C. Roelof (APL), E. T. Sarris (Univ. Thrace), G. M. Simnett (Univ. Birmingham, England), and W. E. Frain (APL), "The ISPM Experiment for Spectral, Composition, and Anisotropy Measurements of Charged Particles at Low Energies," in *The International Solar Polar Mission—Its Scientific Investigations*, European Space Agency Special Pub. SP-1050, K. P. Wenzel et al., eds., pp. 141-153 (1983).

L. J. Lanzerotti and C. G. Maclennan (Bell Labs.), R. P. Lepping (NASA/Goddard), and S. M. Krimigis (APL), "On the Plasma Conditions at the Dayside Magnetopause of Saturn," *Geophys. Res. Lett.* **10**, 1200-1202 (1983).

W. D. Larkin and J. P. Reilly, "Strength/Duration Relationships for Electrocutaneous Sensitivity: Stimulation of Capacitive Discharges," *Percept. Psychophys.* **36**, 68-78 (1984).

R. E. Lenhard, Jr. (JHMI) and B. I. Blum (APL), "Practical Applications of OCIS, A Clinical Information System for Oncology," *Comput. Biol. Med.* **14**, 15-23 (1984).

R. E. Lenhard, Jr. (JHMI), B. I. Blum (APL), and E. E. McColligan (JHMI), "An Information System for Oncology," in *Information Systems for Patient Care*, B. I. Blum, ed., Springer-Verlag, New York, pp. 385-403 (1984).

C. S. Lin (Southwest Research Inst.) and C.-I. Meng (APL), "Observations of a Quiet-Time Pc5 Wave in the Outer Magnetosphere," *Planet. Space Sci.* **32**, 551-559 (1984).

J. S. Lombardo, "A Paravane System for Compensation of Distortions in Towed Arrays," in *Proc. 16th IEEE Electronics and Aerospace Conf.*, pp. 223-226 (1983).

A. T. Y. Lui, "Characteristics of the Cross Tail Current in the Earth's Magnetotail," in *Magnetospheric Currents*, T. A. Potemra, ed., *Geophys. Monogr. Am. Geophys. Union* **28**, p. 158 (1984).

A. T. Y. Lui, T. A. Potemra, and D. J. Williams (APL), T. E. Eastman and L. A. Frank (Univ. Iowa), and S.-I. Akasofu (Univ. Alaska), "Streaming Reversal of Energetic Particles in the Magnetotail during a Substorm," *J. Geophys. Res.* **89**, 1540-1552 (1984).

L. R. Lyons (NOAA) and D. J. Williams (APL), *Quantitative Aspects of Magnetospheric Physics*, D. Reidel Pub. Co., Dordrecht, Holland (1984).

J. L. MacArthur and P. V. K. Brown, "Altimeter for the Ocean Topgraphy Experiment (TOPEX)," in *Proc. SPIE: Recent Advances in Civil Space Remote Sensing*, H. W. Yates, ed., pp. 172-180 (1984).

C. G. Maclennan and L. J. Lanzerotti (Bell Labs.), S. M. Krimigis (APL), and R. P. Lepping (NASA/Goddard), "Low-Energy Particles at the Bow Shock, Magnetopause, and Outer Magnetosphere of Saturn," *J. Geophys. Res.* **88**, 8817-8830 (1983).

K. Makita and C.-I. Meng, "Average Electron Precipitation Patterns and Visual Aurora Characteristics during Geomagnetic Quiescence," *J. Geophys. Res.* **89**, 2861-2872 (1984).

E. E. Mark, O. J. Deters, and M. H. Friedman, "Quasisteadiness of Flow in a Human Coronary Model," in *Mechanics of the Coronary Circulation*, R. E. Mates et al., eds., ASME, pp. 71-74 (1983).

J. K. Markham, "Computer Graphics in the F. T. McClure Computing Center," *Johns Hopkins APL Tech. Dig.* **5**, 286-289 (1984).

W. T. Maughan (JHMI), R. F. Jenkins and W. T. Ebert (APL), and A. Ciuffo, A. A. Shoukas, and K. Sagawa (JHMI), "Multiple Marker Cineventriculogrammetry: A New Technique for Simultaneous Measurement of Regional Wall Motion and Overall Geometry in Animals," in *Ventricular Wall Motion*, U. Sigwart and P. H. Heintzen, eds., Georg Thieme Verlag, Stuttgart, pp. 14-23 (1984).

B. H. Mauk, Review of *Magnetospheric Plasma Physics*, A. Nishida, ed., *Eos* **64**, 617 (1983).

R. H. Maurer, "Dual-in-Line Package Mounting for Space Applications," in *Proc. 34th IEEE Electronic Components Conf.*, pp. 498-510 (1984).

B. H. Mauk and C.-I. Meng, "Dynamical Injections as the Source of Near Geostationary Quiet Time Particle Spatial Boundaries," *J. Geophys. Res.* **88**, 10,011-10,024 (1983).

R. H. Maurer and O. M. Uy, "Dual-in-Line-Package Mounting for Space Applications," in *Proc. 34th Electronic Components Conf.*, IEEE, pp. 498-510 (1984).

R. L. McCally, "Measurements of Gaussian Beam Parameters," *Appl. Opt.* **23**, 2227 (1984).

R. L. McCally and C. B. Bargeron (APL), W. R. Green (JHMI), and R. A. Farrell (APL), "Stromal Damage in Rabbit Corneas Exposed to CO_2 Laser Radiation," *Exp. Eye Res.* **37**, 543-550 (1983).

W. McCloskey, "Hard Times Hit the Bay," *Nat. Wildlife* **22**, 7-14 (1984).

L. F. McGoldrick, "Remote Sensing for Oceanography: Past, Present, and Future," in *Proc. URSI Commission F Symp. and Workshop, Frontiers of Remote Sensing of the Oceans and Troposphere from Air and Space Platforms*, NASA Conf. Pub. 2303, pp. 1-10 (1984).

L. F. McGoldrick (APL), P. M. Woiceshyn (JPL), M. G. Wurtele (Univ. California, Los Angeles), D. H. Boggs (dB Systems, Ltd.), and S. Peteherych (AES, Canada), "A New Parameterization of an Empirical Model for Wind/Ocean Scatterometry," in *Proc. URSI Commission F Symp. and Workshop, Frontiers of Remote Sensing of the Oceans and Troposphere from Air and Space Platforms*, NASA Conf. Pub. 2303, pp. 57-74 (1984).

C.-I. Meng, "Dynamic Variation of the Auroral Oval during Intense Magnetic Storms," *J. Geophys. Res.* **89**, 227-235 (1984).

C.-I. Meng (APL) and S.-I. Akasofu (Univ. Alaska), "Electron Precipitation Equatorward of Midday Oval and the Mantle Aurora," *Planet. Space Sci.* **31**, 889-899 (1983).

C.-I. Meng (APL) and R. E. Huffman (Air Force Geophysics Lab.), "Ultraviolet Imaging from Space of the Aurora under Full Sunlight," *Geophys. Res. Lett.* **11**, 315-318 (1984).

E. E. Mengel (APL) and D. W. Stover (Bendix), "Microprocessor for the NR Maser Frequency Standards," in *Proc. 37th Annual Frequency Control Symp.*, pp. 27-31 (1983).

A. Metropoulos (National Hellenic Res. Foundation) and D. M. Silver (APL), "Rotationally Inelastic Collisions of LiH with He: Quasiclassical Dynamics of Atom-Rigid Rotor Trajectories," *J. Chem. Phys.* **81**, 1682-1691 (1984).

R. A. Meyer, J. D. Mandell, and M. H. Friedman, "Changes in Aortic Bifurcation Geometry during a Cardiac Cycle," *J. Biomech.* **17**, 637-638 (1984).

D. G. Mitchell and E. C. Roelof (APL) and S. J. Bame (Los Alamos National Lab.), "Solar Wind Iron Abundance Variations at Speeds >600 km s^{-1}, 1972-1976," *J. Geophys. Res.* **88**, 9059-9068 (1983).

D. G. Mitchell and E. C. Roelof (APL) and S. J. Bame (Los Alamos National Lab.), "Spatial Variation of Iron Abundance in the Solar Wind, 1972-1976," in *Solar Wind Five*, M. Neugebauer, ed., NASA Conf. Pub. 2280, p. 605 (1983).

G. E. Mitzel, "Single Exponential Identification of Degree-2 Polynomial Systems," *IEEE Trans. Autom. Control* **AC-29**, 263-266 (1984).

G. E. Mitzel, P. G. Barnett, B. E. Kuehne, and S. Sommerer, "Wide-Area Correlation and Tracking of Surface Ships Us-

ing Multiple Sensors," *Johns Hopkins APL Tech. Dig.* **5**, 28-36 (1984).

J. B. Moffett and S. J. DeAmicis, "Computer Assisted Editing," in *Proc. Professional Communication Society Conf.*, pp. 35-43 (1983).

J. B. Moffett and S. J. DeAmicis, "System Review: NBI System 3000," *Tech. Commun.* **30**, 42 (1983).

L. Monchick, "Boundary Conditions and Reversibility in Diffusion Controlled Reactions. II. A Three State Model for Steady State Evaporation of a Spherical Drop," *J. Chem Phys.* **81**, 2010-2015 (1984).

L. Monchick , "Generalized Reorientation Cross Sections. II. Scattering Frame Transformations and Propensity Rules," *J. Chem. Phys.* **80**, 4129-4132 (1984).

L. Monchick, "The International Research Conference on Transport Properties and Molecular Forces," *Johns Hopkins APL Tech. Dig.* **5**, 184-187 (1984).

L. K. Moore, "IEEE's Congressional Fellows in Action," *Impact* **8**, 5-6, 14-15 (1984).

J. S. Murphree and C. D. Anger (Univ. Calgary), C.-I. Meng (APL), and S.-I. Akasofu (Univ. Alaska), "Large Scale Auroral Distribution and the Open Field Line Region," *Planet. Space Sci.* **32**, 105-109 (1984).

J. C. Murphy and L. C. Aamodt, "Reflective Photothermal Imaging," *J. Phys. (Paris)* **C6**, 513-517 (1983).

E. Neter (S.U.N.Y. Buffalo), P. L. Altman (FASEB), M. W. Burgan (APL), N. H. Holmgren (N.Y. Botanical Garden), G. Pollock (ACS), and E. M. Zipf (BIOSIS), eds., *CBE Style Manual: A Guide for Authors, Editors, and Publishers in the Biological Sciences*, 5th Ed., Council of Biology Editors, Inc., Bethesda, Md. (1983).

J. W. Newland and H. G. Tornatore, "Navy Command, Control, and Communications—An Introduction," *Johns Hopkins APL Tech. Dig.* **5**, 3-8 (1984).

A. L. Newman, "Self-Injurious Behavior Inhibiting System," *Johns Hopkins APL Tech. Dig.* **5**, 290-295 (1984).

R. R. Newton, *The Moon's Acceleration and Its Physical Origins*, **2**, The Johns Hopkins University Press, Baltimore (1984).

V. O'Brien, "Discussion on 'The Effect of Transverse Curvature of the Drag and Vortex Shedding of Elongated Bluff Bodies at Low Reynolds Number'," *Trans. ASME: J. Fluids Eng.* **105**, 318-319 (1983).

V. O'Brien, "On Exact Unsteady Navier-Stokes Solutions," *Lett. Appl. Eng. Sci.* **22**, 343-346 (1984).

V. O'Brien, "Two Types of Instream Stagnation," *AIAA J.* **22**, 337-339 (1984).

W. L. Oliver, J. C. Foster, J. M. Holt, and G. B. Loriot (MIT), V. B. Wickwar, J. D. Kelly, and O. de la Beaujardiere (SRI International), P. F. Bythrow, C.-I. Meng, and F. J. Rich (APL), and R. E. Huffman (Air Force Geophysics Lab.), "Initial Millstone Hill, Sondrestrom, and HILAT Observations of Thermospheric Temperatures and Frictional Heating," *Geophys. Res. Lett.* **11**, 911-914 (1984).

D. K. Pace, "A Compendium of Principles for Successful Mangement of Computer Simulation Development," in *Proc. 5th Conf., American Soc. for Engineering Management*, pp. 55-59 (1984).

D. K. Pace, "Review of 'The Apocalyptic Premise: Nuclear Arms Debated'," *J. Am. Sci. Affiliation* **36**, 122-123 (1984).

D. K. Pace, "WG Feature: Naval Warfare Working Group A-4," *Phalanx* **17**, 14 (1984).

J. G. Parker, "The Importance of Singlet Delta Oxygen in Cancer Photoradiation Therapy," *Johns Hopkins APL Tech. Dig.* **5**, 48-50 (1984).

K. Peacock, "The Optical Variability of the Ocean from CZCS Imagery," in *Proc. SPIE Ocean Optics VII* **489**, pp. 208-219 (1984).

D. P. Peletier, "The Application of a Distributed Computer Organization to Ocean Research," *Johns Hopkins APL Tech. Dig.* **5**, 270-273 (1984).

V. L. Pisacane, "Satellite Technology Developments in Gravity Research," in *Proc. 34th Congress, International Astronautical Federation* (1983).

H. D. Pixler, "APLnet—A Local Area Computer Network," *Johns Hopkins APL Tech. Dig.* **5**, 284-285 (1984).

T. O. Poehler, R. S. Potember, R. Hoffman, and R. C. Benson, "Optical Phase Transitions in Organo-Metallic Charge-Transfer Complexes," *Mol. Cryst. Liq. Cryst.* **107**, 91-101 (1984).

H. H. Porter, "Recollections on the Development of Radio-Controlled Proximity Fuzes," *Johns Hopkins APL Tech. Dig.* **4**, 296-300 (1983).

R. S. Potember and T. O. Poehler (APL), D. O. Cowan (JHU), and F. L. Carter and P. Brant (NRL), "Reversible Field Induced Switching in Copper and Silver Radical-Ion Salts," in *Molecular Electronic Devices*, F. L. Carter, ed., Marcel Dekker, Inc. New York, pp. 73-85 (1983).

R. S. Potember, R. C. Hoffman, R. C. Benson, and T. O. Poehler, "Erasable Optical Switching in Semiconductor Organic Charge-Transer Complexes," *J. Phys. (Paris)* **44**, C3-1597 to C3-1604 (1983).

T. O. Potemra, "Images of the Aurora," *Johns Hopkins APL Tech. Dig.* **5**, 96-97 (1984).

T. A. Potemra, "Magnetospheric Currents," *Johns Hopkins APL Tech. Dig.* **4**, 276-284 (1983).

T. A. Potemra, P. F. Bythrow, L. J. Zanetti, F. F. Mobley, and W. L. Scheer, "The HILAT Magnetic Field Experiment," *Johns Hopkins APL Tech. Dig.* **5**, 120-124 (1984).

K. A. Potocki, "The HILAT Spacecraft," *Johns Hopkins APL Tech. Dig.* **5**, 104-108 (1984).

W. R. Powell and R. A. Freeman, "A Missile Scheduling Simulation," in *Proc. 1984 Summer Computer Simulation Conf.*, pp. 1026-1028 (1984).

R. J. Prengaman, R. E. Thurber, and W. G. Bath, "A Retrospective Detection Algorithm for Extraction of Weak Targets in Clutter and Interference Environments," in *16th IEEE Electronics and Aerospace Conf.*, pp. 153-157 (1983).

G. R. Preziotti, I. J. Shepperd, and M. D. Sullivan, "A Communications Systems Test and Evaluation Program," *Johns Hopkins APL Tech. Dig.* **5**, 37-40 (1984).

J. S. Quinn and H. L. Cox, "Data Collection and Recording Instrumentation for Command, Control, and Communications," *Johns Hopkins APL Tech. Dig.* **5**, 41-47 (1984).

J. P. Reilly and W. D. Larkin, "Electrocutaneous Stimulation with High Voltage Capacitive Discharges," *IEEE Trans. Biomed. Eng.* **BME-30**, 631-641 (1983).

J. P. Reilly and W. D. Larkin, "Understanding Transient Electric Shock," *Johns Hopkins APL TEch. Dig.* **5**, 296-304 (1984).

R. P. Rich, "F. T. McClure Computing Center Development," *Johns Hopkins APL Tech. Dig.* **5**, 277-279 (1984).

R. M. Robinson (Lockheed), D. S. Evans (NOAA), T. A. Potemra (APL), and J. D. Kelly (SRI International), "Radar and Satellite Measurements of an F-Region Ionization Enhancement in the Post-Noon Sector," *Geophys. Res. Lett.* **11**, 899-902 (1984).

E. C. Roelof, R. B. Decker, and S. M. Krimigis, "Latitudinal and Field-Aligned Cosmic Ray Gradients 2 to 5 AU, Voyagers 1 and 2 and IMP 8," *J. Geophys. Res.* **88**, 9889-9909 (1983).

D. M. Rust, "The Solar Maximum Observatory," *Johns Hopkins APL Tech. Dig.* **5**, 188-196 (1984).

F. W. Schenkel and B. S. Ogorzalek, "The HILAT Vacuum Ultraviolet Auroral Imager," *Johns Hopkins APL Tech. Dig.* **5**, 131-137 (1984).

M. E. Schmid, "Fault Tolerant Computing via Monitors," *Johns Hopkins APL Tech. Dig.* **5**, 238-244 (1984).

W. Schneider, "Communicating in Code," *Creative Comput.* **9**, 222-232 (1983).

J. Schroeder, J. H. Schummers, B. P. Sandford, and W. J. Tropf, "Infrared Cloud Backgrounds," in *Proc. Tri-Service Infrared Backgrounds Symp.*, AFGL-TR-84-0094, pp. 206-215 (1984).

T. P. Sleight, "Computing at APL," *Johns Hopkins APL Tech. Dig.* **5**, 216-217 (1984).

J. H. Smart, "Spatial Variability of Major Frontal Systems in the North Atlantic—Norwegian Sea Area: 1980-81," *J. Phys. Oceanogr.* **14**, 185-192 (1984).

W. E. Snelling and J. E. Penn, "A Fully Pipelined, Bit-Sliced, VLSI Correlator," in *Digital Signal Processing—84*, V. Cappellini and A. G. Constantinides, eds., Elsevier Pub., Amsterdam, pp. 313-320 (1984).

A. Sommer (JHMI), H. A. Kues (APL), and S. A. D'Anna, S. Arkell, A. Robin, and H. A. Quigley (JHMI), "Cross Polarization Photography of the Nerve Fiber Layer," *Arch. Ophthalmol.* **102**, 864-869 (1984).

J. C. Spall (APL) and K. D. Wall (Univ. Virginia), "Asymptotic Distribution Theory for the Kalman Filter State Estimator," *Commun. Stat. Theory Methods* **13**, 1981-2003 (1984).

J. C. Spall, "Validation of State Space Models in Non-Gaussian Systems," in *Proc. American Control Conf.*, pp. 1072-1076 (1984).

W. D. Stanbro and M. J. Lenkevich, "Kinetics and Mechanism of the Decomposition of *N*-Brominated Alanine in Aqueous Solution," *Int. J. Chem. Kinet.* **15**, 1321-1328 (1983).

W. D. Stanbro and M. J. Lenkevich, "Kinetics and Mechanism of the Reaction of Aqueous Sulfite with N-Chloroalanylalanylalanine," *Int. J. Chem. Kinet.* **16**, 251-258 (1984).

W. I. Sternberger, "Temperature-Compensated Thermistor Anemometer," in *Proc. STD Conf. and Workshop*, Marine Technology Soc., pp. 112-115 (1984).

D. F. Sterne, "Applied Research in ADA," *Johns Hopkins APL Tech. Dig.* **5**, 266-269 (1984).

R. I. Stewart, M. G. Diaz, and M. S. Baldwin, "A Multimedia UNIX-Based Work Station," in *Proc. 5th Annual Conf. on Interactive Videodisc in Education and Training*, Soc. for Applied Learning Technology, pp. 17-20 (1983).

K. Strohbehn, M. D. Foust, and G. A. Heyler, "Space Telescope Alternate Fine Guidance Sensor Performance," in *Proc. AIAA Conf.*, pp. 655-665 (1984).

T. D. Taylor and D. A. Hurdis, "Drag Reduction Studies by Compliant Surfaces and Surface-Active Substances," *Johns Hopkins APL Tech. Dig.* **5**, 56-58 (1984).

T. D. Taylor, R. S. Hirsch, and M. M. Nadworny, "Comparison of FFT, Direct Inversion, and Conjugate Gradient Methods for Use in Pseudo-Spectral Methods," *Comput. Fluids* **12**, 1-9 (1984).

R. J. Taylor, L. B. Richardson, and D. T. Burton, "Ultrasonics for Inhibiting Biofouling," in *Proc. Ultrasonics International '83 Conf.*, pp. 352-357, Butterworth, Boston (1983).

J. W. Thomas, E. L. Brickner, E. P. Lee, and J. Phipps, "The AN/SPS-48C Radar Detection Data Converter," in *Record, 30th Tri-Service Radar Symp.*, Environmental Research Inst. of Michigan, pp. 31-40 (1984).

M. E. Thomas, "The Electrical Properties of Seawater at Microwave Frequencies," in *Proc. URSI/IEEE Meeting*, p. 108 (1984).

R. E. Thurber, "Advanced Signal Processing Techniques for the Detection of Surface Targets," *Johns Hopkins APL Tech. Dig.* **4**, 285-295 (1983).

D. G. Tilley, "Fourier Analysis of SAR Speckle for the Polynomial Synthesis of Spectral Corrections Applied to Seasat Oceanic Data," in *Proc. 1983 International Geoscience and Remote Sensing Symp.* **II**, pp. 4.1-4.6 (1983).

S. G. Tolchin, S.A. Kahn, E. S. Bergan, and G. P. Gafke, "A Distributed Hospital Information System," in *Proc. 4th Jerusalem Conf. on Information Technology*, IEEE Computer Soc. Press, Silver Spring, Md., pp. 620-631 (1984).

S. G. Tolchin, E. S. Bergan, M. A. Espenshade, R. S. Grossman, S. A. Kahn, M. J. Schneider, D. F. Sterne, and R. F. Wachter, "Computer Assisted Requirements Specification System (CARS)," in *Proc. 4th Jerusalem Conf. on Information Technology*, IEEE Computer Soc. Press, Silver Spring, Md., pp. 282-290 (1984).

R. Turner and R. E. Lee, "Particle Sizing in a Fuel Rich Air-Breathing Engine Combustor Discharge," in *Proc. 20th JANNAF Combustion Meeting*, CPIA Pub. 383, **1**, p. 17 (1983).

D. Venkatesan (Univ. Calgary) and R. B. Decker and S. M. Krimigis (APL), "Cosmic Ray Intensity Gradients in the Radial Distance 1-13 AU as Determined from a Comparative Study of Observations by Spacecraft Voyagers 1 and 2, and Earth-Orbiting Satellite IMP-8," in *Proc. 18th International Cosmic Ray Conf.*, p. 156 (1984).

D. Venkatesan (Univ. Calgary) and R. B. Decker and S. M. Krimigis (APL), "Radial Gradient of Cosmic Ray Intensity from a Comparative Study of Data from Voyagers 1 and 2 and IMP 8," *J. Geophys. Res.* **89**, 3735-3746 (1984).

J. P. Villain (Univ. Toulon), R. A. Greenwald (APL), and J. F. Vickrey (SRI International), "HF Ray Tracing at High Latitudes Using Measured Meridional Electron Density Distributions," *Radio Sci.* **19**, 359-374 (1984).

L. L. Warnke and E. E. Westerfield, "Use of GPS for Determining Position of Drifting Buoys," in *NTC '83—IEEE National Telesystems Conf. Record*, pp. 209-213 (1983).

D. J. Webb and S. M. Bhagat (Univ. Maryland) and K. M. Moorjani, T. O. Poehler, and F. G. Satkiewicz (APL), "Magnetic Resonance in Amorphous Fe_xB_{100-x} Sputtered Films," *IEEE Trans. Magn.* **MAG-19**, 1892-1894 (1983).

D. J. Webb and S. M. Bhagat (Univ. Maryland) and K. Moorjani, F. G. Satkiewicz, T. O. Poehler, and M. A. Manheimer (APL), "Study of Magnetic Regimes in a-Fe_xB_{100-x} by DC Magnetization Measurements," *J. Non-Cryst. Solids* **61/62**, 1377-1382 (1984).

L. B. Weckesser, "Some Observations about Radome Boresight Error Performance," in *Proc. Workshop on EM Windows and Domes*, U.S. Army Missile Command (1983).

J. A. Weiner, H. K. Charles, Jr., and B. M. Romenesko, "Thickness Measurement in Microelectronic Fabrication by Beta-Backscatter, *Hybrid Circuit Tech.* **1**, 45 (1984).

J. A. Weiner, O. M. Uy, H. K. Charles, Jr., B. M. Romenesko, and R. von Briesen, "Beta-Backscatter Thickness Measurement: Applications in Microelectronic Fabrication and Control," *Int. J. Hybrid Microelectron.* **6**, 462-470 (1983); also in *Proc. ISHM Conf.* (1983).

D. J. Williams (APL) and L. A. Frank (Univ. Iowa), "Intense Low-Energy Ion Populations at Low Equatorial Altitudes," *J. Geophys. Res.* **89**, 3903-3911 (1984).

F. M. Wiygul and R. M. Metzger (JHU) and T. J. Kistenmacher (APL), "Madelung Energy Systematics in the Heterofulvalene-TCNQ Charge-Transfer Salts," *Mol. Cryst. Liq. Cryst.* **107**, 115-131 (1984).

F. Yasuhara (Chyuko Univ.), R. K. Greenwald (APL), and S.-I. Akasofu (Univ. Alaska), "On the Rotation of the Polar Cap Potential Pattern and Associated Polar Phenomena," *J. Geophys. Res.* **88**, 5773-5777 (1983).

L. J. Zanetti (APL), W. Baumjohann (Max-Planck Inst.), and T. A. Potemra and P. F. Bythrow (APL), "Three-Dimensional Birkeland Ionospheric Current System, Determined from MAGSAT," in *Magnetospheric Currents*, T. A. Potemra, ed., *Geophys. Monogr. Am. Geophys. Union* **28**, pp. 123-130 (1984).

L. J. Zanetti and T. A. Potemra (APL), T. Iijima (Univ. Tokyo), W. Baumjohann (Max-Planck Inst.), and P. F. Bythrow

(APL), "Ionospheric and Birkeland Current Distributions for Northward Interplanetary Magnetic Field: Inferred Polar Convection," *J. Geophys. Res.* **89**, 7453-7458 (1984).

P. A. Zucker, "Credible Use of Models for Untested Conditions," in *Proc. 1984 Summer Conf., Soc. for Computer Simulation*, pp. 237-238 (1984).

PRESENTATIONS

F. J. Adrian, J. Bohandy, and B. Kim, "Magnetophotoselective Photolysis of Randomly Oriented Radical in Solids," Gordon Conf. on Radical Ions, Wolfeboro, N.H. (Jun 18, 1984).

J. R. Apel, "Oceanic Internal Waves," International Union of Geodesy and Geophysics, Hamburg (Aug 17, 1983).

J. R. Apel, "A Review of Major Scientific Results from U.S. Satellite Altimetry and Projections for the Future," International Union of Geodesy and Geophysics, Hamburg (Aug 26, 1983).

W. H. Avery, "Ocean Thermal Energy Conversion (OTEC): A Major New Source of Fuels and Power," Resources for the Future Colloq., Washington (Mar 30, 1983).

W. H. Avery, "Ocean Thermal Energy Conversion Status and Prospects," School of Advanced International Studies, Washington (Mar 28, 1984).

W. H. Avery and D. Richards, "Design of a 160 MW OTEC Plantship for Production of Methanol," Oceans '83, San Francisco (Aug 29-Sep 1, 1983).

W. H. Avery, D. Richards, and G. L. Dugger, "Hydrogen Generation by OTEC Electrolysis and Economical Energy Transfer to World Markets via Ammonia and Methanol," 5th World Hydrogen Energy Conf., Toronto (Jul 15-19, 1984).

C. B. Bargeron, B. H. Nall, and A. N. Jette, "Use of Low-Energy Electron Current Image Diffraction to Determine Surface Structure," 6th Symp. on Applied Surface Analysis, Dayton (Jun 6, 1984).

W. G. Bath, E. W. G. David, and J. T. Miller, "Development and Testing of the Gridlock Demonstration System," 30th Tri-Service Radar Symp., Naval Postgraduate School, Monterey (Jun 26-28, 1984).

R. C. Beal, F. M. Monaldo, and D. G. Tilley, "Properties of the L-Band MTF in the Open Ocean from Precision Seasat SAR Ocean Wave Spectra," URSI Microwave Signature Workshop, Toulouse (Jan 1984).

R. C. Benson, B. H. Nall, F. G. Satkiewicz, and H. K. Charles, Jr., "Surface Analysis of Adsorbed Species from Epoxy Adhesives in Microelectronics," 6th Symp. on Applied Surface Analysis, Dayton (Jun 6, 1984).

F. S. Billig, "Ramjets with Supersonic Combustion," AGARD-NATO PEP Lecture Series No. 136 on Ramjet and Ramrocket Propulsion Systems for Missiles, Naval Postgraduate School, Monterey (Sep 5-6, 1984); also the Royal Aeronautical Soc., London, (Sep 10-11, 1984) and the German Armed Forces University, Munich (Sep 13-14, 1984).

H. D. Black, "Satellites for Land Surveying," 31st Spring Meeting, County Engineers' Assoc. of Maryland, Columbia (May 4, 1984).

S. J. Bockstahler-Brandt and L. Kassof, "Evolution of an Historical Oceanographic Data Base," DEC Users Soc. Symp., Cincinnati (Jun 4-8, 1984).

W. E. Buchanan, "Computer Authoring Systems for Teachers," International Conf., Association for Children with Learning Disabilities, New Orleans (Feb 28, 1984).

M. W. Burgan, "Editorial Consistency," Annual Meeting, Council of Biology Editors, Airlie, Va. (Apr 29-May 2, 1984).

D. T. Burton, "Chemical and Biological Considerations of Power Plant Dechlorination," Electric Power Research Institute Seminar/Workshop on Dechlorination Systems Design and Operations, Chicago (Jul 19-20, 1984).

D. T. Burton, "The Impacts of Chlorine and Chlorine-Related Pollutants Received by the Bay from Sewage Treatment, Electric Generating, and Food Processing Plants," Conf. on Land Use and the Chesapeake Bay, Fort Monroe, Va. (May 15-17, 1984).

D. T. Burton and J. A. Fava, "Toxicity of Chlorine to Aquatic Life and Its Impact on the Environment," 57th Annual Conf., Water Pollution Control Federation, New Orleans (Sep 30, 1984).

D. C. Cetronk, "APL's Hybrid Facility," Spring Meeting, EAI Computer Users Group, Columbia, Md. (Apr 19, 1984).

H. K. Charles, Jr., "Ball Shear Standard Test Method—Update," ASTM F-7 Committee on Electronics Meeting, San Jose, Calif. (Feb 10, 1984).

H. K. Charles, Jr., "Microelectronics Packaging," SRC Advanced Packaging Strategies Workshop, Raleigh-Durham (Dec 9, 1983).

A. F. Cheng, "Escape of Sulfur and Oxygen from Io," JHU Atomic Physics Seminar, Baltimore (Nov 1983).

A. F. Cheng, "Magnetospheres of Earth, Jupiter, and Saturn: Comparative Studies," Canadian Assoc. of Physics Annual Meeting, Universite de Sherbrooke, Quebec (Jun 17-20, 1984).

A. F. Cheng, "Magnetosphere, Rings and Moons of Uranus," Voyager Uranus/Neptune Workshop, JPL, Pasadena (Feb 6-8, 1984); also 164th Meeting, American Astronomical Soc., Baltimore (Jun 11-13, 1984).

A. F. Cheng, "Pulsar Radiation Mechanisms," Astronomy Colloq., Univ. Maryland, College Park (Dec 1983).

A. F. Cheng, "Satellite and Torus Processes in Planetary Magnetospheres," 1984 Yosemite Conf. on Planetary Environments: A Comparative View, Yosemite, Calif. (Jan 30-Feb 3, 1984).

A. F. Cheng, "X-Ray Emission from Fast Pulsars," Workshop on Birth and Evolution of Neutron Stars: Issues Raised by Millisecond Pulsars, National Radio Astronomy Observatory, Green Bank, W. Va. (Jun 5-8, 1984).

M. C. Chiu, M. J. Chandler, and A. G. Bates, "Automated Measurements and Data Recording System for High Resolution Phase Intercomparison for a Set of Precision Clocks," Conf. on Precision Electromagnetic Measurements '84, Delft, The Netherlands (Aug 20-24, 1984).

J. P. Darling, "A Hardware Model for Comparative Quantification of the Propagation Delay from an Inner-Product Step Processor," 15th Annual Pittsburgh Modeling and Simulation Conf., Univ. Pittsburgh (Apr 19-20, 1984).

S. C. Dillon, "INQUIRE: A Management Tool for the Space Department of The Johns Hopkins University Applied Physics Laboratory," INFODATA National Users Meeting, Scottsdale, Ariz. (Oct 23-27, 1983).

E. B. Dobson, J. R. Rowland, M. L. Hill, and R. E. Miller, "An Optical Disdrometer to Measure Dropsize Distributions, Visibility, and Liquid Water Content in an Airborne Environment," International Symp., IEEE Antennas and Propagation Soc., Boston (Jun 1984).

Q. E. Dolecek, "Mainframe Graphics Using the Texas Instruments Professional," Texas Instruments Minicomputer International Users Group Symp., Nashville (Mar 25-28, 1984).

Q. E. Dolecek and D. B. Strake, "VHSIC System Design Methodology," DoD VHSIC Workshop Series, San Diego (Mar 19-21, 1984).

G. L. Dugger, L. L. Perini, and D. Richards, "Hybrid Geothermal-Ocean Thermal Energy Conversion (GEOTEC)

Power Plant Analysis and Cost Estimates," 5th Miami Conf. on Alternative Energy Sources, Miami Beach (Dec 13-15, 1983).

L. W. Ehrlich, "Computational Aspects of Aortic Bifurcation Flows," SIAM Summer Meeting, Seattle (Jul 19, 1984).

L. F. Fehlner and T. W. Jerardi, "Observation of the Performance of the Southwest U.S. Loran-C Chain," Wild Goose Association Technical Symp., Washington (Oct 12-14, 1983).

R. E. Fischell, "A Programmable Implantable Medication System: Application to Diabetes," 3rd Workshop, Study Group of the European Assoc. for the Study of Diabetes, Igls, Austria (Feb 5-7, 1984); also CARDIOSTIM 84 Symp., Monte Carlo (Jun 21-23, 1984).

R. E. Fischell, "A Programmable Implantable Medication System (PIMS)," Univ. Tokyo Faculty of Medicine (Nov 11, 1983).

R. E. Fischell, "A Programmable Implantable Medication System (PIMS) for the Treatment of Diabetes," 4th Congress, International Soc. for Artificial Organs, Kyoto (Nov 14-17, 1983).

R. E. Fischell, "From Space Technology: Implantable Microcomputer Devices to Treat Cardiovascular Diseases," American Heart Association's Advanced Topics in Cardiovascular Nursing 1984, St. Joseph Hospital, Towson, Md. (Jun 14, 1984).

R. E. Fischell, "From Space Technology: Improved Microcomputer Implantable Devices to Treat Cardiovascular Diseases," American Heart Association's 11th Science Writers Forum, St. Petersburg Beach, Fla. (Jan 15-18, 1984).

R. E. Fischell, "The Treatment of Diabetes with a Programmable Implantable Medication System," 5th Annual IEEE-EMBS Conf., Columbus, Ohio (Sep 10-12, 1983).

J. Fluss, K. A. Plantz, and D. K. Pace, "FFG-7 Multi-Warfare Analysis," 52nd Symp., Military Operations Research Soc., Ft. Leavenworth, Kans. (Jun 5-7, 1984).

J. W. Foerster (U.S. Naval Academy) and P. M. Thompson (APL), "Plankton and Whaling Ground Dynamics in the Denmark Strait," International Symp. on Marine Plankton, Tokai Univ., Shimizu, Japan (Jul 23-28, 1984).

M. D. Foust, K. Strohbehn, and G. A. Heyler, "Space Telescope Alternate Fine Guidance Sensor Performance," AIAA Guidance and Control Conf., Seattle (Aug 20-22, 1984).

H. G. Fox, "Relocation and Refurbishment of the APL Space Simulation Laboratory," 31st Meeting, AIAA Working Group on Space Simulation, Tokyo (Sep 18-21, 1984).

E. J. Francis, "A Financing Option for OTEC Plants," 1st Pacific Congress on Marine Technology, Honolulu (Apr 24-27, 1984).

E. J. Francis, "Comments for OTEC Workshop," Workshop on Ocean Thermal Energy Systems, Office of Technology Assessment, Washington (Feb 9, 1984).

J. D. Franson, "Optical Interferometer Data in Support of Local Theories," Conf. on Fundamental Questions in Quantum Mechanics, State Univ. New York, Albany (Apr 12-14, 1984).

M. H. Friedman, "A Model of the Thickening of the Arterial Intima under Shear," Workshop on Cardiovascular and Pulmonary Dynamics, Zuoz, Switzerland (Aug 23, 1984).

M. H. Friedman, "Fluid Mechanics in Atherogenesis," Lovelace Medical Foundation, Albuquerque (Nov 30, 1983).

M. H. Friedman, "Fluid Mechanical Factors in Atherogenesis," 9th Hugh Lofland Conf. on Arterial Wall Metabolism, San Antonio (May 24, 1984).

M. H. Friedman, "Fluid Mechanics and Mass Transport in Atherosclerosis," Special Seminar, Chemical Engineering Dept., Crump Institute for Medical Engineering, Univ. California, Los Angeles (May 21, 1984).

M. H. Friedman, O. J. Deters, and C. B. Bargeron (APL), G. M. Hutchins (JHMI), and F. F. Mark (APL), "The Effect of Wall Shear on the Thickening of Human Arterial Intima," 9th Hugh Lofland Conf. on Arterial Wall Metabolism, San Antonio (May 25, 1984).

R. M. Fristrom, "O Atom Studies Using Pulsed Molecular Beams," Materials and Equipment Workshop, NASA/Goddard, Greenbelt, Md. (Jun 8, 1984).

P. G. Fuechsel, "Field Test to Characterize Submarine-Generated E.F Sources," 52nd Symp. Military Operations Research Soc., Fort Leavenworth, Kans. (Jun 5-7, 1984).

J. R. Gersh, "Rule-Based Automation of Command Action in Naval Combat Systems," 7th MIT/ONR Workshop on C^3 Systems, San Diego (Jun 11-15, 1984).

A. P. Georgopoulos (JHMI), J. F. Kalaska (Univ. Montreal), J. T. Massey (APL), and R. Caminiti (JHMI), "Cortical Mechanisms of Two-Dimensional Aimed Arm Movements: IX. Static (Positional) Factors Cannot Account Fully for Movement-Related Cell Discharge in Motor Cortex and Area 5," Soc. for Neuroscience, Boston (Nov 1983).

A. D. Goldfinger, R. C. Beal, F. M. Monaldo, D. E. Irvine, and D. G. Tilly, "Recovery of Ocean Wave Spectra from SAR Images, a Progress Report," International Soc. Photogrammetry and Remote Sensing, Commission II, SAR Processing Working Group, Tokyo (Nov 9-11, 1983).

J. Goldhirsh, "Rain Attenuation Program: Measurements and Prediction of Rain Attenuation at Frequencies above 10 GHz, August 1983 through June 1984," NASA Program Experimeters Meeting VII, Hanover, N.H. (Jun 29, 1984).

J. Goldhirsh, "Slant Path Rain Attenuations at 28 GHz Derived Simultaneously with a Radiometer and a Radar," 1984 IEEE Antennas and Propagation Soc. International Symp., Boston (Jun 25-28, 1984).

J. Goldhirsh and J. Rowland, "Differential Reflectivity Measurements of Precipitation at Wallops Island, Virginia," 1984 IEEE Antennas and Propagation Soc. International Symp., Boston (Jun 25-28, 1984).

W. J. Grabowski, "Two-Dimensional Mixed Layer Thermostructure," AGU Ocean Science Meeting, New Orleans (Jan 23-28, 1984).

M. E. Greenspan (APL), D. H. Fairfield (NASA/Goddard), and C.-I. Meng (APL), "Simultaneous Polar Cap and Magnetotail Observations of Intense Polar Rain," AGU Chapman Conf. on the Magnetospheric Polar Caps, Fairbanks (Aug 6-9, 1984).

R. A. Greenwald, "Initial Results from the Goose Bay HF Radar," National Radio Science Meeting, Univ. Colorado, Boulder (Jan 11-13, 1984).

R. A. Greenwald, K. B. Baker, and R. A. Hutchins (APL) and C. Hanuise (Univ. Toulon), "New HF Radar for Studying High Latitude F-Region Irregularities," National Radio Science Meeting, Univ. Colorado, Boulder (Jan 11-13, 1984).

W. H. Guier, J. T. Massey, and W. Schneider (APL) and J. L. Weiss (JHMI), "The Use of PC's for On-Line Data Processing in Medical and Clinical Research," 17th Annual Hawaii International Conf. on System Sciences, Honolulu (Jan 4-13, 1984).

T. C. Guo, "Transient Dielectric Responses in Nonsteady State Regimes," Colloq., George Washington Univ., Washington (Jul 16, 1984).

W. W. Guo, "Microwaves for Medical Imagery and Therapy," Colloq., George Washington Univ., Washington (Jul 16, 1984).

G. D. Halushynsky, "An Architecture for the Year 2000 Navy Command and Control," Joint National Meeting, Institute of Management Sciences and Operations Research Soc., San Francisco (May 14-16, 1984).

L. W. Hart and J. W. Sari, "Geomagnetic Noise Measurements near the St. Croix Shoreline," ONR Workshop on Geomag-

netic Properties of Continential Margins, Golden, Colo. (Apr 30-May 1, 1984).

R. A. Henle, "Microcomputer Technology Applying to Authoring Systems," Joint Convention, JHU/Maryland State Dept. of Education, Baltimore (Jan 1984).

R. A. Henle, "Personal Computing in Your Organization—Technical and Managerial Issues: Methodologies for Success," IEEE Computer Soc., Laurel, Md. (Jun 27-28, 1984).

R. A. Henle, "Recent Advances in Microcomputer Technology—Impact on the Handicapped," Association for Rehabilitation in Data Processing, Baltimore (Jan 1984).

R. A. Henle, "Small Computer Systems" (ten-part seminar), IEEE Power Soc., Baltimore (Mar-May 1984).

R. A. Henle, "The Current Struggle to Aid the Handicapped with Microcomputers," Assoc. for Learning Disabled, New Orleans (Feb 6-7, 1984).

R. A. Henle, "The Trend Towards Distributed Computing," Illinois Inst. Tech. Research Facility, Annapolis (Apr 15, 1984).

R. F. Hendrick, J. R. Brannan, and G. P. Forney, "The Uniform WKB Approach Extension to Multiple Channel and Bottom Propagation," 108th Meeting, Acoustical Soc. of America, Minneapolis (Oct 9-12, 1984).

R. E. Hicks, "Overview of Medical Applications for Hybrid Microelectronics," New England Chapter, ISHM Meeting, Mass. (Feb 15, 1984); also Capital Chapter, ISHM Meeting, Linthicum, Md. (Mar 7, 1984).

R. E. Hicks, H. K. Charles, Jr., and B. M. Romenesko, "High Density Interconnects in Biomedical Systems Using Hybrids and Surface Mounted Components," 1984 Microelectronic Interconnect Conf., Welches, Ore. (Jul 31, 1984).

M. L. Hill, "Electrical Disturbances near Thunderstorms Observed by Means of Small Remotely Piloted Aircraft Stabilized with Respect to the Local Field Vector," 7th International Conf. on Atmospheric Electricity, Albany (Jun 3-8, 1984).

E. D. Holm, "A GPS Fast Acquisition Receiver," NTC '83—IEEE National Telesystems Conf., San Francisco (Nov 1983).

G. W. Hoskins (SSPO) and R. J. Danchik (APL), "Joint Paper on Navy Navigation Satellite System Status and Future," The Royal Institute of Navigation Annual Conf., London (May 22, 1984).

D. E. Irvine, "The Giant Wave Problem," Colloq., National Research Inst. of Oceanology, Stellenborsch, South Africa (May 26, 1984).

D. E. Irvine, "The Modulation of Short Waves by Long Waves in the Presence of Wind," Symp. on Wave Breaking, Turbulent Mixing, and Radio Probing of the Ocean Surface, Sendai, Japan (Jul 19-25, 1984).

D. E. Irvine, L. C. Beal, A. D. Goldfinger, F. M. Monaldo, and D. G. Tilley, "A Status Report on SAR Ocean Wave Spectra Research at APL," Conf. on Active Microwave Sensing of Oceans, Royal Aircraft Establishment, Farnsborough, England (Apr 4, 1984).

A. N. Jette, B. T. Nall, and C. B. Bargeron, "Low Energy Electron Channeling Observed by Current Image Diffraction," 30th National Symp. American Vacuum Soc., Boston (Nov 1-4, 1983).

S. C. Jones and V. J. DiLosa, "Computer Model for a Waveguide Relay Link," National Telesystems Conf., San Francisco (Nov 14-17, 1983).

R. J. Keenan, "6 DOF Missile Hybrid Computer Simulation," North American Chapter, EAI Computer Users Group, Columbia, Md. (Apr 1, 1984).

T. J. Kistenmacher, "Conformational Properties of Purine and Pyrimidine Complexes of cis-$[(NH_3)_2PtCl_2]$; Effects of Intermolecular and Intramolecular Forces," Chemistry Dept. Seminar, Towson State Univ., Baltimore (Apr 3, 1984).

T. J. Kistenmacher, "Structure-Physical Property Relationships for Tetramethyltetraselenafulvalenium Salts, $(TMTSF)_2X$," American Crystallographic Assoc. Meeting, Lexington, Ky. (May 21-25, 1984).

T. J. Kistenmacher, "Structure-Physical Property Relationships in the Family of Organic Superconductors, $(TMTSF)_2X$," Chemistry Dept. Seminar, Morgan State Univ., Baltimore (Feb 10, 1984).

S. M. Krimigis, "Active Experiments in the Distant Magnetosphere: The AMPTE Program," Institute for Interplanetary Space Physics, Frascati, Italy (Oct 28, 1983).

S. M. Krimigis, "Particle Injection Experiments in Space: The AMPTE Program," JHU/APL Colloq., Laurel, Md. (May 25, 1984).

S. M. Krimigis, "Space Science Board/European Science Foundation Workshop," Hilton Head, S.C. (Sep 20-23, 1983); also the NASA/ESA/ISAS Solar-Terrestrial Physics Meeting, Washington (Sep 26-27, 1983).

W. H. Lambert, "Cooperative AAW Engagements: Trend of the Future for Naval SAM Systems," Symp. on Fire Control, Picatinney Arsenal, N.J. (Apr 1984).

S. D. Landersman, "Rainbow Reef Exercise and the Near Term Prepositioned Force," Military Sealift Command, Washington (Mar 26, 1984); also Staff, Chief of Naval Operations, Washington (Apr 9, 1984); also Master Mariners Readiness Training Course, U.S. Merchant Marine Academy, Kings Point, N.Y. (May 8, 1984); also Staff, Naval Sea Systems Command, Washington (May 23, 1984).

M. J. Linevsky and R. M. Fristrom (APL) and J. R. Smith (Sandia National Lab.), "Single Eddy Combustion—A New Approach to Turbulent Flames," 20th Symp. on Combustion, Ann Arbor (Aug 12-16, 1984).

A. T. Y. Lui, "Observed Features of the Earth's Cross-Tail Current Sheet," IAU Symp. No. 107 on Unstable Current Systems and Plasma Instabilities in Astrophysics, College Park, Md. (Aug 1983).

F. Marshall (JHMI), J. T. Massey (APL), R. Sanders (JHMI), R. A. Makofski, F. F. Mark, and F. B. Weiskopf, Jr. (APL), F. Leo (JHMI), and W. H. Guier (APL), "Shock Wave Destruction of Renal Calculi: New Technical Modifications," Meeting, American Urological Assoc., New Orleans (May 7, 1984).

R. H. Maurer, "Cosmic Ray Effects on Space-Borne Microelectronics," Joint Colloq. Univ. Delaware Physics Department and the Bartol Research Foundation of the Franklin Inst., Newark, Del. (Feb 15, 1984).

L. F. McGoldrick, "Remote Sensing for Air-Sea Interaction and Oceanography," 5th Conf. on Ocean-Atmosphere Interaction, Miami (Jan 10-13, 1984).

W. F. Mehlman, "Role of Aegis in AAW," Meeting, Assoc. of Senior Naval Engineers, Long Beach, Calif. (Jun 8, 1984).

C.-I. Meng, "Dynamic Variations of the Auroral Precipitation and the Polar Cap," International Conf. on Results of ARCAD 3, Toulouse (May 22-25, 1984).

C.-I. Meng, "Imaging Aurora under Full Sunlight by Vacuum Ultraviolet Observation," International Conf. on Results of ARCAD 3, Toulouse (May 22-25, 1984).

G. E. Mitzel and P. G. Barnett, "Positional Surface Target Discrimination Using Pattern Recognition," 7th MIT/ONR Workshop on C^3 Systems, San Diego (Jun 11-15, 1984).

F. F. Mobley, "Passive Attitude Control," AIAA/NCS Seminar on Spacecraft Attitude Control Systems, NASA/Goddard Space Flight Center, Greenbelt, Md. (Oct 24, 1983).

F. M. Monaldo, "Comparison of Ocean Wave Energy Measurements by the Seasat Synthetic Aperture Radar with SAR Wave Imaging Theories," 1984 International Geoscience and Remote Sensing Symp., Strasbourg (Aug 1984).

F. M. Monaldo, "Variation in Ocean Surface Wave Energy as

Measured by the Seasat SAR," AGU Ocean Sciences Meeting, New Orleans (Jan 1984).

L. K. Moore (APL) and D. L. Plung (Westinghouse Idaho Nuclear), "Getting an Anthology Published with the IEEE Press," IEEE Professional Communication Soc., Atlantic City (Oct 10-12, 1984).

J. C. Murphy, "Thermal Wave Imaging in Non-Destructive Evaluation," Non-Destructive Evaluation of Materials Seminar, Rutgers Univ., New Brunswick, N.J. (Jun 15, 1984).

V. O'Brien, "Blood Flow in Constricted Arteries," Fluid Dynamics Seminar, CSIRO, Canberra (Jun 5, 1984).

V. O'Brien, "Pulsatile Blood Flow in a Constricted Artery," Seminar, Univ. Sydney (Jun 20, 1984).

D. E. Olsen, "The Applied Statistician at APL," Orientation Seminars in Mathematical Sciences," The Johns Hopkins Univ., Baltimore (Feb 28, 1984).

D. K. Pace, "The Mystique of Weapon System Analysis," JHU School of Advanced International Studies, Security Studies Roundtable, Washington (Mar 19, 1984).

D. K. Pace, "The Potential Impact of Third World Military Systems on Future Ship Designs," 52nd Symp., Military Operations Research Soc., Ft. Leavenworth, Kans. (Jun 5-7, 1984).

J. G. Parker, "Optical Determination of O_2 ($^1\Delta_g$) Quenching Rates and Relative Emission Intensities in High Pressure Oxygen Gas Using Pulsed Laser Radiation at 10640 Å," Conf. on Singlet Molecular Oxygen, Clearwater Beach, Fla. (Jan 4-7, 1984).

J. G. Parker and W. D. Stanbro, "Optical Determination of the Rates of Formation and Decay of O_2 ($^1\Delta_g$) in H_2O, D_2O, and Other Solvents," Conf. on Singlet Molecular Oxygen, Clearwater Beach, Fla. (Jan 4-7, 1984).

K. Peacock, "The Optical Variability of the Ocean from CZCS Imagery," SPIE Ocean Optics VII, Monterey (Jun 25-28, 1984).

R. S. Potember, "Erasable Optical Switching," Colloq., E. I. du Pont de Nemours & Co. (Feb 6, 1984).

R. S. Potember, T. O. Poehler, R. C. Hoffman, and R. C. Benson, "Erasable Optical Switching in Organic Charge Transfer Complexes," International Conf. on Physics and Chemistry of Low-Dimensional Synthetic Metals, Albano Termes, Italy (Jun 20, 1984).

T. A. Potemra, "Birkeland Currents," Univ. California, San Diego (Feb 27, 1984).

T. A. Potemra, "Electrodynamic Coupling Processes in Planetary Magnetospheres," Herzberg Inst. Astrophysics, National Research Council of Canada, Ottawa (Mar 29, 1984).

K. A. Potocki, "HILAT—A First Year Status," HILAT Science Team Meeting, La Jolla (May 30, 1984).

W. R. Powell, "A Missile Scheduling Simulation," 16th Summer Computer Simulation Conf., Boston (Jul 23-25, 1984).

A. J. Pue, "High Precision Pointing Control of Space Telescopes," System Theory Colloq., Univ. Maryland, College Park (Oct 12, 1984).

S. N. Raja and J. N. Campbell (JHMI) and R. A. Meyer (APL), "Effects of General Anesthetics on Response of Nociceptive Primary Afferents in Monkey," 3rd International Conf. on Molecular and Cellular Mechanisms of Anesthesia, Calgary (Jun 1984).

S. N. Raja (JHMI), R. A. Meyer (APL), and J. N. Campbell (JHMI), "Halothane Sensitizes Nociceptive C-Fibers in Monkeys," Annual Meeting, American Soc. of Anesthesiologists, Atlanta (Oct 1983).

W. J. Ravich and R. S. Johannes (JHMI), W. Schneider and J. T. Massey (APL), and R. J. Johns and T. R. Hendrix (JHMI), "Portable Continuous pH Monitoring with Computerized Data Analysis," Meeting, American Gastroenterology Assoc., Washington (Oct 25-26, 1983).

J. P. Reilly and W. D. Larkin, "Growth of Sensation with Suprathreshold Current Transients," 6th Annual Bioelectromagnetics Soc. Meeting, Atlanta (Jul 15-19, 1984).

D. Richards (APL), J. S. Seward (Seward Assoc.), F. B. Weiskopf, Jr. (APL), and E. S. Burcher (DOE), "Study of Utilization and Management of Power Generated by a Pneumatic Wave Energy Conversion System," International Conf. on Alternative Energy Systems: Electrical Integration and Utilization, Coventry (Sep 10-12, 1984).

C. L. Rowland, "ALDOT Program," Underwater Systems Group, Range Commanders Council, Bay St. Louis, Miss. (Feb 27-Mar 2, 1984).

L. J. Rueger, "A Satellite Time Dissemination System for the 400.1 MHz Authorized Clear Channel," Interim Working Party 7/4 of International Radio Consultive Committee, Geneva (Nov 22, 1984).

D. M. Rust, "Observations of Fast-Moving Fronts in Solar Flare Loops," International Workshop on Solar Physics and Interplanetary Travelling Phenomena, Yunnan Observatory, Kunming (Nov 1983).

D. M. Rust (APL), G. M. Simnett (Univ. Birmingham, England) and D. F. Smith (Berkeley Research Assoc.), "Thermal Wave Fronts in Solar Flares," 163rd Meeting American Astronomical Soc., Las Vegas (Jan 8-12, 1984).

D. M. Rust (APL) and B. V. Somov (P. N. Lebedev Physics Inst., USSR), "Flare Loops Heated by Thermal Conduction," 164th Meeting, American Astronomical Soc., Baltimore (Jun 10-13, 1984).

W. Seamone, "Morse Code/Computer Interface for Brainstem Infarction Patients," Summer Computer Simulation Conf., Boston (Jul 23-25, 1984).

V. G. Sigillito, "Expert Systems: Present and Future," Assoc. for Computing Machinery, Baltimore (Nov 22, 1983).

D. M. Silver, "Chemical Bonds and Other Electron Pairs," Seminar, Chemistry Dept., Georgetown Univ., Washington (Jan 25, 1984).

D. M. Silver, "Complex Orbital Transformations for Molecular Structure," Kyoto Univ., Japan (May 31, 1984); also Inst. for Molecular Science, Okazaki (Jun 8, 1984); also Tohoku Univ. (Jun 15, 1984); also Hokkaido Univ. (Jun 18, 1984).

J. H. Smart, "Diurnal Variability of Fine-Structure Shear Temperature in the Mixed Layer," AGU Ocean Science Meeting, New Orleans (Jan 23-28, 1984).

J. F. Smola and N. E. Peterson, "The AMPTE Program—An Overview," Star Motor Space Symp., Univ. Delaware (Sep 14-15, 1983).

H. M. South, "Signal Processing Systems for SSBN Sonar Evaluation," Underwater Acoustics and ASW Colloq., Naval Postgraduate School, Monterey (Mar 8, 1984).

J. C. Spall, M. I. Koch, and J. L. Maryak, "On Detecting Sources of Parameter Errors in Invalid Linear Dynamic Models," Joint National Meeting, American Statistical Assoc., Philadelphia (Aug 13-16, 1984).

W. I. Sternberger, "Temperature Compensated Thermistor Anemometer," Salinity-Temperature-Depth 1984 Conf., Marine Technology Soc., San Diego (Feb 27-29, 1984).

J. J. Suter, J. G. Wall, H. D. Black, and T. E. Strikwerda, "Progress Toward Radio-Tracking of Birds via Satellites," Patuxent Wildlife Res. Center, Laurel, Md. (Mar 198-).

R. J. Taylor, "Hazard Analysis for Magnetic Induction from Electric Transmission Lines," 1983 IEEE/EMC Symp., Washington (Aug 23-25, 1983).

R. J. Taylor and L. B. Richardson, "The Use of Ultrasound for the Prevention of Biofouling," Ultrasonics International 83, Halifax (Jul 12-14, 1983).

B. E. Tossman, "Testing Dampers and Attitude Control Subsystems," Workshop, International Federation of Automatic Control, Stanford Univ., Calif. (Aug 22-26, 1983).

W. J. Tropf, A. N. Vavreck, B. P. Sandford, J. H. Schummers,

and J. Schroeder, "Infrared Cloud Backgrounds and Sensor Performance," 2nd Annual Tri-Service Cloud Modeling Workshop, Naval Surface Weapons Center, White Oak, Md. (Jun 26-28, 1984).

D. P. Vasholz and L. J. Crawford, "Dye Dispersion in the Seasonal Thermocline," Seminar, Woods Hole Oceanographic Institution, Mass. (Apr 3, 1984).

R. L. Waddell, Jr., "Satellites: Orbits and Operations," Maryland Junior Academy of Science Meeting, Baltimore (Sep 15, 1984).

J. H. Walker, "Teaching Project Management," American Soc. for Engineering Management, Dallas (Sep 23-25, 1984).

L. B. Weckesser, "APL Program on Sensor Windows," Aero-Structures Workshop, Naval Surface Weapons Center, Dahlgren, Va. (Sep 27, 1983).

L. B. Weckesser, "ENNK Radome Evaluation Program," 1st ENNK Radome Review Meeting, Georgia Institute of Technology, Atlanta (Dec 13, 1983).

L. B. Weckesser, "Test of Oxidation Resistant Carbon-Carbon Candidates for the AWAM Combustor," JANNAF Ramjet Insulator Testing Workshop, Naval Postgraduate School, Monterey (Oct 17, 1983).

E. E. Westerfield, "Use of GPS for Determining Position of Drifting Buoys," NTC '83—IEEE National Telesystems Conf., San Francisco (Nov 1983).

D. J. Williams, "Hot Plasma Effects in the Plasmapause Region," Conf. on Fundamental Magnetospheric Processes in the Plasmapause Region, Univ. Alabama, Huntsville (Oct 25-27, 1983).

A. C. Williamson, "Influence of Low Grazing Angle Sea Clutter on Detection," 6th DARPA Cruise Missile Survivability Workshop, Lincoln Laboratory, Lexington, Mass. (May 1-3, 1984).

L. J. Zanetti, "Magsat Birkeland-Ionospheric Currents, Daylight Auroral Imaging from the HILAT Satellite," Seminar, Uppsala Ionospheric Observatory, Sweden (Oct 7, 1983).

P. A. Zucker, "Establishing Credibility for Multidimensional Models," 9th World Congress, International Federation of Automatic Control, Budapest (Jul 2-6, 1984).

The following papers were presented at the General Assembly, International Association of Geomagnetism and Aeronomy, Hamburg (Aug 1983):

C. B. Baker (APL), K. Pfitzer and W. P. Olson (McDonnell-Douglas), A. Pedersen (European Space Research and Technical Centre), and R. A. Greenwald (APL), "The Effect of Induced Electric Fields on the Electric Coupling between the Magnetosphere and Ionosphere;"

P. F, Bythrow, "Statistical Study of Large-Scale Birkeland Currents Compiled over the Lifetime of Magsat;"

M. Candidi (National Res. Council, Italy) and C.-I. Meng (APL), "Magnetospheric Cusp Electrons and Solar Wind Parameters;"

S. M. Krimigis and B. M. Mauk, "Diamagnetic Effects of Energetic Oxygen Ions in Saturn's Magnetosphere;"

B. H. Mauk and C.-I. Meng, "Geostationary 'Injection Boundary' Signatures;"

C.-I. Meng (APL) and K. Makita (Takushoku Univ.), "Configuration of the Auroral Oval of the Quiescent Magnetosphere;"

C.-I. Meng (APL) and M. Candidi (National Research Council, Italy), "Simultaneous Observations of the Conjugate Polar Cusp;"

C.-I. Meng and B. H. Mauk, "Quiet Time Geostationary Spatial Boundaries as a Manifestation of Dynamical Injection."

L. J. Zanetti (APL), W. Baumjohann (Max-Planck Inst.), and T. A. Potemra and P. F. Bythrow (APL), "Ionospheric and Birkeland Current Distributions Inferred from the Magsat Magnetometer Data."

The following papers were presented at the 1983 International Geoscience and Remote Sensing Symp., San Francisco (Aug 31-Sep 2, 1983):

E. B. Dobson and D. E. Irvine, "Investigation of Gulf Stream Ring Detection with Spaceborne Altimeter Using Mean Sea Height, Wave Height, and Radar Cross Section;"

J. Goldhirsh, "Comparison of Simultaneous Radiometer and Radar Derived Slant Path Attenuation Statistics at 28.56 GHz;"

F. M. Monaldo, "Tracking Ocean Surface Waves Using Spaceborne SAR Image Spectra Corrected for Ocean Surface Movement;"

F. M. Monaldo, E. J. Walsh, and J. Goldhirsh, "The Influence of Rain and Clouds on a Satellite Dual Frequency Radar Altimeter System Operating at 13 and 35 GHz."

The following papers were presented at the Symp. on Electric Shock Safety Criteria, Toronto (Sep 7-9, 1983):

J. P. Reilly, "Body Impedance;"

J. P. Reilly and W. D. Larkin, "Mechanisms for Human Sensitivity to Transient Electric Currents;"

R. J. Taylor, "Body Impedance for Currents of Short Duration."

The following papers were presented as the 5th Washington Area Neighborhood Astronomers Meeting, Naval Research Lab., Washington (Oct 1983):

A. F. Cheng, "X-Rays from Radio Pulsars;"

L. J. Zanetti and C.-I. Meng (APL) and R. A Huffman (Air Force Geophysics Lab.), "Ultraviolet Auroral Imaging from the HILAT Satellite,"

The following papers were presented at the 4th Annual Meeting, American Pain Society, Chicago (Nov 1983):

R. A. Meyer, "Neurophysiology of Neuroma Pain;"

S. N. Raja and J. N. Campbell (JHMI) and R. A. Meyer (APL), "Evidence for Different Mechanisms for Primary and Secondary Hyperalgesia."

The following papers were presented at the Fall Meeting, American Geophysical Union, San Francisco (Dec 5-10, 1983):

K. B. Baker and R. A. Greenwald (APL) and C. Hanuise (Univ. Toulon), "Preliminary Results from the Goose Bay HF-Radar;"

P. F. Bythrow, T. A. Potemra, and C.-I. Meng (APL) and R. E. Huffman, F. J. Rich, and D. A. Hardy (Air Force Geophysics Lab.), "High Density Birkeland Currents Observed by HILAT in the Late Evening and Early Morning Sectors;"

M. Candidi (National Research Council, Italy) and C.-I. Meng (APL), "Double Structure of the Polar Cusp Precipitating Electron Fluxes;"

A. F. Cheng (APL), C. G. Maclennan and L. J. Lanzerotti (Bell Labs.), and M. T. Paonessa and T. P. Armstrong (APL), "Longitudinal Asymmetry in the Io Plasma Torus;"

R. B. Decker, A. T. Y. Lui, and S. M. Krimigis, "Numerical Simulation of Lithium Interactions with Earth's Bow Shock: Transmission Coefficients and Energization in Laminar Field Geometry;"

R. E. Gold (APL) and J. Bamber and D. Venkatesan (Univ. Calgary), "The Relationship between Recurrent Cosmic Ray Increases and Solar Wind Velocity;"

M. E. Greenspan, D. J. Williams, B. H. Mauk, and C.-I. Meng, "ISEE-1 Observations of Particle Injections;"

R. A. Greenwald, K. B. Baker, and R. A. Hutchins (APL) and C. Hanuise (Univ. Toulon), "A New HF Radar for Studying High Latitude F-Region Irregularities;"

R. E. Huffman (Air Force Geophysics Lab.) and C.-I. Meng (APL), "Auroral/Ionospheric Mapper for Ultraviolet Imaging from the HILAT Satellite;"

T. Iijima (Univ. Tokyo) and T. A. Potemra, L. J. Zanetti, and P. F. Bythrow (APL), "Stable Patterns of Large-Scale Birkeland Currents in the Polar Region during Strongly Northward B_Z—A New Birkeland Current System;"

T. W. Jerardi and W. G. Innanen (APL) and B. D. Merritt (DMA), "Kwajalein Test of a New Method of Open Ocean Surveying;"

C. L. Johnson, "Towed Observation of Free Convection in a Winter Mixed Layer;"

S. M. Krimigis, "The Active Magnetospheric Particle Tracer Explorers (AMPTE): Program Overview;"

A. T. Y. Lui and S. M. Krimigis, "Association of Energetic Particle Bursts and Magnetic-Field Aligned Currents in the Magnetotail;"

B. H. Mauk and S. M. Krimigis (APL) and R. P. Lepping (NASA), "The High Pressure Contribution of Energetic (>66 keV) Oxygen Ions in the Inner Saturnian Magnetosphere;"

C.-I. Meng (APL) and R. E. Huffman (Air Force Geophysics Lab.), "Observation of Aurora under Full Sunlit Conditions;"

D. G. Mitchell, A. T. Y. Lui, and D. J. Williams, "Three-Dimensional Energetic Particle Distributions across the Flanks of the Magnetopause and Bowshock;"

L. Monchick and C.-I. Meng (APL) and S. Chakrabarti and S. Bowyer (Univ. California, Berkeley), "Observation of the Auroral Display under Full Sunlit Condition by Using Atmospheric EUV Emissions;"

T. A. Potemra, P. F. Bythrow, and L. J. Zanetti (APL), R. E. Huffman (Air Force Geophysics Lab.), and C.-I. Meng (APL), "The Association of Birkeland Currents and VUV Auroral Emission from HILAT;"

E. C. Roelof, "Orientations of the Interplanetary Magnetic Field, 1964-1965: Solar Cycle Effects;"

E. C. Roelof, D. G. Mitchell, and D. J. Williams, "New Results: Energetic Particle Experiments, IMP 7 & 8;"

E. T. Sarris (Univ. Thrace) and R. B. Decker (APL), "Simultaneous Observations of Shock Accelerated Particles at 1 AU and in the Deep Space;"

L. Varga and D. Venkatesan (Univ. Calgary), and C.-I. Meng (APL), "Intensity Variations of Energetic Electrons in the Outer Radiation Belt during Isolated Substorms;"

D. Venkatesan (Univ. Calgary), R. B. Decker and S. M. Krimigis (APL), and J. A. Van Allen (Univ. Iowa), "Multi-Spacecraft Observations of the Cosmic Ray Minimum of Solar Cycle 21 in the Inner and Outer Heliosphere;"

L. Vlahos (Univ. Maryland) and R. B. Decker and A. T. Y. Lui (APL), "Numerical Simulation of Lithium Interactions with Earth's Bow Shock: Effects of Wave-Particle Interactions between Shock Crossings;"

L. J. Zanetti, T. A. Potemra, and P. F. Bythrow (APL), W. Baumjohann (Max-Planck Inst.), and T. Iijima (Univ. Tokyo), "Birkeland and Hall Current Distributions in the Ionosphere."

The following papers were presented at the AIAA 22nd Aerospace Sciences Meeting, Reno (Jan 9-12, 1984):

F. S. Billig, M. E. White, and D. M. Van Wie, "Application of CAE and CFD Techniques to a Complete Tactical Missile Design;"

S. M. Krimigis and J. Dassoulas, "Active Experiments in the Distant Magnetosphere: The AMPTE Program;"

E. F. Lucero, "Empirical Curves for Predicting Supersonic Aerodynamics of Very Low Aspect Ratio Lifting Surfaces;"

M. E. White, F. S. Billig, and D. M. Van Wie, "Application of CAE and CFD Techniques to a Complete Tactical Missile Design."

The following papers were presented at the JANNAF Propulsion Meeting, New Orleans (Feb 7-9, 1984):

P. P. Pandolfini, P. J. Waltrup, G. A. Sullins, and C. E. Stevens, "Dual-Combustion Ramjet Low Mach Number, High Altitude Connected-Pipe Tests;"

J. R. Stevens, J. L. Keirsey, M. E. White, and D. M. Van Wie, "Multiple Inward-Turning Scoop Investigation for a Hypersonic Dual-Combustor Ramjet Engine;"

M. E. White (APL) and A. Kumar (NASA/Langley), "Viscous Analysis of Supersonic Inlets for the Hypersonic Dual-Combustion Ramjet."

The following papers were presented at the 1984 Naval Aeroballistics Committee Meeting, White Oak, Md. (Feb 14-15, 1984):

R. W. Newman, "Report to the Naval Aeroballistics Heat Transfer Panel for 1984;"

M. E. White and J. C. Hagan, "Computational Viscous Analysis of Supersonic Inlets for the Hypersonic Dual Combustion Ramjet."

The following papers were presented at the Chapman Conf. on Collisionless Shock Waves in the Heliosphere, Napa Valley, Calif. (Feb 20-24, 1984):

R. B. Decker, "The Shock-Drift Acceleration Mechanism at Curved Shocks;"

R. B. Decker (APL) and L. Vlahos (Univ. Maryland), "Effects of Wave-Particle Interactions on the Shock-Drift Acceleration Mechanism."

The following papers were presented at the Annual American Physical Society Meeting, Detroit (Mar 26-30, 1984):

F. J. Adrian, B. F. Kim, and J. Bohandy, "Magnetophotoselective Photolysis of the Formyl Radical in Quartz;"

K. Moorjani (APL) and D. J. Webb and S. M. Bhagat (Univ. Maryland), "Magnetic Phase Diagrams of Amorphous Fe_xB_{100-x};"

T. O. Poehler, R. S. Potember, R. C. Benson, and R. C. Hoffman, "The Electronic and Vibrational Spectra of Electric Field-Induced Phase Transitions in Metal-TCNQ Complexes;"

R. S. Potember, T. O. Poehler, R. C. Hoffman, and R. C. Benson, "Laser-Induced Optical Changes in Organometallic Thin Films."

The following papers were presented at the Spring Meeting, Association for Research in Vision and Ophthalmology, Sarasota (Apr 30-May 4, 1984):

C. L. Aner, L. W. Hirst, H. Abbey, and J. Cohn (JHMI) and H. A. Kues (APL), "Quantitative Analysis of Wide-Field Specular Micrographs;"
R. A. Farrell and R. L. McCally, "Light Scattered from the Cornea at Specular and Other Angles;"
L. W. Hirst (JHMI), H. A. Kues (APL), W. R. Green and S. A. D'Anna (JHMI), and G. Dunkelberger (APL), "Microwave-Induced Corneal Endothelial Changes in Monkeys;"
R. L. McCally and C. B. Bargeron (APL), W. R. Green (JHMI), and R. A. Farrell (APL), "Beam Diameter Dependence and Healing Processes in Co_2 Laser Damaged Corneas;"
E. Young and M. Farazdaghi (JHMI), H. A. Kues (APL), and R. Prendergast (JHMI), "Improved Model of Corneal Allograft Rejection."

The following papers were presented at the Symp. on the Effect of the Ionosphere on C^3I Systems, Alexandria, Va. (May 1-3, 1984):

R. A. Greenwald, K. B. Baker, and R. A. Hutchins (APL) and C. Hanuise (Univ. Toulon), "A New HF Radar for Studying High Latitude F-Region Irregularities;"
R. E. Huffman, J. C. Larrabee, and F. J. Leblanc (Air Force Geophysics Lab.) and C.-I. Meng (APL), "Ultraviolet Remote Sensing of the Aurora and Ionosphere;"
T. A. Potemra, L. J. Zanetti, and P. F. Bythrow, "Global Patterns of Ionospheric and Field-Aligned Birkeland Currents."

The following papers were presented at the NATO Advanced Research Workshop on the Morphology and Dynamics of the Polar Cusp, Lillehammer, Norway (May 6-12, 1984):

R. A. Greenwald, "Coherent Scatter Radar Observations of the Cusp;"
C. Hanuise (Univ. Toulon) and R. A. Greenwald and K. B. Baker (APL), "Problems in the Determination of Cusp-Related Convection Patterns from Single Radar Observations;"
C.-I. Meng, "First Imagery of Aurora in Daylight;"
C.-I. Meng, "The Large Scale Dynamic Motion of the Polar Cusp;"
T. A. Potemra, "Characteristics of Birkeland Currents in the Polar Cap and Cusp."

The following papers were presented at the Spring Meeting, American Geophysical Union, Cincinnati (May 14-18, 1984):

K. B. Baker and R. A. Greenwald, "Early Results from the Goose Bay Ionospheric Radar;"
P. F. Bythrow, T. A. Potemra, and C.-I. Meng (APL) and R. E. Huffman, F. J. Rich, and D. A. Hardy (Air Force Geophysics Lab.), "An Intense Earthward-Directed Birkeland Current: Its Relationship to Energetic Electrons and Plasma Drifts;"
M. E. Greenspan (APL), D. H. Fairfield (NASA/Goddard), and C.-I. Meng (APL), "Simultaneous Polar Cap and Magnetotail Lobe Observations of Hard, Intense Polar Rain;"
A. T. Y. Lui (APL) and A. Hasegawa (Bell Labs.), "Implications of a Steady-State Magnetospheric Convection;"
B. H. Mauk, "Low Energy Particle Measurements within ULF Wave Environments;"
D. G. Mitchell and D. J. Williams (APL) and T. E. Eastman and L. A. Frank (Univ. Iowa), "Magnetospheric Low-Latitude Boundary Layer Convection Investigated in Energetic Particle (MEPI) and Plasma (LEPEDEA) Data;"
M. T. Paonessa and A. F. Cheng, "Energetic Ion Losses in Saturn's Magnetosphere;"
T. A. Potemra, L. J. Zanetti, P. F. Bythrow, and A. T. Y. Lui (APL) and T. Iijima (Univ. Tokyo), "B_y-Dependent Patterns of High-Latitude Phenomena during Periods of Northward IMF;"
E. C. Roelof, D. G. Mitchell, and D. J. Williams, "Energetic Neutral Atoms (E >24 keV) from the Ring Current: Observations from ISEE-1 during a Magnetic Storm;"
L. J. Zanetti and T. A. Potemra (APL), T. Iijima (Univ. Tokyo), W. Baumjohann (Max Planck Inst. Extraterrestial Phys.), and P. F. Bythrow (APL), "Ionospheric and Birkeland Current Distributions for Northward Interplanetary Magnetic Field; Inferred Polar Convection."

The following papers were presented at the COSPAR Meeting, Graz, Austria (Jun 25-Jul 7, 1984):

R. A. Greenwald (rapporteur), "IMS Results on Electric Fields in the Ionosphere and Magnetosphere;"
A. T. Y. Lui, "Streaming Reversal of Energetic Particles in the Magnetotail during a Substorm in the IMS Period;"
C.-I. Meng, "Imaging Aurorae under Full Sunlight;"
C.-I. Meng, "Simultaneous Observation of the Conjugate Polar Cusp Regions;"
T. A. Potemra, "Current Systems in the Magnetosphere and Ionosphere and Their Effects;"
D. M. Rust, "Energy Transfer in Solar Flares;"
D. J. Williams, "Particle Sources, Transport, Storage, and Precipitation;"
D. J. Williams and T. A. Fritz, "The Plasmasheet Boundary as Observed by the ISEE Medium Energy Particles Experiment."

The following papers were presented at the 4th World Congress on Pain, Seattle (Sep 1984):

J. N. Campbell (JHMI), R. A. Meyer (APL), and S. N. Raja (JHMI), "Hyperalgesia: New Insights;"
R. A. Meyer (APL) and J. N. Campbell and S. N. Raja (JHMI), "Coupling of Action Potential Activity between Unmyelinated Fibers in the Normal Peripheral Nerve of Monkey;"
S. N. Raja and J. N. Campbell (JHMI), R. A. Meyer (APL), and S. E. Mackinnon (Univ. Toronto), "Hyperalgesia Following Peripheral Nerve Injury Is Signalled by Myelinated Fibers."

The following papers were presented at Oceans '84, Washington (Sep 10-12, 1984):

C. W. Anderson, "Surface-Operated Profiling Paravane;"
G. J. Farruggia and A. B. Fraser, "Miniature Towed Oceanographic Conductivity Apparatus;"
D. A. Kitchin, A. B. Fraser, R. P. H. Lee, L. A. Meyer, L. E. Karner, and C. S. Best, "Densely Instrumented Towed Sensor Systems."

The following papers were presented at the Workshop on Bank-to-Turn Controlled Terminal Homing Missiles, Laurel, Md. (Sep 19-20, 1984):

A. Arrow, "Influence of Radome-Induced Body Motion Coupling on Bank-to-Turn Controlled Terminal Homing Missiles;"
P. A. Hawley, "Dynamics of the Airframe and Kinematics of the Seeker for Selected Airframes and Control Policies;"

A. J. Pue, "Adaptive Radome Error Correction for Homing Missiles;"

G. B. Stupp, Jr., and A. Arrow, "Influence of Control Policy on Airbreathing Chin Inlet SOJS Missile."

AUTHOR INDEX

AUTHOR INDEX